Philipps Universität Marburg

Adsorption and Thermally Induced Reactions of Methanol on Bimetallic X/Ru(0001) Layers (X = Cu, Pt)

DISSERTATION

zur Erlangung des Doktorgrades
der Naturwissenschaften (Dr. rer. nat.)

dem

Fachbereich Physik
der Philipps-Universität Marburg

vorgelegt von

Dipl.-Phys. Paweł Gaździcki

aus Warschau, Polen

Marburg/Lahn, 2011

Erstgutachter: Prof. Dr. Peter Jakob

Zweitgutachter: Prof. Dr. Wolfram Heimbrodt

Einreichungsdatum: 13.10.2011

Als Dissertation angenommen: 07.12.2011

Tag der mündlichen Prüfung: 20.12.2011

Hochschulkennziffer: 1180

Abstract

This thesis summarizes the results of thermally induced methanol (CH_3OH) reactions on bimetallic Ru(0001)-based catalyst surfaces under ultrahigh vacuum conditions. Specifically, the following clean and oxygen covered surfaces were used: Ru(0001), (sub-) monolayer Cu/Ru(0001), multilayer Cu/Ru(0001), Pt_n/Ru(0001) layers, and Pt_xRu_{1-x}/Ru(0001) surface alloys.

The adsorption and reactions of methanol are of great technological relevance for the direct methanol fuel cell (DMFC). Thereby, it is desirable to influence chemical reactivity and selectivity of catalysts to convert methanol to CO_2 instead of CO which acts as a poison affecting a continued and stable operation. The stability of reaction intermediates and the height of the activation barriers of the various reaction steps critically depends on specific properties of the substrate material. Straightforward methods to design novel catalysts in a controlled way are the deposition of ultrathin metal films on a host material, the building of alloys or the addition of coadsorbates.

In the experiments performed in this work methanol was added at 20 or 80 K to the catalyst surfaces and slowly annealed with 1 K/s to increasingly higher temperatures. Thereby, the surface species were identified using Fourier transform infrared spectroscopy, i.e. the observed vibrational modes were analyzed in detail. For an unambiguous assignment of the observed peaks isotopic labeling was applied using different isotopes of methanol, oxygen, carbon monoxide, and hydrogen. The desorbing species, on the other hand, were analyzed by temperature programmed desorption using a quadrupole mass spectrometer. The desorption temperature provides information about the binding strength of an adsorbate and about the dissociation temperature of stable surface species which decays into gaseous products. Moreover, isotopic labeling (^{18}O and ^{16}O) allows the discrimination of reactions involving surface oxygen, e.g the formation of desorbing water. Similarly, the CD_3OH isotope allows to distinguish whether hydrogen from the CD_3 or the OH group contributes to a certain reaction. For the quantitative analysis of the chemical composition of the surface and the adsorbates, X-ray photoelectron spectroscopy was applied.

The experiments focus on the identification of fundamental reaction steps and stable intermediate species and, in the second step, on the variation of surface parameters, such as the sort and thickness of a deposited metal, the addition of coadsorbates,

changing the adsorbate order and density or modifying the composition of the surface alloy.

The reactions on the investigated surfaces can be subdivided into two major pathways; (i): a total dehydrogenation pathway leading to CO, and (ii): an oxidation pathway which produces gaseous CO_2.

On the clean Ru(0001), Cu/Ru(0001) and Pt/Ru(0001) surfaces either the dehydrogenation pathways are observed or no reaction occurs at all. The CO_2 producing path, on the other hand, can be opened by the adsorption of oxygen. In parallel, the CO formation becomes reduced. In this context, the influence of oxygen on the yielded reaction products was investigated. Generally, it is found that only disordered and dilute oxygen promote methanol reactions; dense and ordered O-overlayers passivate the surface effectively. A significant drawback of adding oxygen is the reaction of the oxygen atoms with hydrogen from methanol dehydrogenation to gaseous water. As hydrogen is the energy provider in a DMFC the desorbing water represents an unwanted drain of H atoms from the surface. Interestingly, the surfaces which produce the highest amount of CO_2 are also most efficient with respect to the formation of water.

As on oxygen covered Pt_xRu_{1-x}/Ru(0001) surface alloys the drain of H atoms is limited and they nonetheless exhibit CO_2 as a final product they represent a compromise regarding the ideal catalyst material for a DMFC. In particular, alloys with a Pt contents of $50 - 80\%$ are found to be most suitable.

Zusammenfassung (Abstract in German)

Diese Arbeit ist eine Zusammenfassung der Ergebnisse zu thermisch induzierten Methanolreaktionen (CH_3OH) auf bimetallischen Ru(0001)-basierten Katalysatoroberflächen unter Ultrahochvakuumbedingungen. Im Einzelnen wurden die folgenden sowohl sauberen als auch mit Sauerstoff vorbedeckten Oberflächen verwendet: Ru(0001), (Sub-) Monolagen Cu/Ru(0001), Multilagen Cu/Ru(0001), Pt_n/Ru(0001) Lagen und Pt_xRu_{1-x}/Ru(0001) Oberflächenlegierungen.

Die Adsorption und die Reaktionen von Methanol sind von größtem technologischen Interesse in Bezug auf die Direktmethanolbrennstoffzelle (DMFC). Dabei ist es wünschenswert, die chemische Reaktivität und Selektivität eines Katalysators so zu steuern, dass Methanol zu CO_2 anstelle von CO umgewandelt wird, da Letzteres einen reibungslosen Betrieb der Brennstoffzelle verhindern würde. Die Stabilität der Zwischenprodukte und die Höhe der Aktivierungsbarrieren der einzelnen Reaktionsschritte hängen dabei stark von den Eigenschaften des Substrats ab. Einfache Methoden zur kontrollierten Funktionalisierung von Oberflächen sind die Deposition ultradünner Metallschichten, die Legierungsbildung oder das Hinzufügen von Koadsorbaten.

In den durchgeführten Experimenten wurde Methanol entweder bei 20 oder 80 K auf die Katalysatoroberflächen dosiert und anschließend mit 1 K/s geheizt. Dabei wurden die Oberflächenspezies anhand ihrer Vibrationsmoden mittels Fouriertransformations-Infrarotspektroskopie identifiziert. Die Verwendung verschiedener Isotope von Methanol, Sauerstoff, Kohlenmonoxid und Wasserstoff lässt eine eindeutige Zuordnung der Vibrationspeaks zu. Die desorbierenden Spezies und ihre Bindungsenergien wurden mit Hilfe von thermischer Desorption mit einem Quadrupol-Massenspektrometer untersucht. Die Desorption gibt dabei auch Auskunft über den Zerfall stabiler Oberflächenspezies, falls diese direkt in Gasphasenmoleküle zerfallen. Dabei ermöglicht die Isotopenmarkierung (^{18}O und ^{16}O) die Unterscheidung zwischen Reaktionen, bei denen Sauerstoff involviert ist. Des Weiteren kann durch die Verwendung des CD_3OH-Isotops unterschieden werden, ob Wasserstoff aus der CD_3- oder der OH-Gruppe an bestimmten Reaktionen teilnimmt. Die quantitative Analyse der chemischen Zusammensetzung der Probe und der Adsorbatmengen fand unter Anwendung der Röntgen-Photoelektronenspektroskopie statt.

Die Untersuchungen konzentrieren sich zunächst auf die Identifikation fundamentaler Reaktionsschritte und stabiler Reaktionsspezies und im Folgenden auf die Variation verschiedener Parameter, wie die Art und Dicke des deponierten Metallfilms, das Hinzufügen von Koadsorbaten, die Änderung der Adsorbatordnung und -dichte oder die Modifikation der Zusammensetzung der Oberflächenlegierung.

Die Reaktionen können in zwei verschiedene Pfade unterteilt werden: (i) in die vollständige Dehydrierung von Methanol zu CO und (ii) in die Umwandlung von Methanol zu CO_2. Auf den sauerstofffreien Oberflächen wurde ausschließlich die Produktion von CO beobachtet. Der CO_2 bildende Reaktionsweg kann durch die Koadsorption von Sauerstoff aktiviert werden, wodurch gleichzeitig die Menge des gebildeten CO verringert wird. In diesem Zusammenhang wurde der Einfluss der Sauerstoffmenge auf die Reaktionsausbeute im Detail studiert. Allgemein begünstigen nur verdünnte und vor allem ungeordnete Sauerstoffschichten die Bildung von CO_2. Durch dichte und geordnete O-Schichten wird die Oberfläche effektiv passiviert. Ein großer Nachteil von Sauerstoff in Verbindung mit der DMFC, bei der Wasserstoff der Energielieferant ist, ist die Bildung von desorbierendem Wasser. Diese Reaktion ist durch die Koadsorption von Sauerstoff bedingt, der mit dem von Methanol abgetrennten H zu Wasser reagiert. Interessanterweise haben Oberflächen, die besonders hohe Mengen CO_2 produzieren gleichzeitig eine hohe Affinität zur Wasserbildung.

Ein Kompromiss sind PtRu/Ru(0001) Oberflächenlegierungen, die trotz begrenzter Wasserbildung CO_2 als Reaktionsprodukt aufweisen. Besonders geeignet als Katalysator für eine DMFC sind Legierungen mit einem Pt-Anteil von $50 - 80\%$.

Acknowledgements

There exist a number of people who contributed directly, or indirectly to this work and whom I would like to thank.

First of all, I thank Prof. Peter Jakob for the excellent supervision of my doctoral research, and for the numerous fruitful and stimulating discussions. I also thank Prof. Wolfram Heimbrodt for providing the second opinion on my thesis.

I am grateful to my sister Marysia for proofreading the manuscript. Moreover, I thank my father and my colleagues Caro R. Braatz and Gregor Öhl for their critical remarks.

Sebastian Thussing supported me in the lab; specifically, he performed some measurements concerning methanol on Pt/Ru(0001), for which I would like to thank him.

I acknowledge technical support by the electronics lab and precision mechanics workshop of the physics department.

Special thanks go to my beloved wife Nina who equipped me with approximately 600 delicious packed lunches within the last three years, to our families for watching our son David, and to my parents for encouraging me to study physics.

Publications: Author's Contributions

This work is a cumulative (article-based) thesis which is based on six scientific articles listed in the following, along with the author's contributions:

Article I: P. Gazdzicki and P. Jakob;
Reactions of Methanol on Ru(0001),
J. Chem. Phys. C **114**, 2655 (2010).

PG performed all experiments, analyzed the data, prepared the figures, and wrote the first version of the manuscript. PG and PJ improved the manuscript and interpreted the results together. PJ supervised the project. *Note that the investigation of the adsorption of methanol on Ru(0001) and the first insight into the reactions was part of the diploma thesis of PG (Marburg 2008).*

Article II: P. Gazdzicki and P. Jakob;
Formation of Methoxy on Cu/Ru(0001) Layers,
J. Phys. Chem. C **115**, 1961 (2011).

PG constructed the Cu evaporator, performed all experiments, analyzed the data, prepared the figures, and wrote the first version of the manuscript. PG and PJ improved the manuscript and interpreted the results together. PJ supervised the project.

Article III: P. Gazdzicki and P. Jakob;
Methanol oxidation on Monolayer Cu/Ru(0001),
J. Phys. Chem. C **115**, 16555 (2011).

PG performed all experiments, analyzed the data, prepared the figures, and wrote the first version of the manuscript. PG and PJ improved the manuscript and interpreted the results together. PJ supervised the project.

Article IV: P. Jakob, A. Schlapka and P. Gazdzicki;
Oxygen adsorption on Pt/Ru(0001) layers,
J. Chem. Phys. **134**, 224707 (2011).

PG performed thermal desorption and IRAS measurements in order to investigate the correlation between the strength of the O-O stretching mode of adsorbed O_2 and the O_2 desorption signal for $0 - 12$ Pt layers. Furthermore, PG analyzed the amount of desorbing O_2 quantitatively. AS performed IRAS measurements identifying different adsorbed O_2 species and demonstrating that the

sticking probability of O_2 strongly depends on n. Additionally, AS analyzed the data. PJ wrote the manuscript and supervised the project.

Article V: P. Gazdzicki, S. Thussing and P. Jakob;
Oxidation of Methanol on Oxygen Covered Pt_n/Ru(0001) Layers,
J. Phys. Chem. C (in revision).[1]

PG performed most of the experiments (in part with ST), analyzed the data, prepared the figures, and wrote the first version of the manuscript. PG and PJ interpreted the results together. PG and PJ improved the manuscript. PJ supervised the project.

Article VI: P. Gazdzicki, S. Thussing and P. Jakob;
Reactions of Methanol on Clean and Oxygen Covered Pt_xRu_{1-x}/Ru(0001) Surface Alloys,
J. Phys. Chem. C (submitted).[2]

PG performed most of the experiments (in part with ST), analyzed the data, prepared the figures, and wrote the first version of the manuscript. PG and PJ interpreted the results together. PG and PJ improved the manuscript. PJ supervised the project.

The publications are referred to as Articles I-VI. Article I deals with methanol reactions on clean Ru(0001) and on Ru(0001) with low oxygen coverages ($\Theta_O \sim$ few percent of a monolayer). In Article II methanol reactions, especially methoxy formation, have been investigated on Cu/Ru(0001) bimetallic layers with submonolyer Cu coverages. The influence of surface oxygen on methanol reactions on 1 ML Cu/Ru(0001) as well as the reactions on thick Cu_{30ML}/Ru(0001) layers are reported in Article III. Moreover, methanol on a second bimetallic system, namely Pt/Ru(0001), has been studied. In advance, Article IV shows the influence of the thickness of the deposited Pt film on Ru(0001) on the adsorption of oxygen. Article V contains results on methanol reactions on molecular and atomic oxygen precovered Pt_n/Ru(0001) layers with thicknesses $n = 3 - 15$ ML. Finally, Article VI presents results obtained on clean and oxygen covered Pt_xRu_{1-x}/Ru(0001) surface alloys.

[1] Final version available at *J. Phys. Chem. C 115, 23013 (2011).*
[2] Final version available at *J. Phys. Chem. C 115, 25379 (2011).*

Contents

Chapter 1

Introduction

This thesis presents the results of a study on fundamental methanol (CH_3OH) reaction steps on functionalized ruthenium-based catalyst surfaces. This topic has a high relevance concerning the direct methanol fuel cell (DMFC), where platinum-ruthenium catalysts are used for the dehydrogenation of methanol. In the DMFC, which is an electrochemical energy conversion device, electrical power is won from the chemical reaction of hydrogen (provided by methanol) and oxygen. The hydrogen industry is a promising alternative to fossil fuels like coal or petroleum. Moreover, due to its small size and different bonds (C-H, O-H, C-O) methanol is a choice model system to study the selective activation of competing chemical pathways.

This work belongs to the interdisciplinary field of research called surface science where the interests of (chemical) physicists and (physical) chemists merge. In particular, the reactions of gases or liquids over a metal surface are known as heterogeneous catalysis. "Heterogeneous" means that the reacting molecules and the catalysts are in different states of matter, namely gas and solid, respectively. Generally, a catalyst is a material which supports a chemical reaction without being changed or consumed by the reaction. This occurs by selective lowering or increasing of activation energies of certain reaction steps of the molecule. Consequently, the corresponding reaction proceeds significantly faster or slower than for the free molecules. Thereby both the bond-breaking and bond-making reactions are of importance. By choosing a proper catalyst and precursor molecules one is able to synthesize new molecules. Such catalytic reactions are widely used in industrial processes; the most prominent of them is the Haber-Bosch process in which hydrogen and nitrogen are converted to ammonia ($\simeq 10^8$ t/year), the precursor of many synthetic fertilizers, over an iron based catalyst [1, 2].

As already mentioned, catalytic reactions proceed over solid state surfaces. Note that under real catalytic conditions (high temperatures and high pressures) the catalysts consist of small (e.g. $10-100$ nm) crystallites with a large specific surface area [2]. In fundamental research, on the other hand, simpler conditions are chosen, allowing for a good control of the experiments, i.e. the measurements are performed under ultra high vacuum ($p < 1 \times 10^{-10}$ mbar) on well defined, atomically flat single crystal surfaces. Nevertheless, in both cases the surface atoms

play the active role in the described processes. Surface atoms have, compared to bulk atoms, unsaturated bonds due to missing neighboring atoms. Thus, they exhibit a high tendency to undergo chemical reactions making them ideal catalysts [3].

Referring to the DMFC, the anode material must be highly reactive toward the conversion of methanol to CO_2 and inert against the so-called CO poisoning which passivates the electrode. In order to design a proper catalyst material it is therefore essential to have detailed knowledge of processes which occur at the molecular or atomic scale. The results of this thesis provide an in-depth analysis of thermally induced methanol reactions on pure Ru(0001) as well as on functionalized bimetallic Cu/Ru(0001) and Pt/Ru(0001) surfaces. Especially, methanol reactions on PtRu/Ru(0001) surface alloys, representing the most realistic catalyst surfaces, were studied.

In a typical experiment methanol is added to the sample (10 mm diameter) at low temperatures ($20 - 80$ K). Then, the reactions are induced thermally by controlled annealing (1 K/s) of the sample. Insight into what is on the surface is meanwhile provided by vibrational spectroscopy. Thermal desorption spectroscopy provides information about what kind of molecules leave the surface at a certain temperature. Thanks to the combination of mainly these two experimental methods a full picture of the processes which occur on the surface can be obtained.

Direct Methanol Fuel Cell

A technological application related to this thesis is the direct methanol fuel cell (DMFC). An important advantage of a DMFC, compared with other fuel cells, is the fuel itself which is liquid at room temperature (high energy density) and thus easy to handle. Furthermore, methanol is cheap and easy to produce. Compared with a H_2 fuel cell which needs either a fuel reformer to extract H_2 from a H-rich compound, or a reservoir with liquid H_2 ($T \approx -253°C$) a DMFC is less complex, smaller, and consequently less expensive. A disadvantage is the power density of a DMFC with typical values around $20 - 60$ mW/cm^2 which is only about 30% of the power density of a H_2 fuel cell [4]. Due to its small size a DMFC is particularly applicable for portable devices with a power in the range $1 - 100$ W. Furthermore, a DMFC is independent of the electrical network and can be recharged continuously by filling it with methanol. In contrast, the working time of batteries is limited by their exhaustion.

The cell basically consists of an anode, a membrane and a cathode. A scheme of a DMFC and the process of electro-oxidation of methanol is depicted in Fig. 1.1. On the anode side of the cell methanol (CH_3OH) and water (H_2O) are being dehydrogenated to CO and O which become removed from the catalyst as CO_2. The membrane, typically made of a polymer material called Nafion, is permeable for positive ions only and can be operated at temperatures up to about 400 K [4–6]. The H^+ ions (protons) pass the membrane directly while the electrons follow them via an external wire as shown in the middle panel of Fig. 1.1 [4, 7, 8]. The reaction at the anode is:

$$CH_3OH + H_2O \rightarrow CO_2 + 6\ H^+ + 6\ e^-. \tag{1.1}$$

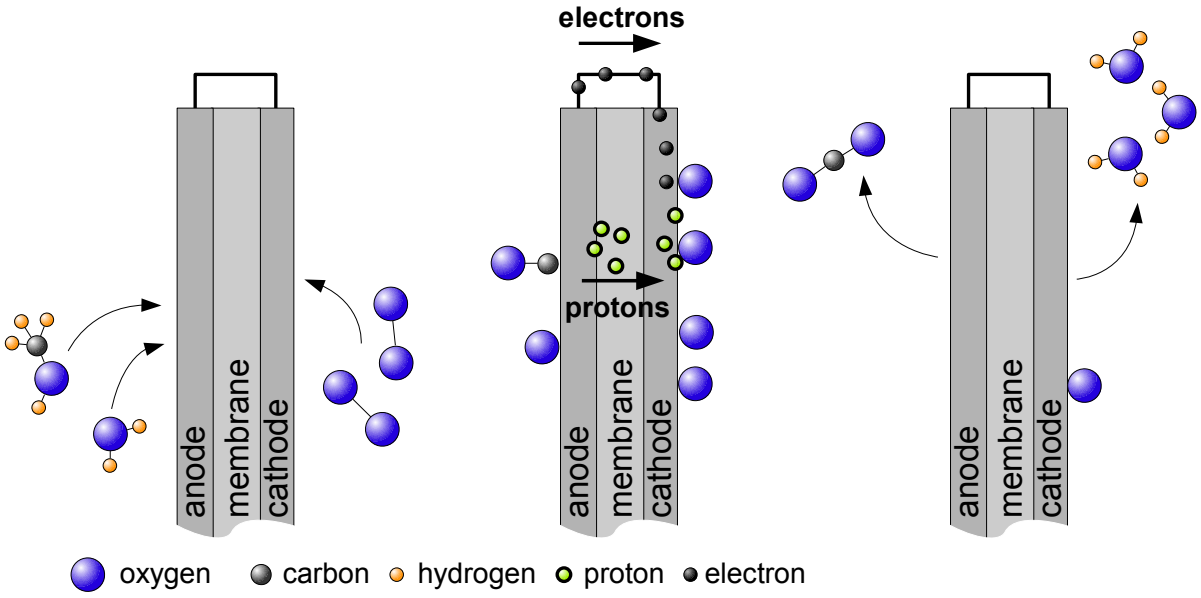

Figure 1.1: Scheme of a direct methanol fuel cell.

On the cathode side of the cell oxygen adsorbs on the catalyst and becomes converted by the incoming H^+ and e^- to water. This process is described by the relation

$$1.5\ O_2 + 6\ H^+ + 6\ e^- \rightarrow 3\ H_2O. \tag{1.2}$$

The net reaction with a theoretical cell voltage of 1.18 V is $CH_3OH + 1.5\ O_2 + H_2O \rightarrow CO_2 + 3\ H_2O$ [4]. Yet, the real cell voltage is significantly lower with typical values around 35% of the theoretical one.

There are two prominent problems which reduce the efficiency (voltage) of a DMFC, namely the CO poisoning of the anode [4, 9] and the crossover of methanol [7, 10]. The porous anode, consistent of crystallites with sizes around 10 nm, becomes poisoned by CO from methanol decomposition when the binding energy between CO and the catalyst is very high, and/or oxidation to CO_2 does not occur [4, 9]. Recent studies on this topic have reported that Pt/Ru alloys are most inert against CO poisoning, compared with pure metals and other binary or ternary catalysts [4, 8, 9, 11–16]. Thereby, the electro-oxidation activity of methanol is highest for a Ru content of $30 - 50\%$ [4, 9, 12, 13, 16]. The cathode material, on the other hand, is typically made of pure Pt or carbon supported Pt [17].

The fuel crossover means that methanol and water can diffuse through the membrane leading to a loss of fuel and consequently reducing the efficiency of the cell [7, 10]. Yet, the efficiency is reduced not only due to the loss of methanol (and water) on the anode side of the cell, but also due to the blocking of adsorption sites on the cathode by these molecules [4]. The diffusion

of the fuel through the membrane can be reduced by the proper design of the membrane or by increasing its thickness (typically $50 - 200$ μm) [4]. The latter approach, however, increases the cell resistance substantially.

Outline

This thesis is organized as follows: Chapter 2 contains an overview of the current status of research. In Chapter 3 the experimental setup is described and basic information concerning vibrational spectroscopy and thermal desorption are given. A brief summary of the most important results is given in Chapter 4. Chapter 5 contains a general discussion of the experimental findings. The main part of this thesis are the research articles provided in Chapter 6.

Chapter 2

Status of Research

In order to study the fundamental reaction steps of methanol on single crystal catalyst surfaces, well defined conditions are needed. Thus, detailed studies of model systems, as in this thesis, are being performed under UHV conditions and on low-index single crystal surfaces. The difference between real catalytic conditions (high pressure, high temperature) and UHV experiments is usually referred to as the "pressure gap". Specifically, the results obtained under UHV conditions cannot be generally translated into real catalytic conditions because the adsorption structures at high temperatures and pressures are not necessarily the same as those under UHV [18]. Moreover, defect, which are negligible in UHV studies, may play an important role under steady state conditions. For some systems, however, the reaction rates calculated for high temperatures and pressures based on results obtained in surface science experiments (UHV) are in excellent agreement with the reaction rates observed in industrial reactors [19]. An example is the synthesis of ammonia over an iron catalyst [19].

Under UHV conditions the adsorption and thermal evolution of methanol has been studied experimentally as well as theoretically on various single crystal catalyst surfaces, for instance Ru [20–26], Cu [27–37], Pt [38–50], Rh [51–53], Pd [54–56], Ag [57, 58], and Mo [59, 60]. In detailed theoretical works the adsorption geometries of possible surface intermediates, their binding energies and activation barriers of individual reaction steps have been calculated [29, 36, 37, 48, 49].

The first publications [28, 33, 40] on this topic appeared around 1980. Yet, up to now, new results are published regularly. In some cases it took decades until a commonly accepted picture of methanol reaction steps emerged. As regards methanol reactions on clean Pt(111) it was first believed that methanol, adsorbed at $T \approx 100$ K, decomposes upon annealing into CO and H [38, 40]. Later, the perfect Pt(111) surface turned out to be inert for methanol decomposition which occurs at defects only [39].

In the case of Ru(0001) it was believed for about 20 years that methanol adsorbs dissociatively at 80 K [20, 22, 24]. However, unambiguous evidence of intact adsorption has been published recently by us [26]. Furthermore, it was erroneously concluded that water formation observed

in thermal desorption experiments is due to a C-O bond breaking reaction of methanol [20, 24]. This problem is discussed in Article I.

With respect to this thesis the most important catalyst surfaces are Ru(0001), Cu(111) and Pt(111), which will be introduced in the following in more detail referring to methanol reactions. Subsequently, important findings concerning bimetallic surfaces will be presented.

2.1 Methanol on Pt(111)

As mentioned above, the clean Pt(111) surface is inert for methanol reactions, i.e. methanol desorbs molecularly at about 180 K [39, 40]. As regards DFT calculations [48–50] methanol is bound to an atop site through its oxygen atom. Moreover, theoreticians found that C-H bond breaking has the lowest activation barrier leading to a hydroxymethyl species (H_2COH) as the first reaction intermediate [48, 49]. This activation barrier, however, is significantly higher than the desorption barrier which is in good agreement with experimental findings of reversible adsorption.

On Pt(111) methanol can be activated by preadsorbed atomic oxygen which leads to methanol decomposition to CO and H [44, 47]. The surface oxygen is easily removed by the abstracted H atoms as desorbing water. Whether a stable surface intermediate is produced or not depends on the ratio of initially adsorbed methanol molecules to oxygen atoms. For submonolayer methanol on 0.25 ML oxygen, a formaldehyde intermediate (H_2CO) has been identified in the temperature range $200 - 220$ K [47]. A further minor reaction step is the oxidation of formaldehyde to produce formate (HCOO) which eventually decays and desorbs as CO_2. The formation of a stable methoxy (CH_3O) intermediate, as precursor of formaldehyde, has also been proposed by some authors [40, 41]. However, according to available vibrational spectroscopy data [40, 44, 47] the observed species most likely represents intact methanol rather than methoxy. Moreover, the loss of intensity of the corresponding vibrational bands correlates well with the desorption of intact methanol. This topic is discussed in Article V.

The reaction pathways look completely different when molecular oxygen is added to the Pt(111) surface prior to methanol adsorption [44, 46]. First, it is notable that oxygen adsorbs molecularly on Pt(111) at $T < 120$ K [61, 62]. By heating the O_2/Pt(111) layer a part of the O_2 molecules desorbs intact at 130 K, while residual oxygen dissociates to atomic oxygen which desorbs associatively around 800 K. Remarkably, the only reaction intermediate produced in the course of methanol reactions on preadsorbed O_2 is formate which desorbs as CO_2 and H_2 at $T \approx 300$ K [44, 46]. Thereby, minor oxidation of methanol starts at $T \approx 80$ K which is well below the dissociation temperature of the molecular oxygen. At $T > 130$ K the HCOO producing reaction is significantly more effective suggesting that it is promoted by disordered atomic oxygen rather than by molecular O_2.

2.2 Methanol on Cu(111)

Similar to the clean Pt(111) surface [39], methanol adsorbs molecularly on Cu(111) [27, 31] without any dissociation and desorbs intact at $T \approx 150$ K. According to DFT studies by Greeley and Mavrikakis [29] it is bound through the oxygen atom to an atop site with its O-H axis oriented nearly parallel to the surface. Due to its low binding energy and the relatively high activation barriers, intact desorption is the favored reaction step. As the O-H bond cleavage exhibits the lowest reaction barrier methoxy is calculated to be the first reaction species which, additionally, has the highest binding energy (besides atomic hydrogen). The adsorption geometry of CH_3O is suggested to be upright on a 3-fold hollow site (C_{3v} symmetry). The next stable intermediate on the way to the total dehydrogenation is a weakly bound formaldehyde (H_2CO) species.

In UHV experiments methanol is converted to methoxy in the vicinity of preadsorbed surface oxygen only [27, 31]. Thereby, surface oxygen facilitates the abstraction of the H atom from methanol's O-H group for low oxygen coverages [27]. For high oxygen coverages, on the other hand, O-H bond breaking is inhibited, turning the surface nonreactive. Such a maximum in the reaction yield for dilute oxygen overlayers has also been reported for methanol on O/Cu(110) [36, 63, 64] and O/Cu(100) [32, 33]. On O/Cu(111) methoxy, formed at about 200 K, loses a hydrogen via C-H bond breaking and desorbs as formaldehyde at 420 K which is again in agreement with theoretical predictions [27, 31]. As on O/Pt(111) [44, 47], surface oxygen atoms react with H atoms to gas phase water. Cu surfaces, and particularly the oxygen covered Cu(100) surface, exhibit a high efficiency for methoxy formation [28, 32, 34, 65, 66]. An ordered (2×2)-methoxy structure with a coverage of 0.5 ML can be produced from an initial oxygen coverage of 0.25 ML. For comparison, the maximum value attained on Ru(0001) amounts to 0.1 ML [Article I].

Furthermore, Russel et al. [27] found CO_2 desorption as the final product of a minor reaction path and concluded that it is produced due to the decomposition of a formate species. Article III focuses, among others, on this specific topic.

2.3 Methanol on Ru(0001)

The reactions of methanol on Ru(0001) are subject of Article I. Nevertheless, the results of Article I and other literature will be introduced in this section in order to complete the picture of methanol reactions on monometallic surfaces.

On clean Ru(0001) methanol adsorbs intact at liquid nitrogen temperatures with its O-H group close to parallel to the surface [26]. At low coverages (≈ 0.1 ML) isolated methanol molecules are observed which build hydrogen bonded clusters upon slight annealing ($T \rightarrow 120$ K) or increasing the coverage. Evidence for intact methanol is provided by a combined theoretical and experimental study which identified out-of-phase $[\delta(\mathrm{OH})+\rho_{inplane}(\mathrm{CH_3})]oop$ and in-phase $[\delta(\mathrm{OH})+\rho_{inplane}(\mathrm{CH_3})]ip$ normal modes of methanol, both containing contributions of the CH_3 and the OH group. The activation of the O-H bond breaking leads to surface methoxy and

hydrogen [Article I] [20, 22]. Thereby, methoxy binds to 3-fold hollow sites [67] with the C-O axis oriented perpendicular to the surface. The amount of produced methoxy reaches maximum around 200−220 K. The final reaction products, CO and H, desorb at 340 and 450 K, respectively. Moreover, thermal desorption spectra of methanol on Ru(0001) exhibit desorption of water around 190 K which was first attributed to a C-O bond breaking reaction [20, 22]. However, in Article I it is unambiguously shown by using isotopic labeling that the desorbing water is due to the reaction of hydrogen from methanol's O-H group and residual surface oxygen.

On the perfect (2×2)-O and (2×1)-O layers on Ru(0001) methanol adsorbs reversibly [Article I]. Note that there are no theoretical works concerning methanol reaction pathways on Ru(0001) so far.

2.4 Bimetallic Surfaces

This section gives a short introduction to strained bimetallic layers and surface alloys.

The effect of strain (compression or expansion) on adsorptive properties of a surface has been provided for the first time by Gsell, Jakob, and Menzel [68, 69] showing that surface reactivity increases with lattice expansion. The authors prepared subsurface argon bubbles in a Ru(0001) sample which lead to protrusions with laterally expanded top areas and compressed edge regions to study the binding strengths of oxygen and CO. Mavrikakis, Hammer and Nørskov [70] explained this effect by means of a strain induced shift of the metal d-bands with respect to the Fermi level. The overlap of the d-bands with molecular orbitals is a measure for the adsorbate-substrate interaction [70–73]. Upon lattice expansion the overlap between the (for transition metals) partially filled d-bands of neighboring atoms becomes reduced which leads to a narrowing of these bands. Consequently, the center of the d-band must shift upwards in energy in order to keep the occupancy of the band constant. Such up-shifts lead to stronger interactions between adsorbates (such as O and CO) and metal surfaces [70, 74].

A straightforward method to prepare strained bimetallic films is to deposit an overlayer of a metal on a host surface made of another metal. Metallic films of a thickness of 1 ML exhibit a pseudomorphic structure for a number of material combinations, such as Cu/Ru(0001) [75–77], Pt/Ru(0001) [74, 78–80], Rh/Ru(0001) [81], Ag/Pd(111) [82], or Ni/Ru(0001) [83]. The d-band position of monolayer metal films on various substrates have been calculated by Ruban et al. [71]. Similarly, Kitchin et al. [84] investigated the influence of monolayer thick metal films on the d-band structure by means of DFT calculations and found that both effects, strain and electronic influence of the substrate, affect surface reactivity.

For the bimetallic material Cu/Ru(0001) only the first monolayer grows pseudomorphically, i.e. Cu matches the lattice constant of Ru(0001) with a mismatch of 5.5% (expansion) relative to Cu(111) [75–77]. Starting from the second layer the surface strain begins to relax losing the pseudomorphic structure. Thick Cu layers with coverages of $30 - 40$ ML behave virtually like the Cu(111) surface [85]. However, for the more interesting thin bimetallic films, which

exhibit surprising properties, the electronic influence of the substrate material represents the dominant contribution to the surface reactivity [74, 86]. This effect has been illustrated in a theoretical work by Laurent et al. [86] using the example of H_2 adsorption on pseudomorphic Cu/Ru(0001) and Pd/Ru(0001), as well as on artificially expanded Cu(111) and compressed Pd(111). The adsorption of H_2 on regular Cu(111) and 5.5% expanded Cu(111) is in both cases an activated process (i.e. adsorption barriers are higher than 25 meV, average kinetic energy of a thermal particle beam at 300 K), with a barrier of $\approx$ 360 meV. The high adsorption barrier is in agreement with experiments which found a negligible sticking probability of $s_0 \approx 10^{-5}$ [87]. As expected by the Hammer-Nørskov model [70–73], the calculated H_2-adsorption barrier for the expanded Cu(111) is slightly lowered (to $\approx$ 290 meV) as compared to regular Cu(111) [86, 88]. In contrast, on 1 ML Cu/Ru(0001) the threshold is reduced significantly to 160 meV (still an activated process). Similarly, the difference between the (non-activated) H_2 adsorption on Pd(111) and 2% compressed Pd(111) is marginal. As expected, the barrier of the latter increases slightly and equals to $\approx$ 20 meV [86]. The barrier on 1 ML Pd/Ru(0001), however, is high and amounts to 130 meV (activated process). Remarkably, both layers, namely Cu(111) and Pd(111), behave completely different referring to H_2 adsorption. Yet, 1 ML Cu/Ru(0001) and 1 ML Pd/Ru(0001) both exhibit a similar activation barrier of $\approx$ 150 meV. Consequently, the influences due to the nearby Ru(0001) surface are significant. Note that for clean Ru(0001) the sticking probability of H_2 equals 0.25 [89].

A further example which underlines the importance of the substrate is the adsorption of O_2 on Cu(111), Ru(0001) and 1 ML Cu/Ru(0001). While on clean Ru(0001) [90] and on 1 ML Cu/Ru(0001) [91] the sticking probabilities are similar with values of 0.75 and 0.6, respectively, the corresponding probability on Cu(111) is negligible (10^{-3}) [92] .

A bimetallic material which allows the separation of the electronic influences of the host metal and the influence due to strain is Pt/Ru(0001) [74]. Pseudomorphic Pt/Ru(0001) films can be grown up to thicknesses of four monolayers; the short range electronic influences of the substrate vanish for the third Pt layer [74]. The results of a study on the adsorption of O_2 on such Pt/Ru(000) layers are reported in Article IV. Furthermore, studies on methanol reactions on thin pseudomorphic Cu/Ru(0001) films and Pt/Ru(0001) layers are presented in Articles II, III and V.

Referring to the DMFC the study of methanol on surface alloys is interesting as such catalyst are more realistic than pure single crystal surfaces. The properties of such bimetallic systems have been studied extensively showing that the behavior of foreign atoms embedded into a surface of a host material (surface alloy) behave substantially different than bulk alloys or elemental surfaces [3, 93]. The effects of alloying can be explained by means of the number of specific surface sites needed to activate a certain reaction (geometric or ensemble effect) [93, 94], the electronic interaction between different types of atoms (electronic or ligand effect) [93, 94], and the difference in atom sizes (strain induced effect) [70]. Various surface alloys, such as PtRu/Ru(0001) [95–98], PdRu/Ru(0001) [98, 99], and AuPt/Pt(0001) [100] have been characterized experimentally. The system Pt/Ru(0001) builds a Pt_xRu_{1-x}/Ru(0001) surface

alloy upon annealing a submonolayer Pt deposited on the clean Ru(0001) surface to 1300 K [78, 95]. The onset of alloy formation is around 850 K. Specifically, a surface alloy means that the barrier for incorporation of foreign atoms into the first atomic layer is significantly lower than the barrier for the diffusion from the surface into the bulk; for a Pt content up to 80% no diffusion of Pt atoms into Ru bulk occurs as verified by STM [95, 98]. Moreover, the group of Behm found that the binding energy of CO as well as H is lowered on the Pt_xRu_{1-x}/Ru(0001) surface alloys as compared to clean Ru(0001) which is an important finding concerning the DMFC [96, 97].

Chapter 3

Experimental

In this chapter the experimental setup is introduced, along with the main experimental methods, infrared absorption spectroscopy and thermal desorption. At the end some basic information concerning methanol are given.

3.1 Experimental Setup

All experiments presented in this thesis were performed with the "FTIRAS"-apparatus at the physics department (Surface Spectroscopy Group of Prof. Peter Jakob) of the Philipps-Universität Marburg. In this section only a brief description of the facility is given. More details can be found in the doctoral thesis of Axel Schiffer [101].

The whole setup, shown in Fig. 3.1, consists of a cylindric stainless steel ultra high vacuum (UHV) chamber equipped with the following components:

Sample: The Ru(0001) single crystal has a 5N (99,999%) purity. Its dimensions are 10 mm diameter and a thickness of 2 mm. It is mounted on a Ag-cryostat and can be cooled with liquid He or N_2. Annealing temperatures up to 1570 K, limited by the melting point of the type K thermocouple spot welded to the side of the sample, are possible with linear heating rates of $0.1 - 10$ K/s controlled by means of a computer operated power supply. The sample was cleaned by Ar^+ sputtering (1.4 keV, 1 μA) and multiple O_2 dosing cycles combined with flashing the sample up to 1570 K.

FTIRAS: The Fourier-transform infrared spectrometer is a Bruker IFS 66/v (for details see Section 3.2.7).

QMS: For gas analysis and thermal desorption experiments a Balzers QMG 112A quadrupole mass spectrometer with a mass range $0 - 100$ u was used. Details on thermal desorption experiments are given in Section 3.3.2.

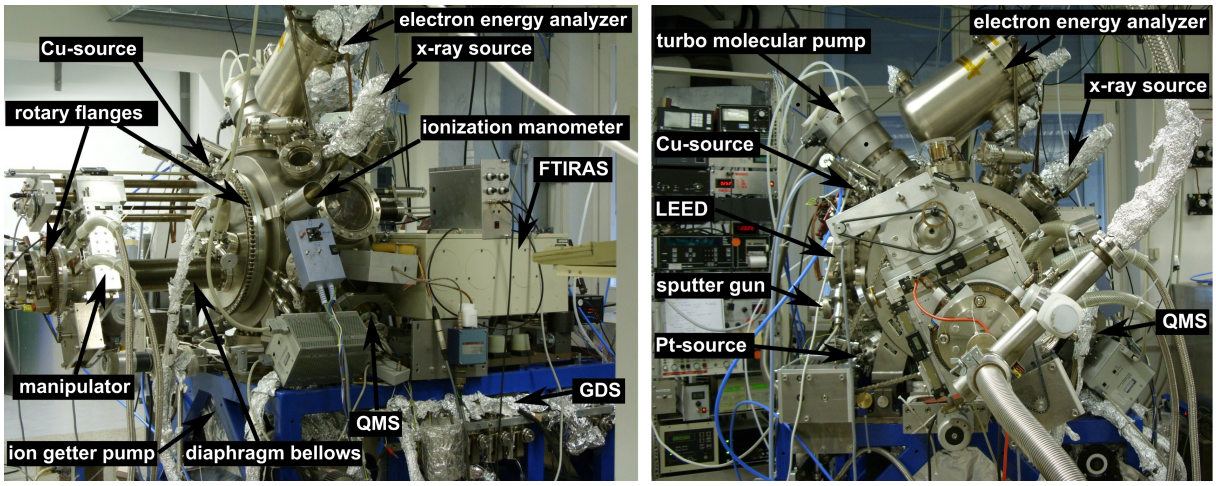

Figure 3.1: Side and front view of the FTIRAS experimental setup.

LEED: The surface structure was analyzed by low energy electron diffraction with a Omicron Spectraleen NGL 10.

XPS: (X-ray source and electron energy analyzer) The chemical composition of the sample was investigated by means of XPS (X-ray photoelectron spectroscopy) with a Fisons Instruments VG Microtech CLAM2 electron energy analyzer in combination with a Fisons instruments Mg Kα or Al Kα X-Ray source.

$\Delta\Phi$-Work function: For the measuring of work function changes of the sample a home made Kelvin probe [102] is available.

Metal sources: The deposition of metals (Cu and Pt) occurred by means of commercial and home made thermal (e^--beam) evaporators.

GDS: The gas dosing system contains Ar, O_2, $^{18}O_2$, CO, ^{13}CO, NO, H_2, D_2, methanol, and C_2H_4 connected to the gas line via leak valves. A constant pressure in the gas line, measured by a MKS Instruments Baratron Type 270, is obtained by continuously dosing a gas through a leak valve and slightly pumping the gas line by a turbo pump. Gas dosage occurs with a multi-capillary array with individual diameters of $\sim$ 10 µm. In order to avoid contaminations by condensable gases the GDS contains a LN_2 cooling trap.

The experiments were performed at a base pressure $p = 6 \times 10^{-11}$ mbar (measured with an ionization gauge) which is achieved by pumping the chamber with a Varian StarCell VacIon ion getter pump (230 ls^{-1}) equipped with an integrated titanium sublimation pump and by a Leybold Turbovac 361 (345 ls^{-1}) turbo molecular pump serially connected to a Varian Turbo V60 (65 ls^{-1}) turbo molecular pump. A second Varian Turbo V60 is used for pumping the

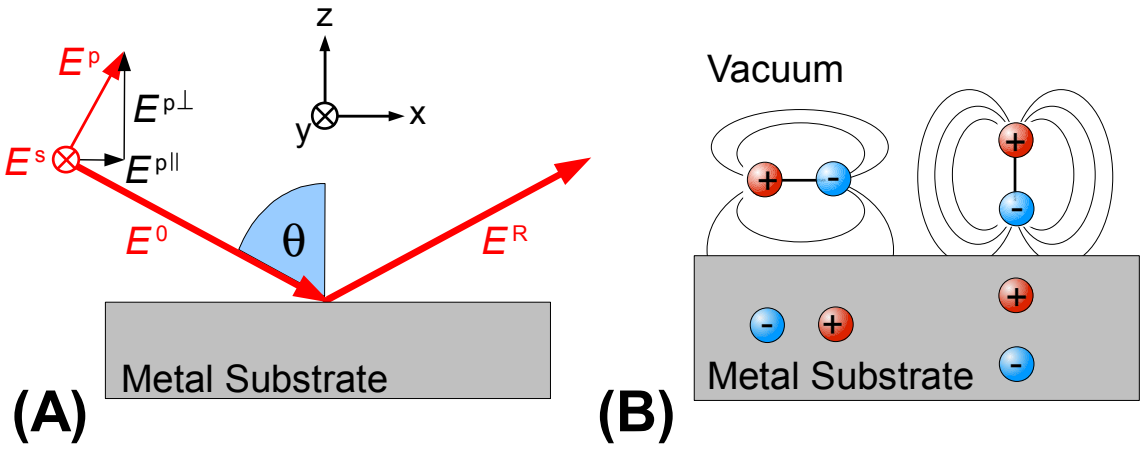

Figure 3.2: Illustration of the electric field vector components impinging a metal surface (A) and demonstration of the surface selection rule (B).

GDS. The fore-pressure ($\approx 10^{-2}$ mbar) is generated by Edwards 2-level rotary vane pumps. For sample positioning the manipulator can be rotated with two differentially two-level pumped rotary flanges (in axis and off-axis of the manipulator). Furthermore, linear adjustments along the x, y and z directions are possible.

3.2 Infrared Spectroscopy

Infrared absorption spectroscopy (IRAS) is a powerful method to investigate molecules and chemical reactions based on the excitation of molecular vibrations. Extended introductions to infrared spectroscopy of adsorbates with many examples have been published by Bradshaw and Schweizer [103], Chabal [104], and Hayden [105]. In the following an overview of infrared spectroscopy on metal surfaces, based on available literature, is given.

3.2.1 Light at Metal Surfaces

The behavior of light upon impact on a solid surface (in vacuum, $\epsilon^{vac} = 1$) is characterized by the complex dielectric function $\epsilon = \epsilon' + i\epsilon''$ of the solid which is associated with the index of refraction n by the relation $n = \sqrt{\epsilon\mu}$ with the permeability $\mu \approx 1$ for non-ferromagnetic materials [104]. In what follows the incident electric field E^0 is separated into a p-polarized component, E^p (in the plane of incidence), and a s-polarized component, E^s (parallel to the plane of incidence), as shown in Fig. 3.2A. Furthermore, E^p is again separated into $E^{p\perp}$ and $E^{p\parallel}$, its perpendicular and the parallel component with respect to the surface, respectively. The components of the reflected electric field E^R at the surface under the angle θ are described by

Fresnel's equations [104]:

$$E^s = \left(1 + \frac{\cos\theta - \sqrt{\epsilon - \sin^2\theta}}{\cos\theta + \sqrt{\epsilon - \sin^2\theta}}\right) E^0, \tag{3.1}$$

$$E^{p\parallel} = \left(1 - \frac{\epsilon\cos\theta - \sqrt{\epsilon - \sin^2\theta}}{\epsilon\cos\theta + \sqrt{\epsilon - \sin^2\theta}}\right) E^0\cos\theta, \tag{3.2}$$

$$E^{p\perp} = \left(1 + \frac{\epsilon\cos\theta - \sqrt{\epsilon - \sin^2\theta}}{\epsilon\cos\theta + \sqrt{\epsilon - \sin^2\theta}}\right) E^0\sin\theta. \tag{3.3}$$

For highly reflective non-transparent material (metals), such as ruthenium, $|\epsilon| = |\epsilon^m| >> 1$ and in particular its imaginary part $\epsilon^{m\prime\prime}$ is large, i.e. of the order of several hundreds [104]. Thus, assuming that $|\epsilon^m| \to \infty$ both, $E^{p\parallel}$ and E^s are negligible with values $\sim E^0/\sqrt{|\epsilon^m|}$. In other words $E^{p\parallel}$ and E^s become effectively screened by the metal surface. In contrast, the relative intensity $E^{p\perp}/E^0$ is high for grazing angles of incidence due to the constructive interference of the reflected and the incident light [103–105]. Hence, only $E^{p\perp}$ needs to be considered in the following.

3.2.2 Selection Rule

The interaction of infrared light (typically $500-4000\ \mathrm{cm}^{-1}$, 1 meV$\hat{=}$8.1 cm^{-1}), or more precisely of its electric field vector E, with an electric dipole m of a molecule induces a vibrational transition of a normal mode only if the dynamic dipole, $\mu = \partial m/\partial x_i$, associated with the displacement of a normal coordinate, x_i, is non-zero. The probability of a transition $T_{\mathrm{i}\to\mathrm{f}}$ with the resonant frequency ω_0 from an initial state $|\mathrm{i}\rangle$ to a final state $|\mathrm{f}\rangle$ is given by Fermi's Golden Rule [106]

$$T_{\mathrm{i}\to\mathrm{f}} \propto |\langle \mathrm{f}|\mu|\mathrm{i}\rangle|^2 \delta(\omega_0 - \omega). \tag{3.4}$$

The screening of s-polarized light and the amplification of p-polarized light described above is the key point of the **surface selection rule** for metal surfaces which says that only dipoles with a non-zero component perpendicular to the surface can be excited. These perpendicular dipoles are amplified by their image dipoles by about $\times 2$ for grazing angles of incidence. In contrast, parallel dipoles become screened by their image dipoles as illustrated in Fig. 3.2B. Referring to Eq. 3.4 only the components μ_z and $E_z = E^{p\perp}$ of the dynamic dipole and the electric field are relevant on metal surfaces. Thus, a vibrational transition of an adsorbate is only allowed if $\int \Psi_f^* \mu_z \Psi_i d^3r$ is non zero. Hence, the integrand $\Psi_f^* \mu_z \Psi_i$ must be totally symmetric. The initial state Ψ_i is determined by the symmetry of the molecule. Consequently, the final state Ψ_f must have the same symmetry as μ_z. In practice, symmetry arguments are sufficient to verify if a transition is allowed or not. Therefore, the integral in Eq. 3.4 does not need to be calculated explicitly.

3.2.3 Symmetry Considerations

A mathematical tool which helps to analyze infrared spectra of polyatomic molecules, based on symmetry considerations, is group theory [107, 108]. For adsorbates the only possible point groups (mathematical groups of symmetry elements that leave at least one point in space unchanged) are C_n with one n-fold rotation axis C_n (n = 1,2,3,4,6), C_{nv} with one n-fold rotation axis C_n and n mirror planes σ_v through the axis (n = 2,3,4,6), and C_s =C_{1v} with one mirror plane σ [103]. Referring to the surface selection rule, all allowed vibrations are totally symmetric with respect to all symmetry operations of a given point group (Fig. 3.3), i.e. they transform similar as the surface normal (z axis) [107]. Such vibrations belong to so called A_1 and A' irreducible representations of the surface normal. Noteworthy, combination vibrations of forbidden modes may again belong to the totally symmetric representation and become dipole allowed. A demonstrative example is formate (HCOO, C_{2v} symmetry) bound through both oxygen atoms to Cu(110) where the combination of the two infrared forbidden modes antisymmetric O-C-O stretch, ν_{as}(OCO), and C-H bend, δ(CH), is allowed and has been observed experimentally with IRAS [109, 110].

From IRAS spectra the adsorption symmetry of a molecule can be determined by comparing the experimentally observed peaks with a theoretical set of peaks expected for a certain adsorption geometry. In the case of surface methoxy (CH_3O), a prominent intermediate in methanol decomposition, the adsorption symmetry has been found to be C_{3v} (CO axis parallel to the surface normal) on various metal surfaces like Ru(0001) [20] [Article I], Cu(111) [31, 111], Cu(100) [34, 66, 112, 113], Mo(110) [59, 60], or Ag(111) [57] (see Fig. 3.3). This is concluded from the observation of only one bending mode, the CH_3 umbrella mode, $\delta_s(CH_3)$. For a tilted methoxy other modes as the asymmetric CH_3 bend, $\delta_{as}(CH_3)$, or the CH_3 rocking mode, $\rho(CH_3)$, would be visible in the spectral range $1000 - 1400$ cm^{-1}.

3.2.4 Fermi Resonance

For polyatomic molecules the expected number of peaks can, on the first sight, deviate from the experimental data. This effect is explained by the Fermi resonance [57, 60, 107, 112], a phenomenon of polyatomic molecules, which occurs when two vibrations belonging to the same symmetry, e.g. a fundamental mode and a weak overtone vibration, have similar vibrational frequencies. The coupling of these modes leads to mixing of the energy levels characterized by the perturbation $W_{1,2}$. For two interacting modes the shifted positions (E_1 and E_2) of the initial modes at E_1^0 and E_2^0 can be described by the relation

$$E_{1,2} = \frac{E_1^0 + E_2^0}{2} \pm \sqrt{4|W_{1,2}|^2 + (E_1^0 - E_2^0)^2}. \tag{3.5}$$

Thereby, the weak overtone borrows intensity from the strong fundamental mode and becomes visible with IRAS.

In the case of methoxy and especially of the CD_3O isotope the Fermi resonance is more complicated. The corresponding IRAS spectra on metal surfaces exhibit four modes in the region of the $\nu(CD_3)$ stretch ($2000 - 2200$ cm^{-1}). Note that only one normal mode ($\nu_s(CD_3)$) is expected in this spectral region. The three other modes are the overtones $2\delta_{as}(CD_3)$ and $2\delta_s(CD_3)$ and the combination band $\nu(CO)+\delta_s(CD_3)$ in Fermi resonance with the $\delta_s(CD_3)$ fundamental mode. The weak overtones and the combination band borrow intensity from the allowed $\nu_s(CD_3)$ vibration and become detectable with IRAS. A detailed analysis of the Fermi resonance of CD_3O is given in the supporting information of Article VI.

The relative intensities of vibrational modes of a specific molecule can vary substantially with isotopic substitution [Article I] [31, 66, 114]. Methoxy exhibits an intensive umbrella mode $\delta(CD_3)$ at 1095 cm^{-1} for the CD_3O isotope but not for CH_3O (at ≈ 1400 cm^{-1}) [31, 66]. The reason for such dissimilar oscillator strengths for two methoxy isotopes is again mode coupling (intensity borrowing) with the nearby C-O stretching mode (≈ 1000 cm^{-1}) which enhances the intensity of $\delta_s(CD_3)$ at 1095 cm^{-1}.

3.2.5 Vibrational Transitions

Under typical experimental conditions the vibrational energies lie between 500 and 4000 cm^{-1} ($60 - 500$ meV) which is significantly higher than the thermal energy which equals to about 25 meV at 300 K. The occupation n_ν of a vibrational state ν with the energy E_ν at a temperature T is given by the Boltzmann-distribution $n_\nu \propto \exp(-E_\nu/kT)$. In the case of CO the probability for the occupation of the first vibrationally excited state $\nu = 1$ at 300 K is about $n_{\nu=1}/n_{\nu=0} \approx 10^{-5}$ [115]. Therefore, it can be assumed that only the vibrational ground state $|0\rangle$ is populated, and, by approximation, only transitions $|0\rangle \rightarrow |1\rangle$ are being excited, i.e. the observed transitions are located at the minimum of the molecule potential. Hence, in the case of infrared spectroscopy a harmonic approximation of this potential is sufficient and no direct information about dissociation energies or potential shapes can be obtained from a single vibrational band. Even though the probability for observing higher harmonics is very low, in high quality experiments and for certain molecules it is possible to observe the weak overtone vibrations [66].

3.2.6 Effect of Adsorption on Vibrational Properties

In the gas phase vibrational transitions are always accompanied by molecular rotations and translations. Yet, in the case of adsorbed molecules only vibrational modes exist. In the following, the formaldehyde molecule (H_2CO) will act as an example. For a molecule with n atoms $3n - 6$ internal vibrational modes can be observed ($3n - 5$ for a linear molecule like CO). Thus, H_2CO exhibits six internal vibrations shown in the top row of Fig. 3.3 (first six modes). For adsorbates, however, translations and rotations turn into new vibrational modes, so-called frustrated translations or rotations. Concerning H_2CO, a frustrated translation is, e.g., the vibration

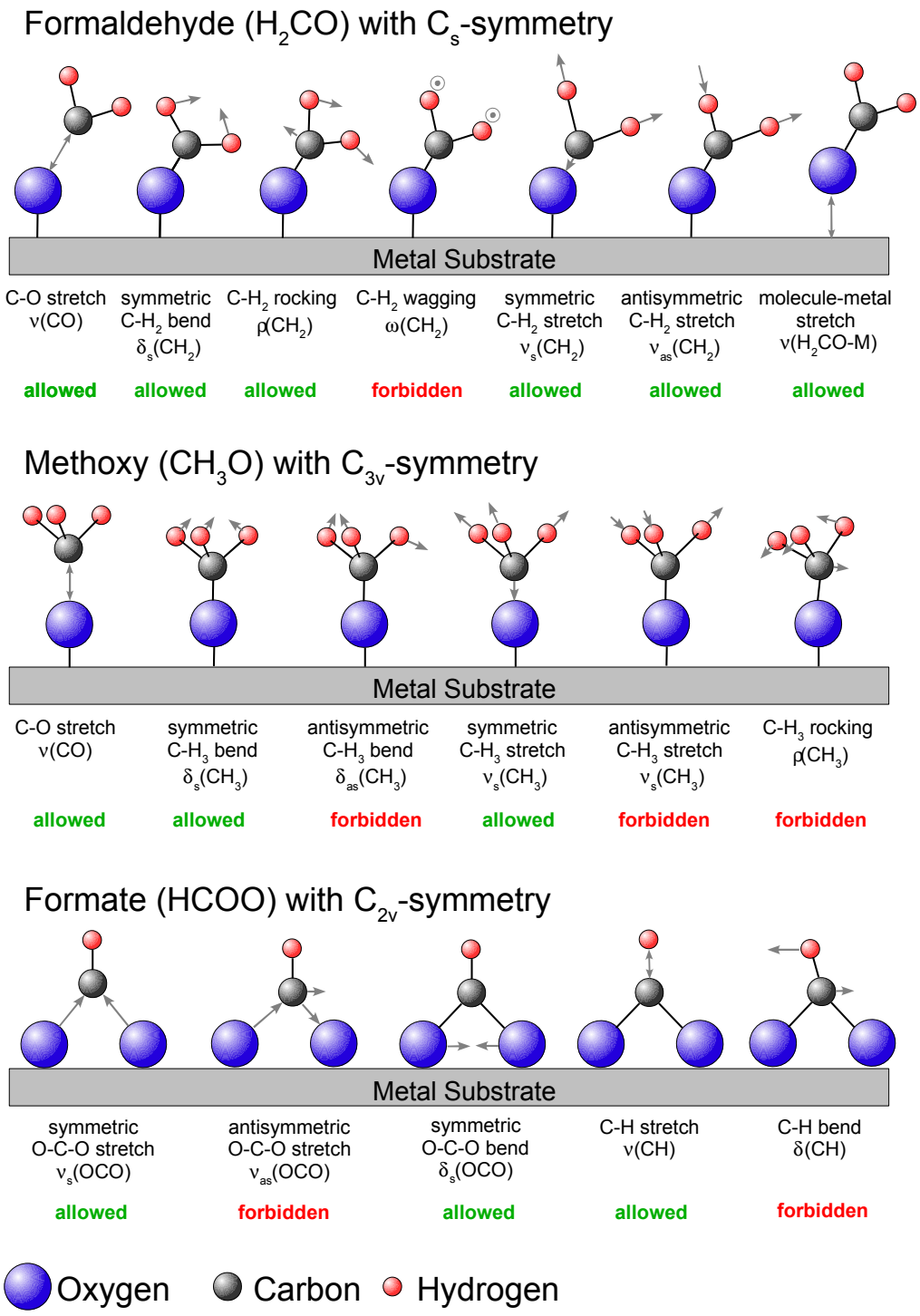

Figure 3.3: Normal modes of the H_2CO, CH_3O, and the HCOO molecule. The molecule symmetries, common mode abbreviations, displacement patterns, and information if a mode is IR-forbidden or allowed are given in the figure.

of the whole molecule against the surface ($\nu(H_2CO\text{-}M)$) as demonstrated in Fig. 3.3 (top row, right cartoon).

The vibrational bands of chemically bound adsorbates are spectrally broadened and shifted as compared to the gas phase. The broadening is in part due to significantly shorter life times of vibrational states of adsorbed molecules than of gas phase molecules. In the gas phase molecular vibrations decay via emission of light or via collisions with other molecules [104]. The fast dissipation of vibrational energy of adsorbates, on the other hand, occurs primarily via coupling of molecular states to electronic states of the substrate [103, 104]. Furthermore, inhomogeneous broadening due to different local environments and dephasing play an important role. Dephasing, a temperature-dependent effect, is the loss of the phase correlation of high frequency modes due to coupling to a thermally excited low frequency mode with a statistically fluctuating occupation [116, 117]. In the case of CO on Pt(111) [118] and Ru(0001) [116, 117, 119, 120], the C-O stretch couples to the frustrated translation of the molecule. This effect leads to slight shifts of line positions and an increase of line widths. Typical energetic widths of vibrational-rotational bands of a molecular gas and of an adsorbate are around 0.001 (Doppler broadening) and 10 cm^{-1}, respectively.

Furthermore, line positions of adsorbates are shifted as compared to the gas phase due to a chemical bond between the molecule and the metal surface. For gaseous CO the fundamental stretch is located at 2143 cm^{-1}. Upon adsorption it shifts down in frequency to 2060 cm^{-1} for a saturated CO layer on Ru(0001) [121]. Moreover, on Pt(111) two adsorption sites, a bridge bonded and an atop site, can be discriminated with IRAS at 2104 and 1855 cm^{-1}, respectively [118].

The shifts of the line positions are coverage (Θ) dependent effects caused by a static (chemical) coupling between molecular orbitals and substrate states (chemical shift Δ_{chem}), as well as by lateral dynamic interactions of a molecule with neighboring molecules and their image dipoles (dipole shift Δ_{dip}) characterized by the lattice sum $U = \sum_{i \neq j} |x_i - x_j|^{-3}$ of interacting dipoles at positions x [105, 122, 123]. The shift of the singleton frequency $\nu_0 = \nu(\Theta = 0)$ of an isolated species to a frequency $\nu = \nu_0 + \Delta_{dip}$ is given by

$$\frac{\nu^2 - \nu_0^2}{\nu_0^2} = \frac{\alpha_v \cdot U}{1 + \alpha_e \cdot U}, \tag{3.6}$$

with the vibrational and electronic part of the polarizability α_v and α_e, respectively. A descriptive experimental demonstration and analysis of coadsorbate effects on vibrational properties has been published by P. Jakob and A. Schiffer [122].

3.2.7 Setup and Data Processing

A scheme of the Fourier transform infrared spectrometer (FTIRAS) is presented in Fig. 3.4. Its optics can be evacuated ($p < 1$ mbar) to avoid absorption by disturbing ambient gases such as CO_2 and H_2O. The IR radiation is produced by a water cooled blackbody source (Globar)

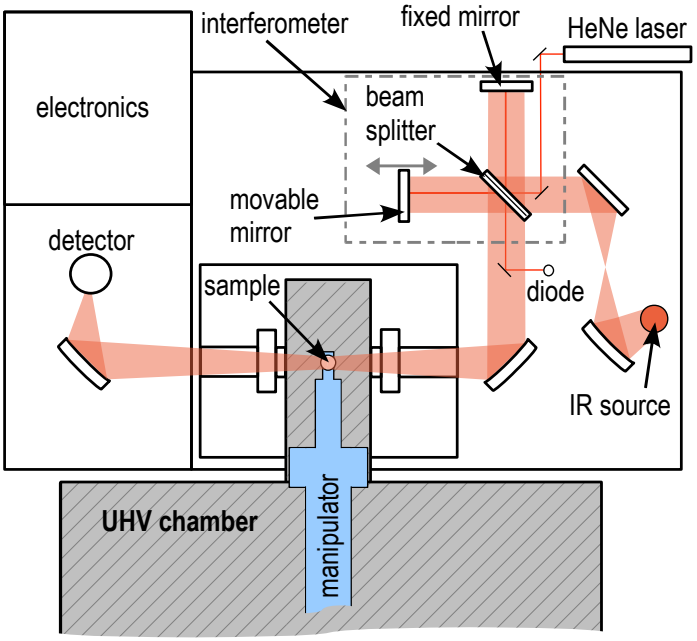

Figure 3.4: Scheme of the IRAS spectrometer. The IR beam is marked orange and the Michelson interferometer is labeled by a gray dashed box.

and it is *p*-polarized by a wire grid (see surface selection rule in Section 3.2). Within this work a LN_2 cooled MCT (HgCdTe) detector was used, allowing for measurements in the spectral range $700 - 4000$ cm^{-1}. All infrared absorption (IRAS) spectra were taken at a resolution of 2 cm^{-1} with typically $500 - 2000$ scans coadded. For the IRAS measurements the sample was positioned in a dedicated IR-cell with KBr windows, which contained a titanium sublimation pump. A uniform gas dosage in the IR-cell is provided by a multi-capillary array.

The heart of a Fourier transform spectrometer is a Michelson interferometer which is labeled by a dashed box in Fig. 3.4. One half of the IR light which enters the interferometer is reflected and a second half is transmitted by a beam splitter. The reflected and the transmitted beams are reflected a second time by a fixed and a movable mirror, respectively. In the next step, both beams pass the beam splitter again and interfere. The interference depends on the wavelength $\lambda = 1/\nu$ and the displacement x of the movable mirror. Evidently, all wavelangths in the IR beam interfere constructively for $x = 0$, i.e. when the lengths of both optical paths are equal. Furthermore, providing

$$2 \cdot x = n \cdot \lambda \text{ with } n = 0,\ 1,\ 2,\ .. \tag{3.7}$$

the light with a certain wavelength λ interferes constructively. Destructive interference occurs for

$$2 \cdot x = \left(n + \frac{1}{2}\right) \cdot \lambda \text{ with } n = 0,\ 1,\ 2,\ ... \tag{3.8}$$

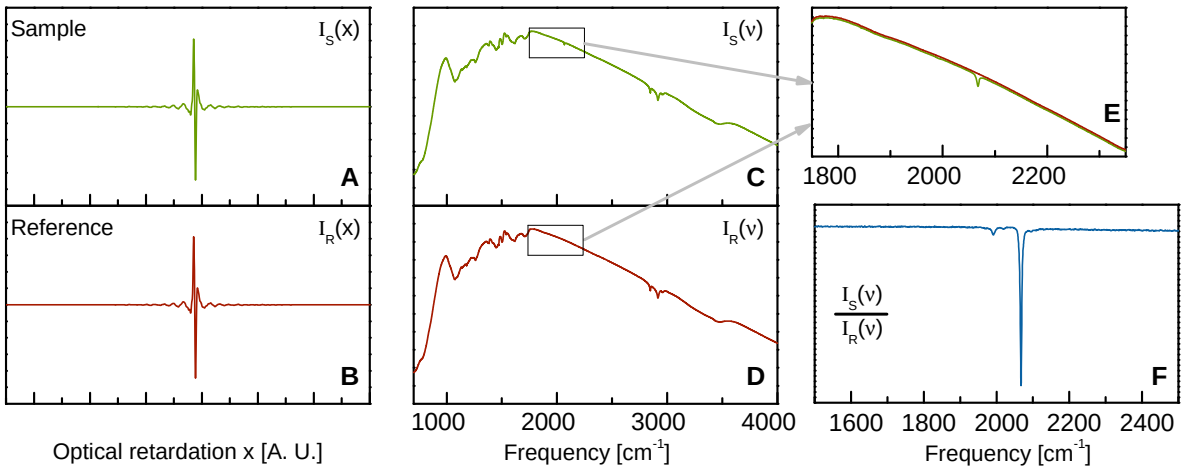

Figure 3.5: Interferograms (2 cm^{-1} resolution) of the clean Cu/Ru(0001) sample (B) and after CO adsorption (A). The data of the sample and the reference were taken at 80 K with 500 and 2000 scans, respectively. Panels (C) and (D) show the corresponding spectra after the Fourier transformation (so called single channel spectra). In panel (E) the difference between the two single channel spectra is highlighted. Finally, panel (F) depicts the reflection spectrum.

Note that the sampling is determined by the equidistant zero crossings of a monochromatic interferogram of a HeNe laser ($\lambda_{\mathrm{HeNe}} = 632.991$ nm or $\nu_{\mathrm{HeNe}} = 15798$ cm^{-1}) which is measured by a photo diode. Hence, the continuous variable x has to be replaced by a discrete one $n \cdot \Delta x$ with $n = 0, 1, 2, 3, \ldots$ The total number N of points of the interferogram depends on the maximum retardation x_{max} of the movable mirror and is given by

$$N = x_{\mathrm{max}}/\lambda_{\mathrm{HeNe}}. \tag{3.9}$$

$\Delta\nu = 1/(N \cdot \Delta x)$ is the spacing of the data points. Furthermore, the resolution of the interferometer equals to

$$\delta\nu = 1/(2 \cdot x_{\mathrm{max}}). \tag{3.10}$$

The intensity $I(n \cdot \Delta x)$, called the interferogram, measured by the detector is a sum over all wavenumbers $k \cdot \Delta\nu$ in the IR beam:

$$I(n \cdot \Delta x) = \sum_k S(k \cdot \Delta\nu) \cdot \cos(2\pi \cdot n\Delta x \cdot k\Delta\nu), \tag{3.11}$$

where $S(k \cdot \Delta\nu)$ is the intensity at a corresponding $k \cdot \Delta\nu$. Typical interferograms are depicted in Fig. 3.5A and B. Note that in order to measure an absorption spectrum, the signal $I_R(n\Delta x)$ of a clean reference sample (without adsorbates) is measured first. Subsequently, the signal $I_S(n\Delta x)$ of the sample after preparation (adding adsorbates) is recorded. The next step in

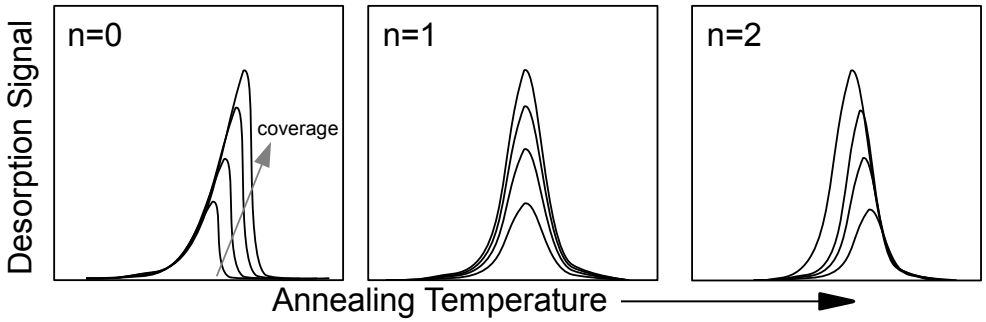

Figure 3.6: Scheme of thermal desorption signals for the orders $n = 0$, 1, and 2 for increasing surface coverages.

data processing, performed by a PC, is the discrete Fourier transformation which calculates the so-called single channel spectrum $I(k\Delta\nu)$ as follows:

$$I(k\Delta\nu) = \sum_{n=0}^{N-1} I(n\Delta x) \exp(2\pi i n k/N). \tag{3.12}$$

The resulting spectra $I_R(k\Delta\nu)$ and $I_S(k\Delta\nu)$ are depicted in Fig. 3.5C and D. Panel E highlights the difference between the spectra from panels C and D. The last step is the calculation of the absorption spectrum with the relative reflectivity $\Delta R/R$ as

$$\Delta R/R = \frac{I_S(k\Delta\nu)}{I_R(k\Delta\nu)} \tag{3.13}$$

depicted in Fig. 3.5F for CO adsorbed at 80 K on 0.95 ML Cu/Ru(0001). For more details on IRAS data processing the reader is referred to additional literature [124, 125].

The signal to noise ratio (S/N ratio) of an IRAS spectrum is proportional to $\sqrt{t}$ with the scan time t. A typical spectrum consists of data from $500 - 2000$ coadded scan cycles of the movable mirror (short: scans). For a resolution of 2 cm^{-1} the time per scan equals 0.27 seconds. In the spectrum presented in Fig. 3.5E, recorded with 2 cm^{-1} resolution and 500 scans coadded, the S/N ratio equals $\sim 12500 : 1$.

3.3 Thermal Desorption

3.3.1 Theoretical Approach

Temperature programmed desorption is an experimental method to measure the adsorption strength and to study the desorption kinetics of adsorbates [126–128]. Thereby, a sample covered with molecules or atoms is heated linearly with a rate $\beta = dT/dt = \text{const}$. In parallel, the desorption rate $R_{\text{des}} = -dN/dt$, which is the change of the number N of adsorbed particles with

time t, is measured by means of a quadrupole mass spectrometer. In general, the increase of the pressure

$$\frac{dp}{dt} = \frac{R_{\mathrm{des}} kT}{V} - \frac{(p - p_0)S}{V} \tag{3.14}$$

upon desorption is the flux of particles into a volume V (e.g. a UHV-chamber with a base pressure p_0) minus the particles pumped by the system with the pumping speed S [126–128]. The desorption rate is described by the Arrhenius equation

$$R_{\mathrm{des}} = -dN/dt = \kappa \Theta^n \exp\left(-\frac{E_d}{kT}\right), \tag{3.15}$$

with the pre-factor κ, the activation/desorption energy E_d, the coverage Θ, and the desorption order n. $T = T_0 + \beta \cdot t$ is the increasing temperature and k is the Boltzmann constant. The activation energy and the pre-factor are again functions of the coverage Θ which changes with T. Typical values of κ are of the order $10^{13} - 10^{19}$ s^{-1} [128, 129]. For simple systems, e.g. multilayer desorption with a desorption rate independent of the coverage, the parameters κ and E_d can be calculated from experimental data; by plotting the logarithmic desorption signal versus the inverse temperature, these parameters can be extracted from the slope and the intercept of the curve [126–128].

By integrating the desorption rate the initial surface coverage can be calculated:

$$\Theta = \int_0^\infty R_{\mathrm{des}} dt. \tag{3.16}$$

The dependency of the desorption rate on the coverage is characterized by the desorption order n as illustrated in Fig. 3.6. Thereby, $n = 0$ corresponds to the desorption of physisorbed particles (multilayer desorption); the maximum desorption signal shifts to higher temperatures with increasing coverage. The intact desorption of chemisorbed molecules is associated with $n = 1$. In this case the maximum desorption rate is independent of the coverage. For the associative (recombinative) desorption, characterized by $n = 2$, the maximum shifts to lower temperatures with increasing coverage. According to Redhead [128] the relation between E_d and the temperature, T_{max}, at which R_{des} is maximum is given approximately by

$$E_d / kT_{\mathrm{max}} = \ln(\kappa \cdot T_{\mathrm{max}}/\beta) - 3.64 \tag{3.17}$$

assuming that κ and β are constant, E_n is independent of Θ, and $n = 1$. Note that T_{max} and the shape of the desorption signal depend on the heating rate; specifically, high heating rates, β, lead to high desorption temperatures, T_{max}. In the present work all thermal desorption experiments were performed at $\beta = 1$ K/s.

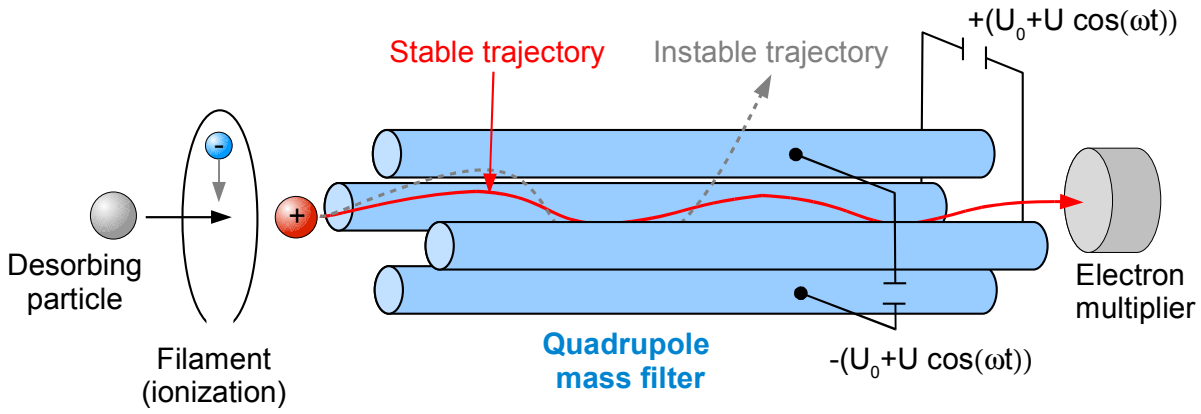

Figure 3.7: Scheme of a quadrupole mass spectrometer.

3.3.2 Experimental Details

For thermal desorption experiments a Balzers QMA112 quadrupole mass spectrometer (QMS) with a mass range $0-100$ u was used. A scheme of a QMS is presented in Fig. 3.7. The desorbing particles become ionized by electrons while passing the filament. Thereby, the molecule can become destroyed (bond breaking) due to the electron impact. Subsequently, the positive ions enter the quadrupole mass filter which consists of four rods. To the two pairs of opposite rods an AC voltage of $U_{AC} = U_0 + U\cos(\omega t)$ and $-U_{AC}$ is applied, respectively. Thus for a certain U_{AC}, only ions with a certain mass to charge ratio m/z can pass the filter (stable trajectory) and become detected by an electron multiplier. All other m/z-ratios exhibit instable trajectories as shown in the figure.

The temperature control (direct current heating) occurred by means of a computer operated proportional-integral-derivative controller. Panels (B) and (C) of Fig. 3.8 show a typical constant temperature gradient and its derivative, respectively. The adjustment from 0 to 1 K/s takes less than 10 s. Moreover, the noise of the temperature ramp amounts to only ± 0.1 K/s.

Quasi simultaneous collection of thermal-desorption spectra with up to 10 different masses was performed by repeatedly scanning through the preset masses. The typical measuring time per data point equals to 0.2 seconds, and it is followed by a waiting period of 30 ms to let the signal settle to its proper value. For each data point and mass individual temperature readings were recorded.

In order to improve the desorption signal the mass spectrometer was equipped with a Feulner cup [130] (glass enclosure). The diameter of the aperture of the cup equals approximately 60% of the diameter of the sample which is positioned in front of the aperture at a distance of about 1 mm. Therefore, it is ensured that the QMS detects the desorption from the front face of the sample only. Furthermore, due to a much smaller volume of the cup as compared to the whole

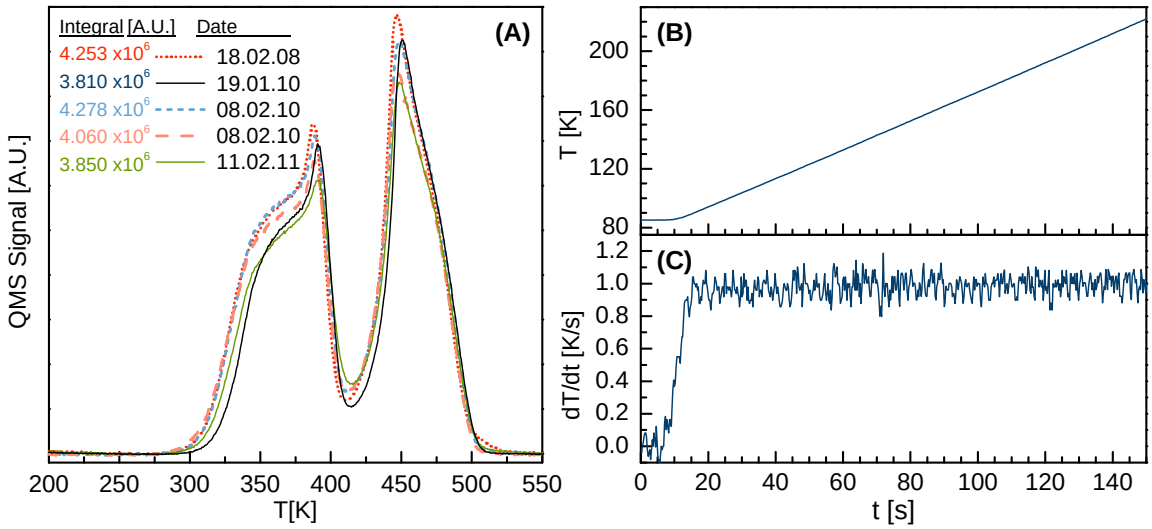

Figure 3.8: **A:** Comparison of thermal desorption spectra (1 K/s, mass 28 u) of CO/Ru(0001) repeated within a time period of several years to check the reproducibility. To each sample CO was dosed at 80 K in the IR cell until the saturation of the $\nu_{\text{C-O}}$ vibrational mode. **B:** A typical temperature ramp at a heating rate of 1 K/s. **C:** Derivative of the temperature ramp from panel (B) showing a fluctuation of the gradient of ± 0.1 K/s.

UHV-chamber, the increase of the local pressure in the Feulner cup is significantly higher than in the UHV-chamber which means an enhancement of the detection probability. If the pumping speed S of the UHV system is significantly larger than the conductance of the cup openings, then S becomes irrelevant and Eq. 3.14 can be reduced to $R_{\text{des}} \propto p$ [130, 131].

For a high reproducibility of the desorption spectra the position of the sample in front of the Feulner cap (QMS) was controlled by measuring the capacitance between the sample and the aperture of the Feulner cap [132]. TPD spectra of saturated CO/Ru(0001) layers with $\Theta_{\text{CO}} = 0.66$ ML [85, 129] are depicted in Fig. 3.8A. The experiments have been repeated over a time period of several years. The dates of the measurements, along with the integrated intensities of the desorption peaks, are summarized in panel (A). Apparently, the reproducibility of the spectra is better than $\pm 10\%$.

3.4 Methanol

Methanol is the smallest alcohol (mass 32 u) which consists of six atoms, namely carbon, oxygen, and four hydrogen atoms, and it exhibits three different chemical bonds (C-O, C-H, and O-H). At 1 bar pressure methanol is a colorless liquid ($\rho = 0.7872$ g/cm^3) with the melting and boiling point at 175.5 and 337.7 K, respectively [133]. It is usually produced from synthesis gas [134, 135] (CO, CO_2, H_2) over a Cu/ZnO [136–138] based catalyst at $50-100$ bar pressure and a

temperature of $200-300°C$. Beside its relevance for the DMFC, methanol is of great importance for the synthesis of formaldehyde via the $CH_3OH + 0.5\ O_2 \rightarrow H_2CO + H_2O$ reaction [139]. Mass spectra of various methanol isotopes can be found in Fig. 3.9. The high intensities of masses 33 and 35 u in the spectrum of CD_3OD are due to an D↔H exchange at the walls of the gas line. Note that this isotopic exchange reaction affects only the OH group of methanol.

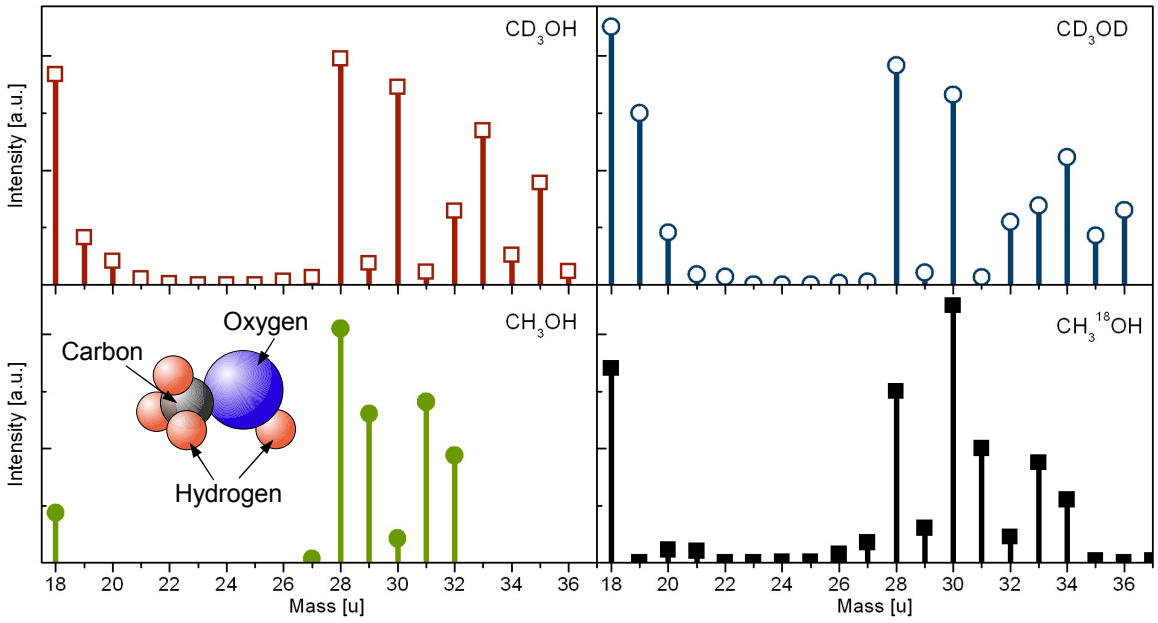

Figure 3.9: Ionization mass spectra of the methanol isotopes used in this work. For each measurement methanol has been dosed in front of the QMS (distance $\sim$ 10 cm) at a pressure of about 10^{-8} mbar. The isotopic purities of the methanol isotopes CD_3OH, CD_3OD and $CH_3^{18}OH$ are 99.8%, 95% and 98.73%, respectively. A scheme of the methanol molecule is given as an inset. Due to a D↔H exchange of the hydroxyl group at the chamber walls of the GDS the CD_3OD spectrum contains a substantial level of CD_3OH.

Chapter 4

Summary of the Results

This chapter contains a summary of the results of the individual research articles, included in Chap. 6, along with key figures which underline important findings and illustrate trends.

The results obtained in this work give a broad overview of the complex methanol reactions on Ru(0001) based catalyst surfaces. In advance, all surface intermediates and desorbing species identified on the studied catalysts are schematically depicted in Fig. 4.1. A comparison of the reaction pathways of methanol (CD_3OH) on various surfaces is given in Fig. 4.2. The symbols and the patterned areas correspond to integrated infrared intensities of characteristic modes of the individual surface intermediates and desorption signals of final reaction products, respectively (indicated in the figure). Fig. 4.2 serves only as a scheme of the reaction pathways intended to help the reader to follow the presentation of the results. Additionally, the approximate temperature stability ranges of the main surface species observed with IRAS are summarized in Tab. 4.1. Noteworthy, the CD_3OH methanol isotope will be used in the following as it exhibits sharper line shapes as compared to the regular one.

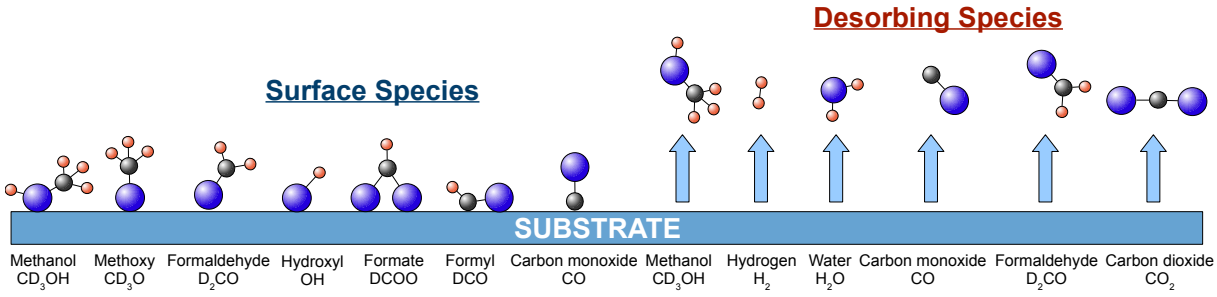

Figure 4.1: Surface intermediates and desorbing species formed from methanol reactions on catalyst surfaces investigated in this work.

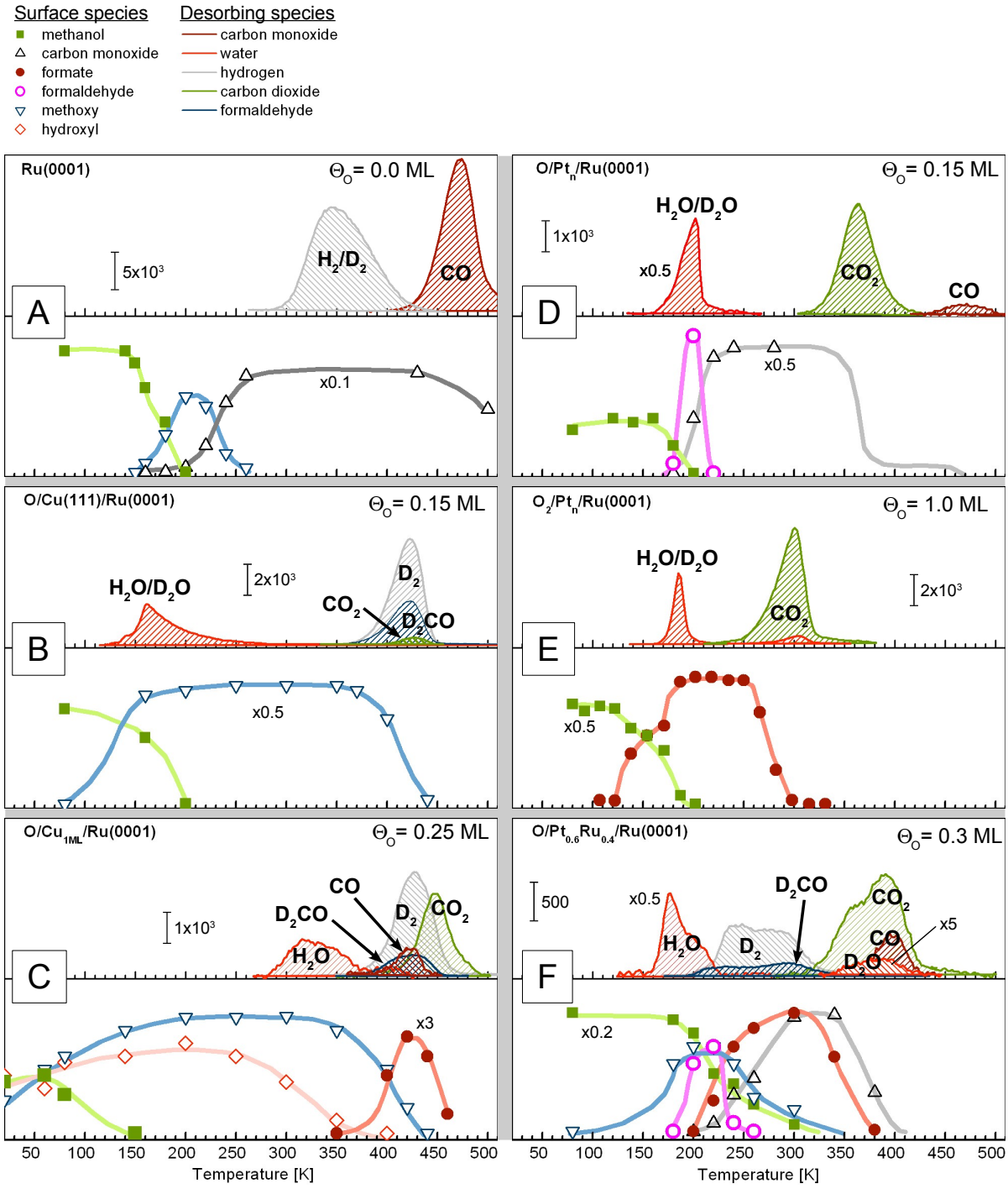

Figure 4.2: Thermal evolution of methanol (CD_3OH) on various catalyst surfaces. The plot comprises stable surface species (symbols) as well as final desorption products (patterned areas). Note that the desorption signals of CO correspond exclusively to desorbing molecules, i.e. they do not contain contributions due to ionization fragments of other molecules. In contrast, the signals of hydrogen (panels A, B, C, and F) refer to raw data. The lines are guides to the eye.

Table 4.1: Approximate temperature stability ranges (in K) of surface species produced from CD_3OH and observed with IRAS. The films deposited on Ru(0001) are listed in the left column. The temperatures in parentheses correspond to: ($^\circ$) methoxy stabilized by postadsorbed oxygen, (*) Ru-bound methoxy, (†) disordered oxygen, (‡) $x \geq 0.3$.

	CD_3OH	CD_3O	D_2CO	DCOO	CO	OH
Ru(0001)	<180	180-240(300)$^\circ$	-	-	240-500	-
$Cu_{<1ML}/Ru$	<180	180-320(300)*	-	-	300-450	-
$O/Cu_{1ML}/Ru$	<250(100)†	(20)†100-400	-	400-450	-	(20)†120-320
$O/Cu_{30ML}/Ru$	<180	150-400	-	-	-	-
$O/Pt_n/Ru$	<190	-	190-210	-	210-360	-
$O_2/Pt_n/Ru$	<160	-	-	160-280	-	-
$O/Pt_xRu_{1-x}/Ru^\ddagger$	<220	180-270	180-250	220-350	280-360	-
Pt_xRu_{1-x}/Ru	<180	180-300	-	-	300-450	-

Reactions of Methanol on Ru(0001)

On the clean Ru(0001) surface (Fig. 4.2A) it has been found that the thermal evolution of methanol starts around 180 K with the breaking of the O-H bond leading to an upright (C_{3v} symmetry) methoxy species (CD_3O). At this temperature, however, its decomposition into CO and deuterium has already started. Yet CD_3O, formed at 220 K, can be stabilized up to $320-340$ K by means of surface site blocking through CO coadsorption. Hydrogen and carbon monoxide, the resulting reaction products from methoxy decomposition, desorb at $330-350$ K and 470 K, respectively. No other reaction intermediates have been identified.

The maximum methoxy coverage of 0.1 ML is low compared to e.g. O/Cu(100) [28, 32, 34, 65, 66]. This is due to the fact that the Cu surfaces are cleaned from the abstracted surface H atoms by removing them (together with surface oxygen) as water. On Ru(0001), on the other hand, H atoms remain on the surface up to about $330-350$ K and block adsorption sites needed for the formation of further methoxy molecules. An entirely new interpretation is presented regarding the production of water detected in thermal desorption at about 190 K. Based on experiments with different methanol and oxygen isotopes it is demonstrated that hydrogen of the hydroxyl group of methanol and residual surface oxygen (most likely at steps and as a relict of the surface cleaning procedure with oxygen) contributes to the formation of water. Note that the hydrogen of the CD_3 group does not participate in the water formation reaction. As an intermixing of the abstracted hydrogen with coadsorbed deuterium is found to be negligible, the hydrogen abstracted from methanol is suggested to react directly with surface oxygen, i.e. without adsorbing on the surface in between. Thus, C-O bond breaking, long believed to act as the primary reaction step towards water formation, can definitely be ruled out.

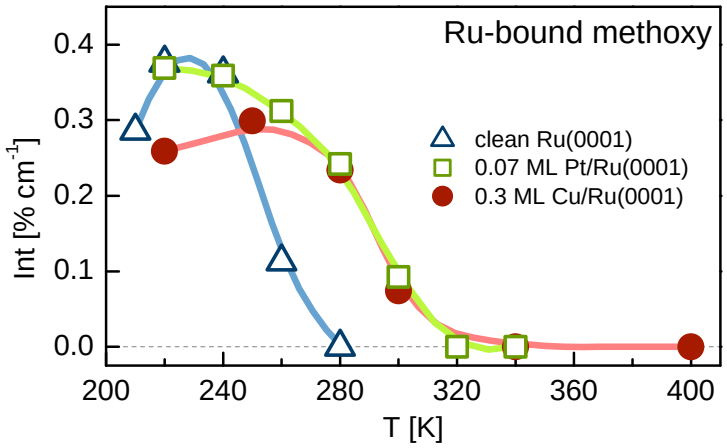

Figure 4.3: Temperature dependence of the integrated IRAS intensities of methoxy ($\delta_s(CD_3)$ at 1074 cm^{-1}) demonstrating the passivation effect of Ru(0001) by deposited Cu or Pt. The triangles thereby refer to a clean Ru(0001) surface, while the circles and squares to Ru(0001) with pre-deposited copper ($\Theta_{Cu} = 0.3$ ML, $T_{growth} = 700-800$ K) and platinum ($\Theta_{Pt} = 0.07$ ML, $T_g = 700$ K), respectively.

Formation of Methoxy on Cu/Ru(0001) Layers

The deposition of one monolayer Cu on Ru(0001) passivates the surface entirely toward methanol reactions. However, various reaction intermediates are discernible for $\Theta_{Cu} < 1$ ML. In the temperature range $220-300$ K two upright methoxy species (local C_{3v} symmetry) on uncovered Ru(0001) areas and on Cu/Ru(0001) can be distinguished. The local methoxy coverage on the Cu monolayer amounts to about 0.04 ML which is half the value found on Ru(0001). This value gradually reduces to zero for Cu coverages exceeding 0.75 ML, i.e. approaching the full Cu-monolayer. Interestingly, the passivation of the Ru(0001) step edges by minute amounts of Cu or Pt effectively delays the decomposition of the Ru-bound methoxy as illustrated in Fig. 4.3 where integrated characteristic vibrational bands of the Ru-bound methoxy on clean Ru(0001), 0.07 ML Pt/Ru(0001), and 0.3 ML Cu/Ru(0001) are shown as a function of the surface temperature. Specifically, the thermal stability of methoxy on uncovered Ru(0001) increases from 220 K for clean Ru(0001) to about 300 K for a partially filled Cu/Ru or Pt/Ru layer. The thermal stability of the Cu-bound methoxy is even higher and at least 380 K is required to transform all methoxy molecules into CO and hydrogen (not shown).

This study clearly shows that a modification of the reaction kinetics on a catalytically active surface can be achieved even for minute amounts of deposited metal atoms, e.g. by passivating various types of reaction centers. For extended monolayer films strain and electronic effects due to the underlying substrate strongly affect stability of intermediate species, as well as their formation and decomposition kinetics.

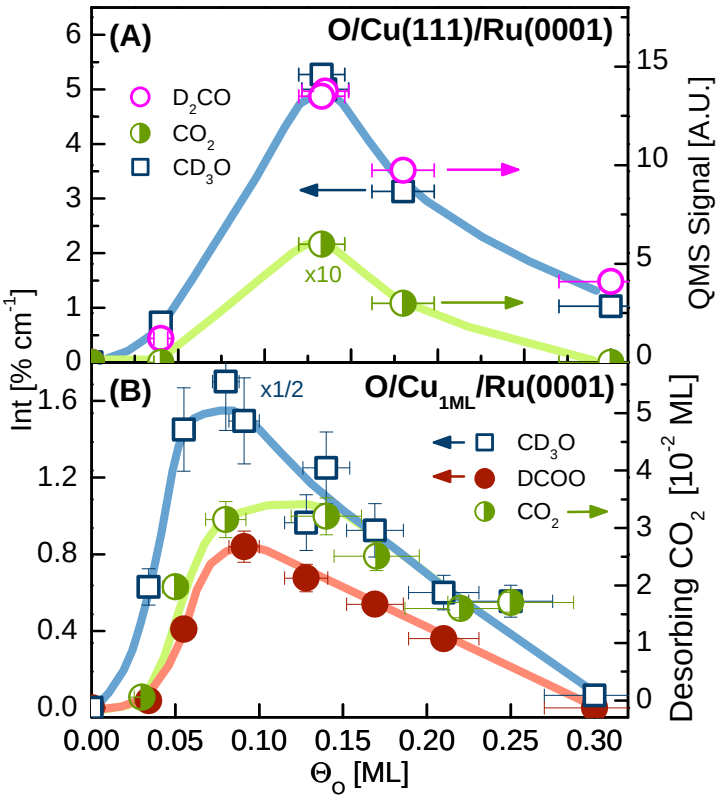

Figure 4.4: Integrated IRAS intensities of surface intermediates and TPD peak areas of desorbing species (CO_2 and D_2CO) as a function of preadsorbed surface oxygen. **(A):** multilayer methanol adsorbed at 80 K on $O/Cu_{30ML}/Ru(0001)$ and heated to 300 K to produce methoxy ($\delta(CD_3)$ at 1086 cm^{-1}). **(B):** 0.15 ML methanol adsorbed at 80 K on ordered $O/Cu_{1ML}/Ru(0001)$ and annealed to 200 and 420 K to produce methoxy ($\nu_s(CD_3)$ at 2050 cm^{-1}) and formate ($\nu(OCO)$ at 1320 – 1330 cm^{-1}), respectively. The amount of surface oxygen has been determined by means of XPS.

Methanol oxidation on Monolayer Cu/Ru(0001)

In contrast to the pure 1 ML Cu/Ru(0001), the oxygen covered Cu/Ru(0001) layer (Fig. 4.2C) exhibits enhanced reactivity toward methanol activation and methoxy formation. Interestingly, the ordered (2×2)-O phase is unreactive, which may indicate a reduced affinity of these aligned oxygen atoms toward hydrogenation. Activation of methanol therefore occurs only in dilute oxygen environments, or, at defects and domain boundaries of the ordered (2×2)-O phase. In Fig. 4.4B the yielded surface and desorbing species on $O/Cu_{1ML}/Ru(0001)$ are plotted versus Θ_O. In panel (A) a corresponding plot is shown for a $O/Cu_{30ML}/Ru(0001)$ layer (Fig. 4.2B) which also exhibits a maximum reaction yield for intermediate oxygen coverages. Under such favorable conditions on $O/Cu_{1ML}/Ru(0001)$ (upright) methoxy formation readily occurs, even at low $T < 80$ K. If oxygen layers are not annealed ($T = 20$ K) prior to methanol admission,

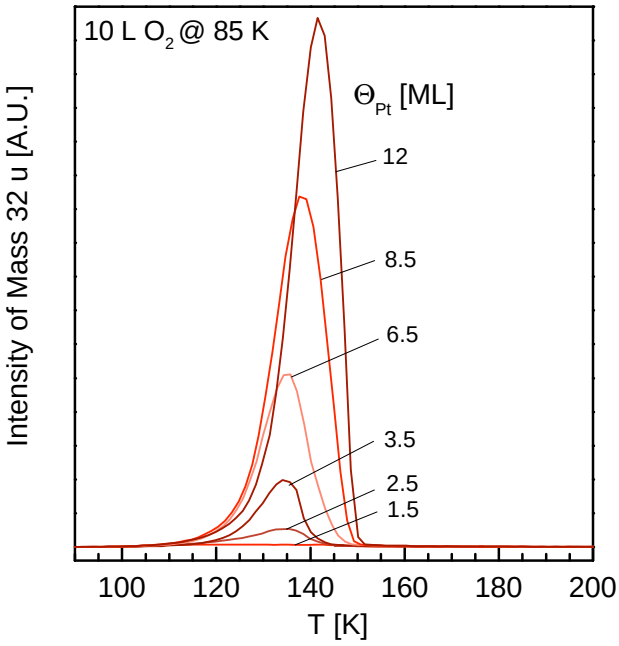

Figure 4.5: TPD spectra (1 K/S) of O_2 from Pt_n/Ru(0001) with n = 1.5, 2.5, 3.5, 6.5, 8.5 and 12 ML. All samples were exposed to 10 L O_2 at 85 K.

methanol adsorbs dissociatively even at 20 K. In general, methoxy formation is accompanied by the formation of surface hydroxyl (OH) which desorbs as water at $300 - 350$ K. Methoxy represents the main intermediate up to 350 K. Reactions upon further annealing depend on the oxygen coverage; for low $\Theta_O < 0.1$ ML the formation of formaldehyde (D_2CO) and CO which desorb instantaneously prevails. For high Θ_O methoxy is oxidized to formate (DCOO) which represents a stable intermediate and eventually desorbs as CO_2 at $T > 450$ K. Additionally, formyl (DCO) has been identified as a minor intermediate species.

Oxygen adsorption on Pt_n/Ru(0001) layers

The adsorption of O_2 on Pt_n/Ru(0001) layers with $n = 1 - 12$ ML was investigated in order to obtain information about the influences of surface strain and of the nearby substrate on the catalytic properties of the Pt/Ru(0001) system. It is found that the sticking probability of oxygen on the Pt/Ru(0001) monolayer is virtually zero and increases stepwise for increasing n, approaching the value of Pt(111) as depicted in Fig. 4.5 where thermal desorption spectra of O_2 from various Pt_n/Ru(0001) layers exposed to 10 L O_2 at 85 K are shown. Furthermore, $n > 2$ is needed to dissociate the chemisorbed O_2. Additionally, a novel state of the chemisorbed O_2, associated with a minority site of the first Pt layer (e.g. steps), has been identified.

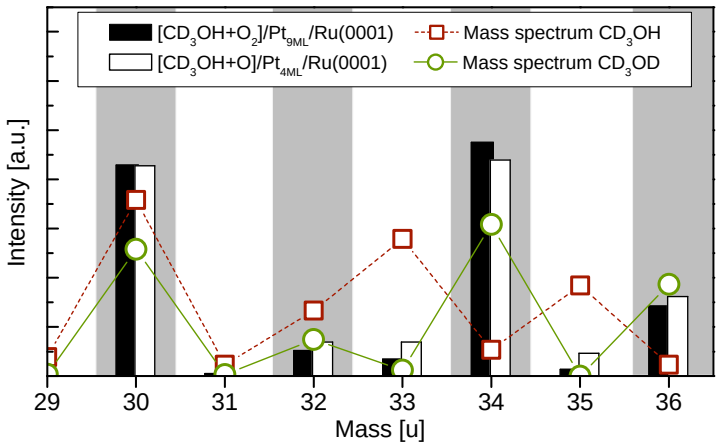

Figure 4.6: QMS signal levels associated with different methanol isotopes. The squares and circles denote the respective QMS signals as CD_3OH or CD_3OD is admitted to our chamber. The black and white bars correspond to the desorption signals at 188 K for $[CD_3OH{+}O_2]/Pt_{9\ ML}/Ru(0001)$ and at 203 K for $[CD_3OH{+}O]/Pt_{4\ ML}/Ru(0001)$, respectively. For better comparison the thermal desorption data have been aligned for mass 30 u. In both cases the observed QMS signals of desorbing methanol are independent of the isotopic nature of preadsorbed oxygen.

Oxidation of Methanol on Oxygen covered Pt_n/Ru(0001) Layers

Thin pseudomorphic as well as thick "Pt(111)-like" Pt/Ru(0001) bimetallic substrates have been used to study the oxidation of methanol (CD_3OH) to CO_2. Specifically, molecular (cold deposited, Fig. 4.2E) and ordered atomic (annealed, Fig. 4.2D) oxygen precovered Pt_n/Ru(0001) layers with $n = 1-15$ ML have been studied. Hereby the thickness of the Pt films primarily influences the adsorption probability of O_2 and much less the energy barriers for methanol reactions. In particular, no indication of a strain effect could be detected and the reactions of methanol on Pt_n/Ru(0001) multilayer films closely follow the known reaction scheme on Pt(111) substrates: On O_2/Pt_n/Ru(0001) methanol is directly oxidized to formate (DCOO) and eventually desorbs as CO_2 (300 K). The formate producing reaction is promoted by dissociating O_2 molecules (130 K) and, at higher temperatures ($130 - 200$ K), by disordered atomic oxygen. This is in contrast to methanol post-adsorbed onto ordered atomic oxygen covered Pt_n/Ru(0001) layers which exhibit formaldehyde formation and decomposition to CO and H. Note that around 300 K the produced CO reacts with residual surface oxygen to gas phase CO_2 until all oxygen atoms become consumed by this reaction. The excess CO desorbs at about 500 K (see Fig. 4.2D).

An interesting finding illustrated in Fig. 4.6 is that during methanol dissociation at $160 - 200$ K a remarkable fraction of methanol molecules experiences an $H \leftrightarrow D$ exchange of the hydroxyl group hydrogen, leading to the dominant desorption of CD_3OD (white and black bars) instead of the intially adsorbed CD_3OH (squares). Our observation that the relative fraction of

desorbing CD_3OH is exceptionally low implies a bold primary isotope effect which we attribute to the dissimilar zero point energies associated with OH and OD vibrations of methanol.

Reactions of Methanol on Clean and Oxygen Covered Pt_xRu_{1-x}/Ru(0001) Surface Alloys

On oxygen-free layers the reaction path corresponds to the one on clean Ru(0001). Yet, Pt increases the thermal stability of methoxy, representing the only stable intermediate, as illustrated in Fig 4.7C (full symbols). Interestingly, even low amounts of Pt (ligand effect) lead to strong shifts of methoxy's vibrational bands. For high $x > 0.4$ the surface becomes gradually less reactive in agreement with the inert full Pt/Ru(0001) monolayer.

On oxygen precovered Pt_xRu_{1-x}/Ru(0001) surface alloys the oxidation of methanol to DCOO, via a surface methoxy (CD_3O), dominates for $x = 0.4 - 0.8$ ML. For $x < 0.4$ ML, on the other hand, total dehydrogenation to CO prevails. This trend is clearly demonstrated in Fig. 4.7A where the amounts of desorbing CO and CO_2 are plotted as a function of x. As evidenced by the strong correlation between DCOO and CO_2 in panel A, CO_2 is primarily produced from formate decomposition. Yet, a contribution due to the reaction CO+O is observed for high amounts of Pt, see panel D. Due to the quadratic increase of the amount of reactively produced DCOO and CO_2 for $x < 0.4$ this reaction is ascribed to an ensemble effect associated with Pt. The Pt content also affects the formation temperatures and the thermal stability of species; e.g. the dissociation temperature of methoxy, the precursor of DCOO, decreases with increasing x (empty symbols in panel C). Consequently, the onset of DCOO formation falls with increasing x too (blue bullets in panel B).

Formaldehyde formation (200 K) and desorption (290 K) is observed for $x = 0.1 - 0.8$. In accordance with methanol reactions on O/Ru(0001) and O/Pt/Ru(0001) no experimental evidence for surface hydroxyl has been found.

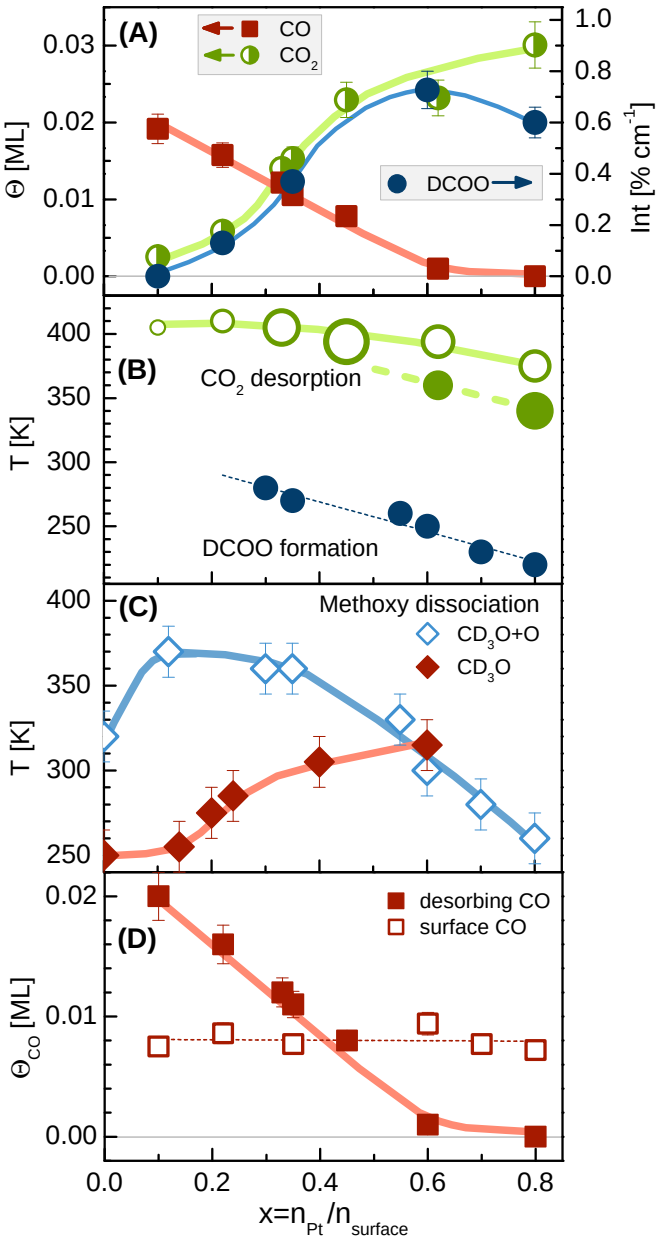

Figure 4.7: A: Integrated IRAS intensities of DCOO after annealing to 320 K, as well as the integrated thermal desorption peaks of CO_2 and of CO as a function of x. All samples were exposed to 4 L oxygen and to 40 mTorr·s CD_3OH, both at 80 K. The amount of DCOO for $x = 0.8$ is below the amount of desorbing CO_2 due to a lowered CO_2 desorption temperature, see panel B.
B: Temperature range of DCOO formation and CO_2 desorption, i.e. DCOO decomposition, for the samples in panel A versus x. The empty and full green symbols correspond to the two maxima in the CO_2 desorption trace; the areal size of the symbols thereby corresponds to the respective integrals.
C: Dissociation temperature of methoxy on oxygen precovered (open diamonds) and oxygen-free (solid diamonds) surface alloys. The low dissociation temperature of CD_3O+O for $x > 0.4$ is due to the onset of DCOO formation which falls with increasing x, see Panel B.
D: Quantities of reactively produced CO, from CD_3O dissociation, determined by TPD (full symbols) and IRAS at $300 - 320$ K (open symbols). For $x < 0.4$ less surface CO than desorbing CO is observed due to the enhanced thermal stability of methoxy for $x < 0.4$ (panel C), i.e. the CD_3O dissociation overlaps with CO desorption. For $x > 0.4$ surface CO (empty squares) reacts with O to gaseous CO_2 rather than desorbing as CO (full squares).

Chapter 5

Discussion

This chapter provides a general discussion of the results obtained in Articles I-VI. The possible reaction pathways, the influence of surface oxygen on the surface reactivity, and the final reaction products are discussed first. Subsequently, the formation and the decay of prominent reaction intermediates is examined. Finally, closing remarks on the relevance of the results for the DMFC are given.

5.1 Reaction Pathways

At low surface temperatures ($20 - 80$ K) methanol adsorbs intact on metal surfaces and is bound through the oxygen atom [140]. The thermally induced reactions of methanol can start either with the cleavage of the O-H, C-D, or the C-O bond. The first reaction species of the O-H bond breaking path is a methoxy (CD_3O) species which becomes stepwise dehydrogenated to formaldehyde (D_2CO), formyl (DCO), and eventually to CO. The C-D bond breaking path provides hydroxymethyl (CD_2OH) as the first intermediate. In the second step CD_2OH can dissociate either to CDOH or D_2CO. If D_2CO is formed the O-H and the C-D bond breaking pathways merge. Otherwise, CDOH decays to CO via a COH species. The final reaction products, CO and hydrogen, eventually desorb and leave a clean surface behind. A scheme of these reaction pathways is depicted in Fig. 5.1.

According to DFT calculations the favored initial reaction step on Pt(111) [48, 49] and Cu(111) [29] is the C-D and the O-H bond breaking, respectively. The barrier for the scission of the C-O bond is significantly higher than the barriers for the activation of the two other bonds [49]. The latter finding agrees with experimental works as the C-O bond breaking has not been observed for any of the investigated systems. Moreover, the absence of a C-O bond breaking path is supported by other experimental works on Cu(111) [27], Cu(100) [35], Pd(111) [56], and Pt(111) [46, 47] which lack evidence for this reaction step. Similarly, there is no experimental evidence for a stable hydroxymethyl species making the C-D bond breaking as the first reaction step unlikely.

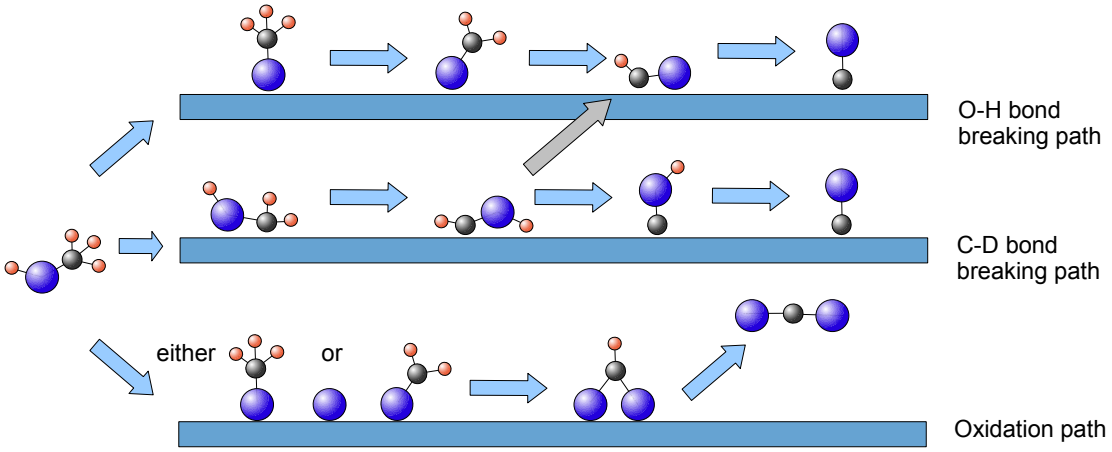

Figure 5.1: A scheme of possible reaction pathways. The adsorbate geometries of the C-D bond breaking path are based on Ref. [49]. The C-O bond breaking path which is energetically unfavored is not shown.

On all surfaces the activation of methanol starts with the dehydrogenation of the OH group. Moreover, only surface intermediates (CD_3O, D_2CO, DCO) associated with the O-H bond breaking path have been observed experimentally. Noteworthy, according to Mavrikakis and Barteau [140] the breaking of the O-H bond is expected to be the first reaction step of methanol on metal surfaces.

Additionally, a new reaction path which exhibits CO_2 as the final product can be opened by the coadsorption of methanol and oxygen (oxidation path). Thereby, the dehydrogenation of methanol is accompanied by an oxidation reaction providing formate (DCOO) as the precursor of CO_2. Depending on the substrate DCOO is formed either from methoxy or formaldehyde.

A more detailed discussion of the individual reaction species is presented in Section 5.5.

5.2 Clean Surfaces

The reactions of methanol on clean, i.e. oxygen-free, metal surfaces are discussed in the following. On such layers CD_3O (and CO) represents the only stable surface intermediate. Noteworthy, among the clean elemental surfaces only Ru(0001) activates methanol; on multilayer Pt/Ru(0001), Cu/Ru(0001) as well as on Pt(111) and Cu(111) methanol adsorbs reversibly. This difference can be explained by means of the *d*-band model [70–73] which predicts a linear relationship between the relative decrease of adsorbate binding energies E_B and the down-shift of the metal's *d*-band center, ϵ_d, relative to the Fermi level. In Fig. 5.2A the dependence of E_B on ϵ_d is plotted for several elemental surfaces. The positions of ϵ_d correspond to the values reported by Ruban et al. [71]. The binding energies E_B were calculated from the desorption temperatures of chemisorbed methanol on the corresponding substrates according to Redhead

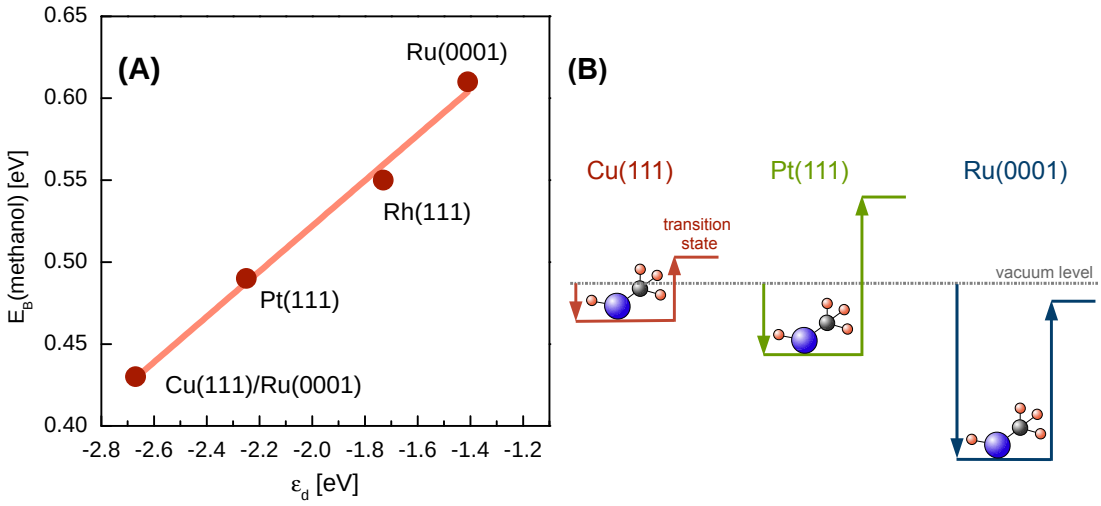

Figure 5.2: **(A):** Dependence of the binding energy, E_B, of methanol on various substrates as a function of the position of the metal's d-band, ϵ_d, relative to the Fermi level. The values of ϵ_d are taken from Ref. [71]. The binding energies have been determined from the desorption temperatures of chemisorbed methanol according to Redhead [128]. The plot comprises data obtained on Cu(111)/Ru(0001) [this work], Pt(111) [39, 40], Rh(111) [52], and Ru(0001) [this work] **(B):** Schematic potential energy surface of the first reaction step of methanol on Cu(111), Pt(111), and Ru(0001).

[128]. On Ru(0001) the binding energy of methanol is significantly higher than on Pt(111) or Cu(111). Therefore, it is likely that on Ru(0001) the dissociation barrier of methanol is located well below the vacuum level preventing the intact desorption of all methanol molecules and allowing for methanol reactions as illustrated in Fig. 5.2B. Because on Cu(111) and Pt(111) E_B is lower than the activation energy intact desorption represents the favored reaction step [27, 29, 31, 39, 40, 49]. Note that the d-band model usually applies to strongly chemisorbed molecules, such as CO, O, or H [70–73], and not to molecules with dominant van-der-Waals interactions as methanol. Therefore, the nearly perfect linear dependence of the experimental values for E_B on ϵ_d is surprising.

5.3 Influence of Θ_O on Surface Reactivity

The reactions of methanol strongly depend on the preadsorption of oxygen. Specifically, oxygen promotes the cleavage of the O-H bond substantially, i.e. it makes the inert surfaces (multilayer Pt/Ru, Cu/Ru) highly reactive. Another effect of oxygen is the opening of the oxidation pathway (CO_2 path) of methanol and the stabilization of additional intermediates (e.g. D_2CO) which are not observed without surface oxygen.

5.3.1 O-H Bond Breaking

The activation of the O-H bond facilitated by surface O is strongly correlated with the effective formation of OH and water which consists of surface O and hydrogen atoms from the dehydrogenation of methanol. This reaction was observed on all surfaces investigated in this work as well as on Pt(111) [44, 47] and Cu(111) [27, 31]. Therefore it is suggested that O actively participates in this reaction by inducing a direct transfer of the H atoms of the methanolic OH group without allowing them to bind to the surface in between. Such a direct H transfer has been unambiguously established on Ru(0001) precovered with oxygen [Article I]. Yet, this mechanism likely applies to the other surfaces as well. For instance, on PtRu/Ru(0001) surface alloys only the H atoms from the OH group of CD_3OH contribute to water formation; the D atoms from the dehydrogenation of the CD_3 group, on the other hand, desorb as D_2 [Article VI].

Another possibility would be that O affects the electronic structure of the substrate leading to a destabilization of methanol and the lowering of the O-H dissociation barrier.

Remarkably, no experimental evidence for stable surface water molecules was found because the formation of water occurs at temperatures above the natural desorption temperature of water. Therefore, H_2O desorbs immediately after its formation. The only detected stable compound consisting of surface oxygen and hydrogen is a surface OH, produced by the reaction $CD_3OH+O \rightarrow CD_3O+HO$. Moreover this reaction was observed exclusively on $O/Cu_{1ML}/Ru(0001)$ [Article III].

5.3.2 Oxidation of Methanol

Evidently, oxygen atoms lower the bond breaking barriers of adsorbed methanol substantially, similar as first layer Ru atoms. In contrast to Ru atoms which promote the total dehydrogenation only, oxygen opens a new oxidation pathway with gaseous CO_2 as the final reaction product. Thereby, surface DCOO represents the precursor of desorbing CO_2. Moreover, DCOO and CO_2 always consist of one O from methanol and another one due to surface O, as deduced from isotopic labeling experiments. This finding suggest an active participation of O in the oxidation reaction, similar as it is the case concerning the formation of water. Note that on Ru(0001), independent of precovered oxygen, exclusively the CO producing path is observed.

5.3.3 Structure of Surface Oxygen

It is to mention that the structure of the adsorbed O layers has a significant effect on the reaction yields. Generally, ordered and dense oxygen layers passivate the surfaces. For instance, the yielded surface intermediates and desorbing species due to methanol decompositions on oxygen covered Cu/Ru(0001) clearly exhibit maxima for intermediate oxygen coverages (0.1 ML, see Fig 4.4). For both, low and high oxygen coverages, the surface reactivity is inhibited. Specifically, high (and ordered) oxygen coverages passivate the surface which agrees with the

results obtained on saturated O/Cu(110) [63, 64], Cu(111)-(2×2)-O [27], and Ru(0001)-(2×2)-O [26] which are all inert toward methanol reactions. On Ru(0001)-(2×2)-O [141] the binding energy of H is substantially lower (by about $0.5 - 0.6$ eV) than on clean Ru(0001). According to the Brønsted-Evans-Polanyi (BEP) principle [142, 143] the decreased binding energy of H on Ru(0001)-(2×2)-O leads to a higher activation energy of the dehydrogenation reaction on this surface as compared to Ru(0001). The BEP principle describes a linear relationship between the activation energy of a certain reaction and the binding energy of the final state. Because of this effect, on Ru(0001)-(2×2)-O [144] no methanol reactions are observed even though methanol is stronger bound to this substrate than to the clean Ru(0001) surface.

Consider that high, but disordered (cold deposited) oxygen layers alone are not sufficient to passivate the surface, but, additionally, an oxygen long-range order is needed [Article III]. The low reactivity of dense and ordered oxygen layers, which seems to be widely spread, has been confirmed by DFT calculations for the system O/Cu(110) by Gross and Sakong [36] who identified edge sites of oxygen islands as reactive centers. Furthermore, the aligned O atoms may also block surface sites needed for the dehydrogenation of methanol.

5.4 Final Reaction Products: CO vs CO_2

Referring to the DMFC the thermally induced methanol reactions can be subdivided into two major pathways: a total dehydrogenation pathway with CO as the final product, and an oxidation pathway which produces gaseous CO_2 (Fig. 5.1). The activation of the CO_2 path by the adsorption of oxygen does not mean that the CO producing path becomes deactivated; generally, the two pathways are competing processes which depend on the substrate composition.

Fig. 5.3 compares the desorption temperatures and quantities of the final reaction products of methanol on various catalyst surfaces. The quantities (proportional to the symbol area) of the desorbing products are indicated in the figure as the percentage of initially adsorbed methanol. Consider that desorbing water is not included in the figure as its absolute amounts have not been estimated. The quantities of desorbing hydrogen from $O/Cu_{1ML}/Ru(0001)$ and $O/Pt_xRu_{1-x}/Ru(0001)$ are lower limits only because the intensity of the hydrogen fragment due to the ionization of formaldehyde could not be determined. In both cases D_2CO and D_2 desorb at the same temperatures. The values have been estimated under the assumption that the D_2/D_2CO ratio for desorbing D_2CO corresponds to the one on $O/Cu_{30ML}/Ru(0001)$.

On oxygen-free catalysts, such as Ru(0001) or submonolayer Cu/Ru(0001), only the dehydrogenation path is observed which starts with an O-H bond break leading to methoxy as the only stable intermediate and ending up with CO and hydrogen [Articles I, II, VI]. Furthermore, the activation of methanol on such coadsorbate-free surfaces only takes place if Ru atoms are present within the first atomic layer. The deposition of Cu or Pt in excess of a monolayer passivates the Ru(0001) surface entirely.

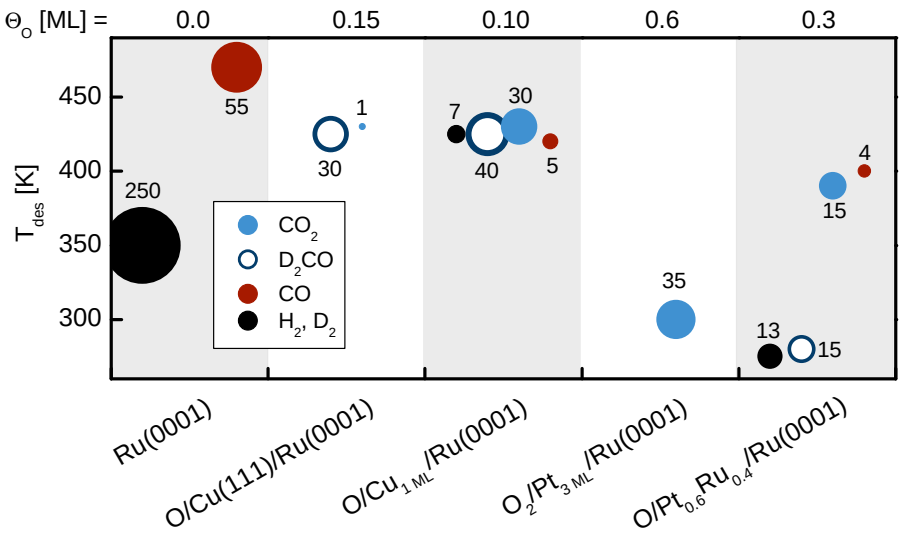

Figure 5.3: Desorption temperatures (vertical scale) and quantities (symbol size) given in percent of initially adsorbed methanol on Ru(0001), O/Cu_{30ML}/Ru(0001), O/Cu_{1ML}/Ru(0001), O_2/Pt_n/Ru(0001), and O/Pt_xRu_{1-x}/Ru(0001). The calibration of absolute amounts of desorbing CO, CO_2, D_2, H_2, and D_2CO is described in Articles I and III. To all surfaces $0.1 - 0.15$ ML methanol was added, except for Cu_{30ML}/Ru(0001), or Cu(111)/Ru(0001), where a methanol multilayer was adsorbed. Thereby, only the chemisorbed methanol molecules (0.4 ML) are of relevance [Article III]. The oxygen coverages are given at the top of the figure.

On oxygen precovered surfaces both pathways, the dehydrogenation path and the CO_2 producing path, are observed. Moreover, surfaces which oxidize methanol to CO_2 exhibit only small amounts of desorbing hydrogen which is removed from the surface as water or leaves the surface as formaldehyde. Concerning the DMFC this means a substantial drain of the energy providing H atoms. In contrast, from the clean Ru(0001) surface where CO is the only final reaction product all hydrogen atoms from methanol dehydrogenation desorb molecularly. Yet, the formation of a highly stable CO ($T_{\mathrm{des}} \approx 470$ K) causes a poisoning of the catalyst and is therefore a serious drawback of Ru(0001). Note that the criterion for the poisoning of the DMFC's anode is a high thermal stability of the corresponding adsorbate, i.e. all adsorbates which survive the operation temperature of the cell (≈ 400 K) represent poisons. A further example of a catalyst poison is DCOO on O/Cu_{1ML}/Ru(0001) which is stable up to around 440 K [Article III].

Pt_xRu_{1-x}/Ru(0001) surface alloys exhibit a relatively low affinity toward water formation, i.e. water is formed most likely via a direct H transfer from the OH group to the surface O which does not affect the CD_3 group [Article VI]. In this case the partial drain of hydrogen atoms proceeds via the desorption of formaldehyde. In parallel a remarkable amount of desorbing CO_2 is observed at relatively low temperatures (390 K).

The surfaces with the, by far, highest reactivity toward oxidation of methanol to CO_2

and the lowest CO_2 desorption temperature are $O_2/Pt_n/Ru(0001)$ layers (especially with $n >$ 6 ML). Another surface with a high selectivity toward the conversion of methanol into CO_2 is $O/Cu_{1ML}/Ru(0001)$. Moreover, the amount of desorbing CO_2 from $O/Cu_{1ML}/Ru(0001)$ is at least a factor $\times 10$ higher than from 30 ML Cu/Ru(0001) where the oxidation of methanol is a minor path only, and, to a large extent, methanol is converted to gaseous formaldehyde. Evidently, D_2CO does not only represent a stable surface intermediate and a precursor of DCOO (see Section 5.5.3), but it is also a final reaction product of the O-H bond breaking path. If D_2CO is weakly bound, as on Cu(111), it desorbs molecularly rather than undergoing further reactions.

5.5 The Formation and Decay of Species

In the following Section general information concerning the formation and the decay of the most prominent reaction species methoxy formate, and formaldehyde are given.

5.5.1 Initial Reaction Step and Formation of Methoxy

The formation of methoxy as a result of the breaking of methanol's O-H bond, which is the expected initial reaction step [140], is widely spread. Interestingly, the adsorption geometry of methoxy is C_{3v}, independent of the substrate. The observation of O-H bond breaking as the initial reaction step in methanol decomposition is in agreement with results obtained on many other metal surfaces, such as Cu(100) [28, 32, 35, 145], Cu(111) [27, 31], Ag(111) [57], Ru(111) [51–53], and Mo(110) [59], and with DFT calculations concerning methanol reactions on Cu(111) where the cleavage of the O-H bond was reported to have the lowest activation barrier [29].

On surfaces which exhibit formaldehyde as the first surface intermediate (O/Pt/Ru(0001) layers) its formation due to the rapid dehydrogenation of a stable, but short living methoxy is unlikely. According to the *d*-band model, on $Pt_n/Ru(0001)$ layers ($\epsilon_d \approx -2.8$ eV) a stable methoxy is expected to survive temperatures as high as 370 K (see Fig. 5.5). Yet, on such layers no experimental evidence for a stable methoxy was found. Nevertheless, the cleavage of the O-H bond, promoted by surface oxygen, plays a key role in the activation of methanol. In parallel, the CD_3 group becomes partially dehydrogenated. As no intermediates are observed between methanol and formaldehyde the activation barriers of the O-H and the C-D bonds seem to be similar. In summary, the cleavage of the O-H bond as the the initial reaction step of methanol on metal surfaces seems to be general.

5.5.2 Decay of Methoxy and CO Desorption

The decay of the methoxy species occurs by the stepwise dehydrogenation of the CD_3 group. Possible surface intermediates on the way to the total dehydrogenation of CD_3O are formaldehyde and formyl, which both have been identified experimentally [Article III, V, VI].

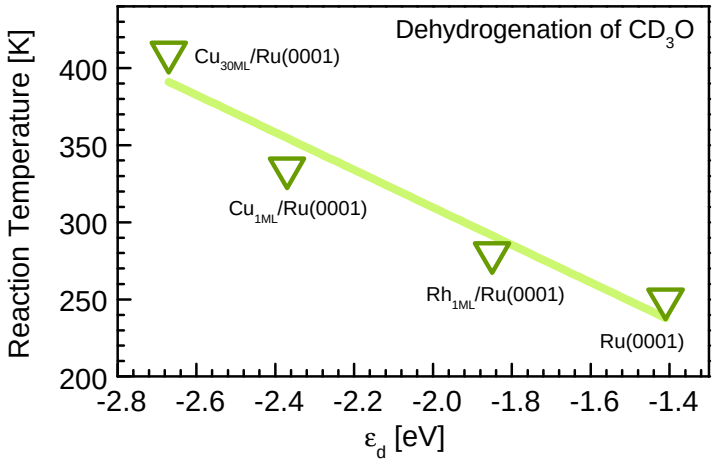

Figure 5.4: Relation between the decomposition temperature of methoxy and the position of the *d*-band, ϵ_d, relative to the Fermi level. The reaction temperature is defined as the temperature at which the integrated IRAS intensities of methoxy have decreased by 50%. The values of ϵ_d are taken from the article by Ruban et al. [71]

The thermal stability of methoxy on metal surfaces can be described by the *d*-band model. Within this model [70–73] the surface reactivity depends on the position of the *d*-band center, ϵ_d, relative to the Fermi level: small energetic distances between ϵ_d and the Fermi level mean a high surface reactivity. In other words, an energetic up-shift of ϵ_d causes a strengthening of the adsorbate-metal interactions which may imply a lowering of the dissociation barrier of a given molecule. Therefore, the usage of the *d*-band model seems to be a good approach to describe the dehydrogenation of CD_3O. The dependence of the dissociation temperature of methoxy on ϵ_d is depicted in Fig. 5.4. The plot comprises various substrates investigated in this work; the corresponding values of ϵ_d are taken from the article by Ruban et al. [71]. Obviously, the data in Fig. 5.4 fit a straight line and the expected trend that methoxy is most stable on surfaces with relatively low ϵ_d can be clearly observed.

On Ru(0001) it has been found that the dissociation of methoxy is strongly promoted by Ru(0001) step edges which can be passivated by minute amounts of Cu or Pt [Article II]. The passivation of these reaction centers leads to an about +40 K higher decomposition temperature of methoxy than the one given in the figure. It is likely that such an effect is general. Yet, as the passivation of steps has not been studied on the other layers, the data point associated with Ru(0001) correspond to the surface with non-passivated steps.

5.5.3 Formation of Formate

The formation of DCOO is an important reaction step as this molecule represents the precursor of gaseous CO_2. The oxidation reaction, which produces DCOO, proceeds via a stable D_2CO or

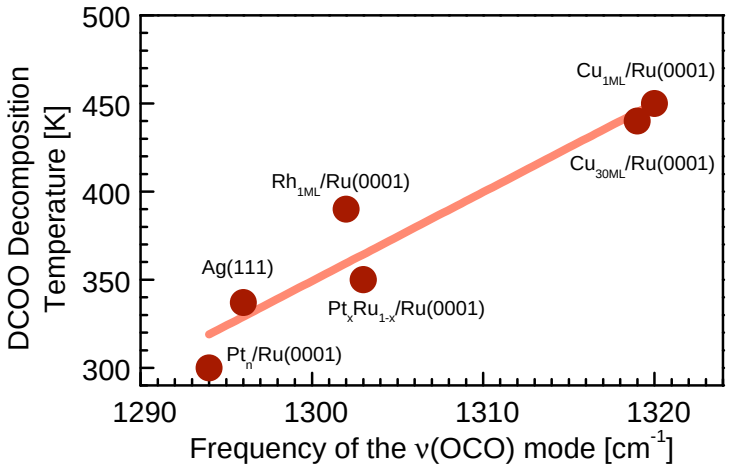

Figure 5.5: Thermal stability of $DC^{16}O^{16}O$ versus its ν(OCO) stretch frequency on various surfaces indicated in the figure. The dissociation temperature of DCOO is defined as the temperature at which the DCOO IRAS signals have decayed by 50%. Except for the values for Ag(111) [57], the plot comprises our own data.

a CD_3O intermediate. As mentioned above these reactions are possible only with preadsorbed surface oxygen. Thereby, the oxidation of either formaldehyde or methoxy is accompanied by a dehydrogenation reaction. Thus, oxygen and formaldehyde must build a compound which immediately loses a hydrogen, or formaldehyde first becomes dehydrogenated to DCO which then becomes rapidly oxidized to DCOO. Yet, the details of this mechanism must remain open as no intermediate species have been observed between methoxy/formaldehyde and formate.

A special case are O_2 covered Pt/Ru(0001) layers where methanol becomes directly converted to DCOO, i.e. without any stable intermediates. It is found that the formation of formate is not primarily promoted by dissociating O_2 as proposed by Endo et al. [44], but it is due to disordered atomic oxygen, especially at temperatures above the O_2 dissociation temperature (130 K) [Article V].

Remarkably, independent of the substrate a C_{2v} adsorption geometry of DCOO was observed. A further general property of the formate species identified on the investigated surfaces is that they always consist of one oxygen from methanol and another one due to preadsorbed oxygen as verified by isotopic labeling experiments [Articles III, V, VI].

5.5.4 Decay of Formate and CO_2 Desorption

On all investigated layers which oxidize methanol to CO_2, the reactions proceed via a stable DCOO which is found to be the precursor of the desorbing CO_2. The abstracted D atoms due to the dehydrogenation of DCOO either desorb molecularly (Cu/Ru) or react with residual surface oxygen to D_2O (Pt/Ru). Similarly, under electro-chemical conditions the oxidation of methanol over a Pt-electrode also occurs via a stable formate [146].

Interestingly, the dissociation temperature of formate and the frequency of its prominent ν(OCO) stretching mode are correlated. Specifically, the higher the dissociation temperature of DCOO, i.e. the desorption temperature of CO_2, the higher the frequency of the O-C-O stretch as depicted in Fig. 5.5. The data largely fit a straight line with an accuracy of ±20 K. This implies that on all surfaces summarized in Fig. 5.5 formate probably favors the same adsorption sites, most likely the short-bridge configuration where each oxygen atom is one-fold coordinated over a metal atom [147, 148]. For different adsorption geometries (e.g. short-bridge vs. cross-bridge) a frequency shift of around 45 cm^{-1} is expected [148]. This value is significantly higher than the scatter of the displayed data. Hence, the knowledge of the line position allows an approximate (±20 K) determination of the activation energy of DCOO to a given surface and the temperature at which CO_2 desorption is expected.

A unambiguous explanation of the correlation of the frequency of the ν(OCO) mode and the dehydrogenation temperature of DCOO cannot be given. For instance, the data cannot be expressed in therms of the simple *d*-band model. A possible contribution are the binding energies of the final reaction products. However, at this point DFT calculations concerning the binding of DCOO on metal surfaces will be helpful in order to give a clear reason for the trend observed in Fig. 5.5.

5.5.5 Formaldehyde

Besides methoxy and formate, formaldehyde is a further prominent reaction product. As mentioned above, it represents not only a stable surface intermediate and a precursor of DCOO, but it is also a possible final reaction product of the O-H bond breaking path. If D_2CO is weakly bound, as on Cu(111), it desorbs molecularly rather than undergoing further reactions.

The formation of a formaldehyde species has been observed in the presence of surface oxygen only. Furthermore, the experiments are in agreement with the expectation [140] that in the vicinity of preadsorbed O, which reduces the electron density of the substrate, formaldehyde preferably adsorbs in the η^1(O)-configuration, i.e. it binds through the oxygen atom to the surface. On O/Pt_n/Ru(0001) formaldehyde represents the main surface intermediate which eventually dissociates to CO and hydrogen. In contrast, on O/Cu/Ru(0001) only gaseous D_2CO is produced.

The intact desorption (400 K) of formaldehyde from Cu/Ru(0001) layers, as opposed to the dissociation (200 K) on Pt/Ru(0001) layers, can be explained by different binding energies of D_2CO on these surfaces. In particular, DFT calculations show that the binding energy of D_2CO on Cu(111) [29, 149] is two times lower than on Pt(111) [48, 150, 151]. Hence, at the high temperatures (400 K), at which formaldehyde is produced on Cu(111), it desorbs instantaneously. On Pt(111) D_2CO is strongly bound and additionally formed at relatively low temperatures (200 K) making it a stable surface species.

The comparison of the theoretical studies with our own data has to be handled with care as in our experiments a η^1-formaldehyde was detected; in the theoretical works which refer to

oxygen-free surfaces a η^2-formaldehyde, i.e. bound through the C and O atoms to the surface, is preferred [29, 48, 140, 149–151]. Moreover, aldehydes adsorbed in a η^2-configuration are more stable than in the η^1-configuration [140].

5.6 Strained Pt Layers

A number of experimental [68, 69, 74] and theoretical [70, 74] works have demonstrated that strain, e.g. within pseudomorphic layers, may have a significant effect on the surface reactivity due to strain induced shifts of metal *d*-bands with respect to the Fermi level [68–70]. Yet, the strain effect and the influence caused by the nearby substrate cannot be separated easily as the most metallic films, such as Cu/Ru(0001), lose their pseudomorphic structure already for the second atomic layer; for one monolayer thick films the effects due to the substrate clearly dominate [74, 86]. A possibility to separate these two contributions is provided by the system Pt_n/Ru(0001) which exhibit pseudomorphic growth up to the 5th atomic layer [74]. For such thick films (> 3 ML) the electronic effects of the substrate can be neglected. Beyond film thicknesses of 5 ML the lattice constant of the Pt layer gradually relaxes approaching the value of Pt(111).

In this context it is natural to expect that thin ($n < 5$ ML) compressed Pt_n/Ru(0001) films should behave differently referring to methanol reactions than thick ($n > 5$ ML) Pt_n/Ru(0001) layers or the Pt(111) surface. Surprisingly, the thickness of the deposited Pt film ($3 - 15$ ML) does not affect the reaction energies of the individual reaction steps within an uncertainty of ± 5 K [Article V]. Yet, the sticking probability of oxygen dramatically depends on the thickness of the deposited Pt film on Ru(0001) and consequently affects the methanol reactions indirectly [Articles IV, V]. Starting with $n = 1$ ML the sticking probability is zero and increases gradually with increasing n approaching the value of Pt(111).

Another interesting finding concerning oxygen precovered Pt_n/Ru(0001) layers is a D→H exchange of the H atoms of methanol's OH group with surface D (from methanol dehydrogenation) which leads to the desorption of CD_3OD instead of the initially adsorbed CD_3OH isotope. This behavior is due to a primary isotope effect attributed to the lower zero point energy of OD as compared to OH group. Such an isotope effect has not been observed on the other surfaces and is thus a unique property of the Pt_n/Ru(0001) layers. As this finding does not depend on n it is not due to the strain within thin pseudomorphic Pt films.

5.7 Relevance for the DMFC

The requirements of the anode material of a DMFC are a high reactivity toward the oxidation of methanol to CO_2 and a high resistance against CO poisoning. There exist a number of steady-state electrochemical studies on methanol oxidation on PtRu alloys [13–16], nano-particles [12], and Ru/Pt surfaces [14–16] performed with various techniques, such as cyclic voltammetry, mass

spectrometry and FT-IRAS. In accordance with the findings of this thesis, the electro-chemical studies [4, 8, 9, 11–16] agree that PtRu alloys are suitable as catalysts for methanol oxidation. For realistic anode potentials (0.5 V), PtRu alloys with a Ru content of $20-50\%$ has been found to oxidize methanol most efficiently [12, 13, 16]. Remarkably, this trend is also confirmed in Article VI. Even though the methanol reactions over single crystal surfaces represent a model system only, the obtained results clearly demonstrate the problems of the individual catalysts and provide a detailed overview of the reaction pathways.

Among the investigated surfaces the chemisorbed molecular or disordered atomic oxygen covered Pt_n/Ru(0001) layers ($T_{ads} = 80$ K) exhibit the highest reactivity for methanol oxidation to CO_2. However, oxygen deposited at room temperature exhibits an ordered phase [47] which hardly converts methanol to CO_2; on such layers CO formation is preferred. Furthermore, the CO desorption temperature is about 100 K higher than the one of CO_2. Similarly, ordered O layers on Cu/Ru(0001) or Pt_xRu_{1-x}/Ru(0001) are significantly less reactive than the disordered (cold deposited) layers which are stable at low temperatures only. In spite of that, the high temperature (440 K) of CO_2 desorption means that the problem of the oxygen covered Cu/Ru(0001) surfaces is a formate poisoning instead of CO poisoning. In other words the stable surface species desorb above the operation temperature of a DMFC (≈ 400 K) which is limited by the operation temperature of the proton conducting membrane.

The clean Cu and Pt surfaces are either inert toward methanol oxidation or, if first layer Ru atoms are available, they dehydrogenate methanol to a highly stable surface CO. Yet, the advantage of such layers is that the hydrogen, which is the energy provider in a DMFC, desorbs molecularly at around 350 K. On Pt_n/Ru(0001) virtually all reactively produced hydrogen atoms are removed from the surface as water due to a reaction with surface oxygen. In contrast, on the Pt_xRu_{1-x}/Ru(0001) surface alloys, hydrogen atoms from methoxy decomposition desorb molecularly rather than react with surface oxygen. In this case, however, the desorption of formaldehyde represents the major drain of hydrogen. Nevertheless, the Pt_xRu_{1-x}/Ru(0001) surface alloys with $x = 0.5 - 0.8$ are most suitable for practical use. The most stable surface species (formate, CO) remain on the surface up to about 400 K which is significantly lower than on e.g. Ru(0001).

This thesis provides a detailed picture of fundamental reaction steps and stable intermediate species of methanol reaction pathways on bimetallic Cu/Ru(0001) and Pt/Ru(0001) surfaces. Subsequently it demonstrates how to functionalize the surfaces by the variation of surface parameters, such as the sort and thickness of a deposited metal, coadsorbates, the adsorbate order and density or the composition of the surface alloy.

Chapter 6

Scientific Articles

This chapter, consisting of six scientific articles, is the main part of this thesis. A brief summary of the results is provided in Chapter 4.

6.1 Article I: Reactions of Methanol on Ru(0001)

Reactions of Methanol on Ru(0001)

Pawel Gazdzicki and Peter Jakob*

Fachbereich Physik und Zentrum für Materialwissenschaften, Philipps-Universität Marburg, Renthof 5, D-35032 Marburg, Germany

Received: October 2, 2009; Revised Manuscript Received: December 25, 2009

Fourier transform infrared absorption spectroscopy and temperature programmed desorption have been used to study the reactions of methanol (CH_3OH, CD_3OH and $CH_3{}^{18}OH$) on the clean Ru(0001) surface in the temperature range 80−600 K. It has been found that the methanol thermal evolution is initiated by a breaking of the O—H bond, forming an upright (C_{3v} symmetry) methoxy species (CH_3O). This reaction requires annealing to about 180 K and, for dense layers, proceeds in parallel to molecular desorption. At 220 K, methoxy is found to be the dominant surface species. However, its decomposition into CO + 3H already starts at this temperature, as deduced from the appearance of the ν(CO) mode of CO; that is, methoxy is stable in a narrow temperature range only. Yet, CH_3O formed at 220 K can be stabilized up to 320−340 K by means of surface site blocking through CO coadsorption. Hydrogen and carbon monoxide, the resulting reaction products from methoxy decomposition, desorb at 330−350 and 470 K, respectively. No other reaction intermediates have been identified. An entirely new interpretation is presented regarding the production of water detected in thermal desorption at about 190 K. On the basis of experiments with different methanol and oxygen isotopes, we demonstrate that it is the hydrogen of the hydroxyl group of methanol and residual surface oxygen (most likely at steps and a relict of the surface cleaning procedure with oxygen) which contributes to the formation of water. As intermixing of abstracted hydrogen with coadsorbed deuterium is found to be negligible, the hydrogen abstracted from methanol is suggested to react directly with surface oxygen, that is, without adsorbing on the surface in between. C—O bond breaking, long believed to act as the primary reaction step toward water formation, can definitely be ruled out.

Introduction

The importance of the system studied within this paper, namely, methanol (CH_3OH) and ruthenium, is related to the direct methanol fuel cell. Thanks to their high tolerance toward CO contamination, ruthenium−platinum alloys bear a high potential to be used as catalysts for the dehydration of CH_3OH. Furthermore, because of its small size and three different chemical bonds, methanol is very attractive when studying selective activations of competing reaction pathways. The mainly used experimental method, infrared absorption spectroscopy (IRAS), is particularly suitable for the identification of reaction intermediates on a surface.

In the literature, a high number of publications related to the reactions of methanol on late transition-metal surfaces can be found, for example, Ru,[1−8] Cu,[9−20] Ag,[21,22] Mo,[23,24] Rh,[25,26] Pd,[27−29] or Pt.[30−38]

Recently, it has been demonstrated that, at $T \leq 80$ K, methanol adsorbs as intact molecule on the clean Ru(0001) surface as well as on O-precovered Ru(0001).[8] This finding revised earlier work[1,3,5] dealing with the adsorption and reaction of methanol on Ru(0001) which suggested spontaneous O—H bond breaking of methanol to form methoxy, even at 80 K. Agreement, on the other hand, exists that annealing to 200−220 K leads to a dominant surface species which unequivocally has been identified as methoxy (CH_3O) with an orientation of the CO axis parallel to the surface normal.[8] Also, there is no dispute regarding the final reaction products, CO and H, formed during CH_3O decomposition at $T \geq 220$ K and which desorb at higher T. Not quite settled are discussions on processes related to the formation of water (desorbing at ∼190 K) which seems to indicate a breaking of the C—O bond in addition to O—H bond breaking leading to the formation of methoxy. This topic will be further elaborated on in this work by using isotopically labeled surface species.

By applying IRAS, Barros et al.[3,5,6] suggested a variety of reaction intermediates of methanol on Ru(0001) such as upright and tilted methoxy, as well as formaldehyde. Despite various efforts, we were, however, unable to reproduce their findings. In particular, we found no evidence for a tilted geometry of methoxy; rather, our data suggest an upright methoxy with a local C_{3v} symmetry at all coverages, and its spectral appearance agrees very well with similar results of methoxy on other surfaces such as Cu(111),[13] Cu(100),[14−17] Ag(111),[22] and Mo(110).[23,24] We are not sure whether the discrepancies to Barros et al. have to do with their different surface preparation procedure or a somewhat erroneous temperature reading in their experiments. For example, multilayer desorption occurs at 110 K in their experiments, whereas agreement exists in the literature that methanol multilayers desorb at 140−150 K (at few Kelvins-per-second heating rate).[1,2,39] Likewise, a ν(CO) mode of adsorbed CO from methanol dissociation appears already at 130 K in their spectra,[3] that is, at a temperature of about 80 K lower than that at which methoxy decomposition yields the first CO molecules in our experiments.

For Ru(0001), no theoretical works dealing with the reaction pathways of methanol have been published sofar. Yet, density-functional-theory (DFT) calculations referring to the reaction steps of methanol on other hexagonally close packed surfaces are available in the literature: on Cu(111) by Greeley and Mavrikakis[19] and on Pt(111) by Greeley and Mavrikakis,[38] as

* Corresponding author. E-mail: peter.jakob@physik.uni-marburg.de.

10.1021/jp9094722
Published on Web 01/22/2010

well as Desai et al.[37] On Cu(111), methanol is suggested to be weakly bound, and molecular desorption should be favored with respect to the various decomposition pathways. Once formed, the methoxy species represents a stable (and the most favored) reaction intermediate. Other possible intermediates are formaldehyde (H_2CO) and formyl (HCO). On the more reactive surfaces, these species might, however, be difficult to isolate because of their low barriers toward decomposition to CO and H. On Pt(111), C—H bond breaking is found to be the favored primary reaction process of adsorbed methanol as compared to the competing O—H scission, with the energy barrier for the latter being at least 25% higher than that for the former.[37,38] The species hydroxymethyl (H_2COH) or methoxy then would represent the first stable reaction intermediates. However, the barriers for both reactions are quite high, and similar to Cu(111), methanol rather desorbs than dissociates on Pt(111). This is in agreement with the experimental observation that methanol decomposition on Pt(111) occurs at steps and defects only.[34]

Interestingly, O—H bond breaking of methanol is considerably enhanced on the various Cu surfaces if surface O is present, leading to dense layers of methoxy after moderate annealing to about 300 K.[9−11,13,14] Such annealing also desorbs reactively produced water and cleans up the surface from abstracted H. On Cu(100), up to 0.5 ML of the methoxy species may be formed, leading to an ordered c(2 × 2) structure at an O precoverage of 0.25 ML.[11,12,16] A similar role of coadsorbed O to act as a promotor for methanol activation is reported for Pt,[30−33,35−38] Ag,[21,22] and Pd[27,28] surfaces.

According to IRAS experiments performed during this study, methoxy is the only stable intermediate of methanol on its way to the total dehydrogenation to CO. Yet, various thermal-desorption experiments suggested a minor reaction path starting with a C—O bond breaking and, eventually, producing water.[1,4] The calculations mentioned above did not consider C—O bond scission due to its activation barrier being over three times higher than those associated with C—H or O—H bond breaking. This constellation of barriers seems to apply for Ru(0001) as well, because our data (employing various isotopically labeled species) reveal that water formation does not involve the O of the methanol hydroxyl group. Instead, it is surface O (most likely a residue of the surface cleaning procedure) which contributes to the reactively formed water; in addition, we detected variable amounts of water contaminants in the methanol manifolds. We therefore conclude that the formation of water as a result of C—O bond breaking can definitely be ruled out for the clean Ru(0001) surface.

Experimental Methods

The measurements were performed in an UHV chamber with a base pressure $p = 6 \times 10^{-11}$ mbar. The Ru(0001) sample (10 mm diameter, 2 mm thickness, 99.999% purity) is mounted on a lq. He- or N_2-cooled cryostat, and it can be heated up to 1570 K (limited by our K-type thermocouple) with linear heating rates of 0.1−10 K/s. The used FTIR instrument is a Bruker IFS 66v with evacuable optics ($p < 1$ mbar) in order to avoid bothersome absorptions of water or CO_2. The polarized IR radiation is produced by a water-cooled blackbody source (Globar), in conjunction with a wire grid polarizer. Within this work, a liquid-nitrogen-cooled MCT (HgCdTe) detector was used, allowing for measurements in the spectral range 600−4000 cm^{-1}. IRAS spectra were taken at a resolution of 2 cm^{-1} with 1000−2000 scans coadded, unless otherwise stated. For the IR measurements, the sample was positioned in a dedicated IR cell, which contains an additional titanium sublimation pump (TSP). A uniform gas exposure is provided by a multicapillary array with individual diameters of 10 μm. The Ru(0001) sample was cleaned by Ar^+ sputtering (1.4 keV, 1 μA) and multiple O_2 dosing cycles combined with flashing the sample up to 1570 K; such annealing leaves less than 1% O on the Ru(0001) surface, as determined by XPS. Linear heating (0.01−10 K/s) to perform temperature programmed desorption (TPD) experiments was achieved by a microcomputer-controlled power supply. Thermal-desorption spectra were obtained by using a glass enclosure (Feulner cup)[40] to ensure desorption from the front face only and to enhance desorption signals in the quadrupole mass spectrometer (QMS). Quasi simultaneous collection of thermal-desorption spectra (up to 10 different masses m_i) is achieved by repeatedly scanning through the desired masses. The setting typically comprises a data-collection time of 0.2 s per data point in conjunction with a waiting period of 30 ms in advance to let the signal settle to its proper value. For each data point and mass m_i, individual temperature readings are recorded. A more detailed description of the used apparatus is given elsewhere.[8]

The methanol was cleaned by repeated freeze-and-thaw cycles. The methanol exposures are given in terms of the product of the pressure in the gas dosing system (mTorr) and the exposure time (s). Thus, the exposures are specific to the used experimental setup and can be compared with each other only. A value of 10 mTorr•s approximately leads to 10% saturation of the first layer. One monolayer (ML) is defined as the maximum amount which can be accommodated on Ru(0001) before multilayers build up.

The isotopic purity of the used molecules is 99.8% for CD_3OH, 99.5% for CH_3OD, 95% for $CH_3{}^{18}OH$, and 98.73% for $^{18}O_2$.

Results and Discussion

Main Reaction Pathway: O—H Bond Breaking. In the course of this work, several methanol isotopes ($CH_3{}^{18}OH$, CH_3OH, CH_3OD, and CD_3OH) have been used. A comparison of the respective spectra of isolated molecules adsorbed on Ru(0001) at 80 K are shown in Figure 1. It is apparent that the various modes are subject to characteristic isotopic shifts; an assignment of the vibrational modes is given in Table 1. The isotopic shifts of CH_3OH and CH_3OD were discussed in detail in a previous publication,[8] along with a discussion of the displacement patterns of the strongly coupled modes.

Figure 2 shows a contour plot of vibrational spectra describing the thermal evolution of CH_3OH multilayers adsorbed on Ru(0001) at 80 K.

Figure 2A covers the spectral range 700−1550 cm^{-1}, displaying strong bands at 740, 1048, 1130, and ∼1450 cm^{-1} at 80−140 K; they are assigned to the multilayer modes: O—H out-of-plane bending δ_{oop}(OH), C—O stretching ν(CO), CH_3 rocking $\rho(CH_3)$, and C—H bending $\delta(CH_3)$, respectively.[1,41] In Figure 2C, the $\nu(CH_3)$ modes which are in Fermi resonance with overtones of various CH_3 bending modes[13] are visible at 2800−3000 cm^{-1} (for a detailed discussion on this topic, we refer to the literature).[15,22,24] A strong ν(OH) band is positioned at 3285 cm^{-1} for the multilayer spectra at $T < 140$ K. Figure 2B covers the range of ν(CO) of on-top CO produced during CH_3O decomposition at $T > 210$ K.

At temperatures above 140 K, the multilayer modes δ_{oop} (OH) and ν(OH) vanish completely. The annealed spectra exhibit significantly smaller and narrower peaks. This observation is obviously correlated with the desorption of the methanol multilayers (mass 31 u) at 139 K[8] as depicted in the left TPD

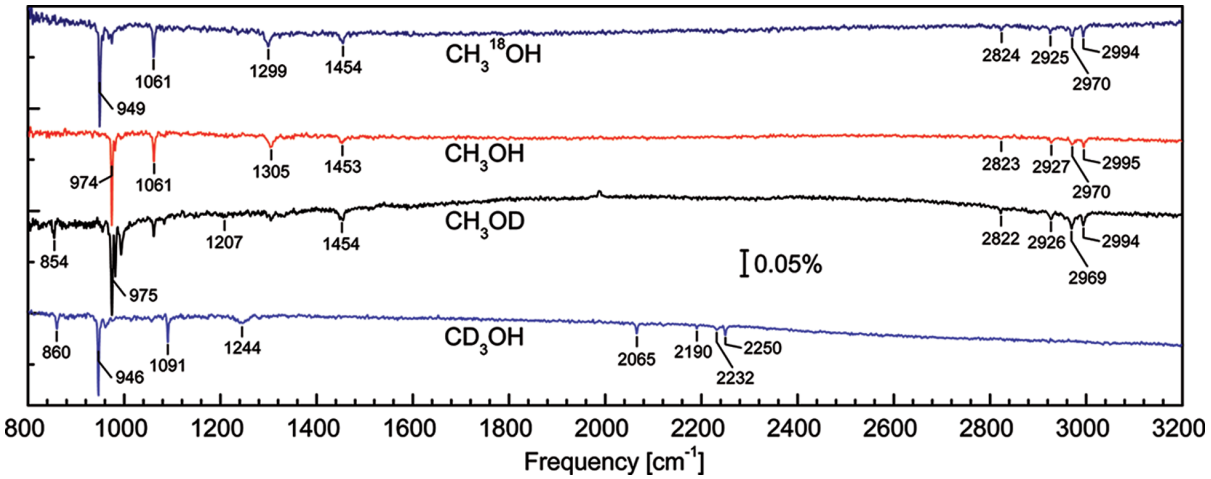

Figure 1. IRAS spectra (2 cm^{-1} resolution) of various methanol isotopes on Ru(0001) adsorbed $T = 80$ K (low-coverage spectra, representative of isolated molecules). The bands at 1061 and 1305 cm^{-1} in the spectrum of CH_3OD belong to regular methanol which is formed because of hydroxyl H ↔ D exchange at the walls of the gas dosing system.

TABLE 1: Vibrational Modes (Frequencies Given in cm^{-1}) of Different Methanol Isotopes Adsorbed on Ru(0001) at 80 K (Low-Coverage Spectra, Representative of Isolated Molecules)[a]

$CH_3{}^{18}OH$	CH_3 OH	CH_3 OD	CD_3 OH	mode assignment
949	974	975	946	ν(CO)
1061	1061	854	860	[δ(OH)+ $\rho_{ip}(CH_3)$] out of phase
1299	1305	1207	1244	[δ(OH)+ $\rho_{ip}(CH_3)$] in phase
1454	1453	1454	1091	$\delta_{as}(CH_3)$
2824	2823	2822	2065	$\nu(CH_3)$ stretching modes
2925	2927	2926	2190	in Fermi Resonance
2970	2970	2969	2232	with various
2994	2995	2994	2250	CH_3 bending modes

[a] Note that the mode notation refers to regular methanol; for other methanol isotopes, O and H have to be replaced by ^{18}O and D, respectively.

in Figure 3. The 31 u signal shows additional peaks at 170 and 216 K, consistent with available literature.[1,2] It is suggested that the former is due to desorption of weakly bound methanol molecules in the second layer or desorption out of a densely packed chemisorbed first layer (decompression peak). The third desorption peak of mass 31 u at 216 K has been attributed to the desorption out of the chemisorbed methanol layer;[8] in parallel, a gradual change in the vibrational spectra occurs at 200−220 K. Specifically, it is the reaction $CH_3OH \rightarrow CH_3O + H$ which is speeding up in this temperature range. At 220 K, the IRAS spectrum in Figure 2A,C is dominated by this methoxy species with its bands listed in Table 2. In Figure 2B, a new peak begins to grow at about 2000 cm^{-1} which is assigned to the ν(CO) stretching vibration of CO.[42] The final reaction products, H and CO, remain on the surface until they eventually desorb at 330−350 K (H_2) and 470 K (CO), see Figure 3. The desorption of CO is thereby correlated with the vanishing of the ν(CO) mode in the IRAS spectra (not shown).

The integrals of desorbed H_2 and CO in the left TPD in Figure 3 equal 0.48 and 0.10 ML, respectively. In the right TPD, these values equal 0.44 and 0.09 ML, respectively. Thus, the H:CO ratio is slightly higher than 4:1, which would be the expected value for dissociated CH_3OH with H_2 and CO as the only desorbing product species. The quantities of desorbing H_2 and CO were specified by comparing the mass 2 u and 28 u desorption signals with TPDs of a saturated Ru(0001)-(1 × 1)-H layer[43] and a Ru(0001)−CO layer with $\Theta_{CO} = 0.66$ ML.[42] In agreement with our results, the amount of CO formed during the reaction of methanol on Ru(0001) obtained by Deckert et al.[2] equals 0.09 ML.

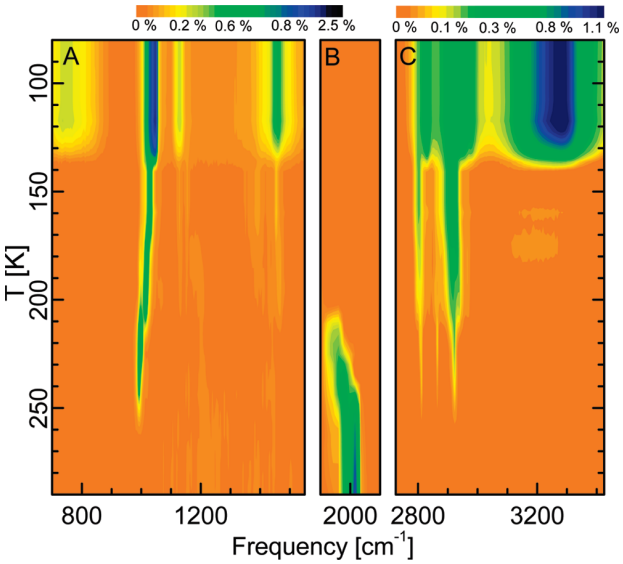

Figure 2. IRAS contour plot of CH_3OH multilayers on Ru(0001) (exposure 245 mTorr·s) after heating the sample in 20 K steps and recooling to the adsorption temperature $T = 80$ K. The spectra between each 20 K step have been interpolated in order to smooth the plotted data. The color scale is indicated at the figure top; panels A and B have the same color scale.

Even though regular IR spectra have been used to build the 3D contour plot in Figure 2, the color coding merely gives an overview of possible intermediates and transition temperatures; that is, it does not exhibit enough details in order to allow an in-depth discussion of the reactions of methanol on Ru(0001); therefore, we will additionally present individual spectra obtained after the stepwise annealing (and recooling) of small amounts of methanol (≤0.1 ML) on Ru(0001). In Figure 4, IRAS spectra of about 0.1 ML CD_3OH and CH_3OH adsorbed at 80 K are displayed for comparison. Low-coverage layers consisting of mostly isolated molecules lead to a relatively small number of narrow peaks. These are easier to discuss than dense layers with their broad bands due to interaction of the adsorbates with each other, for example, clustering of methanol molecules by building hydrogen bonds.[8] The assignment of the vibrational modes is summarized in Table 2.

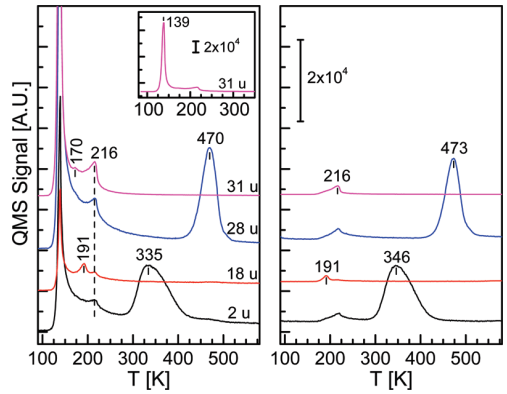

Figure 3. Multiple mass TPD spectra of CH_3OH adsorbed on Ru(0001) at 80 K. The sample was heated linearly with 1 K/s from 80 to 600 K. The initial methanol exposures were 245 mTorr•s (left panel) and 50 mTorr•s (right panel). The inset shows the full range of the mass 31 amu signal. The noise levels are below the line thickness. The signals of masses 28 u (CO), 18 u (H_2O) and 2 u (H_2) below 250 K contain contributions due to fragmentation of desorbing methanol, which was monitored by its largest ionic fragment at 31 u.

Interestingly, already a slight increase in temperature up to 100 K changes the methanol spectra significantly. A broadening of several bands and the growth of new bands can be observed, which is ascribed to methanol-cluster formation. For example, the loss in intensity of the narrow ν(CO) mode of CH_3OH (CD_3OH) at 975 cm^{-1} (947 cm^{-1}) and, in parallel, the growth of the broad ν(CO) mode at 1004 cm^{-1} (966 cm^{-1}) are signatures of this transformation.

At 120 K, the modes belonging to isolated methanol molecules have virtually vanished; that is, only H-bonded methanol clusters are present on the surface. Vibrational frequencies of these small clusters are shifted only slightly with respect to isolated methanol molecules. For CD_3OH, they are located at 900, 966, 1058, 1097, and in the range 2050−2250 cm^{-1}; for CH_3OH, various bands are observed at ∼1000, 1081, 1455, and in the range 2800−3000 cm^{-1} (see Table 2). Up to this temperature, no desorption of methanol or other species is observed as shown in the right panel of Figure 2.

The next IRAS spectrum of Figure 4 (annealing to 180 K) exhibits a mixture of vibrational modes: the majority of them is still due to clustered methanol, whereas new, narrow bands belonging to an upright oriented methoxy species (CH_3O or CD_3O) emerge. As the temperature is raised to 200−220 K, this species produced by H abstraction of the methanol OH group becomes the dominant surface compound. In parallel to its formation, molecular desorption of methanol is observed for intermediate and dense layers, starting at about 180 K and with its maximum at 215−220 K (see right panel of Figure 3); apparently, activation barriers for both processes are not too different.

Methoxy exhibits C—O stretching vibrations at 985 and 980 cm^{-1} for CH_3OH and CD_3OH, respectively. The $\delta_s(CD_3)$ and $\delta_s(CH_3)$ modes of the upright methoxy are visible in Figure 4A,C at 1074 and 1421 cm^{-1}, respectively. Additional peaks of methoxy in the spectral range of ν(CD) or ν(CH) are displayed in Figure 4B (2066, 2114, and 2163 cm^{-1}) and Figure 4D (2812, 2866, and 2926 cm^{-1}). The assignment of the vibrational modes of CD_3O and CH_3O at 220 K is summarized in Table 2. Remarkably, the $\delta_s(CD_3)$ mode of CD_3O at 1074 cm^{-1} is 10 times more intensive than the $\delta_s(CH_3)$ mode of regular methoxy (1421 cm^{-1}), which we attribute to its pronounced coupling to the (spectrally) close and intensive methoxy C—O stretching vibration at 980 cm^{-1}.

Our IR spectra provide unambiguous evidence that methoxy is adsorbed in a C_{3v} symmetry with the C—O axis parallel to the surface normal. Specifically, only one $\delta_s(CH_3)$ or $\delta_s(CD_3)$ mode is observed in the region of the methyl bending vibrations. In a tilted geometry, other modes, for example, $\delta_{as}(CH_3)$ should be visible as well. Available literature concerning methoxy on other metal surfaces[13−17,23,24] reports spectra very similar to those shown in Figure 4, and we are quite confident regarding its identity.

By using DFT cluster calculations, the geometry of methoxy on Ru(0001) has been studied by Cordeiro et al.[44] Thereby, an upright methoxy species (C_{3v} symmetry) chemisorbed on hcp and fcc hollow sites has been predicted to represent the preferred geometry, in perfect agreement with our experimental data. Likewise, a very good matching of vibrational frequencies is attained.

At 220 K, a few small features are detected in Figure 4, which are not included in Table 2: a low-energy shoulder of the ν(CO) mode at 967 cm^{-1} in Figure 4A, a small peak at 2042 cm^{-1} in Figure 4B, and the shoulder at 2912 cm^{-1} in Figure 4D. This latter feature can be explained by the presence of surface H produced by the dissociation of CH_3OH to form methoxy. Adsorbing methanol on a H-precovered Ru(0001) surface causes an increase of this peak at the expense of the 2926 cm^{-1} band and a blue shift of the ν(CO) peak to about 995−1000 cm^{-1} which matches with the position of the high-energy tail of the peak at 985 cm^{-1}. It is speculated that the features at 967 and 2042 cm^{-1} are equivalent bands of the CD_3OH isotope.

On Ru(0001), methoxy is stable in a quite narrow temperature range only. At 220 K, it is the dominant surface species; nevertheless, it already begins to decompose to form CO and H. Evidence for this decomposition ($CH_3O \rightarrow CO + 3H$) is the growth of the ν(CO) stretching vibration at about 2000 cm^{-1} (see Figure 4B). Desorption signals of accumulated H (mass 2 u) at 330−350 K and CO (mass 28 u) at 470 K (see Figure 3) support this conclusion. Our observation of a direct transition of methoxy to adsorbed CO verifies that the second step in the methanol decomposition involving an activation of the C—H bond does not produce any stable intermediates (such as formaldehyde and formyl).

The formation and decomposition of methoxy is illustrated in Figure 5 which displays the temperature-dependent integrals of characteristic peaks of methanol, methoxy, and CO. The decomposition of methoxy is completed at 260 K, where virtually all features of methoxy have vanished in the IRAS spectra and the CO band reaches its maximum intensity. The ν(CO) signal remains constant up to about 430 K and then decays because of CO desorption in accordance with the TPD spectra in Figure 3. At about 600 K, the IRAS spectrum of the clean Ru(0001) surface is reproduced.

Interestingly, methoxy can be stabilized on Ru(0001) up to 320−340 K by coadsorbing ample amounts of CO as shown in Figure 6 for the CD_3O/Ru(0001) layer. ^{13}CO was chosen instead of ^{12}CO in order to avoid overlapping of the ν(CO) peak with ν(CD) stretching modes of methoxy. One may also choose the combination CH_3O and regular CO to avoid overlapping of CO and methoxy related modes. However, CD_3O exhibits more intense and narrow peaks than CH_3O. Especially, the $\delta_s(CD_3)$ mode at 1074 cm^{-1} is significantly larger than the tiny $\delta_s(CH_3)$ band at 1421 cm^{-1} for the same methanol exposure (see bottom spectra of Figure 4); as it turned out afterward, this particular band loses most of its intensity after CO coadsorption, rendering it almost invisible, that is, useless for our quantitative analysis. Spectrum a in Figure 6 represents the initial CD_3OH layer which

TABLE 2: Vibrational Modes (Frequencies Given in cm^{-1}) of Low-Coverage Layers of CH_3OH and CD_3OH Adsorbed on Ru(0001) at 80 K[a]

CH_3OH, 80 K	$(CH_3OH)_n$, 120 K	CD_3OH, 80 K	$(CD_3OH)_n$, 120 K	CH_3O, 220 K	CD_3O, 220 K	mode assignment
975	1004	947	966	985	980	ν(CO)
1061	1081					[δ(OH)+ $\rho_{ip}(CH_3)$] out of phase
		860	900			[δ(OH)+ $\rho_{ip}(CD_3)$] out of phase
1305						[δ(OH)+ $\rho_{ip}(CH_3)$] in phase
		1243				[δ(OH)+ $\rho_{ip}(CD_3)$] in phase
				1421		$\delta_s(CH_3)$
			1058		1074	$\delta_s(CD_3)$
1454	1455					$\delta_{as}(CH_3)$
		1091	1097			$\delta_{as}(CD_3)$
2823	2813	2065	2061	2812	2066	$\nu(CH_3)/\nu(CD_3)$ stretching modes
2927	2926	2190	2197	2866	2114	in Fermi Resonance
2969	2953	2231	2218	2926	2163	with various
2994	2983	2250	2241			CH_3 or CD_3 bending modes

[a] The respective slightly shifted values obtained after annealing to 120 K are ascribed to methanol dimers or small clusters. The modes at 220 K are assigned to an upright methoxy species (CH_3O and CD_3O).

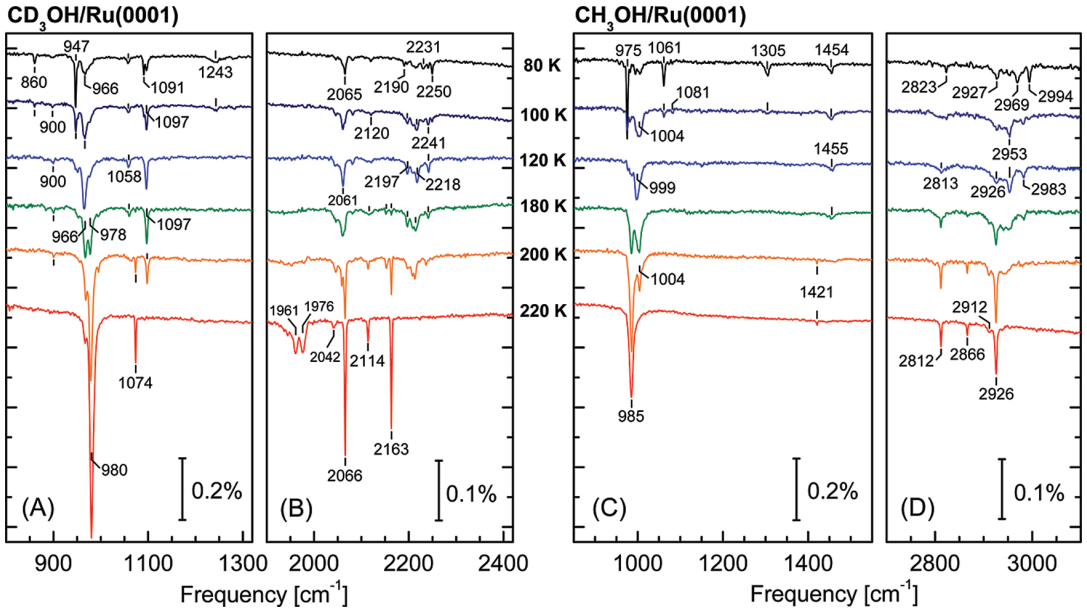

Figure 4. Thermal evolution of a subML of CD_3OH (left) and CH_3OH (right) on Ru(0001) adsorbed at 80 K (exposures ~10 mTorr·s). The sample was heated with 1 K/s to the indicated temperatures and recooled to 80 K before IRAS spectra were taken at 2 cm^{-1} resolution.

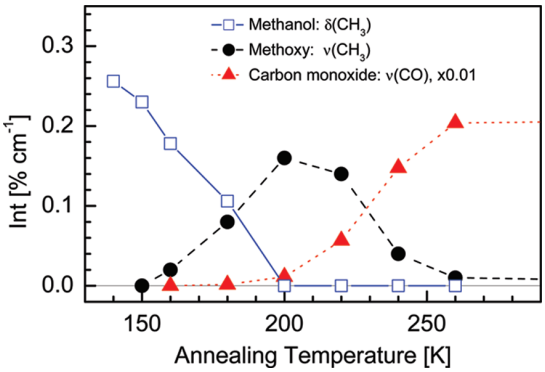

Figure 5. Integrals of the characteristic modes of methanol ($\delta_{as}(CH_3)$ at 1455 cm^{-1} (□)), methoxy ($\nu(CH_3)$ at 2812 cm^{-1} (●)), and CO (ν(CO) at ~2000 cm^{-1} (Δ)) as a function of increasing surface annealing temperature. The adsorption temperature was 80 K, and the initial exposure equals ~10 mTorr·s for the shown data set.

was heated to 220 K thereafter in order to create methoxy (spectrum b). In accordance with Figure 4, the bands at 1950−1980 cm^{-1} in spectrum b are attributed to $\nu(^{12}CO)$ of regular CO resulting from minor methoxy dissociation at 220 K. ^{13}CO was then stepwise postadsorbed until the layer was close to saturation. For spectrum c, the sample was again annealed up to 220 K before data acquisition, resulting in a resharpening of the methoxy peaks. The $\nu(^{13}CO)$ mode begins growing at 1920−1940 cm^{-1} and finally reaches 2002 cm^{-1} as shown in the inset of Figure 6. The prominent extra band at 1935 cm^{-1} in spectra c and d is attributed to $\nu(^{13}C^{18}O)$ because our ^{13}CO gas (99% ^{13}C content) also contained 11% of the $^{13}C^{18}O$ isotope. We note that the ν(CO) bands due to postadsorbed CO are identical to those arising from dissociated methoxy (not shown); that is, the local environment of both types of CO (referring to their prehistory) is the same. Because postadsorbed CO is distributed randomly across the surface, we conclude that the same applies to methoxy and its decomposition products, which rules out enhanced reaction rates at special sites, for example, steps or chemical impurities.

The overall weaker intensities of methoxy vibrational modes in the presence of CO is attributed to electronic screening.[45−47] Specifically, coadsorbed ^{13}CO causes a weakening of all CD_3O modes by about 70%, except for the $\delta_s(CD_3)$ mode at 1074 cm^{-1}

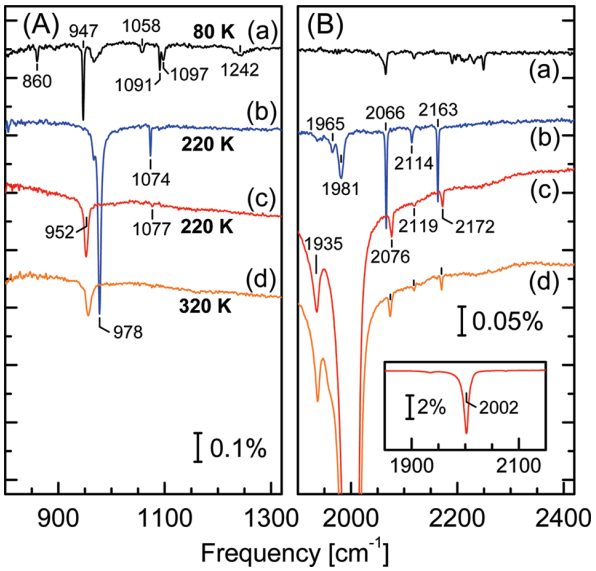

Figure 6. CD_3OH (~0.1 ML) adsorbed on Ru(0001) at 80 K. Spectrum a represents the initial CD_3OH layer at 80 K, which was annealed to 220 K with 1 K/s to obtain spectrum b, representative of methoxy (CD_3O) on Ru(0001). Spectrum c was taken after adsorbing ^{13}CO (at 80 K) and again heating up to 220 K. Before taking spectrum d, the sample was annealed to 320 K. All layers were recooled to 80 K for data acquisition. Note that the vertical scale in panel (B) is enlarged by factor two with respect to the scale in panel (A). The inset covers the full range of the $\nu(^{13}CO)$ vibrational mode of spectrum c.

which has virtually vanished. In addition, slight displacements of the various bands (chemical frequency shifts) are observed. For example, the ν(CO) mode of methoxy exhibits a red shift from 978 to 952 cm^{-1}, whereas all $\nu(CD_3)$ modes as well as the $\delta_s(CD_3)$ band shift to higher energies.

When annealing to 320 K, spectrum d causes the methoxy peaks to become smaller, most likely because of its decomposition, because CO desorption starting at about 300 K produces empty sites needed for such a process to occur. The integral of the methoxy C—O stretch mode decreases by about 15% and displays a broadened line shape; the ν(CD) modes, on the other hand, simply lose intensity without broadening. The dissimilar behavior probably is due to a less strong coupling of the CD_3 group to the substrate and, consequently, a less pronounced sensitivity to the more heterogeneous surroundings. After annealing to ≥340 K, only the C—O stretch mode of CO could be detected. A similar site-blocking effect in the primary decomposition step of methanol when using coadsorbed CO has been identified by Deckert et al.[2] by using isothermal LITD.

Figure 7 shows the relative fraction of the two main reaction pathways of methanol on Ru(0001), namely, molecular desorption and methoxy formation. Specifically, the integral of the narrow $\nu(CH_3)$ stretching mode of methoxy at 2812 cm^{-1} and the integral of mass 31 u desorption signal are plottet as a function of the amount of initially adsorbed CH_3OH at 80 K. The integral of the CH_3 stretching region (2800−3000 cm^{-1}) was taken as an approximate measure for the initial methanol coverage. For low methanol coverages up to 0.5 ML, corresponding to a methanol $\nu(CH_3)$ intensity of 10%·cm^{-1} (equivalent to 50 mTorr·s in terms of the exposure units used), the amount of produced methoxy grows linearly with the methanol exposure. For initial methanol coverages equivalent to 10−20%·cm^{-1} (Figure 7), the maximal amount of methoxy is nearly reached, and the integral of the $\nu(CH_3)$ peak of methoxy remains about constant, converging toward 0.6%·cm^{-1}. Yet,

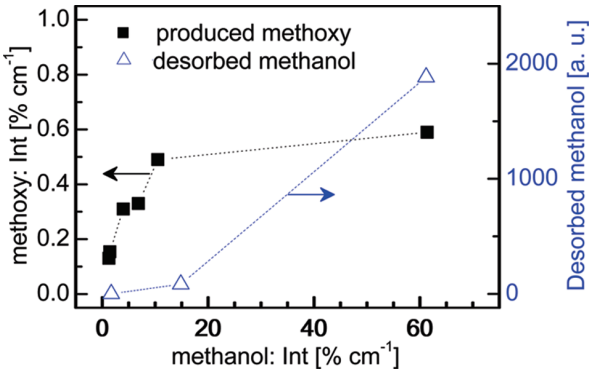

Figure 7. Integral of the 2812 cm^{-1} peak of methoxy measured after heating the sample up to 220 K (left scale) and integral of the mass 31 u thermal-desorption signal (right scale) versus the integral of the C—H stretching modes of the methyl group of intact methanol (T_{ads} = 80 K).

the quantity of desorbing methanol is still more than an order of magnitude lower than for about 2−3 ML (60%cm^{-1}). It is suggested that H abstraction of methanol to form methoxy is the preferred reaction pathway for low and intermediate methanol coverages (unless other factors such as coadsorbates interfere), whereas for thick layers, molecular desorption takes over more and more.

We also find evidence that H abstraction is inhibited for dense methanol layers, most likely because of site blocking. For example, low methanol coverages lead to slightly reduced onset temperatures (about 160 K) of methoxy formation. Vice versa, the formation of methoxy is somewhat delayed for dense methanol layers, and H abstraction proceeds in parallel to desorption of the chemisorbed CH_3OH layer at 170−180 K. Furthermore, the fact that the integral of the methoxy peak is saturated at initial methanol coverages clearly below 1 ML is consistent with the idea that methoxy formation on Ru(0001) is a self-limiting process due to accumulation of the reaction products methoxy and H; that is, once again, site blocking is effective. We note that neither extended methanol exposures at a sample temperature in the range 180−220 K nor postadsorption of methanol on a CH_3O/Ru(0001) layer at low temperature followed by annealing to 220 K could increase the amount of adsorbed methoxy. Because of the onset of methoxy dissociation at T > 220 K, higher temperatures could not be used here. According to thermal-desorption spectra of desorbing CO (see Figure 3), the maximum methoxy coverage equals about 0.1 ML with respect to Ru(0001) surface atoms. This relatively low CH_3O coverage correlates well with our lack of detecting any ordered methoxy layer by using LEED. In order to obtain additional information regarding the coverage of methanol and its reaction products, XPS data (O_{1s} core level) were taken. By using the Ru(0001)-(2 × 2)-O surface as a reference, we find that the methanol monolayer corresponds to an O-equivalent coverage of 0.4 ML, and this value reduces to 0.11 ML when annealed to 220 K to produce methoxy, corroborating the thermal-desorption data. This observation is in contrast to the much denser CH_3O layer with (2 × 2) long-range order which is attained for methanol adsorbed on a O(2 × 2) precovered Cu(100) surface[10,12,16] after annealing to 200 K to desorb reactively produced water from surface oxygen and abstracted H.

Alternative Reaction Pathways. Water, which is found to desorb at about 190 K, represents another possible reaction product of adsorbed methanol. The TPD spectra in Figure 3 show desorption peaks of mass 18 u (H_2O) at 190 K which are

not a fragment ion of desorbing methanol. In order to explain the observation of desorbing water, a C—O bond-breaking reaction was suggested by Hrbek et al.: up to 20% of adsorbed methanol has been allotted to produce water and, as side products, H and surface carbon.[1] No direct spectroscopic detection of surface water or any precursor thereof was, however, achieved, which could be due to its instantaneous desorption once it is formed. This finding has been confirmed recently by Barros et al.[3] by using IRAS, and it is in accordance with the data presented in this work.

In the course of our investigation, this topic was further looked into by performing a series of TPD measurements by using a number of isotopically labeled species and different surface-preparation procedures. The somewhat surprising outcome of these experiments was that the formation of water is primarily driven by residual surface O and in part stems from a water contamination of methanol. Specifically, we find unequivocal evidence that it is not the O of the hydroxyl group of methanol which is contained in the desorbing water molecules. Rather, the O atom of desorbing water originally is a surface oxygen species; more precisely, it represents a remnant (less than 1%, as determined by XPS) of the preceding O cleaning treatment of Ru(0001) to remove surface carbon (see Experimental Methods).

The formation of water due to the reaction of methanol with surface O exhibits unexpected behavior: (i) H atoms of the methyl group do not contribute to the formation of water, but exclusively the H from the OH group does and (ii) coadsorbed surface H/D does not contribute to the water formation. One important message from this latter finding is that no exchange of the hydroxyl-group H and surface H/D occurs, which differs substantially from the system benzene (C_6D_6) + H which displays a prominent D ↔ H exchange.[48] These observations lead us to conclude that the O—H bond breaking of methanol to form methoxy + H is an irreversible process, at least under UHV conditions. Furthermore, point (ii) demonstrates that methanol transfers its hydroxyl H atom directly to surface O (with no intermediate surface-H species). A direct transfer of hydroxyl H to surface O has likewise been suggested on Rh(111)[26] and Pd(111)[28] surfaces. These observations would be in accordance with a suggestion (based on DFT) of Desai et al.[37] that surface O on Pt(111) acts as a Brønsted base that facilitates the breaking of the O—H bond of methanol. Experimentally, the promotion of methanol O—H bond breaking by surface-O atoms is frequently observed on Cu, Ag, Pt, and Pd substrates.[9,10,14,21,22,30−33]

A very similar observation has been reported by Clay et al.[49] and Bauer et al.[50] when studying the peculiarities of water thermal desorption on Ru(0001). In their studies, they identified efficient H-atom transfer to nearby surface-O atoms as the main source of temporary dissociation of H_2O. For D_2O, this process is probably active as well, albeit at a reduced rate due to a smaller O—D bond zero-point energy,[50] which might explain the observed bold isotope effect in thermal-desorption spectra of the water/Ru(0001) system.

For moderate O coverages Θ_O, the reaction kinetics of surface H and O on Ru(0001) has been studied some time ago,[51] and thermal activations equivalent to 300−400 K were needed to initiate water formation (followed by instantaneous desorption); the removal of trace amounts of O required even higher temperatures, in conjunction with substantial H background pressures, that is, very different conditions than those encountered here, with water-formation reactions occurring at T ≈ 200 K.

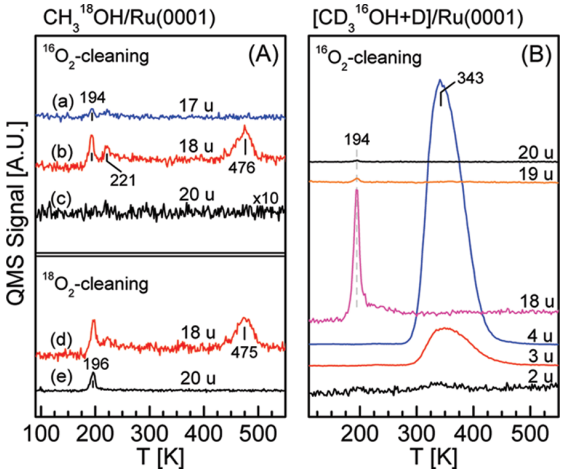

Figure 8. (A) TPD spectra (dT/dt = 1 K/s) of masses 17, 18, and 20 u of $CH_3{}^{18}OH$ adsorbed on Ru(0001) at 80 K. Spectra a−c have been measured after cleaning the sample with regular $^{16}O_2$. Note that the mass 20 u signal in spectrum c is displayed at a x10 enlarged vertical scale. Spectra d and e have been obtained after cleaning the sample with the $^{18}O_2$ isotope. (B) TPD spectra (dT/dt = 1 K/s) of $CD_3{}^{16}OH$ coadsorbed with about 0.3 ML D on Ru(0001) at 80 K after cleaning the sample with $^{16}O_2$. The increased noise levels for mass 2 and 18 u signals are due to high background levels of regular H and water compared to their less abundant isotopes. Other masses, e.g., 2, 12, 28, 30, and 31 u (33 u for $^{18}O_2$ sample cleaning) were measured simultaneously (not shown) to support our conclusions.

The spectra a−c in Figure 8A have been measured after the adsorption of $CH_3{}^{18}OH$ on a Ru(0001) surface (T_{ads} = 80 K) which was cleaned by using $^{16}O_2$. The curves represent the desorption signals of the masses 17 u (^{16}OH), 18 u ($H_2{}^{16}O$), and 20 u ($H_2{}^{18}O$), respectively. Quite clearly, a desorption peak at 194 K is found for the 18 u signal, that is, of desorbing $H_2{}^{16}O$, whereas an equivalent feature, which would indicate the desorption of $H_2{}^{18}O$, is entirely missing for mass 20 u. The peak in the 17 u curve is a fragment of regular water. The features at 221 and 476 K in the mass 18 u trace indicate ion fragments ($^{18}O^+$) of desorbing $CH_3{}^{18}OH$ and $C^{18}O$, respectively rather than $H_2{}^{16}O$. We conclude that the O atom contained in the desorbing water molecules definitely cannot stem from $CH_3{}^{18}OH$, that is, from adsorbed methanol. Note that this finding also excludes the possibility of CH_3 abstraction and transfer to surface O to produce methoxy. For Pt(110)-(2 × 1), this topic has been discussed earlier by Lee et al.,[33] and the associated C—O bond-breaking process has been discarded by means of similar isotopic mixing experiments.

Spectra b and c will now be compared to equivalent experiments with $CH_3{}^{18}OH$ adsorption after repeatedly cleaning the sample by using the $^{18}O_2$ isotope (98.73% ^{18}O, 0.59% ^{17}O). Again, the desorption traces of $H_2{}^{16}O$ (18 u) and $H_2{}^{18}O$ (20 u) were recorded (spectra d and e). Most significantly, the formation of $H_2{}^{18}O$, which is associated with the presence of surface ^{18}O, is now clearly observed. The 18 u signal ($H_2{}^{16}O$), however, definitely can stem neither from the dissociation and water-formation reaction of $CH_3{}^{18}OH$ nor from a reaction with surface ^{18}O. Therefore, it is concluded that the signal of regular water is due to water contamination in the methanol reservoir. This hypothesis is corroborated by substantial variations (up to a factor 10) of the 18 u signals at 190−195 K when adsorbing different methanol isotopes ($CH_3{}^{16}OH$, $CH_3{}^{18}OH$, $CD_3{}^{16}OH$) at similar initial methanol coverages. Furthermore, the amount of desorbing $H_2{}^{18}O$ scales directly with the amount of surface ^{18}O (prepared by flashing to different temperatures T = 1500−1570

K after surface cleaning by using $^{18}O_2$), whereas the 18 u signal remains about constant. Another possibility we took into consideration was the formation of H_2O due to a reaction of methanol with the walls of the gas dosing system. However, flooding of the gas dosing system with either $^{16}O_2$ or $^{18}O_2$ right before dosing methanol had no influence on the desorption signals of 18 and 20 u. Thus, this possibility can be discarded.

Figure 8B displays a (multimass) TPD spectrum measured after adsorbing $CD_3{}^{16}OH$ and 0.3 ML deuterium onto Ru(0001) which was cleaned by using $^{16}O_2$. When assuming for a moment that all hydrogens of the methanol molecules contribute equally and the water formation proceeds via surface hydrogen as an intermediate, one would expect to observe the desorption of masses ranging from 18 u ($H_2{}^{16}O$) to 20 u ($D_2{}^{16}O$). Moreover, the 20 u peak should be considerably larger than the peak of the 18 u signal because of the contribution of D from the methyl group of methanol as well as because of the substantial amount of preadsorbed deuterium. However, only mass 18 u exhibits a significant desorption signal at 194 K, thereby providing additional clear evidence that the desorption of water (mass 18 u) is due to a slight $H_2{}^{16}O$ contamination of methanol and $H_2{}^{16}O$ produced in the reaction of methanol and surface oxygen (^{16}O isotope). The peak of 20 u amounts to only 1% of 18 u. One may reason whether it is a $CD_3{}^{16}OD$ residue within our $CD_3{}^{16}OH$ methanol, a $CD_3{}^{16}OH + D \rightarrow CD_3{}^{16}OD + H$ exchange reaction, or a nonzero reaction rate of surface oxygen and surface hydrogen which contributes to the tiny mass 19 and 20 u signals in Figure 8B. Also, one should bear in mind that regular O contains 0.2% of the ^{18}O isotope which will contribute to the mass 20 u signal. All in all, we conclude that only H of the hydroxyl group contributes to the formation of water. Furthermore, our data demonstrate that this H atom must be transferred directly to the surface O without first adsorbing on the Ru(0001) surface; otherwise, intermixing of preadsorbed D and abstracted H would lead to an immense amount of D_2 O to be formed, which is not the case. It is therefore suggested that the water-forming reaction proceeds in the following way:

$$2CD_3{}^{16}OH + {}^{18}O_{surface} \rightarrow H_2{}^{18}O + 2CD_3{}^{16}O$$

It is quite feasible that the two hydrogenation steps of O to form water are not entirely independent because methanol has already formed small clusters at temperatures $T \approx 120$ K. Dimers or larger units will then migrate as a unit and may transfer their hydroxyl H atoms to surface O, thereby producing water. Decay of the unstable (or short-living) OH species,[51] which sofar has never been detected on Ru(0001), could be outpaced this way.

The onset of methoxy formation by means of H-atom abstraction as observed in the IRAS spectra (160−180 K) agrees favorably with water synthesis and desorption at 180−200 K. The abstraction of the H atom during methoxy formation therefore produces water when residual surface O is available or simply adsorbed H on clean Ru(0001). We note that consecutive methanol-adsorption and thermal-desorption cycles yielded less and less of the reactively produced water which is attributed to a gradual removal of surface O. Intentional O preadsorption produced by annealing an O-covered Ru(0001) surface to 1500 K (instead of 1570 K) gave $\Theta_O = 0.07$ ML, and this value could be lowered to 0.02 ML after two cycles comprising methanol adsorption at 80 K followed by annealing to 600 K. Although we did observe extra bands associated with coadsorbed O in our IR spectra (closely resembling spectra

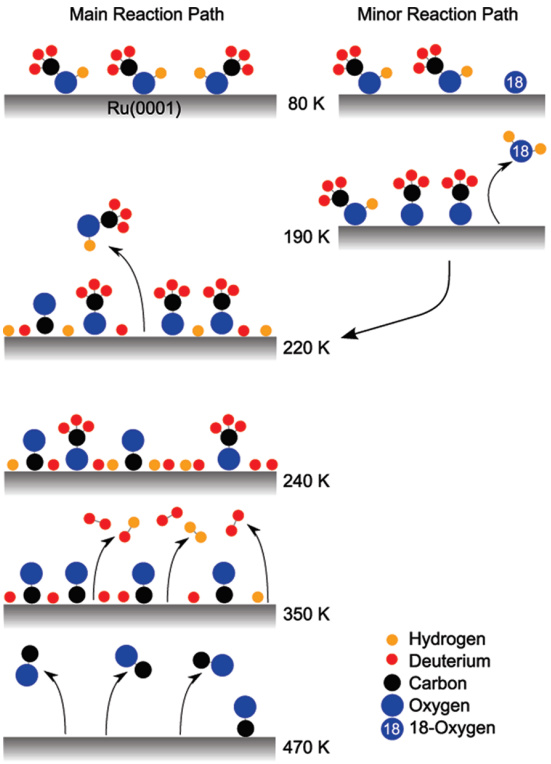

Figure 9. Schematic reaction pathway of methanol on Ru(0001). For a better discrimination of the configuration of the reaction products, the methanol isotope $CD_3{}^{16}OH$ was chosen. ^{18}O represents residual O after $^{18}O_2$ surface cleaning.

obtained for methanol adsorption onto the Ru(0001)-(2 × 2)−O surface), no new desorption species could be detected. Also, the amount of methoxy formed could not be enhanced this way. We stress that we did not find any evidence of a C residue (as invoked by Hrbek et al.)[1] in our experiments, for example, by means of subsequent O adsorption and detection of reactively produced desorbing CO (detection limit less than 0.001 ML). Removal of surface O is exclusively proceeding via the water-formation reaction pathway by means of direct H-atom transfer from the hydroxyl group.

Conclusions

In this work, the adsorption and thermal evolution of methanol on Ru(0001) has been investigated. At low temperatures (≤80 K) and low coverages (<0.1 ML), isolated methanol molecules are found. With increasing coverages or by means of slight annealing ($T \rightarrow 120$ K), methanol forms clusters, driven by the building of H bonds.[8]

The schematic presentation in Figure 9 summarizes the various processes and reactions of methanol on Ru(0001) on the basis of our observations. Not included is the desorption of weakly bound methanol at 140 and 170 K, which does not participate in the various reactions.

As the primary reaction process of chemisorbed methanol, O−H bond breaking produces methoxy and surface H at 160−180 K. For denser layers, this reaction proceeds at slightly higher T because molecular desorption of methanol is required to produce empty adsorption sites for the reaction-product species, methoxy and surface H.

At about 190 K, methanol reacts with surface O (which is a remnant of the surface-cleaning process described in the Experimental Methods) and desorbs as water. Only the H from

the OH group contributes to this reaction, and this H-atom transfer does not involve a surface intermediate; that is, it proceeds without adsorbing on Ru(0001) in between.

At 220 K, both processes come to an end, leaving upright methoxy (C_{3v} symmetry) as the dominant surface species. Even though 220 K is required to fully convert methanol to methoxy, this temperature suffices to cause methoxy decomposition, as deduced from the weak CO stretching mode growing at about 1950 cm^{-1}; that is, methoxy is found to be stable in a narrow temperature range (180−220 K) only and readily dissociates to CO + 3H, with no evidence for additional stable intermediates.

Dissociation of methoxy is completed at 260 K, leaving the reaction products H and CO behind, which desorb at about 330−350 and 470 K, respectively. A stabilization of the methoxy species up to 320−340 K can be achieved by CO coadsorption, thereby effectively taking advantage of a site-blocking effect for the methoxy dissociation products CO + 3H.

A substantial revision of existing knowledge regarding water formation during methanol thermal evolution on Ru(0001) is proposed, based on experiments using various isotopically substituted species. The commonly observed desorption of $H_2{}^{16}O$ has two different origins: (i) it is produced by H-atom transfer from the methanol hydroxyl group to surface O, or (ii) it is due to a slight water contamination in the methanol reservoir. A C−O bond-breaking process of methanol as suggested in the literature can definitely be ruled out. This conclusion is in agreement with a complete lack of methane thermal desorption and the absence of any O residue after methanol adsorption and decomposition by annealing to 600 K. The absence of C−O bond scission agrees with DFT calculations for methanol on Pt(111) which find that the energetic barrier for this reaction pathway is substantially higher (2.2 eV) than that for C−H or O−H bond breaking (0.5−1 eV).

It is left to mention that under no conditions did we observe the formation and/or desorption of methane, formaldehyd, or CO_2 in TPD for methanol on Ru(0001), either with or without coadsorbed O.

References and Notes

(1) Hrbek, J.; DePaola, R. A.; Hoffmann, F. M. *J. Chem. Phys.* **1984**, *81*, 2818.
(2) Deckert, A. A.; Brand, J. L.; Mak, C. H.; Koehler, B. G.; George, S. M. *J. Chem. Phys.* **1987**, *87*, 1936.
(3) Barros, R. B.; Garcia, A. R.; Ilharco, L. M. *J. Phys. Chem. B* **2001**, *105*, 11186.
(4) Sasaki, T.; Itai, Y.; Iwasawa, Y. *Surf. Sci.* **1999**, *443*, 44.
(5) Barros, R. B.; Garcia, A. R.; Ilharco, L. M. *Surf. Sci.* **2003**, *532*, 185.
(6) Barros, R. B.; Garcia, A. R.; Ilharco, L. M. *Surf. Sci.* **2004**, *572*, 277.
(7) Pinto, A. S. S.; Brito de Barros, R.; Cordeiro, M. N. D. S.; Gomes, J. A. N. F.; Garcia, A. R.; Ilharco, L. M. *Surf. Sci.* **2004**, *566*, 965.
(8) Gazdzicki, P.; Uvdal, P.; Jakob, P. *J. Chem. Phys.* **2009**, *130*, 224703.
(9) Wachs, I. E.; Madix, R. J. *J. Catal.* **1978**, *53*, 208.
(10) Sexton, B. A. *Surf. Sci.* **1979**, *88*, 299.
(11) Ryberg, R. *Chem. Phys. Lett.* **1981**, *83*, 423.
(12) Ryberg, R. *Phys. Rev. B* **1985**, *31*, 2545.
(13) Chesters, M. A.; McCash, E. M. *Spectrochim. Acta, Part A* **1987**, *43*, 1625.
(14) Camplin, J. P.; McCash, E. M. *Surf. Sci.* **1996**, *360*, 229.
(15) Asmundsson, R.; Uvdal, P. *J. Chem. Phys.* **2000**, *112*, 366.
(16) Mudalige, K.; Warren, S.; Trenary, M. *J. Phys. Chem. B* **2000**, *104*, 2448.
(17) Andersson, M. P.; Uvdal, P.; MacKerell, A. D., Jr. *J. Phys. Chem. B* **2002**, *106*, 5200.
(18) Sakong, S.; Groβ, A. *J. Phys. Chem. A* **2007**, *111*, 8814.
(19) Greeley, J.; Mavrikakis, M. *J. Catal.* **2002**, *208*, 291.
(20) Singnurkar, P.; Bako, I.; Koch, H. P.; Demirci, E.; Winkler, A.; Schennach, R. *J. Phys. Chem. C* **2008**, *112*, 14034.
(21) Wachs, I. E.; Madix, R. J. *Surf. Sci.* **1978**, *76*, 531.
(22) Sim, W. S.; Gardner, P.; King, D. A. *J. Phys. Chem.* **1995**, *99*, 16002.
(23) Uvdal, P.; Weldon, M. K.; Friend, C. M. *Phys. Rev. B* **1994**, *50*, 12258.
(24) Uvdal, P.; MacKerrell, A. D., Jr. *Surf. Sci.* **1997**, *393*, 141.
(25) Solymosi, F.; Berko, A.; Tarnoczi, T. I. *Surf. Sci.* **1984**, *141*, 533.
(26) Houtman, C.; Barteau, M. A. *Langmuir* **1990**, *6*, 1858.
(27) Davis, J. L.; Barteau, M. A. *Surf. Sci.* **1987**, *187*, 387.
(28) Davis, J. L.; Barteau, M. A. *Surf. Sci.* **1988**, *197*, 123.
(29) Guo, X.; Hanley, L.; Yates, J. T., Jr. *J. Am. Chem. Soc.* **1989**, *111*, 3155.
(30) Sexton, B. A. *Surf. Sci.* **1981**, *102*, 271.
(31) Akhter, S.; White, J. M. *Surf. Sci.* **1986**, *167*, 101.
(32) Wang, J.; DeAngelis, M. A.; Zaikos, D.; Setiadi, M.; Masel, R. I. *Surf. Sci.* **1994**, *318*, 307.
(33) Lee, W. T.; Thomas, F.; Masel, R. I. *Surf. Sci.* **1998**, *418*, 479.
(34) Gibson, K. D.; Dubois, L. H. *Surf. Sci.* **1990**, *233*, 59.
(35) Endo, M.; Matsumoto, T.; Kubota, J.; Domen, K.; Hirose, C. *J. Phys. Chem. B* **2000**, *104*, 4916.
(36) Sawada, T.; Liu, Z.; Takagi, N.; Watanabe, K.; Matsumoto, Y. *Chem. Phys. Lett.* **2004**, *392*, 334.
(37) Desai, S. K.; Neurock, M.; Kourtakis, K. *J. Phys. Chem. B* **2002**, *106*, 2559.
(38) Greeley, J.; Mavrikakis, M. *J. Am. Chem. Soc.* **2004**, *126*, 3910.
(39) Schwaner, A. L.; White, J. M. *J. Phys. Chem. B* **1997**, *101*, 10414.
(40) Feulner, P.; Menzel, D. *J. Vac. Sci. Technol.* **1980**, *17*, 662.
(41) Serrallach, A.; Meyer, R.; Günthard, H. H. *J. Mol. Spectrosc.* **1974**, *52*, 94.
(42) Pfnür, H.; Menzel, D.; Hoffmann, F. M.; Ortega, A.; Bradshaw, A. M. *Surf. Sci.* **1980**, *93*, 431.
(43) Feulner, P.; Menzel, D. *Surf. Sci.* **1985**, *154*, 465.
(44) Cordeiro, M. N. D. S.; Pinto, A. S. S.; Gomes, J. A. N. F. *Surf. Sci.* **2007**, *601*, 2473.
(45) Jakob, P.; Schiffer, A. *Surf. Sci.* **2009**, *603*, 1135.
(46) Ehlers, D. H.; Esser, A. P.; Spitzer, A.; Lüth, H. *Surf. Sci.* **1987**, *191*, 466.
(47) Hoffmann, F. M.; Lang, N. D.; Nørskov, J. K. *Surf. Sci. Lett.* **1990**, *226*, L48.
(48) Jakob, P.; Menzel, D. *Langmuir* **1991**, *7*, 134.
(49) Clay, C.; Haq, S.; Hodgson, A. *Chem. Phys. Lett.* **2004**, *388*, 89.
(50) Bauer, U.; Neppl, S.; Menzel, D.; Feulner, P.; Shaporenko, A.; Zharnikov, M. *Low Temp. Phys.* **2007**, *33*, 511.
(51) Koch, M. H.; Jakob, P.; Menzel, D. *Surf. Sci.* **1996**, *367*, 293.

JP9094722

6.2 Article II: Formation of Methoxy on Cu/Ru(0001) Layers

THE JOURNAL OF PHYSICAL CHEMISTRY C

ARTICLE

pubs.acs.org/JPCC

Formation of Methoxy on Cu/Ru(0001) Layers

Pawel Gazdzicki and Peter Jakob*

Fachbereich Physik und Zentrum für Materialwissenschaften, Philipps-Universität Marburg, Renthof 5, 35032 Marburg, Germany

ABSTRACT: The adsorption and reactions of methanol are of considerable technological relevance for the direct methanol fuel cell. Thereby, the stability of intermediates and activation barriers of the various reaction pathways depend critically on specific properties of the substrate materials. Deposition of ultrathin metal layers represents an established means to tune these in a controlled way. In the present study, Fourier transform infrared spectroscopy and temperature-programmed desorption have been employed to study the thermal evolution of adsorbed methanol on Ru(0001) precovered by Cu. While the full Cu monolayer turns out to be inert in the absence of coadsorbates such as oxygen, various reaction intermediates are discernible for $\Theta_{Cu} < 1$ ML. In the temperature range 220−300 K, two upright methoxy species (local C_{3v} symmetry) on uncovered Ru(0001) areas and on Cu/Ru(0001) can be distinguished. The local methoxy coverage on the Cu monolayer amounts to about 0.04 ML which is half the value found on Ru(0001). This value gradually reduces to zero for Cu coverages exceeding 0.75 ML, i.e., approaching the full Cu monolayer. Interestingly, passivation of the Ru(0001) step edges by minute amounts of Cu or Pt effectively delays decomposition of Ru-bound methoxy. Specifically, the thermal stability of methoxy on uncovered Ru(0001) increases from 220 K for clean Ru(0001) to about 300 K for a partially filled Cu/Ru or Pt/Ru layer. The thermal stability of Cu-bound methoxy is even higher, and at least 380 K is required to transform all methoxy molecules into CO and hydrogen. Our study clearly shows that a modification of the reaction kinetics on a catalytically active surface can be achieved even for minute amounts of deposited metal atoms, e.g., by passivation of various types of reaction centers. For extended monolayer films, strain and electronic effects due to the underlying substrate strongly affect stability of intermediate species, as well as their formation and decomposition kinetics.

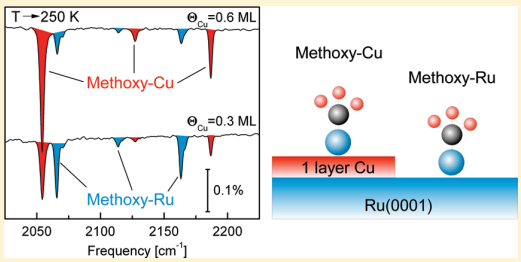

INTRODUCTION

In this paper, the thermal evolution of methanol on Cu/Ru(0001) is presented. Special emphasis is thereby devoted to the effect of preadsorbed Cu on the formation and decay of the main intermediate methoxy. Despite its seminoble character, Cu in conjunction with other materials may display exceptional catalytic behavior. For example, copper is an important component of the Cu/ZnO catalysts which is used for the synthesis of methanol from H_2, CO, and CO_2.[1]

On Ru(0001), the first Cu layer grows pseudomorphically despite a bold lattice mismatch of 5.5% with respect to Cu(111).[2] Starting from the second Cu layer, the lattice strain begins to relax. Detailed studies on the growth and properties of Cu/Ru(0001) layers were conducted by several groups.[3−7]

Since the work of Gsell et al.,[8,9] it is well-known that strain has a direct influence on adsorption energies and may significantly affect surface reactivity. A simplified picture says that surface reactivity increases with lattice expansion. DFT calculations for CO and O adsorption, as well as CO dissociation on Ru(0001), explain this effect by means of strain-induced shifts of metal d-bands with respect to the Fermi level.[10]

For thin pseudomorphic (strained) films, theory and experiments show that the electronic influence of the substrate represents the dominant contribution to surface reactivity.[11,12] This was demonstrated by calculations of Laurent et al.[12] for the adsorption of H_2 on Cu/Ru(0001) and Pd/Ru(111) as well as on artificially strained Cu(111) and compressed Pd(111). The adsorption of H_2 on normal Cu(111) and and that of Cu(111) expanded by 5.5% (i.e., matched to the Ru(0001) lattice) are both activated processes with barriers of a few hundred millielectronvolts; in agreement with expectation, the calculated surface barrier is slightly reduced (130 meV) for the latter system.[12−14] The experimentally observed sticking coefficient for Cu(111) is $\sim 10^{-5}$;[15] on monolayer Cu/Ru(0001), the activation threshold is reduced significantly to 160 meV, starting from 360 meV for Cu(111).[12] Yet, for practical applications, the sticking probability is still negligible. For Pd(111), on the other hand, DFT calculations show that H_2 adsorption is nonactivated with a sticking probability $s_{H_2} \simeq 1$. For a 2% compressed lattice constant (matched to Ru(0001)), s_{H_2} is still close to unity, yielding a negligible activation threshold of 20 meV. In contrast, a strongly activated H_2 adsorption (130 meV) is suggested for the (compressed) pseudomorphic Pd/Ru(0001) monolayer.[12] Even though the strained and normal Cu and Pd surfaces behave completely different in terms of H_2 adsorption, the pseudomorphic Cu/Ru(0001) and Pd/Ru(0001) monolayers are similar insofar as they yield similar barriers of about 150 meV leading to negligible sticking, $s_{H_2} \rightarrow 0$. Note that $s_{H_2}=0.25$ for Ru(0001).[7]

Received: August 23, 2010
Revised: December 2, 2010
Published: December 21, 2010

Interestingly, the sticking probability of oxygen s_{O_2} on pseudomorphic Cu/Ru(0001) equals ~0.6;[16] i.e., it is similar to s_{O_2} = 0.75 on the clean Ru(0001).[17] In contrast, on the clean Cu(111) surface s_{O_2} is only in the range 10^{-3}.[18] From this comparison, it becomes clear that besides strain the nearby substrate represents another source of considerable influence on the adsorptive/reactive properties of ultrathin metallic films.

The effect of these two influences on the characteristics of a pseudomorphic strained layer has been disentangled in the case of Pt/Ru(0001) where Pt grows pseudomorphically up to the fourth atomic layer.[11,19] By means of experiments and theory, it has been shown that the substrate predominantly influences the epitaxial Pt monolayer and that this contribution has largely vanished for three Pt layers, leaving the lattice strain as the dominant effect.

Consequently, for submonolayer Cu/Ru(0001), the surface reactivity regarding methanol is expected to be influenced by the residual empty Ru(0001) substrate. This does not necessarily mean that the reaction path must be the same like on Ru(0001). An example for an unexpected effect of a submonolayer Cu/Ru(0001) sample is the strong reduction of s_{H_2} on Ru(0001) even at small Cu coverages: for Θ_{Cu} = 0.1 ML sticking reduces to $s_{H_2} \sim 0.05$,[7] starting from $s_{H_2} \sim 0.25$ for clean Ru(0001). It is therefore invoked that the passivation of step edges or other types of reactive centers represents another important aspect to be considered when investigating reactivity of bimetallic surfaces.

The only study dealing with methanol on Cu/Ru(0001) has been conducted by Paul and Hoffmann[20] with HREELS (high-resolution electron energy loss spectroscopy) and TPD (temperature-programmed desorption) used as surface analytical methods. They identified a methoxy species as the primary reaction product on clean and Cu precovered Ru(0001). This finding, however, applies only to Cu layers in the submonolayer regime since Cu films at or exceeding monolayer thickness turned out to be inert in terms of methanol reactions. The lack of any reaction of methanol on the complete Cu/Ru(0001) monolayer as well as a Cu-induced stabilization of Ru-bound methoxy could indeed be verified in this work. Additionally, the superior spectral resolution of infrared absorption spectra allows us to distinguish two different methoxy species, Ru-bound as well as Cu-bound methoxy, and study their thermal evolution in detail for various Cu submonolayer coverages.

On Cu(111), experimental and theoretical works agree that no reactions of methanol occur.[21−23] Methoxy on Cu is formed only when preadsorbed oxygen is available, promoting the O−H bond breaking of methanol and leading to the removal of hydrogen from the surface by water formation and desorption.[23] Especially, the Cu(100) surface turned out to be particularly effective in this respect as high methoxy coverages up to 0.5 monolayers (ML) can be attained.[24−28] In comparison, the maximum amount of methoxy produced from methanol dissociation on the clean Ru(0001) surface is 0.1 ML.[29] On submonolayer Cu/Ru(0001) layers, the highest local Cu-methoxy coverage is 0.04 ML, i.e., about half as much as found on Ru(0001) areas. On all of these surfaces, an upright geometry of an oxygen-bound methoxy has been suggested.

EXPERIMENTAL SECTION

The experiments were performed at a base pressure $p = 6 \times 10^{-11}$ mbar. The Ru(0001) crystal has a diameter of 10 mm, a thickness of 2 mm, and a purity of 5 N. It is mounted on a liquid He or N_2 cooled cryostat, and it can be heated to 1570 K (limited by the type K thermocouple) with linear heating rates of 0.1−10 K/s. The Fourier transform infrared spectrometer (FTIRAS) is a Bruker IFS 66v with evacuable optics (p < 1 mbar). The polarized IR radiation is produced by a water-cooled blackbody source (Globar), in conjunction with a wire grid polarizer. Within this work, a LN_2-cooled MCT (HgCdTe) detector was used, allowing for measurements in the spectral ranges 600−4000 cm^{-1}. All infrared absorption (IRAS) spectra were taken at a resolution of 2 cm^{-1} with 500−2000 scans coadded. For the IRAS measurements, the sample was positioned in a dedicated IR cell, which contained an additional titanium sublimation pump. A uniform gas dosage is provided by a multicapillary array with individual diameters of ~10 μm. The sample was cleaned by Ar^+ sputtering (1.5 keV, 1 μA) and multiple O_2 dosing cycles combined with flashing the sample up to 1570 K. For the X-ray photoelectron spectroscopy (XPS) measurements, a VG Microtech Clam2 electron energy analyzer in combination with a Mg Kα source have been used. A more detailed description of the experimental setup has been published recently.[29,30]

The homemade Cu evaporator consists of a tantalum boat which encloses a melted copper wire (GoodFellow, 99.99+% purity, 1 mm diameter). For temperature control, a tantalum wire (5 mm length) inserted into the molten Cu contacts a NiCr−Ni thermocouple. Cu was evaporated at T_{Cu} = 910 K for about 45 min with a deposition rate of 4×10^{-2} ML min^{-1} at a growth temperature T_g = 700−800 K. During the evaporation time, the pressure increases up to $2-4 \times 10^{-10}$ mbar.

The Cu/Ru(0001) samples were prepared by evaporating 1.5−2 ML Cu and then flashing to 1100−1150 K to desorb redundant copper. The prepared Cu/Ru(0001) layers were characterized with IRAS by the adsorption of CO which exhibits characteristic vibrational modes at 1991, 2068, and 2074 cm^{-1} for the uncovered Ru(0001), the first Cu/Ru layer, and the second Cu/Rulayer, respectively.[31] The corresponding IRAS spectra of CO on 2 ML Cu/Ru(0001) and on 1 ML Cu/Ru(0001) are shown in panels (A) and (C) of Figure 1. Panels (B) and (D) show thermal desorption spectra of Cu from these layers.

The methanol was cleaned by repeated freeze-and-thaw cycles. The isotopic purity of CD_3OH and $CH_3{}^{18}OH$ (both from Sigma-Aldrich Co.) was 99.8% and 95%, respectively. All methanol exposures in this paper are specific to our experimental setup only, and they are given as the product of the pressure in our gas dosing system and the exposure time; the units used are mTorr·s.

In the following, a monolayer (ML) is defined as the ratio of the number of adsorbed particles to the number of substrate atoms in the topmost layer. An amount of 10 mTorr·s of methanol approximately leads to 10% saturation of the first layer and equals 0.04 ML referring to the above definition as determined by XPS measuring the integral of the O_{1s} peak and comparing the result with the one of O(2 × 2)/Ru(0001).

RESULTS AND DISCUSSION

Our database regarding the adsorption and reaction of methanol on bimetallic Cu/Ru(0001) layers comprises the isotopic species CH_3OH, $CH_3{}^{18}OH$, and CD_3OH. The data shown in this work correspond to the CD_3OH isotope only, as its vibrational modes exhibit somewhat sharper line shapes with respect to regular methanol. In addition, for the most prominent

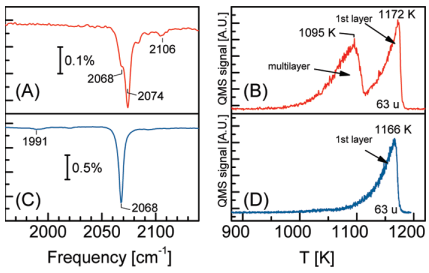

Figure 1. (A) IRAS spectrum of CO ($\Theta_{CO} \simeq 0.03$ ML) adsorbed on 2 ML Cu/Ru(0001) at 80 K. (B) TPD of 2 ML Cu/Ru(0001). The QMS signal of mass 63 u was recorded while annealing the sample with 1 K s^{-1}. (C) IRAS spectrum of CO ($\Theta_{CO} \simeq 0.07$ ML) adsorbed at 80 K on 1 ML Cu/Ru(0001) recorded before the TPD on the right was measured. (D) TPD (mass 63 u) of 1 ML Cu/Ru(0001) measured with 1 K s^{-1}.

reaction intermediate methoxy on Ru(0001), the CD_3O isotope exhibits a 10 times stronger umbrella mode $\delta_s(CD_3)$ (symmetric CD_3 stretch) than CH_3O which allows a more accurate qualitative analysis.[29] A similar observation was reported in the literature for methanol on oxidized Cu(111)[23] and Cu(100)[28] where the methoxy umbrella mode was not at all observed for CH_3O but for CD_3O only.

A series of IRAS spectra taken from equal amounts of methanol adsorbed at 80 K on Cu/Ru(0001) for different Cu coverages is presented in Figure 2. Panels (A) and (B) cover the spectral ranges 800−1550 and 1975−2400 cm^{-1}, respectively. In the range 1550−1975 cm^{-1}, no features have been identified. We have omitted an extra adsorption series here because, on Ru(0001) areas, these spectra simply reproduce the well-known behavior,[30] while on the Cu/Ru(0001) monolayer at 80 K, all vibrational modes of methanol grow in parallel not showing any change in relative intensities and in line position. Such monotonic behavior is in contrast to the adsorption of methanol on the clean Ru(0001) surface.[30] In that case, a coverage-dependent variation in vibrational frequencies and intensities is observed and has been attributed to clustering of individual methanol molecules. This conclusion is mainly based on a low methanol coverage ($\Theta_{Methanol}$) thermal annealing series starting at 30 K which exhibits clustering behavior at temperatures above about 100 K (high and intermediate methanol coverages led to clustering even at low T).

Strictly speaking, a similar scenario applies to methanol on Cu/Ru(0001); the difference is simply due to a higher lateral mobility as compared to Ru(0001). Specifically, on Cu/Ru(0001), cluster formation sets in already at 60 K (even for low methanol coverages of 0.1 ML), and therefore no isolated methanol exists at 80 K. As this paper focuses on methanol reactions which set in at $T > 180$ K, the clustering behavior will not be discussed further.

In this respect, we note that on clean Ru(0001) methanol adsorbs as isolated molecules at rather low exposures <20 mTorr·s only; i.e., the bottom spectrum in Figure 2 already corresponds to clustered methanol $(CD_3OH)_n$/Ru(0001).

In Figure 2, two sets of vibrational bands can be discriminated: the one (e.g., peaks at 1106 and 1341 cm^{-1}) scales with the Cu coverage Θ_{Cu}, while the other set (e.g., bands at 948, 1097, and 1242 cm^{-1}) is proportional to $(1 - \Theta_{Cu})$, i.e., to the remaining empty Ru(0001) area. For $\Theta_{Cu} \rightarrow 0$ ML, the spectra look more and more like those of methanol on the clean Ru(0001) surface.

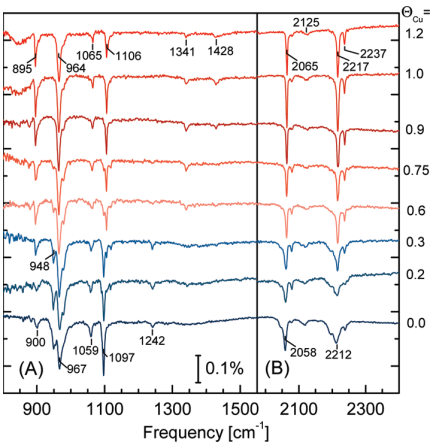

Figure 2. Series of IRAS spectra taken from CD_3OH adsorbed at T_{ads} = 80 K on various Cu precovered Ru(0001) layers. The Cu coverages in monolayers are denoted on the right side of the figure. Two different spectral regions are displayed. The amount of adsorbed CD_3OH was about 40 mTorr·s. The vertical scale is identical in panels A and B, and the spectra are offset vertically for better clarity of presentation.

These modes, on the other hand, begin to shrink with increasing Cu coverage, and they are completely gone for the complete Cu monolayer. A number of modes (located at ∼900, ∼965, and ∼1060 cm^{-1} and in the range of 2050−2250 cm^{-1}) overlap, and a clear-cut separation is not possible, even though in the limit of very low Θ_{Cu} and close to completion of the Cu monolayer distinctly different line positions are observed for the respective vibrational bands.

The feature at 1428 cm^{-1} in Figure 2 is observed for $\Theta_{Cu} >$ 0.9 ML and in a rather narrow sample temperature range (80−160 K) only, and it seems to be correlated with clustering of methanol on Cu/Ru(0001). Yet, we will refrain from giving a more explicit assignment of this peak in this work since it is irrelevant for the thermal evolution of methanol on the Cu/Ru(0001) monolayer and disappears upon slight annealing (160 K).

Clear evidence for an intact adsorption of methanol is provided by the identification of the $[\delta(OH) + \rho_{ip}(CH_3)]$ *out of phase* and $[\delta(OH) + \rho_{ip}(CH_3)]$ *in phase* modes. On Ru(0001), these modes of CD_3OH have been observed at 900 and 1243 cm^{-1}, respectively;[29] for a detailed description of these coupled normal modes, see our previous publication.[30] The corresponding peaks for CD_3OH on 1 ML Cu/Ru(0001) are located at 895 and 1341 cm^{-1} (compare the topmost and the bottom spectrum in Figure 2). An assignment of the vibrational modes is summarized in Table 1. Other prominent modes in the topmost spectrum (methanol on a complete Cu/Ru(0001) monolayer) are the $\nu(CO)$ stretching mode at 964 cm^{-1}, as well as the $\delta(CD_3)$ antisymmetric and symmetric bending modes at 1065 and 1106 cm^{-1}, respectively. The modes in the range 2050−2250 cm^{-1} are assigned to the $\nu(CD_3)$ stretching modes in Fermi resonance[32−34] with $\delta(CD_3)$ bending overtones.

Figure 3 displays IRAS spectra of the layers in Figure 2 after annealing to increasingly higher temperatures. Specifically, panels (A), (B), and (C) show spectra after heating the samples to 220, 300, and 400 K, respectively. Similar to Figure 2, two different species can be distinguished for submonolayer Cu/Ru(0001) (panel (A) of Figure 3), one being dominant at negligible Cu coverages and the other for high Θ_{Cu}. The corresponding sets of peaks are found at 980, 1074, 2065, 2114, and 2163 cm^{-1} and at

Table 1. Vibrational Modes (Frequencies Given in cm^{-1}) of Clustered Methanol (CH_3OH and CD_3OH) and CD_3O on Cu/Ru(0001) as Well as CD_3OH Clusters and CD_3O on Clean Ru(0001)[a]

CH_3OH T = 80 K Θ_{Cu} = 1.0	CD_3OH T = 80 K Θ_{Cu} = 1.0	CD_3OH T = 80 K Θ_{Cu} = 0.0	CD_3O-Cu T = 220 K Θ_{Cu} = 0.9	CD_3O-Ru T = 220 K Θ_{Cu} = 0.0	mode assignment
1005	964	967	990	980	ν(CO)
~1110	895	900			[δ(OH) + $\rho_{ip}(CD_3)$] out of phase
1378	1341	1242			[δ(OH) + $\rho_{ip}(CD_3)$] in phase
~1470	1065	1059			$\delta_{as}(CD_3)$
1435	1106	1097	1090	1074	$\delta_s(CD_3)$
2818	2065	2058	2054	2065	
2912	2125	2118	2128	2114	$\nu(CD_3)$ stretching modes in Fermi resonance with various CD_3 bending modes
2948	2217	2212	2187	2163	
2975	2237	2239			

[a] Note that the mode notation refers to CD_3OH. Θ_{Cu} is given in monolayers.

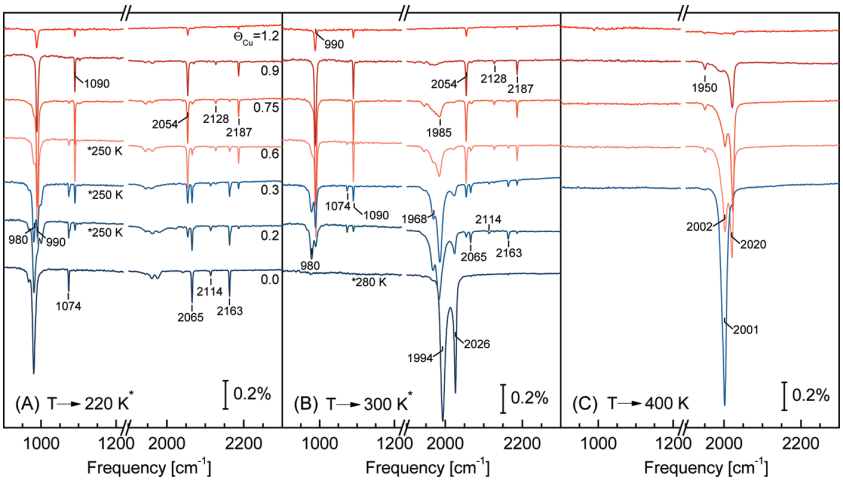

Figure 3. Set of IRAS spectra of CD_3OH (T_{ads} = 80 K) on Cu/Ru(0001) with Θ_{Cu} from 0 to 1.2 ML. The Cu coverage of each layer is denoted in panel A. The three panels refer to the layers of Figure 2, annealed (heating rate 1 K/s) to 220 K in panel (A), to 300 K in panel (B), and to 400 K in panel (C). All initial methanol coverages correspond to 40 mTorr·s, and spectra were taken at 80 K. Note that the spectra labeled with an asterisk were heated to a slightly different temperature as indicated in the figure (which resulted in negligible modifications as verified by other experimental runs). In the left out spectral range 1220−1900 cm^{-1}, no vibrational peaks are observed. For better clarity of presentation, the spectra are offset vertically. The spectra at a certain vertical position (or color) belong to identical samples heated to different temperatures.

990, 1090, 2054, 2128, and 2187 cm^{-1}, respectively. The complete assignment of these modes is also included in Table 1, referring to spectra obtained at Θ_{Cu} = 0.0 and 0.9 ML. Quite clearly, the observed spectral features act as fingerprints of an upright methoxy species (CD_3O) on uncovered Ru(0001) areas and on the Cu/Ru(0001) monolayer. CD_3O is formed due to the breaking of the hydroxyl bond of the methanol molecule. Note that the formation and characteristics of methoxy on clean Ru(0001) have been discussed elsewhere.[29] It is apparent that the spectra at high Cu coverages exhibit a signature very similar to methoxy on clean Ru(0001), i.e., typical for an oxygen-bound methoxy on a metal surface with local C_{3v} symmetry.[23,29,33] Since the detected bands mostly refer to internal vibrations of the methoxy species, the substrate effect is relatively minor and consists of slight shifts in the positions of individual modes up to about 20 cm^{-1}.

In panel (B), after annealing to 300 K, the vibrational modes assigned to CD_3O on uncovered Ru(0001) have decreased in intensity by a factor of 2−3, and additional features around 2000 cm^{-1} due to reactively produced CO appear. This observation is in accordance with expectations for methanol on the clean Ru(0001) surface (Θ_{Cu} = 0 ML) which yields complete decomposition of CD_3O to CO and D at 300 K. The detection of intact Ru-bound methoxy for Θ_{Cu} > 0.1 ML in panel (B) suggests that methoxy decomposition is catalyzed by Ru defect sites (most likely step edges) which became passivated by Cu. Interestingly, methoxy on Cu/Ru(0001) remains virtually unchanged upon annealing to 300 K. These findings are visualized in Figure 4 where integrated intensities of Cu- and Ru-bound methoxy as well as of CO from methoxy decomposition are plotted as a function of the sample annealing temperature for Θ_{Cu} = 0.6 and 0.3 ML. It is apparent that CD_3O-Cu is more stable ($\Delta T \approx 40$ K) compared to CD_3O-Ru. This result implies that the reaction pathways of Cu- and Ru-bound methoxy are decoupled; i.e., migration between these two areas is negligible.

The only peaks observed in the spectra of panel (C) (Figure 3), i.e., after annealing to 400 K, are located at about 2000 cm^{-1}, and they are assigned to CO as a result of methoxy decomposition (on the Ru(0001) as well as the Cu/Ru(0001)

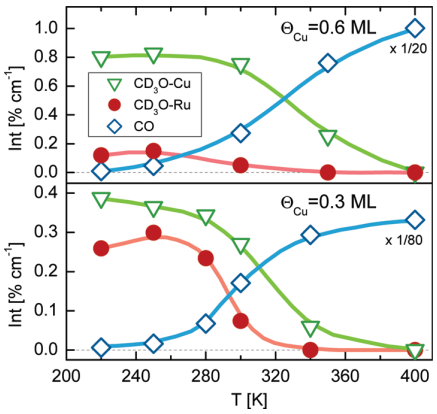

Figure 4. Temperature dependence of integrated IRAS intensities: (i) ν(CO) (located at about 2000 cm^{-1}) of the methoxy decomposition product CO (rhombus), (ii) $\delta_s(CD_3)$ mode of Cu-bound methoxy at 1090 cm^{-1} (triangle), and (iii) $\delta_s(CD_3)$ mode of Ru-bound methoxy at 1074 cm^{-1} (circle). The top and bottom panels refer to Cu coverages of 0.6 and 0.3 ML, respectively. CD_3OH was adsorbed at 80 K, heated (1 K/s) to the respective temperatures, and then recooled to 80 K before the IRAS spectra were taken. The initial methanol exposures equal 40 mTorr·s. The colored curves are guides to the eye.

areas). Since all ν(CO) vibrational bands are located well below 2070 cm^{-1}, it is concluded that all of the produced CO migrates to uncovered Ru(0001) sites, which is in agreement with the literature;[31] it is furthermore corroborated by our observation that CO is more weakly bound to monolayer Cu/Ru(0001) which desorbs already at about 230 K, i.e., at temperatures which are substantially lower than the 400 K applied in panel (C) and the 480 K required to desorb CO from Ru(0001).[36]

For the sample with Θ_{Cu} = 1.2 ML, all vibrational bands in panels (A) and (B) are strongly attenuated. This observation may indicate that the complete Cu monolayer is more or less unreactive; i.e., reversible adsorption of methanol prevails.

An enhanced reaction yield for the partially covered Cu/Ru(0001) layers strongly suggests a vital role of bare Ru(0001) areas in activating methanol and forming methoxy on Cu/Ru(0001) areas. To elucidate this hypothesis, we plotted the Cu-dependent intensities of the characteristic methoxy $\nu_s(CD_3)$ vibrational mode due to reactively produced methoxy on Ru(0001) and on Cu/Ru(0001) (see Figure 5). The various integrated intensities were taken after annealing to 300 K; in the case of methoxy on Ru(0001), an additional curve (annealing to 220 K) has been added since, at 300 K, methoxy has already started to dissociate. This is particularly true for low Cu coverages due to incomplete passivation of the more reactive Ru steps. As expected, the methoxy/Ru(0001) bands gradually lose intensity as Θ_{Cu} increases, eventually vanishing completely at about Θ_{Cu} = 1 ML. Our data therefore suggest that complete pseudomorphic Cu layers on Ru(0001) are inert with respect to methanol reactions, in agreement with the literature.[20] Similarly, reversible adsorption of methanol has been reported for Cu(111) as well.[21,22]

Yet, submonolayer Cu/Ru(0001) definitely yielded Ru as well as Cu-bound methoxy. Specifically, for methoxy on Cu/Ru(0001), the $\nu_s(CD_3)$ band initially increases linearly with Θ_{Cu}, reaches a maximum at Θ_{Cu} = 0.75 ML, and gradually decays to zero after completion of the Cu monolayer (the elimination of residual empty Ru(0001) areas actually required a little more than 1 ML of deposited copper).

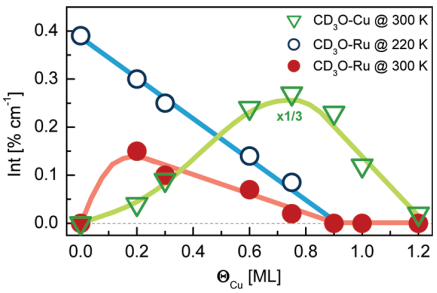

Figure 5. Integrated IRAS intensities ($\nu_s(CD_3)$ vibrational mode) of reactively produced methoxy on Ru(0001) and Cu/Ru(0001) for increasing amounts of deposited Cu (T_g = 700−800 K). The underlying spectra were obtained after adsorbing 40 mTorr·s CD_3OH at 80 K, heating (1 K/s) to 220 or 300 K, and then recooling to 80 K for data taking. The curves are guides to the eye.

To analyze the special role of Ru in the formation of methoxy on the Cu/Ru(0001) monolayer islands, the uncovered areas of Cu/Ru(0001) (Θ_{Cu} = 0.75 ML) were passivated by the preadsorption of hydrogen before exposure to methanol. This treatment resulted in a 70% reduction in the methoxy yield on Cu/Ru(0001), which led us to conclude that, indeed, residual ruthenium areas represent a key factor in the formation of Cu-bound CD_3O. In this respect, we note that at 80 K H_2 does not easily adsorb on Cu/Ru(0001).[20] The reported reduction of the H_2 sticking coefficient on Cu/Ru(0001) by at least a factor 50 with respect to clean Ru(0001) was confirmed by our TPD experiments: a sample with about 0.9 ML Cu/Ru(0001) was exposed to 16 Langmuir H_2; this amount of hydrogen is found sufficient to achieve saturation of H/Ru(0001). The integrated mass 2 u desorption signal, however, corresponded to only 4.5% of a monolayer H/Ru(0001), and for the most part it stems from residual Ru areas. For 2 ML Cu/Ru(0001), the corresponding 2 u signal equaled <1% of a monolayer.

A reaction scheme with the steps (perimeter) of Cu/Ru(0001) monolayer islands representing the key component to formation of Cu-bound methoxy (instead of residual Ru(0001) areas as discussed above) can be ruled out, as an increased number of small Cu islands on Ru terraces (sample temperature held at 80 K during 0.5 ML Cu deposition) had virtually no effect on the formation or thermal evolution of CD_3O. We conclude that methoxy is primarily formed on uncovered Ru(0001) areas and then partially migrates to Cu/Ru(0001) where it remains bound as CD_3O−Cu. Thereby, the location of Cu-bound methoxy is not restricted to the Cu/Ru boundaries but most likely extends over the entire Cu areas. This is concluded from the largely linear dependence of the CD_3O−Cu signal (Figure 5) as the Cu coverage increases. Otherwise, the CD_3O signal on Cu/Ru(0001) should saturate for rather low Θ_{Cu}, i.e., as soon as Ru step edges become decorated by a few atomic rows of Cu. The relatively small amount of CD_3O−Cu is ascribed to a poisoning of more reactive Ru(0001) sites by relatively strongly bound methanol decomposition fragments CD_3O, CO, and hydrogen which accumulate at $T \simeq$ 200 K and which start desorbing only at T > 350 K. This means that active sites for the production of additional methoxy become unavailable at an early stage of methoxy formation.

The next thing that is important to mention is that even for low methanol coverages (15 mTorr·s) and low Θ_{Cu} = 0.3 ML CD_3O−Cu decomposition nonetheless occurs at higher temperatures than CD_3O−Ru. It is concluded that the increased

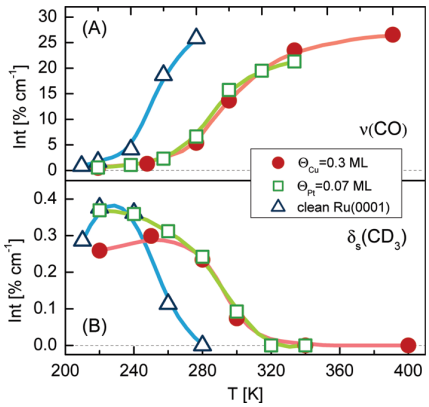

Figure 6. Temperature dependence of the integrated IRAS intensities of methoxy (panel B, $\delta_s(CD_3)$ at 1074 cm^{-1}) and its decomposition product CO (panel A, $\nu(CO)$ mode at 2000 cm^{-1}), demonstrating the passivation effect of Ru(0001) by deposited Cu or Pt. In both panels, the integrals comprise the Ru-bound methoxy and CO species only. The triangles thereby refer to a clean Ru(0001) surface and the circles and squares to Ru(0001) with predeposited copper (Θ_{Cu} = 0.3 ML, T_g = 700−800 K) and platinum (Θ_{Pt} = 0.07 ML, T_g = 700 K), respectively. CD_3OH was adsorbed at 80 K, heated (1 K/s) to the respective temperatures, and then recooled to 80 K for IRAS data taking. The initial methanol exposure on Ru(0001) was 15 mTorr·s. On Cu/Ru(0001) and Pt/Ru(0001), the corresponding value was 40 mTorr·s. We note that the methoxy decomposition on Ru(0001) does not depend on the initial methanol coverage.

stability of CD_3O−Cu is a genuine effect of the Cu/Ru(0001) monolayer rather than a consequence of a poisoning of free Ru areas by methoxy decomposition products (we originally speculated that the more reactive Ru(0001) areas might be responsible for decomposition of Ru- as well as Cu-bound methoxy). In this regard, we conclude that CD_3O−Cu decay does not involve methoxy migration onto Ru(0001) areas.

A particular interesting property of the Cu/Ru(0001) layers is the increased thermal stability of Ru-bound methoxy on these surfaces as compared to clean Ru(0001). This observation is visualized in Figure 6 where the umbrella mode $\delta_s(CD_3)$ of CD_3O−Ru and $\nu(CO)$ of CO are shown as functions of the annealing temperature for clean Ru(0001), Cu/Ru(0001) at Θ_{Cu} = 0.3 ML, and Pt/Ru(0001) at Θ_{Pt} = 0.07 ML. On clean Ru(0001), methoxy begins decomposing to CO and 3H right after it is formed;[29] i.e., CD_3O (triangles, panel (B)) decays for T > 220 K, while the CO entity (triangles, panel (A)) increases in parallel. At 280 K, methoxy decomposition is completed, and the amount of CO reaches its maximum value. In the presence of preadsorbed copper (located at Ru step edges due to our growth temperature T_g = 700 K),[4] Ru-bound methoxy (circles, panel (B)) is fully stable up to 250 K. Even at 300 K a notable fraction of intact CD_3O molecules on copper-free Ru sites are found (see the IRAS spectra in panel (B) of Figure 3).

Similar to the clean Ru(0001) surface, the amount of produced CO increases in parallel to methoxy decomposition (bullets, Figure 6(A)). It is quite evident that the decomposition of Ru-bound methoxy proceeds slower on Cu/Ru(0001) than on the clean Ru(0001) surface. These observations suggest that the process of methoxy decomposition is driven by Ru step edges and can be suppressed by Cu attachment. A similar observation is made for Ru(0001) samples with Ru step edges passivated by 0.07 ML Pt,[35] deposited at T = 700 K (squares, Figure 6).

In Figure 7, multiple mass thermal desorption spectra of CD_3OH (and various reaction products) are presented for different Cu coverages on Ru(0001). The initial methanol coverages correspond to those used in Figure 2 and Figure 3 and equal 40 mTorr·s ($\Theta_{Methanol}$ = 0.15 ML). Following methanol adsorption at 80 K, the samples were heated at 1 K/s, and the masses 2, 3, 4, 28, and 33 u were measured in parallel. To monitor CD_3OH mass, 33 u was used which is the most intensive fragment of the d_3-methanol isotope. Desorption of intact methanol molecules (33 u) thereby always occurs at 170−200 K, with a slight dependence on the Cu coverage. This peak is due to chemisorbed methanol and not due to multilayer desorption which can be observed at about 140 K for higher methanol exposures.[29] At 80−250 K, other masses with signals resembling the 33 u trace are due to ionization fragments of desorbing methanol. Desorption of the final reaction products of methanol decomposition, i.e., H_2, HD, D_2, and CO, is observed at 340−380 K (masses 2, 3, and 4 u) and at 380−480 K (mass 28 u), respectively.

For a full Cu monolayer ($\Theta_{Cu} \geq 1$ ML), the amount of desorbing CO and hydrogen is very low (Figure 7); the integral of the 28 u signal (marked blue in the figure) corresponds to less than 1% of a monolayer CO. This value increases steadily if less Cu has been deposited; e.g., a sample with 0.9 ML Cu produces 0.02 ML CO. To a good approximation, the amount of desorbing CO scales with the fractional area of non-Cu-covered Ru(0001). Since CO is the only dissociation product of methoxy on the studied surfaces, the integral coverage of this species can be derived from analyzing the amount of desorbing CO. In this respect, we note that we have not found any evidence for the presence of formaldehyde, both as a desorbing or a surface species (detection limit 10^{-3} ML). In the case of a rather low Cu coverage (Θ_{Cu} = 0.2 ML), for example, the maximum amount of methoxy (after repeated CD_3OH dosing and annealing $T \rightarrow$ 250 K) calculated from CO desorption equals 0.085 ML. This value is in good agreement (~15% variation) with the value obtained from the decomposition of methanol on the clean Ru(0001) surface (see Figure 7(D)) which is about 0.1 ML.[29] These findings corroborate our conclusions that methoxy formation from methanol proceeds until saturation of non-Cu-covered Ru(0001) areas by methanol decomposition products impedes further activation of adsorbed methanol.

For high Θ_{Cu}, the hydrogen isotopes H_2, HD, and D_2 desorb at different temperatures, namely, ~340, ~350, and ~365 K, respectively. Regular hydrogen desorbs first, and the signal is exclusively caused by the hydrogen from the initial abstraction of the hydroxyl hydrogen atom ($CD_3OH \rightarrow CD_3O + H$) which occurs at 180−200 K when methoxy is built. D_2 on the other hand exclusively stems from the dissociation of the methyl group which occurs at higher temperatures (350−360 K) when methoxy decays into CO and 3D. Consequently, the 3 u signal (HD) is due to the coexistence of H and D on the surface.

The sequential desorption of H_2, HD, and D_2 on Cu-rich samples is in contrast to the observation that all hydrogen isotopes desorb simultaneously in the absence of Cu on Ru(0001) (see the very right panel of Figure 7). We attribute this to the fact that on the clean Ru(0001) methoxy dissociates well below 300 K; i.e., the dissociation temperature of methoxy is lower than the desorption temperature of hydrogen, so that accumulation of H and D occurs until both of them desorb in common and associatively at about 370 K.

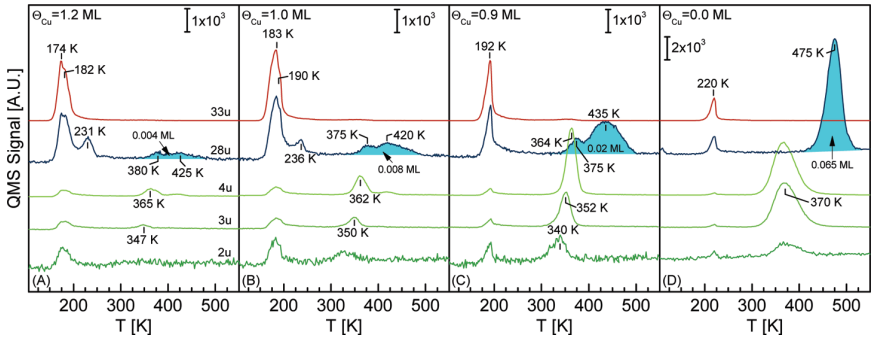

Figure 7. Multiple mass TPD spectra of CD_3OH adsorbed on different Cu/Ru(0001) layers at 80 K. The Cu coverages in panels (A), (B), (C), and (D) are equal to 1.2, 1.0, 0.9, and 0 ML, respectively. The sample was linearly heated (1 K/s) from 80 to 600 K. The initial methanol exposures were 40 mTorr·s. The 28 u desorption peaks at 350−500 K are emphasized, and they correspond to reactively produced CO (methoxy decomposition). The integral amounts (given in monolayers) are denoted in the image.

The 28 u desorption signals at ~400 K consist of two peaks for Θ_{Cu} = 1.2, 1.0, and 0.9 ML, one around 380 K and a second one at 430 K. On the clean Ru(0001) surface, CO likewise exhibits two desorption peaks for CO coverages Θ_{CO} > 0.33 ML.[36,37] Due to small Ru areas which are not covered by Cu at 1.2 ML ≥ Θ_{Cu} ≥ 0.9 ML, and in conjunction with a pronounced preference of CO for non-Cu-covered Ru(0001), the local CO coverage in these areas can likely exceed 0.33 ML and lead to the well-known double peak signature in the CO desorption trace. This hypothesis is corroborated by the relative ratio of these two 28 u peaks which changes with Cu coverage: the higher the Cu coverage, the higher the intensity of the low temperature peak, i.e., the higher the local CO coverage of the Cu-free Ru areas. For the clean Ru(0001) surface, only one CO desorption peak is observed at about 475 K.

The small amount of desorbing CO from samples with high Cu coverages, e.g., Θ_{Cu} = 0.9 ML, seems to be in contradiction to the intensive methoxy vibrational peaks in the spectra in Figure 3 and may indicate an alternative decomposition pathway avoiding CO formation. Specifically, the intensities of the CD_3 stretch and bending vibrations of Cu-bound CD_3O are comparable to those of methoxy on clean Ru(0001); hence, one would expect similar CD_3O coverages for both samples. On the sample with 0.9 ML Cu, however, the overall amount of produced methoxy, as calculated from the CO desorption signal (or deduced from the CO internal stretch intensities), equals 0.02 ML only, which is 5 times less than on the clean Ru(0001). This result was confirmed by XPS: The quantities of CD_3O and CO were determined by measuring the O_{1s} peak and comparing the result with the one of O(2 × 2)/Ru(0001) which corresponds to Θ_O = 0.25 ML. On a sample with about 0.7−0.8 ML Cu several CD_3OH dosing (T = 80 K) and annealing ($T \rightarrow$ 250 K) cycles were performed until maximum IRAS intensity of the CD_3O−Cu species was obtained. The integrated O_{1s} peak of this sample equaled 0.048 ML oxygen. From the CO thermal desorption peak (identical layer), the corresponding value was determined to be 0.043 ML confirming the XPS results. It seems, therefore, that the dynamic dipoles of Cu-bound methoxy modes are significantly stronger than equivalent ones of Ru-bound methoxy.

For a more detailed investigation of the exceptionally strong modes of the CD_3O−Cu species, we performed additional experiments with methanol adsorbed on Cu(111)/Ru(0001) ($\Theta_{Cu} \simeq$ 30 ML held at 900 K for 30 min after Cu deposition). Our IRAS, TPD, and XPS data confirm previous findings that the clean Cu(111) surface is fully inert regarding methanol reactions and that surface oxygen is needed to convert methanol to surface methoxy (which mainly desorbs as formaldehyde at 400 K).[21−23] A fractional amount of methoxy undergoes further oxidation to surface formate which eventually desorbs as CO_2 and H_2 as suggested for Cu(111) single-crystal surfaces by Russell et al.[21]

Similar to Cu/Ru(0001), we found that for a methoxy coverage of about 0.1 ML (measured with XPS) the vibrational bands of Cu-bound methoxy on multilayers Cu(111)/Ru(0001) are once again much stronger than equivalent ones of Ru-bound methoxy on clean Ru(0001). Specifically, we determined enhancement factors of ×1.5 for the methoxy C−O stretching mode, ×10 for the symmetric CD_3 bend (umbrella mode), and ×5 for the symmetric CD_3 stretching modes. These findings are consistent with our data on methoxy on Cu/Ru(0001) submonolayers. While we cannot give a convincing explanation for this increase at present, we suspect that for Cu-bound methoxy the coupling between methoxy dynamic dipoles and Cu surface states may lead to exceptionally strong dynamic charge oscillations associated with methoxy vibrational excitations. At this point, DFT calculations for normal mode intensities as well as for coupled modes (Fermi resonance) of methoxy on Cu/Ru(0001) layers would be helpful.

Kind of puzzling, the 28 u signal shows a peak at about 230 K for Cu/Ru(0001) layers close to Cu monolayer coverage (two left panels of Figure 7). The temperature matches the desorption temperature of CO from the first Cu/Ru(0001) layer;[31] in addition, these peaks correlate well with the 12 u signal (not shown), which represents a fragment of desorbing CO. Specifically, the trace of the mass 12 u signal multiplied by 10 resembles the 28 u curve for temperatures above 210 K. At lower T both curves differ because in this temperature range the mass 12 u signal represents a fragment of desorbing methanol and not of CO. The 230 K peak, however, is probably not caused by CO stemming from methanol decomposition, but it is, most likely, due to a CO contamination which was accumulated during sample positioning in front of our mass spectrometer. The amount of CO desorbing at 230 K in Figure 7 equals about 0.005 ML which matches the amount after positioning the clean sample (T = 80 K) for 1 h in the IR cell and then taking a TPD spectrum. For lower Θ_{Cu}, this peak is missing since CO will migrate to the remaining empty Ru sites, leading to desorption at about 430 K.

For completion, we like to mention another possible reaction path which involves C−O bond breaking of methanol as the primary activation step. Yet, this path can be excluded as there is no experimental evidence for this reaction which would likely produce water ($2CH_3OH \rightarrow 2OH + 2CH_3 \rightarrow H_2O + O + 2CH_3$) or methane ($CH_3OH \rightarrow OH + CH_3 \rightarrow O + CH_4$). In the TPD experiments, no 18 (H_2O), 19 (HDO), or 20 u (D_2O) signals are detected except for methanol fragments. The same applies to the TPD signal of mass 15 u (CH_3^+) which would be a major fragment of desorbing CH_4 in an experiment with CH_3OH/Cu/Ru(0001). As already mentioned above, D_2CO represents another potential intermediate species which, however, is not observed under the conditions of our experiment, i.e., in the absence of surface oxygen. Furthermore, in the IRAS spectra no indication for surface water or OH could be found. We note that in previous work on "clean" Ru(0001) H_2O formation and desorption has been traced to the reduction of residual oxygen by means of direct H transfer of methanol hydroxyl hydrogens.[29]

SUMMARY

In this work, the reaction of methanol on Cu/Ru(0001) has been studied. At low T methanol adsorbs intact on Cu/Ru(0001). Due to an enhanced mobility on Cu/Ru(0001) monolayer areas, clustering of methanol occurs at 80 K, even for low $\Theta_{Methanol}$; this is in contrast to methanol adsorption on clean Ru(0001) which exhibits isolated molecules at 80 K and low $\Theta_{Methanol}$. For a closed Cu monolayer, reversible adsorption of methanol is observed, in agreement with previous experiments on Cu/Ru(0001)[20] and with measurements of methanol on Cu(111).[21,22] For $\Theta_{Cu} < 1$ ML, annealing to 200−220 K leads to methanol desorption and, in parallel, to a decomposition via O−H bond breaking forming upright methoxy molecules. The IRAS spectra allow us to discriminate methoxy on uncovered Ru(0001) areas as well as Cu-bound methoxy. The maximum local methoxy coverage on Cu/Ru(0001) monolayer areas equals 0.04 ML which is about half the quantity formed in the course of methanol decomposition on clean Ru(0001).[29]

The formation of Cu-bound methoxy requires free Ru(0001) sites to be present. Blocking of these by preadsorbed hydrogen or by completion of the Cu/Ru(0001) monolayer effectively suppresses methoxy formation. Similarly, the methanol decomposition products hydrogen and methoxy lead to a self-poisoning of Ru(0001) with respect to methanol activation. Another passivation effect concerns the decomposition of methoxy on Ru(0001). Our data clearly demonstrate that the thermal stability of Ru-bound methoxy can be enhanced by 40−50 K by means of Cu passivation of Ru step edges. This passivation of Ru step edges could also be achieved by deposition of submonolayer amounts of Pt. Cu-bound methoxy is notably more stable than CD_3O−Ru and can be observed up to 380 K. At 350−400 K, the decomposition of virtually all methoxy is completed, leading to the final reaction products, namely, carbon monoxide and hydrogen. They desorb at 380−480 and 340−380 K, respectively. For CO we find unequivocal evidence for migration to free Ru(0001) areas in advance of desorption. Contrary to methoxy decomposition, methoxy formation is not affected by predeposited Cu or Pt, which rules out any influence of steps in the initial activation of methanol on Ru(0001).

AUTHOR INFORMATION

Corresponding Author

*E-mail: peter.jakob@physik.uni-marburg.de.

REFERENCES

(1) Chinchen, G. C.; Denny, P. J.; Jennings, J. R.; Spencer, M. S.; Waugh, K. C. *Appl. Catal.* **1988,** *36,* 1.
(2) Houston, J. E.; Peden, Z. H. F.; Blair, D. S.; Goodman, D. W. *Surf. Sci.* **1986,** *167,* 427.
(3) Christmann, K.; Ertl, G.; Shimizu, H. *Thin Solid Films* **1979,** *57,* 241.
(4) Günther, C.; Vrijmoeth, J.; Hwang, R. Q.; Behm, R. J. *Phys. Rev. Lett.* **1995,** *74,* 754.
(5) Zajonz, H.; Baddorf, A. P.; Gibbs, D.; Zehner, D. M. *Phys. Rev. B* **2000,** *62,* 10436.
(6) Calleja, F.; García-Suárez, V. M.; Hinarejos, J. J.; Ferrer, J.; Vázquez de Parga, A. L.; Miranda, R. *Phys. Rev. B* **2005,** *71,* 125412.
(7) Shimizu, H.; Christmann, K.; Ertl, G. *J. Catal.* **1980,** *61,* 412.
(8) Gsell, M.; Jakob, P.; Menzel, D. *Science* **1998,** *280,* 717.
(9) Jakob, P.; Gsell, M.; Menzel, D. *J. Chem. Phys.* **2001,** *114,* 10075.
(10) Mavrikakis, M.; Hammer, B.; Nørskov, J. K. *Phys. Rev. Lett.* **1998,** *81,* 2819.
(11) Schlapka, A.; Lischka, M.; Gross, A.; Käsberger, U.; Jakob, P. *Phys. Rev. Lett.* **2003,** *91,* 016101.
(12) Laurent, G.; Busnengo, H. F.; Rivière, P.; Martín, F. *Phys. Rev. B* **2008,** *77,* 193408.
(13) Sakong, S.; Gross, A. *Surf. Sci.* **2003,** *525,* 107.
(14) Kroes, G. J. *Prog. Surf. Sci.* **1999,** *60,* 1.
(15) Anger, G.; Winkler, A.; Rendulic, K. D. *Surf. Sci.* **1989,** *220,* 1.
(16) Otero, R.; Calleya, F.; García-Suárez, V. M.; Hinarejos, J. J.; de la Figuera, J.; Ferrer, J.; Vázquez de Parga, A. L.; Miranda, R. *Surf. Sci.* **2004,** *550,* 65.
(17) Madey, T. E.; Engelhardt, H. A.; Menzel, D. *Surf. Sci.* **1975,** *48,* 304.
(18) Habraken, F. H. P. M.; Kieffer, E. Ph.; Bootsma, G. A. *Surf. Sci.* **1979,** *83,* 45.
(19) Jakob, P; Schlapka, A. *Surf. Sci.* **2009,** *601,* 3556.
(20) Paul, J.; Hoffmann, F. M. *Surf. Sci.* **1986,** *172,* 151.
(21) Russell, J. N., Jr.; Gates, S. M.; Yates, J. T., Jr. *Surf. Sci.* **1985,** *163,* 516.
(22) Greeley, J.; Mavrikakis, M. *J. Catal.* **2002,** *208,* 291.
(23) Chesters, M. A.; McCash, E. M. *Spectrochim. Acta, Part A* **1987,** *43,* 1625.
(24) Sexton, B. A. *Surf. Sci.* **1979,** *88,* 299.
(25) Ryberg, R. *Chem. Phys. Lett.* **1981,** *83,* 423.
(26) Camplin, J. P.; McCash, E. M. *Surf. Sci.* **1996,** *360,* 229.
(27) Ryberg, R. *J. Chem. Phys.* **1985,** *82,* 567.
(28) Mudalige, K.; Warren, S.; Trenary, M. *J. Phys. Chem. B* **2000,** *104,* 2448.
(29) Gazdzicki, P.; Jakob, P. *J. Phys. Chem. C* **2010,** *114,* 2655.
(30) Gazdzicki, P.; Uvdal, P.; Jakob, P. *J. Chem. Phys.* **2009,** *130,* 224703.
(31) Hoffmann, F. M.; Paul, J. *J. Chem. Phys.* **1987,** *86,* 2990.
(32) Asmundsson, R.; Uvdal, P. *J. Chem. Phys.* **2000,** *112,* 366.
(33) Uvdal, P.; Weldon, M. K.; Friend, C. M. *Phys. Rev. B* **1994,** *50,* 12258.
(34) Herzberg, G. *Infrared and Raman Spectra of Polyatomic Molecules*; D. Van Nostrand Company: New York, 1960.
(35) Käsberger, U.; Jakob, P. *Surf. Sci.* **2003,** *540,* 76.
(36) Pfnür, H.; Feulner, P.; Menzel, D. *J. Chem. Phys.* **1983,** *79,* 4613.
(37) Kneitz, S.; Gemeinhardt, J.; Steinrück, H.-P. *Surf. Sci.* **1999,** *440,* 307.

6.3 Article III: Methanol Oxidation on Monolayer Cu/Ru(0001)

THE JOURNAL OF PHYSICAL CHEMISTRY C

ARTICLE

pubs.acs.org/JPCC

Methanol Oxidation on Monolayer Cu/Ru(0001)

Pawel Gazdzicki and Peter Jakob*

Fachbereich Physik und Zentrum für Materialwissenschaften, Philipps-Universität Marburg, Renthof 5, 35032 Marburg, Germany

Supporting Information

ABSTRACT: A versatile though straightforward process to functionalize materials is to deposit thin metal films or add coadsorbates in a controlled way. Referring to the direct methanol fuel cell, it is desirable to influence chemical reactivity and selectivity of catalysts to convert methanol to CO_2 instead of CO, which acts as a poison affecting continued and stable operation. In this study Fourier transform infrared spectroscopy, temperature-programmed desorption, and X-ray photoelectron spectroscopy were used to study the reactions of methanol (CD_3OH) on Cu monolayers on Ru(0001). In contrast to the inert pure Cu/Ru(0001) monolayer, the oxygen-covered Cu/Ru(0001) layer exhibits enhanced reactivity toward methanol activation and methoxy (CD_3O) formation. Interestingly, the ordered (2×2)-O phase is unreactive as well, which indicates a reduced affinity of this ordered array of oxygen atoms toward hydrogenation. Activation of methanol therefore occurs primarily in dilute oxygen environments or at defects and domain boundaries of the (2×2)-O phase. Under such favorable conditions (upright) methoxy is formed readily, even at low $T < 80$ K. If oxygen layers are not annealed ($T \leq 80$ K) prior to methanol admission methanol adsorbs dissociatively even at 20 K. In general, methoxy formation is accompanied by the formation of surface hydroxyl (OH) which desorbs as water at 300−350 K. Methoxy represents the main intermediate up to 350 K. Depending on the oxygen coverage, further annealing transforms methoxy into formaldehyde (D_2CO), which desorbs instantaneously, or methoxy is oxidized to formate (DCOO), which represents a stable intermediate and eventually produces (desorbing) CO_2 at $T > 450$ K. As a minority species formyl (DCO) is identified.

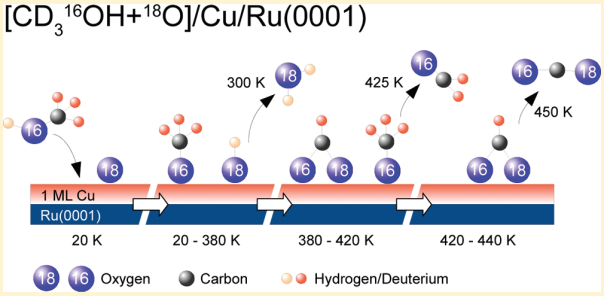

INTRODUCTION

This study concerns methanol (CD_3OH) reactions on oxygen-covered Cu_{1ML}/Ru(0001) layers ($\Theta_{Cu} \approx 1$ ML) which exhibit reactivity toward complete methanol oxidation and thus formation of CO_2. In general, catalysts that convert methanol to CO_2 are of interest with respect to the direct methanol fuel cell (DMFC) where CO poisoning of the electrodes represents a longstanding problem.[1−3]

Methanol reaction pathways eventually leading to CO_2 formation may proceed via a CO formation and oxidation reaction or the dehydrogenation of a formate (DCOO) species. Thereby formate can be formed by oxidation of formyl (DCO) or of methoxy (CD_3O) with the latter releasing excess D atoms. Because of CO poisoning, catalysts that dehydrogenate methanol without oxidation of CO may be unsuitable for practical use. Usually PtRu alloys are used as electrode materials in a DMFC.[2,3] Copper, or more specifically Cu/ZnO, is the material used for methanol synthesis from syngas.

Reactions of methanol on Ru(0001) have recently been analyzed and methoxy as well as CO were identified as the only stable surface intermediates.[4] Residual oxygen thereby is identified to induce a direct H-transfer from the methanol OH group, eventually leading to water formation and desorption removing surface oxygen. Ordered $O(2 \times 2)$ or $O(2 \times 1)$ overlayers on Ru(0001), on the other hand, turned out to be entirely unreactive under the (ultrahigh vacuum) conditions of our experiment.[4]

The growth of Cu on Ru(0001) has been investigated by a number of groups.[5−7] Their experimental results agree that a pseudomorphic first Cu layer on Ru(0001) is formed with a lattice mismatch of 5.5% (expansion) with respect to Cu(111). Starting with the second Cu layer the strain begins to relax, and the pseudomorphic structure is lost. Thick Cu layers (≈40 ML) behave virtually identical to the Cu(111) surface referring to their adsorptive properties.[8]

The reactions of methanol on various (oxygen free) submonolayer Cu/Ru(0001) surfaces have been studied previously.[9,10] The complete Cu/Ru(0001) monolayer thereby turned out to be unreactive; that is, methanol desorbs intact at 180 K rather than reacts. For $\Theta_{Cu} < 1$ ML dehydrogenation of methanol via an upright (local C_{3v} geometry) methoxy (CD_3O) intermediate, formed at 180−200 K, occurs. The final reaction products hydrogen and CO desorb at 350−370 and 380−470 K, respectively. One of the main differences between clean Ru(0001) and submonolayer Cu/Ru(0001) is that Ru step edges which play an

Received: May 20, 2011
Revised: July 15, 2011
Published: July 21, 2011

active role in methoxy decomposition become passivated by Cu, increasing the methoxy decomposition temperature from 220 K for clean Ru(0001) to 300 K.[4,10]

Similar to the clean Cu(111) surface,[11,12] preadsorbed oxygen is needed for the Cu/Ru(0001) monolayer to initiate methanol reactions via O−H bond breaking as the first step. On Cu(111), hydrogen abstracted from the methanol OH group reacts with surface oxygen and desorbs from the surface as water, leaving a methoxy[11,12] layer behind. Upon further annealing methoxy is dehydrogenated and desorbs as formaldehyde.[11] A low binding energy of formaldehyde which desorbs rather than undergoes further reaction is in accordance with theoretical predictions.[13,14] In parallel, minor CO_2 desorption was observed, suggesting methoxy oxidation and a formate intermediate.[11] Experiments and theory agree that without preadsorbed oxygen no reactions occur.[11−13]

The oxidation of methanol on oxygen-precovered Cu(100) has been investigated by Ryberg and Trenary's group.[15−18] Using IRAS, the authors identified methoxy as the major reaction intermediate which decomposes to gas phase formaldehyde and, as a minor reaction species, formate.

Similarly, methoxy which decays to gaseous formaldehyde also represents the dominant reaction intermediate of the methanol reaction path on O/Cu(110).[19,20] Remarkably, on Cu(100), Cu(110), and Cu(111) surfaces, dense oxygen layers are found to inhibit methanol activation; for Cu(110) edge sites of the oxygen islands were identified as reaction centers.[11,17−20]

Similar to Cu surfaces, preadsorbed oxygen is also needed to activate methanol on Pt(111).[21] On O/Pt(111) methanol simply decomposes to CO and H.[22,23] For submonolayer methanol coverages formaldehyde is identified as an intermediate which again decomposes to CO and H; further oxidation to formate represents a minor reaction pathway.[22] In contrast, for the O_2-covered Pt(111) surface the oxidation of methanol leads to formate as the main reaction product species.[23] In parallel, released H efficiently produces water on Pt(111), as long as surface oxygen is available; this latter process represents an unwanted drain of H atoms in the fuel cell.

To the best of our knowledge, the only work dealing with methanol on oxygen-precovered Cu/Ru(0001) layers has been published by Paul and Hoffmann.[9] In their study partial dehydrogenation of methoxy to formaldehyde desorbing at about 400 K was observed. This specific finding is in agreement with results presented in this work. Yet, neither spectroscopic evidence for surface formate nor CO_2 desorption, which could act as a hint for complete methanol oxidation, has been reported by Paul and Hoffmann.

EXPERIMENTAL SECTION

The experiments were performed at a base pressure $p = 6 \times 10^{-11}$ mbar. The sample is a Ru(0001) crystal (5 N purity) with 10 mm diameter and a thickness of 2 mm. It can be cooled with liquid He or N_2, and it can be heated up to 1570 K (limited by the type K thermocouple) with linear heating rates of 0.1−10 K/s. The quadrupole mass spectrometer (Balzers QMA112) is equipped with a Feulner cup[24] (glass enclosure) to ensure desorption from the front face of the sample only and to enhance the desorption signals. The Fourier transform infrared spectrometer (FTIR) is a Bruker IFS 66v with evacuable optics ($p < 1$ mbar). Polarized IR radiation is produced by a water-cooled blackbody source (Globar) in conjunction with a wire grid polarizer. Within this work a LN_2 cooled MCT (HgCdTe) detector was used, allowing for measurements in the spectral range 700−4000 cm^{-1}. All infrared absorption (IRAS) spectra were taken at a resolution of 2 cm^{-1} with typically 500−2000 scans coadded. For the IRAS measurements the sample was positioned in a dedicated IR cell, which contained a titanium sublimation pump. A uniform gas dosage is provided by a multicapillary array with individual diameters of ≈10 μm. The sample was cleaned by Ar^+ sputtering (1.4 keV, 1 μA) and multiple O_2 dosing cycles combined with flashing the sample up to 1570 K. For the X-ray photoelectron spectroscopy (XPS) measurements, a VG Microtech Clam2 electron energy analyzer in combination with a Mg Kα source has been used. In the following a monolayer (ML) is defined as the ratio of the number of adsorbed molecules or atoms to the number of substrate atoms in the top layer.

For Cu deposition homemade thermal evaporators were used. The typical deposition rates were ≈0.1 ML min^{-1} at a growth temperature T_g = 700−800 K. During the evaporation time the pressure increases up to $(2-4) \times 10^{-10}$ mbar. A more detailed description of the experimental setup has been published recently.[4,25] The Cu/Ru(0001) monolayer samples were prepared by evaporating 1.5−2 ML Cu and then flashing to 1100−1150 K to desorb redundant copper. The prepared Cu/Ru(0001) monolayers were characterized by measuring the ν(CO) mode of adsorbed CO with IRAS.[10] The error of the Cu coverage is estimated to be 5%. In our recent paper the preparation of the Cu/Ru(0001) layers has been described in detail.[10]

Methanol was cleaned by repeated freeze-and-thaw cycles. The isotopic purity of CD_3OH and $CH_3{}^{18}OH$ was 99.8% and 95%, respectively. All methanol exposures in this paper are specific to our experimental setup only, and they are given as the product of the pressure in our gas dosing system and the exposure time; the units used are mTorr·s. 10 mTorr·s of methanol approximately leads to 10% saturation of the first layer and equals 0.04 ML referring to the above definition as determined by XPS (integral of the O_{1s} peak) and comparing the result with O(2 × 2)/Ru(0001) (Supporting Information). Accurate O(2 × 2)/Ru(0001) layers with Θ_O = 0.25 ML were prepared according to Koch et al.[26] The oxygen coverages, Θ_O, on Cu/Ru(0001) have been determined analogous by measuring the O_{1s} peak by means of XPS; errors in the given values are estimated to ±10%.

The data shown in this work comprise the CD_3OH isotope only, as its vibrational modes exhibit somewhat sharper line shapes with respect to regular methanol (see Supporting Information). In addition, CD_3O (methoxy) on Ru(0001) exhibits a 10 times stronger umbrella mode $\delta_s(CD_3)$ (symmetric CD_3 stretch) than CH_3O, which allows a more accurate quantitative analysis.[4] A similar observation was reported in the literature for methanol on oxidized Ag(111),[27] Cu(111),[12] and Cu(100)[28] where the umbrella modes were not at all observed for CH_3O but for CD_3O only.

RESULTS AND DISCUSSION

As it will turn out in the course of this study, oxygen-free Cu_{1ML}/Ru(0001) and the well-ordered (2 × 2)-O phase on this substrate are more or less unreactive with respect to methanol activation. This is why the majority of presented data refer to intermediate oxygen coverages. Another important aspect will be whether the oxygen layers have been annealed (to induce at least

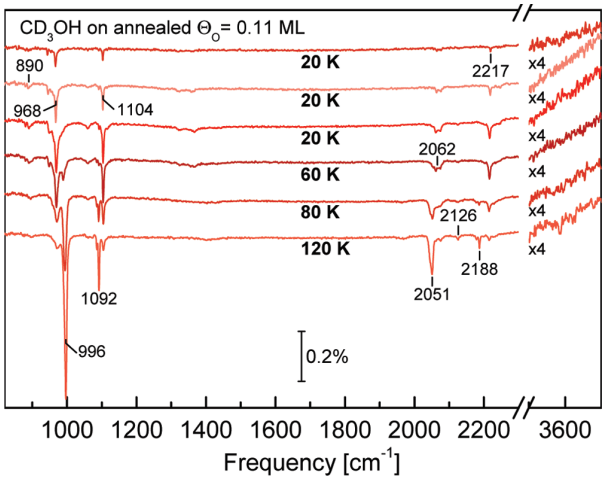

Figure 1. Thermal evolution of infrared absorption spectra of CD_3OH adsorbed on $O/Cu_{1ML}/Ru(0001)$ (Θ_O = 0.11 ML, annealed to 600 K). Initial methanol exposures (T_{ads} = 20 K) amount to 10, 20, and 40 mTorr·s. After annealing to the indicated temperatures the sample has been recooled to 20 K for data collection. The spectra are offset vertically for better clarity of presentation.

Table 1. Vibrational Modes (Frequencies in cm^{-1}) of $CD_3{}^{16}O$ and $CH_3{}^{16}O$ on $O/Cu_{1ML}/Ru(0001)$ and on Clean $Cu_{1ML}/Ru(0001)$[10] [a]

O/Cu/Ru(0001)		Cu/Ru(0001)		
CD_3O	CH_3O	CD_3O	CH_3O	mode
1001	1025	990	1013	ν(CO)
1094		1090		$\delta_s(CD_3)$
2050	2801	2054	2813	$\nu(CD_3)$ stretching modes
2126	2875	2128	2880	in Fermi resonance
2187	2917	2187	2915	with various $\delta(CD_3)$

[a] The quoted line positions deviate slightly from those in Figure 1 as they were derived from layers annealed to 300 K; in addition, coadsorbed oxygen may lead to slight shifts in line positions. Note that the mode description and notation refers to CD_3O.

partial ordering) in advance of methanol adsorption or whether methanol has been admitted onto nonannealed, disordered $O/Cu_{1ML}/Ru(0001)$. Molecular adsorbed (chemisorbed) oxygen species could not be identified even at 20 K.

Methanol on Ordered Oxygen Layers. *Adsorption and Initial Activation.* In this study, oxygen has been generally adsorbed at low T (20−80 K); ordered oxygen layers were achieved by annealing the sample to 600 K. Below 350 K only Ru spots were observed with LEED. Between 350 and 450 K a (2 × 2) LEED overstructure appeared (see Supporting Information). Using LEED and STM, the structure of oxygen layers on $Cu_{1ML}/Ru(0001)$ has been investigated by Ammer et al.,[29] and a complex $\begin{pmatrix}3&0\\2&4\end{pmatrix}$-O structure has been found after the Cu/Ru(0001) monolayers have been exposed to ≈100 langmuirs of O_2 at 520 K. In our case moderate oxygen exposures up to 15 langmuirs were used, leading to the simpler (2 × 2)-O superstructure.

IRAS spectra monitoring the adsorption and the initial reaction step of methanol on 0.11 ML oxygen on 1 ML Cu/Ru(0001) are presented in Figure 1. Increasing amounts of methanol were adsorbed at 20 K and then heated as indicated in the figure before recooling for data acquisition. At 20 K CD_3OH adsorbs intact very much the same as on Ru(0001)[4,25] or Cu/Ru(0001)[10] at 80 K. Unlike these system, however, the initial activation of methanol occurs well below LN_2 cooling temperatures (80 K). Specifically, we identified an O−H bond breaking leading to the formation of methoxy already at 60 K.

The vibrational modes providing unambiguous evidence for methanol dissociation at 60 K are those associated with the methoxy species (CD_3O), the most prominent one being the ν(CO) mode at 995 cm^{-1}. At 80 K weaker methoxy peaks at 1092 and 2188 cm^{-1} can be recognized as well. At about 120 K all peaks of methoxy are clearly visible at 996, 1092, 2051, 2126, and 2188 cm^{-1}; they are assigned to the ν(CO) stretch, $\delta_s(CD_3)$ symmetric bend, and $\nu(CD_3)$ stretching modes in Fermi resonance[30,33,34] with various CD_3 bending modes (see Table 1). The spectral signature fits well to an upright methoxy occupying 3-fold hollow sites and with its C−O axis oriented normal to the surface, as observed on Cu(111) and on various transition metal surfaces.[4,10,12,27,30−32] In parallel to the growth of methoxy vibrational features the original bands indicative of intact methanol fade away. On the clean Ru(0001) surface methoxy formation requires much higher temperatures (about 200 K). This points at a significantly lower barrier for methanol decomposition on the oxygen-precovered Cu/Ru(0001) monolayer. The abstracted H atoms react with surface oxygen to O−H which becomes clearly visible at T > 120 K: in the spectrum at 120 K a tiny peak evolves at 3590 cm^{-1} which we take as a clear indication for the presence of an OH species.

In Figure 2, IRAS spectra of CD_3OH adsorbed at 80 K on $O/Cu_{1ML}/R(0001)$ are displayed. The initial oxygen coverages in panels A and B are 0.04−0.05 and 0.2−0.25 ML, respectively. In the following these layers will be called Θ_O^{low} and Θ_O^{high} as they are representative of two dissimilar reaction pathways. It is apparent that in both cases a mixture of intact methanol (spectral signature according to Figure 1 and Table 1) and its dissociation product methoxy is present at low $T \approx$ 80 K.

Annealing to 200 K leads to characteristic changes in the IRAS spectra in both panels. For Θ_O^{low} and Θ_O^{high} the vibrational bands of methoxy represent the dominant features in the spectra. Yet, the thermal evolution proceeds distinctly different for the two oxygen precoverages of panels A and B, as will be outlined in the following.

For low Θ_O (panel A) an additional feature at 3622 cm^{-1} is observed which is assigned to the ν(OH) stretching mode of surface hydroxyl (OH). It exhibits maximum intensity at 250 K and then decreases gradually as the annealing temperature increases further, until it is completely gone at 350 K as depicted in Figure 3A. Alternative assignments such as the O−H vibration of methanol can be excluded as the respective O−H stretch mode is located at about 3500 cm^{-1} for adsorbed isolated methanol (on the Ru(0001) surface) and at about 3200 cm^{-1} for methanol clusters and multilayers.[25] Our interpretation is further supported by the detection of an equivalent band, slightly shifted in frequency, when regular surface oxygen is replaced by ^{18}O. Preadsorption of a mixture of ^{16}O and ^{18}O then produces vibrational bands at 3622 and 3611 cm^{-1} (see inset of panel A) which are assigned to the $\nu(^{16}OH)$ and $\nu(^{18}OH)$ modes of the two hydroxyl isotopes. The derived $^{16}O \leftrightarrow {}^{18}O$ isotopic shift factor of 1.00305 agrees with expectations for isolated OH, giving 1.0033.

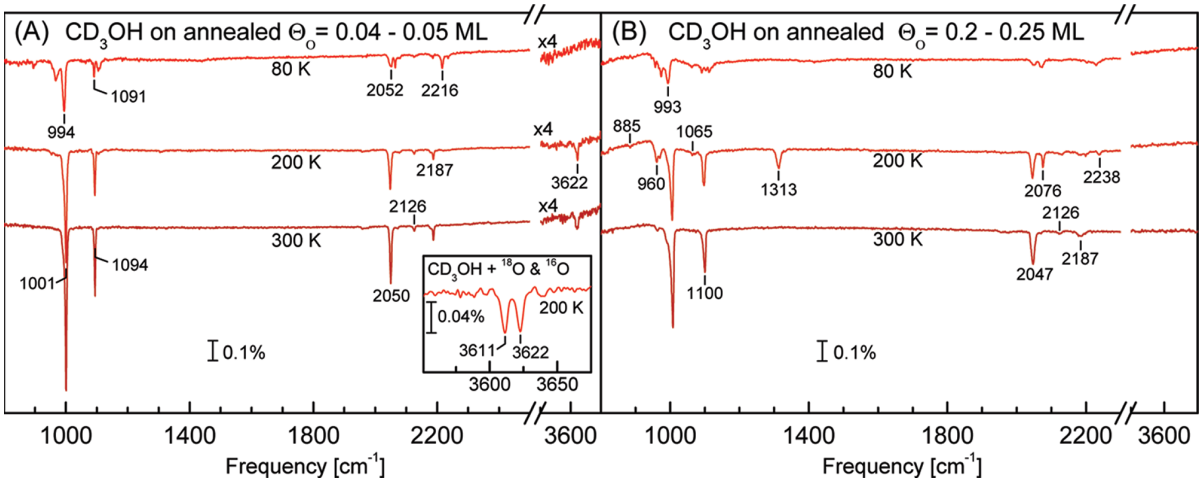

Figure 2. IRAS spectra of CD_3OH adsorbed at T_{ads} = 80 K on annealed $O/Cu_{1ML}/Ru(0001)$ layers: (A) Θ_O = 0.04−0.05 ML (Θ_O^{low}) and (B) Θ_O = 0.2−0.25 ML (Θ_O^{high}). The initial methanol exposures correspond to 40 mTorr·s, and the spectra were taken at 80 K after heating with 1 K/s to the indicated temperatures. Note that in the spectral range 2300−3500 cm^{-1} no vibrational peaks have been observed. The inset in (A) shows an IRAS spectrum of CD_3OH on a mixed (^{18}O + ^{16}O)/Cu/Ru(0001) layer ($\Theta_O^{total} \approx$ 0.05−0.1 ML) after annealing to 200 K. The spectra are offset vertically for better clarity of presentation.

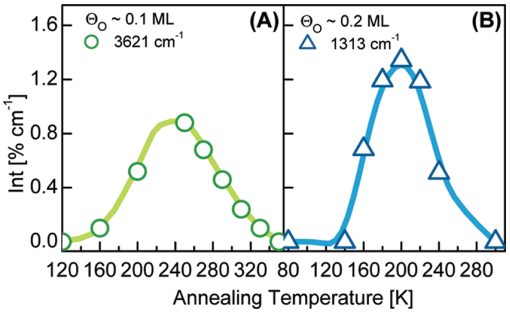

Figure 3. (A) Integrated IRAS intensity of the surface hydroxyl O−H stretch mode, ν(OH), at 3622 cm^{-1} on the annealed $O/Cu_{1ML}/Ru(0001)$ layer ($\Theta_O \approx$ 0.1 ML) as a function of annealing temperature. (B) Integrated IRAS intensity of the in-phase [δ(OH) + $\rho_{in\text{-}plane}(CD_3)$] mode at 1313 cm^{-1} of CD_3OH on the annealed $O/Cu_{1ML}/Ru(0001)$ layer ($\Theta_O \approx$ 0.2 ML) as a function of annealing temperature. The initial methanol exposures were 40 mTorr·s.

The proposed reaction is $CD_3OH + O \rightarrow CD_3O + OH$; i.e., the hydrogen of methanol's OH group is transferred to a surface oxygen atom and eventually desorbs associatively as water H_2O (see below). A similar behavior is encountered on Ru(0001) where a direct transfer of methanol's hydroxyl hydrogen to surface oxygen is found without intermediate binding of abstracted H to Ru(0001).[4] On Ru(0001) this very process has been verified by coadsorption of CD_3OH, O, and D. In the resulting TPD spectra only H_2O (18 u) was observed (peak areas of masses 19 and 20 u amounted to less than ≈1% of 18 u). In the case of $O/Cu_{1ML}/Ru(0001)$ such a direct transfer could not be investigated because the sticking probability of H_2 is close to zero. As to the primary activation of methanol on Cu/Ru(0001), we can clearly exclude any transfer of hydrogen (D) from the CD_3 methyl group because ν(OD) should exhibit a peak at about 2600 cm^{-1} which was not observed in the course of our experiments.

For high oxygen coverages on Cu/Ru(0001) (annealed layer) the thermal evolution of methanol proceeds differently. Specifically, an extra set of vibrational bands, the most prominent one located at 1313 cm^{-1}, is observed upon annealing to $T > 150$ K. This mode scales directly with other vibrational features at 885, 960, 1065, 2076, and 2239 cm^{-1} as the annealing temperature is raised. As will be detailed below, using isotopic substitution, they can be ascribed to intact methanol, most likely embedded in a well-ordered (2 × 2)-O environment. In the following we call this species $CD_3OH^{(2\times2)\text{-}O}$. This interpretation is supported by the close similarities to spectra of adsorbed methanol on (i) clean Ru(0001) and (ii) an ordered oxygen-precovered Ru(0001)-(2 × 2)-O surface (see Table 2).

By further annealing the methanol layers to 300 K, the vibrational signature changes significantly for the layer with Θ_O^{high}, as $CD_3OH^{(2\times2)\text{-}O}$ has vanished completely; methoxy, on the other hand, remains. In panel A methoxy and hydroxyl coexist on the surface. In fact, the modes of methoxy have even increased by about 30% (same for the layer in panel B), as compared to the spectrum at 200 K; a narrowing of vibrational bands indicates an improved local order, or, equivalently, a less heterogeneous environment.

The temperature-dependent integrated intensity of the peak at 1313 cm^{-1} is depicted in Figure 3B, demonstrating that this species begins forming at 160 K and passes through a maximum at 200 K followed by gradual loss in intensity until it is virtually gone at 300 K. We note that for layers with $\Theta_O \geq$ 0.2 ML methanol desorption is observed at 250 K (see below), supporting our interpretation of the 1313 cm^{-1} band to intact methanol ($CD_3OH^{(2\times2)\text{-}O}$).

In order to unambiguously identify the observed species, additional experiments with isotopically labeled methanol and preadsorbed oxygen were performed. The resulting spectra of $CH_3{}^{18}OH$ + ^{18}O and $CD_3{}^{16}OH$ + ^{16}O, taken after annealing to 200 K, are presented in Figure 4. From the isotopic shifts of the individual peaks (marked with dashed lines in the figure) the new species is identified as intact methanol in an ordered (2 × 2) oxygen overlayer with the following modes (referring to CD_3OH): the out-of-phase [δ(OH) + $\rho_{in\text{-}plane}(CD_3)]_{oop}$ mode

Table 2. Vibrational Modes (Frequencies in cm^{-1}) of Various (Isolated) Methanol Isotopes on $Cu_{1ML}/Ru(0001)$-(2 × 2)-O (Θ_O = 0.2−0.25 ML)[a]

$Cu_{1ML}/Ru(0001)$-(2 × 2)-O			Ru(0001)			Ru(0001)-(2 × 2)-O		
CH_3OH	$CH_3{}^{18}OH$	CD_3OH	CH_3OH	$CH_3{}^{18}OH$	CD_3OH	CH_3OH	CD_3OH	mode assignment[25]
988	970	960	975	949	946	982	958	ν(CO)
1110	1110	885	1061	1061	860	1089	875	$[\delta(OH) + \rho_{ip}(CD_3)]$ out of phase
1347	1342	1313	1304	1299	1244	1322	1285	$[\delta(OH) + \rho_{ip}(CD_3)]$ in phase
1460	1460	1065					1061	$\delta_s(CD_3)$
		1095	1454	1454	1091	1461	1097	$\delta_{as}(CD_3)$
2842	2840	2076	2822	2824	2065	2840	2075	$\nu(CD_3)$ stretching modes
		2129					2127	in Fermi resonance
2946	2943	2182	2926	2925	2190	2948	2203	with various
2983	2979	2238	2969	2970	2232	3000	2243	CD_3 bending modes
			2994	2994	2250		2257	

[a] For comparison, the line positions of methanol on clean Ru(0001) and Ru(0001)-(2 × 2)-O are listed as well. Note that the mode notation refers to CD_3OH. All spectra were measured at 80 K.

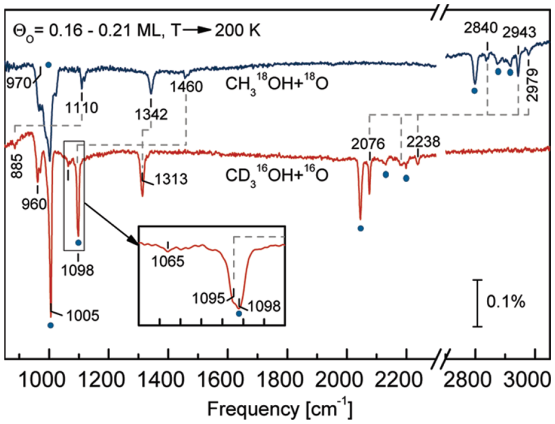

Figure 4. IRAS spectra of methanol (T_{ads} = 80 K) on an annealed $O/Cu_{1ML}/Ru(0001)$ layer (Θ_O = 0.16−0.21 ML) after $T \rightarrow$ 200 K. Individual spectra refer to different methanol and oxygen isotopes: $CH_3{}^{18}OH$ + ^{18}O (top) and $CD_3{}^{16}OH$ + ^{16}O (bottom). The initial methanol exposures were ≈40 mTorr·s. The modes belonging to $CD_3OH^{(2\times2)\text{-}O}$ and the isotopic shifts of these modes are marked with gray dashed lines. The remaining peaks are due to methoxy (labeled with blue dots). In the range 2300−2700 cm^{-1} no additional features were detected. An expanded view of the double peak feature at 1097 cm^{-1} is shown in the inset; as the 1095 cm^{-1} shoulder decays at lower temperatures than the 1098 cm^{-1} band, the former is ascribed to intact methanol and the latter to methoxy. For better clarity of presentation the spectra are offset vertically.

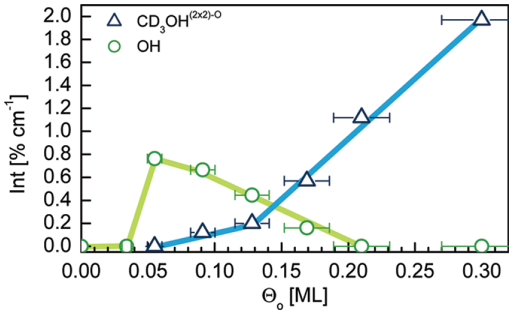

Figure 5. Integrated IRAS intensities of prominent modes in Figure 2 as a function of the surface oxygen coverage on $Cu_{1ML}/Ru(0001)$: (i) ν(OH) mode of surface OH at 3622 cm^{-1} and (ii) in-phase $[\delta(OH) + \rho_{in\text{-}plane}(CD_3)]$ mode of $CD_3OH^{(2\times2)\text{-}O}$ at 1313 cm^{-1}. The data refer to layers after annealing to 200 K. The initial methanol exposures were 40 mTorr·s. Oxygen coverages, Θ_O, have been determined using XPS.

at 885, ν(CO) at 960, $\delta_s(CD_3)$ at 1065, $\delta_{as}(CD_3)$ at 1095 (shoulder), the in-phase $[\delta(OH) + \rho_{in\text{-}plane}(CD_3)]_{ip}$ mode at 1313, and $\nu(CD_3)$ stretching modes (in Fermi resonance with $\delta(CD_3)$ overtones) at 2076, 2129, 2182, and 2238 cm^{-1}. We note that the observed frequencies are independent of the isotopic nature of preadsorbed oxygen. The complete assignment of the peaks of all used isotopes is given in Table 2. For comparison, the frequencies of isolated methanol on Ru(0001) and on (2 × 2)-O/Ru(0001) are listed as well. The other peaks in the spectra in Figure 4 are assigned to methoxy (labeled with blue dots; also compare Table 1, Figure 1, and Figure 2), in accordance with our very recent work.[10]

Next to mention is that the amount of $CD_3OH^{(2\times2)\text{-}O}$ increases dramatically with the coverage of preadsorbed oxygen. This dependence is depicted in Figure 5 where the IRAS peak areas of characteristic modes (after annealing to 200 K) of $CD_3OH^{(2\times2)\text{-}O}$ and OH are plotted as a function of surface oxygen coverage Θ_O (derived by XPS). Interestingly, only small quantities of $CD_3OH^{(2\times2)\text{-}O}$ are present when the amount of produced OH is high, and vice versa. Up to about 0.03 ML, neither species is observed and methoxy represents the only stable intermediate. From 0.04 to 0.1 ML the ν(OH) signal steeply increases and falls off continuously until, for $\Theta_O \approx$ 0.2 ML, its intensity has vanished completely. $CD_3OH^{(2\times2)\text{-}O}$, on the other hand, is formed preferentially for layers with high oxygen coverages, i.e., $\Theta_O \geq$ 0.13 ML. This observation is in accordance with our interpretation of a less reactive (2 × 2)-O overlayer which stabilizes methanol until it desorbs at 250 K. As mentioned above, methoxy occupies 3-fold sites on Cu(111).[31,32] Thus, if methanol is embedded into a (2 × 2)-O structure, the adsorption sites required by methoxy may be unavailable and methanol desorbs rather than reacts. A similar conclusion has been drawn in the case of methanol on O/Cu(100) by Ryberg,[18] who argued that free nearest-neighbor

sites next to oxygen are necessary for the initial reaction step (methoxy formation) to occur. Only at vacancies, defects, or phase/domain boundaries is activation of methanol and methoxy formation possible. Such preferential reactions of methanol at the edges of oxygen rows/islands has been observed on Cu(110) by Bowker's group.[19,20]

Formate Formation. Further reactions can be initiated by heating the sample; at 400 K (not shown) methoxy has already begun to decay but still represents the dominant surface species. Surface hydroxyl (Figure 2A), on the other hand, has vanished completely by desorbing associatively as water (H_2O). At 420 K (Figure 6A) the decay of methoxy has further progressed, rendering only small peaks as compared to the spectra in Figure 2. A closer look at the top spectrum in Figure 6A reveals that the residual methoxy peaks must be ascribed to two different methoxy species which are each labeled (see solid colored lines). The majority methoxy with the features at 988, 1090, 2055, 2126, and 2187 cm^{-1} fits well to methoxy on clean Cu/Ru(0001).[10] For comparison, a spectrum of CD_3O on 0.9 ML Cu/Ru(0001) is depicted in Figure 6A as well. We note that on incomplete Cu/Ru(0001) monolayers methanol activation can be achieved even in the absence of coadsorbed oxygen. The other set of peaks at 982, 1086, 2065, and 2181 cm^{-1} is most likely due to a minority methoxy species affected by nearby surface oxygen.

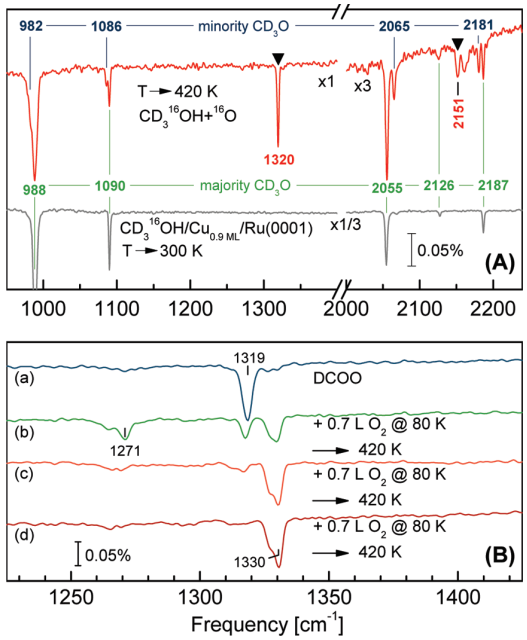

Figure 6. (A) Complex IRAS spectrum of CD_3OH (exposure equivalent to 40 mTorr·s at T_{ads} = 80 K) on O/Cu_{1ML}/Ru(0001) (Θ_O = 0.1 ML) after annealing to 420 K (top spectrum). For comparison, the bottom spectrum shows CD_3OH (exposure equivalent to 40 mTorr·s at T_{ads} = 80 K) on 0.9 ML Cu/Ru(0001) after annealing to 300 K which produces a single methoxy surface species only. The upper spectrum apparently contains two methoxy species with slightly shifted sets of peaks; they are each interlinked by connecting lines. The remaining features, belonging to formate, are marked with triangles. (B) IRAS spectra of DCOO produced from 40 mTorr·s CD_3OH adsorbed at 80 K on 0.1 ML (annealed) oxygen/Cu_{1ML}/Ru(0001) heated to 420 K (a). Spectra b–d were measured after dosing increasingly higher amounts of oxygen at 80 K and again annealing to 420 K.

Interestingly, a new band at about 1320 cm^{-1} has developed after annealing to 420 K. We note beforehand that the near degeneracy with the prominent 1313 cm^{-1} band reported in the previous section is accidental as isotopic substitution yields entirely different shifts (see below). In order to achieve a well-founded assignment of the new feature at 1320 cm^{-1}, measurements with isotopically labeled methanol and oxygen have been performed. Because of the observed frequency shifts, which are summarized in Table 3, the new species is identified as formate DCOO with a symmetric ν(OCO) stretch at 1320 cm^{-1}. The corresponding ν(CD) mode which scales in intensity with the ν(OCO) mode is observed at 2151 cm^{-1}. Other modes in the C–D stretching region are due to residual methoxy and will be discussed shortly. The frequencies of both our formate vibrational modes agree favorably with data reported in the literature: For Cu(100)[15,36] and Pt(111)[37] the ν(OCO) modes of HCOO are located at 1330–1340 and 1315 cm^{-1}, respectively. The ν(CH) stretch on Cu(100)[36] was observed at 2840 cm^{-1}, matching the value observed in our experiments with regular methanol (see Table 3).

According to theory,[35,38] two geometries of formate on Cu(111) seem possible: the short-bridge and the cross-bridge configurations of HCOO with ν(OCO) frequencies at 1368 and 1331 cm^{-1}, respectively, with the former being favored energetically on Cu(111).[35] At variance with this finding formate exhibits an O–C–O band at 1325 cm^{-1} on Cu(111)[39] which fits well the calculated frequency of a cross-bridge bound HCOO. Yet, in a NEXAFS study on Cu(110) a formate orientation along the Cu chains (short-bridge) has been reported.[40] In our experiments virtually identical ν(OCO) frequencies have been found for Cu_{1ML}/Ru(0001) and Cu_{30ML}/Ru(0001) substrates (see Table 3). As our measured vibrational frequency for HCOO on Cu_{1ML}/Ru(0001) (1347 cm^{-1}, Table 3) lies exactly between the calculated vibrational frequencies of short-bridge and cross-bridge HCOO, an unambiguous determination of formate's binding site is not possible at this point.

The band at 2160 cm^{-1} in the top spectrum of Figure 6A could not be correlated with any of the modes of formate or with one of the methoxy species. The appearance of this peak seems to be unclear and varies from one measuring series to another. Thus, an assignment of this mode is not given in this work.

Figure 6B demonstrates the influence of the amount of surface oxygen on the vibrational signature of DCOO. Spectrum a shows formate produced analogous to Figure 6A. Spectra b–d depict DCOO after dosing extra oxygen at 80 K and again heating to 420 K. For Θ_O < 0.15 ML exclusively the peak at 1319 cm^{-1} is

Table 3. Vibrational Modes (Frequencies in cm^{-1}) of Various Formate Isotopes on O/Cu_{1ML}/Ru(0001) in Comparison with DCOO on "Cu(111)" (Cu_{30ML}/Ru(0001))[a]

$DC^{16}O^{16}O$	$DC^{16}O^{18}O$	$HC^{16}O^{16}O$	$HC^{16}O^{18}O$	$HC^{18}O^{18}O$	$DC^{16}O^{16}O$/"Cu(111)"	mode
1320 (1330)	1298	1347 (1358)	1322 (1335)	1309 (1321)	1320	ν(OCO)
2151 (2184)		2844				ν(CD)

[a] Values in parentheses correspond to oxygen-rich environments of the formate species. Note that the mode notation refers to DCOO.

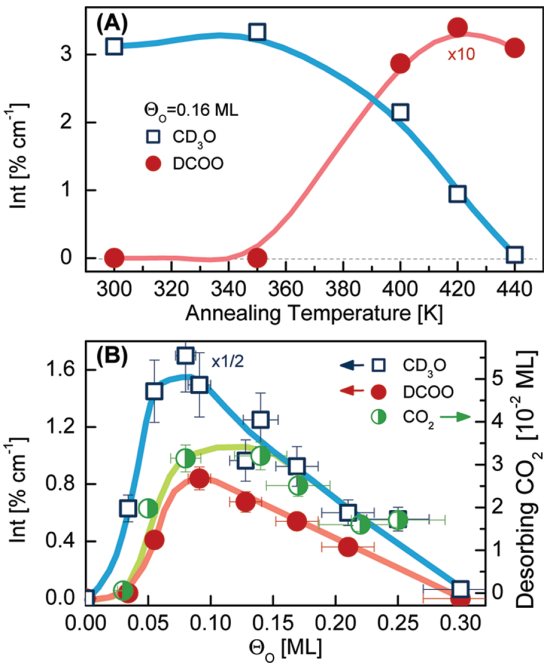

Figure 7. (A) Thermal evolution of integrated IRAS intensities of the DCOO (ν(OCO) mode at 1320 cm^{-1}) and of the CD_3O ($\nu_s(CD_3)$ mode at 2050 cm^{-1}) produced by methanol postadsorption onto annealed $O/Cu_{1ML}/Ru(0001)$ ($\Theta_O \approx 0.16$ ML). The initial methanol exposure was 50 mTorr·s. (B, left scale) Integrated IRAS intensities of DCOO (ν(OCO) modes at 1320−1330 cm^{-1}) and of CD_3O ($\nu_s(CD_3)$ modes at 2050−2065 cm^{-1}) as a function of preadsorbed surface oxygen coverage Θ_O (annealed layer). The initial methanol exposure was 40 mTorr·s, and the data points refer to annealing temperatures of 200 K (CD_3O) or 420 K (DCOO), which display maximum yield of the respective surface intermediate. In addition, the amount of desorbing CO_2 (derived from the 46 u desorption signal at $T \approx 400-470$ K of $C^{16}O^{18}O$ after adsorption of 40 mTorr·s CD_3OH on $^{18}O/Cu_{1ML}/Ru(0001)$ is overlaid (right scale, half-filled circles).

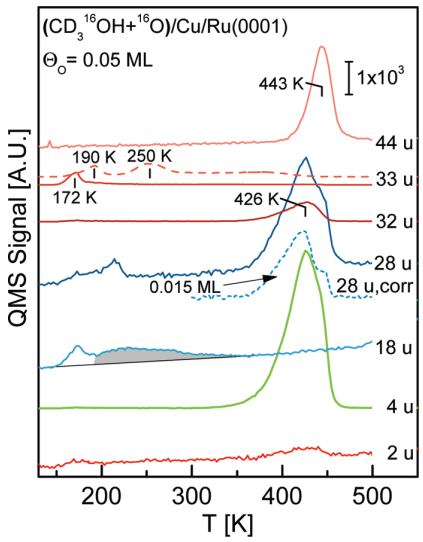

Figure 8. Multiple mass TPD spectra of CD_3OH adsorbed at 80 K on annealed $O/Cu_{1ML}/Ru(0001)$ with $\Theta_O \approx 0.05$ ML. The initial methanol exposure was 40 mTorr·s, and the sample was heated with 1 K/s from 80 to 600 K. In order to isolate the contribution of desorbing CO from the mass 28 u signal, the contributions of CO^+ fragments from desorbing CO_2 (44 u) and formaldehyde (32 u) are subtracted; the corrected curve 28 u,corr, has been calculated according to 28 u,corr = 28 u − 0.35 × 44 u − 1.7 × 32 u. The 28 u/44 u and 28 u/32 u ratios are known from CO_2 desorption experiments on Pt/Ru(0001) and from desorption of D_2CO from multilayer Cu/Ru(0001), respectively (see Supporting Information). Desorption of reactively produced water (18 u) is emphasized by a gray background. The dashed 33 u signal refers to a sample with $\Theta_O \approx 0.2$ ML.

observed (spectrum a). For $\Theta_O \approx 0.2$ bands at 1272 and 1330 cm^{-1} appear (spectrum b). While the former disappears again for higher Θ_O the 1330 cm^{-1} feature dominates for layers with $\Theta_O \approx 0.25-0.3$ ML (spectra c and d). Thus, the 1319 and 1330 cm^{-1} features can easily be attributed to DCOO in an oxygen-poor and an oxygen-rich environment, respectively. Additionally, the shifts of the line positions induced by isotopic labeling give consistent results for these two bands. The shifts for the 1271 cm^{-1} peak, however, do not show a clear correlation with the other two peaks. Furthermore, the band at 1271 cm^{-1} correlates with a tiny peak at 2192 cm^{-1} and is stable up to slightly higher temperatures (+20 K) than the bands at 1319 and 1330 cm^{-1}. Therefore, it must be due to another surface species which is discussed in the following.

A possible candidate for a peak in the 1250−1300 cm^{-1} region (depending on the used isotope) is a η^2-D_2CO species (formaldehyde bound through the C and O atoms to the surface). Yet, D_2CO (32 u) desorption (the TPD is discussed later) at 425 K is observed not only for high initial oxygen coverages (which cause the growth of the 1271 cm^{-1} peak) but also for $\Theta_O \leq 0.15$ ML, i.e., for layers which definitely do not exhibit a peak at 1271 cm^{-1}. A second argument against a formaldehyde surface species is provided by the TPD peak of 32 u at 425 K which is observed at clearly lower temperatures than the decay of the 1271 cm^{-1} feature at 440−460 K. As we neither could detect any CH_2 scissor nor wagging modes, we exclude η^2-D_2CO as a stable reaction intermediate.

On the basis of a relatively small line shift of the mode at 1271 cm^{-1} upon D ↔ H isotope substitution (+6 cm^{-1}) and, on the other hand, a strong blue shift upon $^{18}O \leftrightarrow {}^{16}O$ substitution (+33 cm^{-1}), we conclude that it is a mode with predominately C−O stretch character and some (much smaller) C−H bending or stretching contribution. A species with its C−H bond aligned parallel to the C−O axis, however, is expected to exhibit a much stronger shift (≈25 cm^{-1}) of this mode upon D ↔ H isotopic exchange (equivalent to a $^{14}C \leftrightarrow {}^{13}C$ replacement of a CO species); therefore, we conclude that the C−H bond is substantially inclined with respect to the C−O bond. We are therefore confident that the set of modes can be attributed to a η^2-formyl (DCO bound through the C and O atom to the substrate) with the ν(CO) and ν(CD) stretching modes at 1271 and 2192 cm^{-1}, respectively. We note that formyl represents a minority species which is most likely formed due to the partial dehydrogenation of methoxy which is still available at 420 K.

According to a quantitative analysis of spectra obtained after annealing to successively higher T, vibrational bands associated with methoxy shrink in parallel to the uprise of features belonging to formate (with no extra bands showing up in the transition regime) as illustrated in Figure 7A. Our observation of a surface formate species is therefore attributed to a reaction of

methoxy with surface oxygen: $CD_3O + O \rightarrow DCOO + 2D$ with no stable intermediates in between. Clear evidence for such a synthesis of formate from methoxy and surface oxygen comes from isotopic shifts of the various formate modes as listed in Table 3. Note that, according to our thermal desorption data (see below), this reaction is accompanied by the formation and immediate desorption of formaldehyde (see below): it is therefore very likely that such species actually represents a temporary intermediate in the decomposition of methoxy to formate.

As surface reactions at elevated T are usually accompanied by the desorption of product species, thermal desorption experiments provide valuable extra information to surface spectroscopies such as IRAS. The decomposition of formate, for example, leads to the production of CO_2 which then opens up the possibility for a qualitative and quantitative analysis of reactions schemes and yields (see Figures 7 and 8).

Additional evidence for a methoxy to formate reaction is provided by TPD experiments using $CD_3{}^{16}OH$ and ^{18}O, with masses 46 u ($C^{16}O^{18}O$) and 48 u ($C^{18}O_2$) being detected. In these experiments only the 46 u signal exhibits a significant desorption signal. Thus, desorbing CO_2 and consequently its precursor (formate) always contains one oxygen from methanol and another one due to preadsorbed surface oxygen. We note that coadsorption of CO and O on Cu/Ru(0001) does not produce any CO_2 (44 u) in thermal desorption experiments. In agreement with our data of $CD_3{}^{16}OH$ on $^{18}O/Cu_{1ML}/Ru(0001)$ the desorbing $C^{16}O^{18}O$ from $Cu_{30ML}/Ru(0001)$ (~30 ML Cu deposited onto Ru(0001) and annealed to 900 K for 30 min) contains one O from methanol and another one from preadsorbed surface oxygen. According to Kneitz et al.,[8] such Cu/Ru(0001) multilayers largely behave like a Cu(111) surface.

The transformation of methoxy to formate and its decomposition to produce gas-phase CO_2 are illustrated in Figure 7B where integrated intensities of the most prominent vibrational modes of DCOO and CD_3O as well as the amount of desorbing CO_2 are plotted versus the oxygen coverage. Apparently, the amount of produced formate (after annealing to 420 K) is correlated with the amount of methoxy available at 200−300 K. Both species exhibit maximum yield for 0.07−0.11 ML oxygen. This is attributed to zero reactivity of methanol on the bare $Cu_{1ML}/Ru(0001)$ monolayer as well as on the annealed $O/Cu_{1ML}/Ru(0001)$ surface with $\Theta_O \approx 0.3$ ML. We suspect that activation of methanol occurs only at the borders of (2×2)-O areas or on imperfectly ordered oxygen layers. Such a maximum in the yield of the reaction products was reported by Russel et al.[11] for methanol on oxidized Cu(111) (methoxy is found to decompose at ≈350 K, producing formaldehyde as the main reaction product). Maximum yield is reported for $\Theta_O \approx 0.26$ ML. For $\Theta_O > 0.26$ ML side blocking becomes more and more important. Similarly, calculations[41] as well as experiments[19,20] of methanol on O/Cu(110) show a high reactivity toward methanol oxidation for isolated oxygen atoms and atoms terminating the CuO chains only; for dense oxygen layers, i.e., for complete CuO chains, the dehydrogenation of methanol is endothermic by 1.29 eV[41] and the surface becomes inert.

A closer inspection of the formate and methoxy entities (Figure 7B) shows that the probability of methoxy to convert to formate is not constant. Rather this yield is close to zero for $\Theta_O < 0.04$ ML and reaches its maximum level (not necessarily 100%) only for $\Theta_O > 0.1$ ML. By means of monitoring the surface composition using IRAS, as well as the entity of desorbing species using TPD (see Figure 8), a direct comparison can be attained. In particular, we find that the amount of desorbing CO_2 is proportional to the intensity of the ν(OCO) IRAS mode of formate as shown for several oxygen coverages (half-filled green circles in Figure 7B). The amount of desorbing CO_2 is derived from a comparison of the CO_2 desorption signals from Cu/Ru(0001) layers in this work with TPD data (masses 28, 32, and 44 u) of reactively produced CO_2 from coadsorbed CO and O on Pt multilayer films on Ru(0001 (see Supporting Information).

We note that the CO_2 desorption yield can be enlarged by adding extra oxygen to a $(CD_3O + O)/Cu_{1ML}/Ru(0001)$ layer. Specifically, under optimal conditions (see Figure 7B), i.e., with 0.1 ML oxygen preadsorbed and after the annealing step to 300 K to produce methoxy, exposure to another 3 langmuirs of O_2 at 80 K yields a × 2.6 increased amount of CO_2 desorption as compared to an identical layer without the extra oxygen dose (see Figure 6A). In this experiment the absolute amount of CO_2 was increased from 0.03 to 0.08 ML (see Supporting Information). In parallel, a 40% reduction of desorbing CO was observed. Thus, it is concluded that efficient transformation of methoxy to formate requires a high concentration of oxygen in the vicinity of methoxy. Such a high oxygen coverage right from the beginning, however, lowers the fraction of methanol to transform into methoxy. Ironically, under conditions when maximum methoxy is produced (0.1 ML oxygen) there is not enough oxygen left on the surface to efficiently convert all CD_3O to DCOO; according to our findings this constraint can be eliminated by oxygen postadsorption. A similar conclusion has been drawn by Sakong and Gross[41] based on DFT calculations of methanol oxidation on Cu(110) where the presence of oxygen in the vicinity of methoxy is needed to produce formate. Furthermore, STM measurements show that the amount of produced formate on Cu(110) can be increased significantly by dosing a gas mixture of methanol and oxygen at 300 K.[42]

For methanol on O/Cu(111) Russel et al.[11] identified a minor reaction path leading to CO_2 at ≈480 K, and they concluded that this observation is due to the decomposition of a D containing intermediate, namely DCOO (formate). In our own experiments of methanol on $O/Cu_{30ML}/Ru(0001)$ the main results of Russell et al.[11] concerning methanol reactions on O/Cu(111) are confirmed. Additionally, we were able to directly detect surface formate (ν(OCO) at 1320 cm^{-1}) after annealing a methanol multilayer postadsorbed on oxygen precovered $Cu_{30ML}/Ru(0001)$ to 440 K (see Supporting Information). We note that the amount of produced formate and of desorbing CO_2 from Cu_{30ML} (with 0.1 ML oxygen) is at least a factor 10 lower than for $O/Cu_{1ML}/Ru(0001)$, as the dominant dissociation channel of methoxy on Cu(111) is dehydrogenation to formaldehyde (D_2CO).

Desorption of formaldehyde actually represents yet another dissociation pathway of methoxy molecules on $O/Cu_{1ML}/Ru(0001)$ layers, as verified by our multimass TPD in Figure 8. Specifically, a 32 u desorption peak is observed at 425 K with zero signal for mass 33 u (33 u represents the most intense methanol peak in the QMS spectrum, besides the more ambiguous 28 u and 30 u signals). In our IRAS spectra the only vibrational bands which decrease in this temperature range belong to CD_3O. Hence, the produced formaldehyde results from methoxy decomposition and desorbs immediately.

We like to stress that we did not find any evidence for a C−O bond breaking for the whole reaction path as the produced surface OH species consist exclusively of preadsorbed surface oxygen. Also, C−O bond breaking is rather unlikely

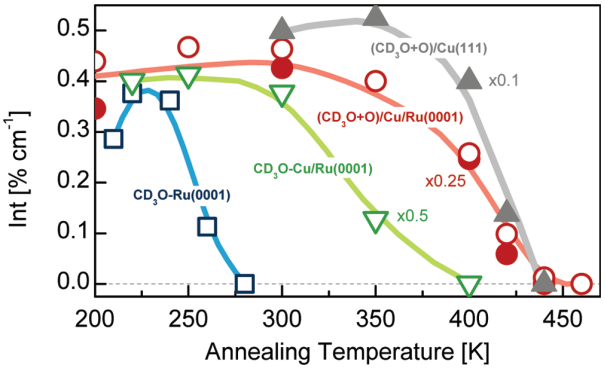

Figure 9. Temperature dependency of the integrated IRAS intensities of the umbrella mode $\delta_s(CD_3)$ of various methoxy species (CD_3O): (i) on clean Ru(0001) (blue squares, 1074 cm^{-1}), (ii) Cu-bound CD_3O on 0.5 ML Cu/Ru(0001) (green triangles, 1090 cm^{-1}), and (iii) CD_3O on O/Cu_{1ML}/Ru(0001) (bullets/circles, 1094 cm^{-1}, Θ_{Cu} = 1 ML). The bullets (circles) correspond to samples with (without) annealing of the oxygen layer (Θ_O = 0.2−0.25 ML) to 600 K before methanol adsorption. The initial methanol exposures (80 K) correspond to 40 mTorr·s. For comparison, the curve derived for CD_3O on oxygen-covered "Cu(111)" is shown as well (full gray triangles). "Cu(111)" was prepared by deposition of 30 ML Cu on Ru(0001) followed by annealing to 900 K for 30 min. This surface was then exposed to 50 langmuirs of oxygen at 300 K before a multilayer methanol was added at 80 K and successively annealed to higher *T*. The colored lines are guides to the eye.

according to reports for methanol on different metal substrates.[4,10,11,15,22,37] Referring to DFT calculations for methanol on Pt(111), the barrier for C−O activation is 3 times higher than for C−H or O−H.[1]

The high dissociation temperature of formate (and CO_2 desorption) and the fact that it is the most stable surface intermediate are in accordance with theoretical works. The calculated binding energy of HCOO on Cu(111)[35,38] and Cu(110)[41,43] equals ≈3.3−3.5 eV. For comparison, the second-most stable intermediate on Cu(111), methoxy, has a binding energy of ≈2 eV.[13,31] The binding energy of formaldehyde, on the other hand, amounts to only 0.1−0.3 eV,[13,14] which is in agreement with our findings, i.e., its rapid desorption once it is formed.

The complex structure of the 28 u desorption peak at 420−440 K suggests several contributions. Besides desorbing genuine CO, the CO^+ ionization fragments of desorbing formaldehyde and of CO_2 contribute as well. In the 28 u,corr trace the contributions of CO_2 (44 u) and formaldehyde (32 u) have been subtracted (determination of ionization fragments: see Supporting Information). The remaining signal corresponds to 0.015 ML CO which is produced in the course of methanol reactions (methoxy decomposition) on oxygen-covered Cu_{1ML}/Ru(0001) layers. Our IRAS data did not detect any ν(CO) band of surface CO on Cu_{1ML}/Ru(00001), which we attribute to the rapid CO desorption from Cu/Ru(0001) (at temperatures below 250 K), that is, at temperatures significantly lower than the dissociation temperature of methoxy. For Cu/Ru(0001) ample amounts of CO on Ru(0001) have been detected only if uncovered Ru(0001) areas were still available, i.e., for Θ_{Cu} < 1 ML. The 4 u peak (D_2) at about 430 K has contributions of formaldehyde and due to desorption of deuterium from formate and methoxy decomposition.

In the low-temperature region ($T \leq$ 300 K) desorbing species comprise water and methanol. The water (18 u) desorption has two contribution. The broad feature at 200−350 K (highlighted by a gray background) is attributed to hydrogen of methanol's OH group which is transferred to surface oxygen, leading to the associative desorption as water (H_2O); the mass 18 u signal at ∼170 K is probably caused by a contamination in the methanol reservoir.[4] Both contributions have been discriminated in an isotopic labeling experiment using the ^{18}O isotope instead of ^{16}O for preadsorbed oxygen. In this case the broad feature at 200−350 K merely yielded desorption of $H_2{}^{18}O$ (20 u) while the equivalent 18 u signal is missing. The 28 u peak at 230 K is observed in the TPD spectra independent of the initial oxygen coverage. As its desorption temperature matches the desorption temperature of CO from a clean Cu/Ru(0001) layer,[44] we attribute this signal to a slight CO contamination (0.003 ML) accumulated during sample positioning in front of the mass spectrometer.[10] IRAS spectra obtained in advance of TPD experiments never displayed any CO features beyond 0.001 ML.

Interestingly, there is no real big difference in TPD spectra for different Θ_O as long as Θ_O > 0.04 ML, besides a variation of the intensities of individual desorption peaks. Yet, the trace of 33 u, indicative of desorbing methanol (CD_3OH) makes an exception. Therefore, the dashed line has been added to Figure 8, and it represents the 33 u signal obtained from a layer with $\Theta_O \approx$ 0.2 ML. The peak at 250 K is correlated with the decrease of vibrational features associated with $CD_3OH^{(2\times2)\text{-}O}$. The desorption of methanol from the clean Cu_{1ML}/Ru(0001) exhibits a peak in the range 170−190 K.[10] The position of the maximum of this peak thereby depends critically on the exact Cu coverage: The two peaks at 170 K (solid line) and 190 K (dashed line) are likely due to slightly different Cu coverages (e.g., 1.05 and 0.95 ML) of the two samples. Below 0.04 ML the spectra resemble those obtained for methanol on oxygen-free Cu/Ru(0001) layers. Therefore, the TPD in Figure 8 can be considered representative of an arbitrary O/Cu_{1ML}/Ru(0001) layer.

Another interesting property of the oxygen-precovered Cu_{1ML}/Ru(0001) layer is that methoxy decays at higher temperatures as compared to other layers, e.g., the clean Ru(0001)[4] surface or submonolayer Cu/Ru(0001).[10] In order to illustrate this, integrated IRAS intensities of methoxy on clean Ru(0001), Cu/Ru(0001), Cu_{30ML}/Ru(0001), and O/Cu_{1ML}/Ru(0001) are plotted as a function of surface temperature in Figure 9. While on the clean Ru(0001) methoxy begins decomposing already at 220 K, dissociation on Cu/Ru(0001) is slowed down and starts only at 280−300 K. On oxygen-precovered Cu/Ru(0001) monolayers this onset is delayed by another 30−40 K, and methoxy decomposition occurs at temperatures similar to O/Cu_{30ML}/Ru(0001) layers. Possibly, these variations in methoxy decomposition temperatures are due to different CO (methoxy decomposition product) binding energies. From Ru(0001)[45,46] and monolayer Cu/Ru(0001)[8,44] small amounts of CO desorb at 490 and 250 K, respectively. When oxygen is preadsorbed on Cu_{1ML}/Ru(0001), the CO desorption temperature is further lowered to about 180 K (not shown). A similar value is reported for $Cu_{multilayer}$/Ru(0001).[8] In other words, the methoxy decomposition temperatures is proportionately lower the higher the CO binding energy. Such a correlation between the reaction (or adsorption) energy and the activation energy of a certain reaction pathway is called the Brønsted−Evans−Polanyi relation.[47,48] DFT calculations confirm linear dependencies of the dissociation barriers on adsorption energies for diatomic[49,50] (e.g., CO, N_2, NO, or O_2) and more complex[51] (CH_4, NH_3, H_2O) molecules on various transition metal surfaces. A recent

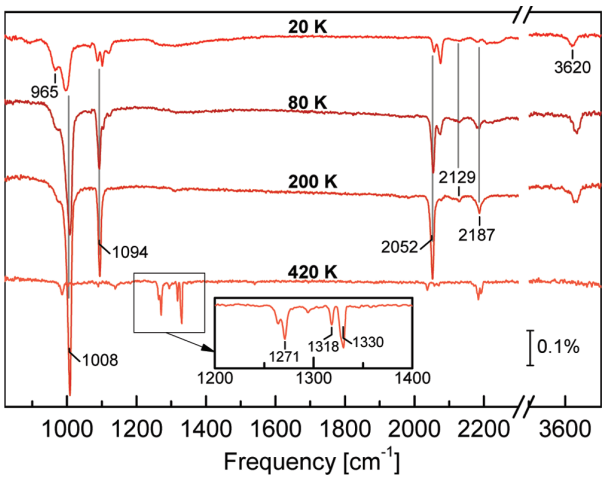

Figure 10. IRAS spectra of CD_3OH adsorbed at T_{ads} = 20 K on disordered (nonannealed) $O/Cu_{1ML}/Ru(0001)$ with $\Theta_O \approx 0.25$ ML. The initial methanol exposure was ~40 mTorr·s, and the spectra were taken at 20 K after annealing to the indicated temperatures with 1 K/s. Note that in the spectral range 2300−3500 cm^{-1} no vibrational bands have been observed. For better clarity of presentation the spectra are offset vertically.

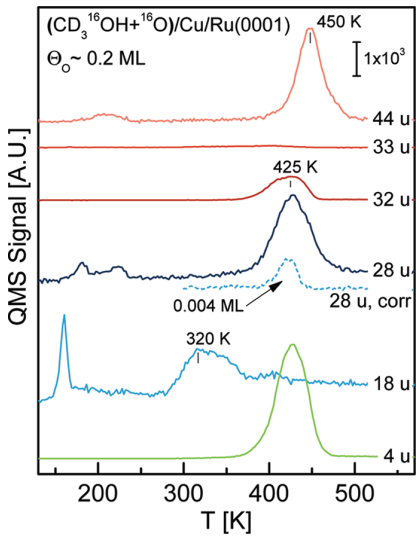

Figure 11. Multiple mass TPD spectra of CD_3OH adsorbed at 80 K on disordered $O/Cu_{1ML}/Ru(0001)$ with $\Theta_O \approx 0.2$ ML. The initial methanol exposure was 40 mTorr·s, and the sample was heated with 1 K/s from 80 to 600 K. Regarding the 28 u,corr curve, see explanatory remarks in the caption of Figure 8.

experimental example of the Brønsted−Evans−Polanyi principle is given for the system $O_2/Pt_n/Ru(0001)$[52] where the energetic barrier for the transition of molecular O_2 from the physisorbed state to the molecularly chemisorbed state depends on the binding energy E_B^{chem} of the chemisorbed state; as E_B^{chem} increases with the number of Pt layers, the mentioned transition into the molecular chemisorbed state become easier and the O_2 sticking coefficient increases dramatically.

Methanol on Disordered Oxygen. The effect of oxygen long-range order on methanol adsorption and reactions will be studied in this section. Here, Cu/Ru(0001) monolayers have been exposed to oxygen at $T \leq 80$ K, and no annealing is applied before methanol adsorption.

In Figure 10, IRAS spectra of CD_3OH on such disordered $O/Cu_{1ML}/Ru(0001)$ with $\Theta_O \approx 0.25$ ML are depicted. Oxygen and methanol were successively adsorbed at 20 K followed by annealing to increasingly higher temperatures (as indicated in the figure) and recooling to 20 K before data acquisition. According to the multitude of vibrational features at 20 K (1000, 1100, 2000−2200, and 3620 cm^{-1}) we conclude that a mixture of species is present. The vertical gray lines thereby mark peaks belonging to methoxy which are observed at 1008, 1094, 2052, 2129, and 2187 cm^{-1} (compare with Figure 1). These bands grow to maximum intensity upon slight annealing, while the modes associated with intact methanol (965, 1104, 1120, 2074, and 2210 cm^{-1}) gradually disappear. Apparently, methoxy is formed already at 20 K, suggesting a dissociative adsorption of methanol. Even though the methoxy peaks are relatively small at low temperatures and they overlap with additional features belonging to intact methanol, they are clearly discernible.

A dissociative adsorption of methanol at 20 K is corroborated by our observation of the hydroxyl band at 3620 cm^{-1} which is visible right from the beginning even at 20 K. It vanishes in the range 300−380 K, which is about 50 K higher than on annealed O-layers. Similar to the previous section, isotopic labeling experiments underline its nature as adsorbed OH and exclude an alternative assignment as the hydroxyl group of intact methanol.[25] Hence, surface hydroxyl is formed spontaneously via methanol O−H bond breaking and, most likely, direct transfer of the separated H to a surface oxygen. The possibility of C−D bond breaking of CD_3OH which should exhibit an O−D stretch at ≈2600 cm^{-1} can be ruled out because no features are observed in the spectral range 2300−3500 cm^{-1}. In parallel to OH formation the creation of CD_3O at 20 K must occur, which is indeed observed. In a DFT study such dissociative adsorption of methanol, spontaneously producing methoxy and OH on Cu(110), was reported by Sakong and Gross.[43]

By annealing to 80 K the bands associated with methoxy (vertical gray lines in Figure 10) and OH increase significantly. In the region of C−D stretch modes even the weakest methoxy $\nu(CD_3)$ stretch at 2129 cm^{-1} is clearly visible now.

Annealing to 200 K further enhances the CD_3O bands, while features associated with intact methanol are virtually gone. The TPD shown in Figure 11 does not exhibit any peaks of the 33 u (CD_3OH) signal in the entire temperature range 80−600 K (no desorption of intact methanol occurs). This observation is in contrast to the TPD in Figure 8 where small amounts of intact methanol are found to desorb after the oxygen layer has been annealed. It is evident that the disordered oxygen layer is more reactive in terms of methanol dehydrogenation than annealed oxygen on $Cu_{1ML}/Ru(0001)$.

For temperatures above about 350−380 K, that is, after all OH have desorbed associatively as water, the thermal evolution of methanol on $O/Cu_{1ML}/Ru(0001)$ layers proceeds largely independent of the original oxygen long-range order. The only differences arise due to the fact that some surface species have been produced with higher efficiency for the nonannealed layers. In brief, the thermal evolution proceeds as follows: methoxy partially reacts with surface oxygen to form DCOO (see Figure 10 at 420 K) while another fraction of the CD_3O molecules becomes dehydrogenated to D_2CO (formaldehyde) which desorbs immediately at about 425 K (see Figure 11).

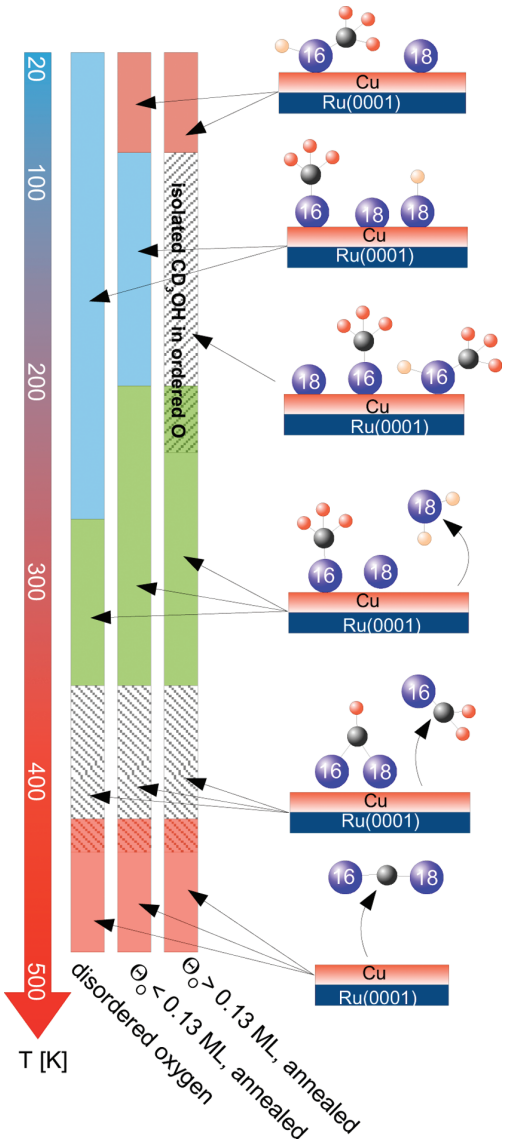

Figure 12. Simplified reaction scheme of $CD_3{}^{16}OH$ + ^{18}O on the Cu/Ru(0001) monolayer. For details see text.

The multiple peaks in the range 1260−1330 cm^{-1} can be assigned to (i) formate in an oxygen-rich environment, (ii) formate in an oxygen-poor environment, and (iii) to a formyl species as described in the previous section (compare with Figure 6B).

In the TPD in Figure 11 only masses 28 and 18 u develop notable peaks below 250 K. However, these features are due to slight H_2O and CO (≈0.0025 ML) contaminations. The weak 28 u signals at 170 and 220 K resemble CO desorption from a $O/Cu_{1ML}/Ru(0001)$ layer; as IRAS does not detect any adsorbed CO, these features are attributed to CO accumulated in front of the QMS. Similar to Figure 8, the 28 u desorption curve at ≈400 K in Figure 11 contains a multitude of contributions (CO^+ ionization fragments of desorbing CO_2 and D_2CO), which overlay the true desorption signal of CO. This latter signal (28 u,corr), i.e., CO resulting from the decomposition of methoxy, can be derived by subtracting the fragmentation contributions.

Reaction Pathways. In the following the reaction paths discussed above will be briefly summarized. For better clarity a simplified reaction scheme is presented in Figure 12.

For ordered (annealed) as well as disordered oxygen on Cu/Ru(0001) monolayers the primary activation of methanol involves the breaking of methanol's O−H bond to form methoxy. In parallel, surface OH is formed by means of H transfer from methanol's hydroxyl group to surface oxygen, a process which requires very little thermal activation since it proceeds at temperatures of 60 K and below; eventually these OH species desorb associatively as water (≈300−380 K). Such a breaking of methanol's O−H bond as the initial reaction step is also observed on clean Ru(0001),[4] on submonolayer Cu/Ru(0001),[10] and on O/"Cu(111)" (30 ML Cu/Ru(0001) annealed at 900 K for 30 min).

Ordered areas of the oxygen phase (prevailing at higher Θ_O > 0.1 ML) lead to a stabilization of intact methanol, and methoxy formation proceeds at a lower rate or requires higher temperatures, probably involving defects of the ordered (2 × 2)-O phase. For temperatures above 350 K the reaction pathways, starting with ordered or disordered oxygen layers, merge. The second reaction step occurs via C−D bond breaking of the methoxy methyl group. Depending on the local environment, i.e., the local oxygen concentration, either formate alone or formate including formyl as a minority species is produced. Additionally, a fraction of the methoxy molecules dehydrogenates and desorbs instantaneously as formaldehyde. For low Θ_O complete dehydrogenation of methoxy, leading to correlated desorption of D_2 and CO represents a competitive channel to formaldehyde desorption (420−450 K). The final reaction step, once formate has been produced, is the C−D bond breaking of DCOO, leading to the desorption of CO_2 and D_2.

CONCLUSIONS

In this work the reactions of methanol on oxygen-covered Cu/Ru(0001) layers with Θ_{Cu} = 1 ML were investigated. One of the major findings thereby is that the initial activation step critically depends on the lateral ordering of the precovered oxygen layer.

On disordered O layers methanol adsorbs dissociatively even at 20 K. Such an efficient activation of all molecules is corroborated by the absence of desorption of intact methanol. On the less reactive annealed $O/Cu_{1ML}/Ru(0001)$ layer the reaction starts at 60 K. In this case a small amount of intact methanol is found to desorb. Layers with Θ_O < 0.13 ML which display only local long-range order despite annealing lead to the formation of surface O−H; no such reaction of the methanol hydroxyl group and surface oxygen is, however, observed for layers with Θ_O > 0.13 ML, displaying extended long-range order.

Decomposition of the main reaction product methoxy requires temperatures T > 350 K. Depending on the amount of coadsorbed oxygen different processes and product species were identified: (i) methoxy oxidation to formate (favored at high Θ_O), (ii) partial dehydrogenation to formaldehyde which desorbs instantaneously into the gas phase, and (iii) or complete dehydrogenation to CO (favored at low Θ_O), again leading to immediate desorption from Cu/Ru(0001). In addition, a stable formyl species has been detected.

Because of a complex reaction pathway, with methoxy representing an important intermediate, the maximum amount of formate is found for O layers at $\Theta_O \approx 0.10$ ML after annealing to T = 420 K. The amount of formate has been estimated by the

quantity of desorbing CO_2 which represents the only dissociation product, besides abstracted hydrogen. The CO_2 yield (and consequently of formate) can be substantially enhanced by at least a factor 2 by adsorbing extra oxygen onto a methoxy/$O/Cu_{1ML}/Ru(0001)$ layer.

Compared to the clean Ru(0001) surface which dehydrogenate methanol to CO (T_{des} = 470 K), the $O/Cu_{1ML}/Ru(0001)$ layers, which convert methanol to gas phase CO_2 at 440 K, are not a real improvement referring to practical use (e.g., in a DMFC). The dissociation temperatures of formate on $O/Cu_{1ML}/Ru(0001)$ and the desorption temperature of CO from Ru(0001) or Pt(111) differ only slightly. This means that the problem of the oxygen-covered Cu/Ru(0001) surface is a formate poisoning instead of CO poisoning.

Our study clearly demonstrates that surfaces can be efficiently functionalized and chemical properties of materials altered by deposition of single monolayers; similar to the paradigm system Pt/Ru(0001),[52,53] the behavior of such materials cannot be simply interpolated between its components but yields entirely novel characteristics.

■ ASSOCIATED CONTENT

Supporting Information. IRAS spectra of different methoxy isotopes and of formate on oxygen precovered Cu/Ru(0001) layers (Figure 1); calibration of the oxygen coverage (Figure 2); LEED patterns of $O/Cu_{1ML}/Ru(0001)$ layers (Figure 3); intensity ratios of ionization fragments of CO_2 and D_2CO (Figure 4); methoxy oxidation on $Cu_{1ML}/Ru(0001)$: control of formate product yield by oxygen postadsorption (Figure 5). This material is available free of charge via the Internet at http://pubs.acs.org.

■ ACKNOWLEDGMENT

We acknowledge support by the Deutsche Forschungsgemeinschaft through GK790.

■ REFERENCES

(1) Greeley, J.; Mavrikakis, M. *J. Am. Chem. Soc.* **2004**, *126*, 3910.
(2) Ralph, T. R.; Hogarth, M. P. *Platinum Met. Rev.* **2002**, *46*, 3.
(3) Ralph, T. R.; Hogarth, M. P. *Platinum Met. Rev.* **2002**, *46*, 117.
(4) Gazdzicki, P.; Jakob, P. *J. Phys. Chem. C* **2010**, *114*, 2655.
(5) Houston, J. E.; Peden, Z. H. F.; Blair, D. S.; Goodman, D .W. *Surf. Sci.* **1986**, *167*, 427.
(6) Christmann, K.; Ertl, G.; Shimizu, H. *Thin Solid Films* **1979**, *57*, 241.
(7) Günther, C.; Vrijmoeth, J.; Hwang, R. Q.; Behm, R. J. *Phys. Rev. Lett.* **1995**, *74*, 754.
(8) Kneitz, S.; Gemeinhardt, J.; Steinrück, H.-P. *Surf. Sci.* **1999**, *440*, 307.
(9) Paul, J.; Hoffmann, F. M. *Surf. Sci.* **1986**, *172*, 151.
(10) Gazdzicki, P.; Jakob, P. *J. Phys. Chem. C* **2011**, *115*, 1961.
(11) Russell, J. N., Jr.; Gates, S. M.; Yates, T. J., Jr. *Surf. Sci.* **1985**, *163*, 516.
(12) Chesters, M. A.; McCash, E. M. *Spectrochim. Acta, Part A* **1987**, *43*, 1625.
(13) Greeley, J.; Mavrikakis, M. *J. Catal.* **2002**, *208*, 291.
(14) Gomes, J. R. B.; Gomes, J. A. N. F. *Surf. Sci.* **2001**, *471*, 59.
(15) Mudalige, K.; Trenary, M. *Surf. Sci.* **2002**, *504*, 208.
(16) Ryberg, R. *Phys. Rev. B* **1985**, *504*, 2545.
(17) Ryberg, R. *J. Chem. Phys.* **1985**, *82*, 567.
(18) Ryberg, R. *Phys. Rev. Lett.* **1982**, *49*, 1579.
(19) Francis, S. M.; Leibsle, F. M.; Haq, S.; Xiang, N.; Bowker, M. *Surf. Sci.* **1994**, *315*, 284.
(20) Davies, P. R.; Bowker, M. *Catal. Today* **2010**, *154*, 31.
(21) Desai, S. K.; Neurock, M.; Kourtakis, K. *J. Phys. Chem. B* **2002**, *106*, 2559.
(22) Liu, Z.; Sawada, T.; Takagi, N.; Watanabe, K.; Matsumoto, Y. *J. Chem. Phys.* **2003**, *119*, 4879.
(23) Endo, M.; Matsumoto, T.; Kubota, J.; Domen, K.; Hirose, C. *J. Phys. Chem. B* **2000**, *104*, 4916.
(24) Feulner, P.; Menzel, D. *J. Vac. Sci. Technol.* **1980**, *17*, 662.
(25) Gazdzicki, P.; Uvdal, P.; Jakob, P. *J. Chem. Phys.* **2009**, *130*, 224703.
(26) Koch, M. H.; Jakob, P.; Menzel, D. *Surf. Sci.* **1996**, *367*, 293.
(27) Sim, W. S.; Gardner, P.; King, D. A. *J. Phys. Chem.* **1995**, *99*, 16002.
(28) Mudalige, K.; Warren, S.; Trenary, M. *J. Phys. Chem. B* **2000**, *104*, 2448.
(29) Ammer, C.; Meinel, K.; Wolter, H.; Neddermeyer, H. *Surf. Sci.* **1997**, *401*, 138.
(30) Uvdal, P.; Weldon, M. K.; Friend, C. M. *Phys. Rev. B* **1994**, *50*, 12258.
(31) Gomes, J. R. B.; Gomes, J. A. N. F. *J. Mol. Struct.* **1999**, *463*, 163.
(32) Hofmann, Ph.; Schindler, K. M.; Bao, S.; Fritzsche, V.; Ricken, D. E.; Bradshaw, A. M.; Woodruff, D. P. *Surf. Sci.* **1994**, *304*, 74.
(33) Asmundsson, R.; Uvdal, P. *J. Chem. Phys.* **2000**, *112*, 366.
(34) Herzberg, G. *Infrared and Raman Spectra of Polyatomic Molecules*; D. Van Nostrand Co.: New York, 1960.
(35) Gomes, J. R. B.; Gomes, J. A. N. F. *Surf. Sci.* **1999**, *432*, 279.
(36) Sexton, B. A. *Surf. Sci.* **1979**, *88*, 319.
(37) Sawada, T.; Liu, Z.; Takagi, N.; Watanabe, K.; Matsumoto, Y. *Chem. Phys. Lett.* **2004**, *392*, 334.
(38) Mei, D.; Xu, L.; Henkelman, G. *J. Catal.* **2008**, *258*, 44.
(39) Nakamura, I.; Nakano, H.; Fujitani, T.; Uchijima, T.; Nakamura, J. *Surf. Sci.* **1998**, *402*, 92.
(40) Puschmann, A.; Haase, J.; Crapper, M. D.; Riley, C. E.; Woodruff, D. P. *Phys. Rev. Lett.* **1985**, *54*, 2250.
(41) Sakong, S.; Gross, A. *J. Phys. Chem. A* **2007**, *111*, 8814.
(42) Jones, A. H.; Poulston, S.; Bennett, R. A.; Bowker, M. *Surf. Sci.* **1997**, *380*, 31.
(43) Sakong, S.; Gross, A. *J. Catal.* **2005**, *231*, 420.
(44) Hoffmann, F. M.; Paul, J. *J. Chem. Phys.* **1987**, *86*, 2990.
(45) Käsberger, U.; Jakob, P. *Surf. Sci.* **2003**, *540*, 76.
(46) Pfnür, H.; Feulner, P.; Menzel, D. *J. Chem. Phys.* **1983**, *79*, 4613.
(47) Brø nsted, N. *Chem. Rev.* **1928**, *5*, 231.
(48) Evans, M. G.; Polanyi, M. *Trans. Faraday Soc.* **1938**, *34*, 11.
(49) Logadottir, A.; Rod, T. H.; Nørskov, J. K.; Hammer, B.; Dahl, S.; Jacobsen, C. J. H. *J. Catal.* **2001**, *197*, 229.
(50) Bligaard, T.; Nø rskov, J. K.; Dahl, S.; Matthiesen, J.; Christensen, C. H.; Sehested, J. *J. Catal.* **2004**, *224*, 206.
(51) Cheng, J.; Hu, P.; Ellis, P.; French, S.; Kelly, G.; Lok, C. M. *J. Phys. Chem. C* **2008**, *112*, 1308.
(52) Jakob, P.; Schlapka, A.; Gazdzicki, P. *J. Chem. Phys.* **2011**, *134*, 224707.
(53) Schlapka, A.; Lischka, M.; Gross, A.; Käsberger, U.; Jakob, P. *Phys. Rev. Lett.* **2003**, *91*, 016101.

Supporting information for: Methanol oxidation on monolayer Cu/Ru(0001)

Pawel Gazdzicki, and Peter Jakob*

Fachbereich Physik und Zentrum für Materialwissenschaften, Philipps-Universität Marburg, Renthof 5, 35032 Marburg, Germany

Supporting Information

References

(1) Koch, M. H.; Jakob, P.; Menzel, D., Surf. Sci. **1996**, 367, 293.

(2) Shi, S.-K.; Schreifels, J. A.; White, J. M., Surf. Sci. **1981**, 105, 1.

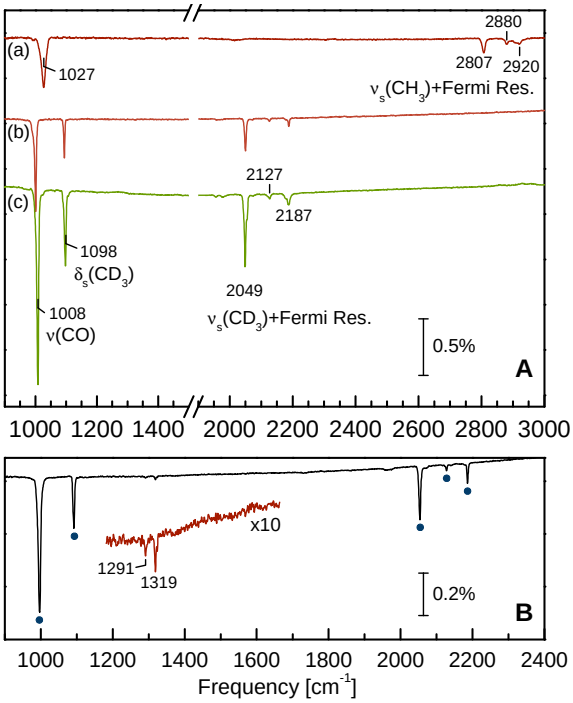

Figure 1: **A: IRAS spectra of different methoxy isotopes and of formate on oxygen precovered Cu/Ru(0001) layers** IRAS spectra of (a): CH_3O on O/$Cu_{1\ ML}$/Ru(0001) ($\Theta_O = 0.2$), and (b): CD_3O on O/$Cu_{1\ ML}$/Ru(0001) ($\Theta_O = 0.2$ ML). 0.15 ML CD_3OH or CH_3OH have been adsorbed at 80 K onto annealed oxygen layers. (c) For comparison a spectrum of CD_3O on O/'Cu(111)'/Ru(0001) is included. CD_3O is produced by heating a CD_3OH+O coadsorbate layer ($\Theta_O = 0.14$ ML, $\Theta_{CD3OH} = 1-2$ ML). In all cases the sample was annealed to 300 K to produce methoxy and recooled to 80 K for data taking. 'Cu(111)'/Ru(0001) was prepared by deposition of $\sim$30 ML Cu on Ru(0001) followed by annealing to 900 K for 30 min. The comparison of spectra demonstrates that CD_3O exhibits significantly narrower line shapes than CH_3O. In addition it is apparent that the $\delta_s(CH_3)$ mode, expected at $\sim$1400 cm^{-1}, cannot be detected for the regular methoxy isotope on Cu/Ru(0001), while it is clearly visible for the CD_3OH isotope. This peculiarity is attributed to mode coupling of $\delta_s(CD_3)$ with the nearby ν(CO) mode which enhances the intensity of this mode; for $\delta_s(CH_3)$ such coupling is negligible due to the frequency mismatch. The mode assignment is denoted in the figure. **B: Formate on Cu_{30ML}/Ru(0001).** DCOO produced by annealing the layer in (c) to 440 K. As on 1 ML Cu/Ru(0001) (see figure 6 of the article) the two peaks at 1291 and 1319 cm^{-1} correspond to the C-O and O-C-O stretching modes of formyl and DCOO, respectively. Methoxy bands are marked by blue dots.

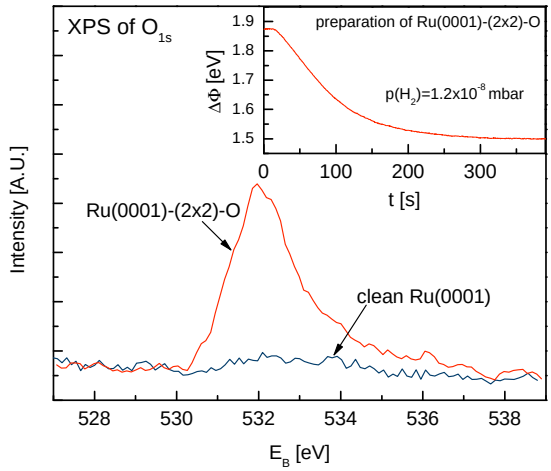

Figure 2: **Calibration of the oxygen coverage.** XPS spectra of the O 1s peak on the nominally clean Ru(0001) surface and on Ru(0001)-(2×2)-O measured with a MgK$_\alpha$ source. The Ru(0001)-(2×2)-O layer with $\Theta_O = 0.25$ ML was prepared by adsorption of 0.5 ML O, flashed to 1250 K to obtain $0.5 > \Theta_O > 0.25$ ML, and dosing H_2 to remove redundant oxygen (beyond 0.25 ML) as desorbing water. The required H_2 exposure is derived from $\Delta\Phi$ (work function) measurements with a Kelvin Probe shown in the inset. At a sample temperature of 350 K $\Delta\Phi$ decreases until a perfect (2×2)-O overlayer is attained which is largely inert towards further titration with hydrogen.[1,2]

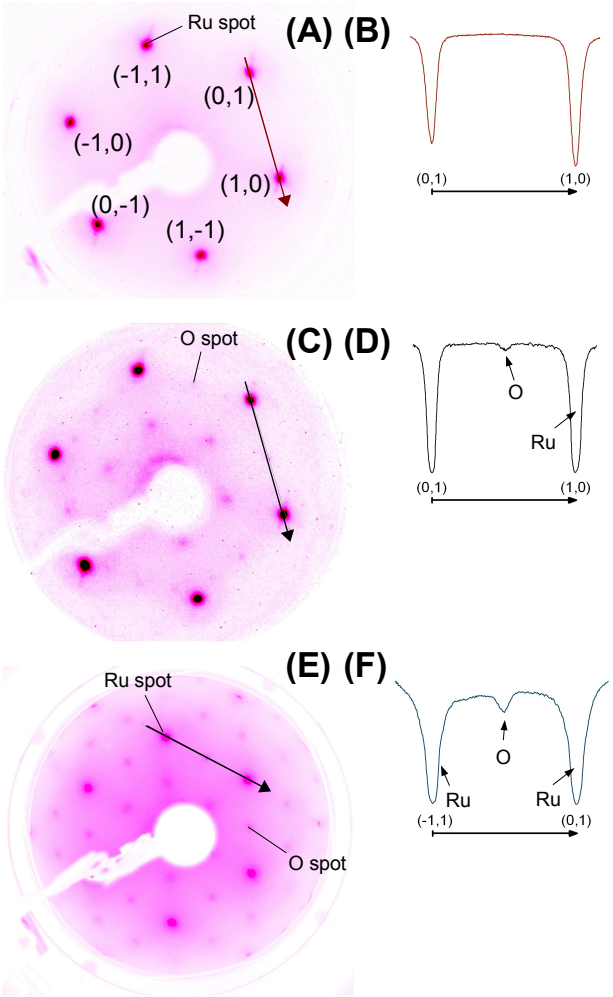

Figure 3: **LEED patterns of O/Cu_{1ML}/Ru(0001) layers.** Image (A) shows a LEED pattern of 1 ML Cu/Ru(0001) confirming the pseudomorphic structure of the Cu monolayer. The line scan in panel (B) corresponds to the arrow in panel (A). Image (C) was taken after dosing 0.5 L O_2 (equivalent to $\sim$0.1 ML) at 80 K followed by annealing to 500 K. The line scan (arrow in panel (C)) is depicted in panel (D). Besides Cu/Ru additional spots due to the oxygen (2×2)-overlayer are discernible. The LEED pattern of the Cu/Ru(0001) monolayer after an exposure of 14 L O_2 at 80 K (and annealing to 400 K) and the corresponding line scan are depicted in panels (E) and (F), respectively.

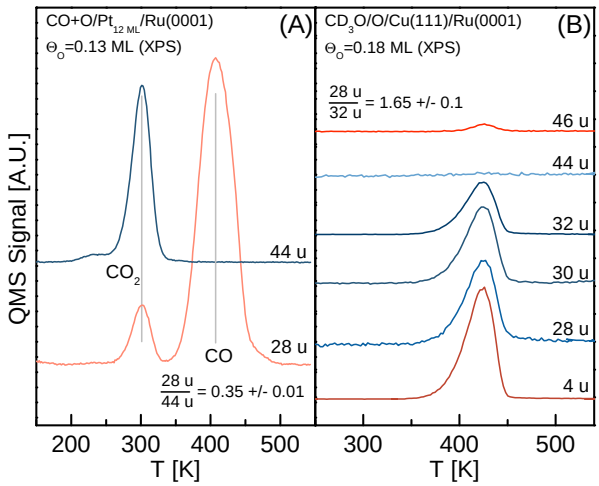

Figure 4: **Intensity ratios of ionization fragments of CO_2 and D_2CO.** The intensity ratios of the ionization fragments of CO_2 and D_2CO have been derived from the TPDs (1 K/s) in panels (A) and (B), respectively. **(A):** TPD of coadsorbed CO and O on 12 ML Pt/Ru(0001). At 300 K reactively produced CO_2 (44 u) desorbs until all surface oxygen is consumed. Thus, the 28 u peak at 300 K is exclusively due to cracking of CO_2 and a value of $\frac{28\text{ u}}{44\text{ u}} = 0.35 \pm 0.01$ is derived. The desorption of excess CO is observed at 410 K. Due to measuring the amount of preadsorbed oxygen with XPS this TPD also acts as a calibration of the quantity of desorbing CO_2. **(B):** multiple mass TPD of CD_3O on $^{18}O/Cu_{30ML}/Ru(0001)$. Virtually all methoxy (CD_3O) desorbs as formaldehyde (D_2CO, mass 32 u). The masses 30, 28 and 4 u are due to cracking products of D_2CO in the QMS. The peak of 46 u is due to minute amounts of desorbing $C^{18}O^{16}O$ caused by formate decomposition; formate is produced by minor oxidation of methoxy. The ratio of CO/CO_2 for CO_2 desorption is known from panel (A). The intensity ratio of the CO^+ ionization fragment of desorbing D_2CO is $\frac{28\text{ u}}{32\text{ u}} = 1.65 \pm 0.1$.

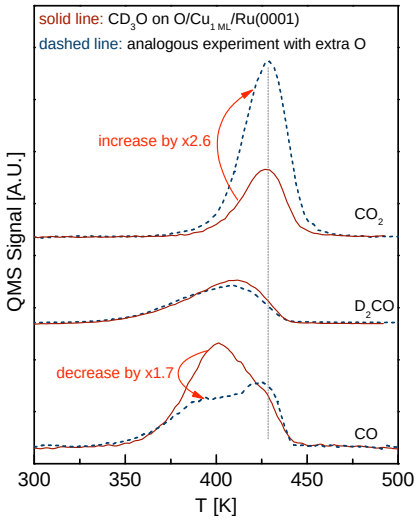

Figure 5: **Methoxy oxidation on Cu_{1ML}/Ru(0001): Control of formate product yield by oxygen post-adsorption.** Solid lines: TPD of CD_3OH (exposure 40 mTorr·s) post-adsorbed at 80 K onto annealed 0.1 ML oxygen on $Cu_{1\ ML}$/Ru(0001); before the TPD the sample was heated to 300 K to produce CD_3O. Dashed lines: analogous experiment as above with extra oxygen added (3 L O_2 at 80 K) after the annealing step to 300 K. The plotted masses correspond to CO_2 (44 u), D_2CO (32 u) and CO (28 u). Note that the CO_2 and D_2CO ionization fragment contributions have been subtracted from the measured 28 u signal. The data demonstrate that the relative yield of produced CO_2 and CO can be controlled by adding extra O to the methoxy layer on the $Cu_{1\ ML}$/Ru(0001) monolayer.

6.4 Article IV: Oxygen on Pt/Ru(0001) Layers

Oxygen adsorption on Pt/Ru(0001) layers

Peter Jakob,[a] Andreas Schlapka, and Pawel Gazdzicki
Fachbereich Physik und Wissenschaftliches Zentrum für Materialwissenschaften, Philipps-Universität Marburg, D-35032 Marburg, Germany

(Received 8 October 2010; accepted 18 May 2011; published online 14 June 2011)

Chemical properties of epitaxially grown bimetallic layers may deviate substantially from the behavior of their constituents. Strain in conjunction with electronic effects due to the nearby interface represent the dominant contribution to this modification. One of the simplest surface processes to characterize reactivity of these substrates is the dissociative adsorption of an incoming homonuclear diatomic molecule. In this study, the adsorption of O_2 on various epitaxially grown Pt films on Ru(0001) has been investigated using infrared absorption spectroscopy and thermal desorption spectroscopy. Pt/Ru(0001) has been chosen as a model system to analyze the individual influences of lateral strain and of the residual substrate interaction on the energetics of a dissociative adsorption system. It is found that adsorption and dissociative sticking depends dramatically on Pt film thickness. Even though oxygen adsorption proceeds in a straightforward manner on Pt(111) and Ru(0001), molecular chemisorption of oxygen on Pt/Ru(0001) is entirely suppressed for the Pt/Ru(0001) monolayer. For two Pt layers chemisorbed molecular oxygen on Pt terraces is produced, albeit at a very slow rate; however, no (thermally induced) dissociation occurs. Only for Pt layer thicknesses $N_{Pt} \geq 3$ sticking gradually speeds up and annealing leads to dissociation of O_2, thereby approaching the behavior for oxygen adsorption on genuine Pt(111). For Pt monolayer films a novel state of chemisorbed O_2, most likely located at step edges of Pt monolayer islands is identified. This state is readily populated which precludes an activation barrier towards adsorption, in contrast to adsorption on terrace sites of the Pt/Ru(0001) monolayer. © *2011 American Institute of Physics*. [doi:10.1063/1.3598957]

I. INTRODUCTION

The tailoring of the chemical characteristics of catalytically active materials represents a major, though elusive task. The aim is to control selectivity and productivity of chemical reactions by proactively influencing the available adsorption sites, the respective adsorption energies, the sticking coefficients for impinging gaseous species and the various activation energies of processes encountered along the reaction pathways. Due to a large number of parameters this represents a formidable endeavour and the extraction of unambiguous and generally applicable information is both, rare and cumbersome. Besides the chemical nature of a catalyst material, its activity may be influenced in particular by the type of adsorption sites (coordination number, terrace, step, or kink sites),[1–3] the number and chemical nature of neighboring atoms (ensemble and ligand effect),[4–6] as well as strain imposed on a lattice by means of various types of heterogeneity.[5,7–9] Yet another degree of freedom (which will not be discussed any further) may be introduced by gas mixtures and the utilization of promotors.[10]

In order to extract reproducible, clear-cut, and well-founded information from catalytic studies, it is advisable to keep good control of experimental (sample) parameters and to add heterogeneity very selectively and systematically. A common approach in the past has been to employ vicinal surfaces and compare the findings to ideal, single crystal surfaces.[1,2,11–13] However, more often than not definite conclusion, i.e., the ascription to a particular interaction process, is hampered by ill-defined experimental conditions, e.g., the combined variation of too many parameters, or a multitude of influences contributing to the detected quantity. For example, the addition of different chemical elements to a catalyst material (e.g., alloying) may introduce novel characteristics either due to the ensemble or the ligand effect, as well as due to strain imposed on the lattice as a result of atoms with a different atomic diameter or number of valence electrons.[6,14,15]

Another procedure to functionalize surfaces is to epitaxially grow metallic layers.[4,16,17] A key characteristic of such bimetallic systems is the lattice mismatch between the adlayer and the substrate. In order to maintain a high degree of surface homogeneity it is desirable to grow pseudomorphic, or otherwise lattice-matched layers.[8,18,19]

In the present paper the adsorption of oxygen on epitaxially grown bimetallic Pt/Ru(0001) layers has been analyzed. For Pt on Ru(0001), up to at least 4 monolayers (ML) Pt grow pseudomorphically, i.e., they adopt the lattice constant of the Ru(0001) substrate and, consequently, are laterally compressed by 2.5%.[8,18] Due to this structural lattice distortion, the Pt electronic structure will deviate from Pt(111), in addition to the remaining influence of the Ru(0001) substrate and of the Pt/Ru interface. In a combined experimental and theoretical approach these two effects have

[a]Electronic mail: peter.jakob@physik.uni-marburg.de.

recently been disentangled for CO on Pt layers of various thickness on Ru(0001).[8] It has been shown that the electronic influence of the substrate, while dominant for Pt islands of monatomic height, has largely vanished for three Pt layers (N_{Pt}). The contribution due to surface strain, on the other hand, is still fully operative until $N_{Pt} = 4$–5 ML when the Pt film starts to relax (and gradually approaches the Pt lattice constant), as indicated by the formation of a dislocation network.[8,18]

For thick Pt layers $N_{Pt} > 10$ ML adsorption of CO strongly resembles CO on Pt(111); slight deviations in terms of step density, CO binding energy and vibrational frequencies, however, remain.[18] According to recent experimental as well as theoretical studies, adsorbate binding energies on laterally expanded lattices are higher (stronger bonding) than on laterally compressed ones.[7,20,21] In the case of CO adsorption on pseudomorphic Pt/Ru(0001) layers, both effects (compressive lateral strain and influence of the Pt/Ru interface) lead to a substantial weakening of the CO-substrate bond strength, in agreement with expectations. The deviations from the behavior on Pt(111) thereby are most significant for thin Pt films, indicating that the influence of lateral strain within the pseudomorphic layers on the adsorption energetics is of subordinate importance as compared to the substrate/interface effect.[8] Only for $N_{Pt} \geq 3$ ML, the strain effect dominates. According to theory oxygen adsorption energies on Pt/Ru(0001) films will be modified (reduced) too, in particular for very thin Pt films.[22]

Despite its notable degree of complexity, the system O_2 on platinum has a number of characteristics which renders it a favorable choice. Specifically, various types of adsorbed oxygen species exist and can be distinguished using infrared absorption spectroscopy (IRAS): physisorbed O_2, two types of chemisorbed O_2, as well as chemisorbed atomic oxygen; since all of them are separated by an activation barrier, the various states can be prepared separately and characterized by standard surface analytical tools.[23–27]

The used IRAS setup is designed for low temperature measurements down to 30 K, providing in-depth insight in the adsorption behavior of oxygen on deposited Pt films on Ru(0001). On Pt(111) there exist various transient stages of O_2 adsorption, depending on sample temperature. At $T <$ 40 K, O_2 is molecularly physisorbed with an intramolecular O-O stretching frequency very close to the free O_2 molecule in the gas phase at 1556 cm^{-1}.[28] At $T > 45$ K, physisorbed O_2 is transformed into two types of molecular chemisorbed states: a paramagnetic so called "superoxo" O_2^- state and a nonmagnetic "peroxo" O_2^{2-} species have been suggested.[25,29–31] The respective internal vibrational modes $\nu_{O\text{-}O}$ are located at about 875 cm^{-1} and 700 cm^{-1}.[32–35] According to theoretical calculations[30] and, in particular, a careful STM investigation[26,36] the two oxygen species are centered above bridge and fcc sites, respectively (Fig. 1). Their abundances depend critically on the adsorption temperature (low T favors the bridge bonded superoxo state), which is due to dissimilar activation energies to reach these states, starting from a highly mobile (intrinsic) precursor state.[36] A third state located at Pt step edges with ⟨111⟩ microfacets (B-type) has additionally been identified using STM; no molecules have been detected at steps with ⟨100⟩ microfacets (A-type).[26,36]

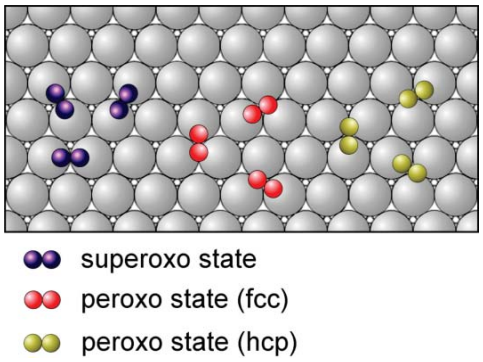

FIG. 1. Adsorption sites of the peroxo and the superoxo species adsorbed on Pt(111), according to a theoretical (Ref. 30) and an experimental study (Ref. 26). They all display three equivalent orientations.

Heating beyond 150 K causes thermal dissociation of molecularly chemisorbed O_2.[32,34] This process is usually accompanied by molecular desorption. In case CO is present, a reaction to form CO_2 proceeds in parallel as well.[37–39] For stepped Pt(111) surfaces (steps along Pt atom rows, i.e., the ⟨1, −1, 0⟩ direction) extra O_2 desorption peaks have been reported at 170-180 K and 220 K (Refs. 2, 12, 13, 40, 41, and 42) with the former being related to O_2 in the vicinity of atomic oxygen and the latter representing a genuine O_2 step species.[40,42]

Atomic oxygen on Pt(111) preferentially occupies fcc sites[30,36] and is characterized by a Pt-O stretch frequency at about 480 cm^{-1}, when arranged in an ordered (2×2)-O overlattice.[34,43]

In this study on the adsorption behavior of chemisorbed O_2 on Pt/Ru(0001) layers a detailed description in terms of vibrational frequencies, binding energies and sticking coefficients will be presented. Direct observation of the internal O-O stretch modes ($\nu_{O\text{-}O}$) of chemisorbed O_2, and of $\nu_{Pt\text{-}O}$ for atomic oxygen thereby allows us to distinguish the various adsorption states of molecular and atomic oxygen species. The data are supplemented by vibrational spectra of coadsorbed CO, acting as a probe molecule which distinguishes between Pt layers of different thickness and which additionally responds sensitively to the presence of nearby oxygen.

II. EXPERIMENTAL

All experiments were performed in an UHV chamber with a base pressure $p = 6 \times 10^{-11}$ mbar, containing facilities for XPS (X-ray photoelectron spectroscopy), low energy electron diffraction, TPD (temperature programmed desorption), FT-IRAS (Fourier transform infrared absorption spectroscopy), and for measurements of work function changes using a Kelvin probe. The sample is a Ru single crystal with a diameter of 10 mm, a thickness of 2 mm, an orientation in the (0001) direction and a purity of 99.999%. It is mounted on a liquid (lq.) He or N_2 cooled cryostate and it can be heated up with linear heating rates of 0.01–10 K/s; the sample

temperature is limited to 1570 K due to a K-type thermocouple spot-welded to the side of the sample. The Ru(0001) surface was cleaned by Ar^+ sputtering (1.5 keV, 1 μA) and multiple O_2 dosing cycles combined with flashing the sample up to 1570 K. The used FTIR instrument is a Bruker IFS 66v with evacuable optics (p < 1 mbar) in order to avoid bothersome absorptions of water or carbon dioxide. Within this work a liquid nitrogen cooled MCT (mercury-cadmium-tellurium) detector was used, allowing for measurements in the spectral range 600–4000 cm^{-1}. Spectra ranging down to 400 cm^{-1} used a liquid He cooled Si:B detector. Unless otherwise specified, IRAS spectra were taken at a resolution of 4 cm^{-1} with 500–1000 scans coadded. For the IR measurements the sample was positioned in a dedicated IR-cell, which contained an additional titanium sublimation pump to reduce contamination. A uniform gas exposure is provided by a multi-capillary array (MCA) with individual diameters of $\simeq$ 10 μm. Linear heating (0.01–10 K/s) to perform temperature programmed desorption (TPD) experiments was achieved by a microcomputer-controlled power supply. Thermal desorption spectra were obtained using a glass enclosure (Feulner cup) (Ref. 44) to ensure desorption from the front face only and to enhance desorption signals in the quadrupole mass spectrometer.

Our Pt films were typically deposited at substrate growth temperatures T_G = 600–700 K at deposition rates of R $\approx 10^{-3}$ ML/s. Post-annealing was restricted to the temperature range of 700–800 K, which assures low defect densities and excludes the possibility of surface alloying.[6,14,15,45]

III. RESULTS

A. Molecular chemisorbed oxygen and conversion to the atomic state

As outlined in Sec. I the adsorptive properties of epitaxially grown Pt layers on Ru(0001) are modified by a combined effect of the Pt/Ru interface as well as lateral strain imposed on the Pt lattice.[8,18] Using CO as a probe particle it has been found that the Pt/Ru interface is perceptible only for thin layers ($N_{Pt} \leq 3$ ML), while the influence of lateral strain persists until the Pt lattice is relaxed by means of dislocation formation ($N_{Pt} \geq 5$ ML). Pt films in excess of 10 ML exhibit only minute deviations from a genuine Pt(111) substrate.[18]

To confirm these characteristics, $^{18}O_2$ and $^{16}O_2$ isotopic species have been adsorbed at T_{ads} = 80 K onto a 10 ML Pt/Ru(0001) film (growth temperature T_G = 700 K). The respective vibrational spectra are displayed in Fig. 2 for the peroxo and superoxo species of molecularly chemisorbed O_2; the various line positions are summarized in Table I, along with the respective isotopic shift factors. Also included in Table I are data on adsorbed atomic oxygen (O-(2 × 2) phase), which forms upon slight annealing of molecularly chemisorbed oxygen to T ≥ 150 K (see Figs. 2(c) and 2(d)). Note, that the values in Table I deviate slightly from Figs. 2(c) and 2(d), as the displayed spectra were obtained from an incomplete O-(2 × 2) phase; only after several adsorption/annealing cycles a perfect p(2 × 2) long range order of the produced atomic oxygen layers is obtained. It is apparent that the vibrational bands

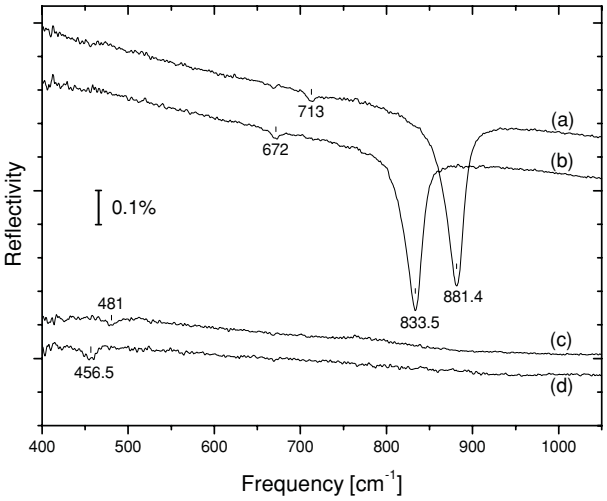

FIG. 2. Infrared absorption spectra of $^{16}O_2$, (a), and $^{18}O_2$, (b), adsorbed at 80 K (exposure 30 L) on epitaxially grown Pt/Ru(0001) films (N_{Pt} =10 ML, T_G = 700 K). IR spectra of atomic oxygen, obtained after annealing the molecular adsorbates to 300 K, are reproduced in curves (c) and (d) for ^{16}O and ^{18}O, respectively. All spectra were taken at a sample temperature of T_m = 80 K, using a lq. He cooled Si:B detector and at a spectral resolution of 2 cm^{-1}.

associated with $^{18}O_2$ and $^{16}O_2$ display a bold isotopic shift for both molecular chemisorbed oxygen species, which confirms their identity as oxygen derived vibrational modes. The $\nu_{O\text{-}O}$ frequencies for oxygen adsorbed on a 10 ML Pt film are somewhat higher as compared to Pt(111) which is attributed to a slightly weaker interaction of O_2 with the not yet fully relaxed Pt film. This observation is in accordance with CO adsorption on the very same Pt film, which likewise displays only marginal deviations in vibrational frequencies as compared to CO on Pt(111), along with slightly lower desorption temperatures in TD-spectra.[8,18] The close similarities of our Pt films and Pt(111) in particular comprises the isotopic shift factors k_{iso} of atomic and molecular oxygen species; in particular, they deviate only slightly from the value of gas phase O_2 ($k_{iso} = 0.943$).[28]

B. Adsorption series for different N_{Pt}

In order to investigate the dependence of the adsorption probability of impinging O_2 molecules on Pt/Ru(0001)

TABLE I. Experimentally observed $\tilde{\nu}_{O\text{-}O}$ line positions of the peroxo and the superoxo O-O stretch modes for the two isotopic species $^{18}O_2$ and $^{16}O_2$. Also included are the respective Pt-O stretch frequencies $\tilde{\nu}_{Pt\text{-}O}$ of atomic oxygen (O-(2 × 2) phase). All line positions are given in cm^{-1} and they refer to a sample temperature of 80 K during IR measurements. The data for Pt(111) are quoted from the literature for comparison (Refs. 27, 35, and 43).

Substrate	10 ML Pt on Ru(0001)			Pt(111)		
Oxygen isotope	$^{18}O_2$	$^{16}O_2$	k_{iso}	$^{18}O_2$	$^{16}O_2$	k_{iso}
$\tilde{\nu}_{O\text{-}O}$ (peroxo species)	672	713	0.942	...	703	...
$\tilde{\nu}_{O\text{-}O}$ (superoxo species)	833.5	881.4	0.946	830	875	0.949
$\tilde{\nu}_{Pt\text{-}O}$ (atomic oxygen)	458	484	0.946	452	477	0.948

layers of varying thickness, the $\nu_{O\text{-}O}$ mode of the superoxo species has been monitored for increasingly higher O_2 exposures. Thereby a thermal beam, aligned by means of a micro-capillary array has been directed at the sample (normal incidence) which was held at a temperature of 80 K (unless otherwise specified).

Unfortunately, the determination of absolute values of the sticking coefficient s was impeded due to the fact that the MCA is located inside the IRAS measurement cell which contains an extra titanium sublimator pump to ensure negligible contaminations; the pressure increase as measured in the UHV main chamber therefore remained in the low 10^{-10} mbar range even if substantial amounts of gas were introduced.

Exposures are therefore based on the pressure reading in the dosing line × exposure time (day-to-day reproducibility about ±5%). In order to obtain equivalent exposures in langmuir (L), a calibration has been carried out lateron. Here, identical O_2 surface coverages have been prepared in two different ways: (i) by means of the directed MCA gas dosing beam and (ii) using isotropic dosing.

The pressure reading in the gas dosing line is provided by a bakable MKS baratron held at a constant temperature to minimize thermal drifts. The pressure in the gas dosing system is dynamically held constant by adjusting a permanent flow from the reservoir while slightly pumping with a turbomolecular pump. A lq. N_2 cold trap inserted in the gas dosing line ensures removal of residual condensable contaminants.

In Fig. 3, three series of IR-spectra taken as the O_2 coverage increases are displayed. The Pt layer thicknesses have been chosen to be 1.3, 2.0, and 10 ML. It is apparent that independent of Pt layer thickness, the spectral appearances, as well as coverage dependent $\nu_{O\text{-}O}$ line shifts of the superoxo species at 870–880 cm^{-1} are quite similar to the findings on Pt(111).[34,35] The same applies to $\nu_{O\text{-}O}$ of the peroxo species at about 710 cm^{-1} except for the fact that this band is missing for thin Pt films ($N_{Pt} \leq 4$ ML). A remarkable difference with respect to adsorption on Pt(111), however, are the substantially increased oxygen gas exposures necessary to reach a certain O_2 coverage.

Another quite startling observation is represented by the 790 cm^{-1} band which is associated with $N_{Pt} \simeq 1$ ML and which grows to its final strength already for rather low exposures at 80 K; annealing to 175 K causes this species to disappear. An extra paragraph will be devoted to this novel species (see below).

C. Extraction of sticking coefficients

According to a quantitative analysis of the O-O stretch mode intensity $I(\nu_{O\text{-}O})$ in Fig. 3, the amount of chemisorbed O_2 initially increases about linearly with O_2 exposure for each of the Pt/Ru(0001) layers; eventually, the increase of $I(\nu_{O\text{-}O})$ slows down which is attributed to the onset of saturation of the Pt/Ru(0001) surface, and probably, electronic screening (depolarization) of $\nu_{O\text{-}O}$. The linear dependence between $I(\nu_{O\text{-}O})$ and the amount of chemisorbed O_2 (derived from thermal desorption spectroscopy) has been verified for Pt-layers N_{Pt} = 1.5-12 ML (see supplementary material[46]). This means that, independent of Pt layers thickness, the $\nu_{O\text{-}O}$ oscillator strength for adsorbed O_2 remains more or less constant.

From these traces the averaged initial sticking coefficient $s_0(\bar{N}_{Pt})$ is extracted for the various layers. Specifically, it is found that s_0 grows dramatically with increasing average Pt layer thickness $\bar{N}_{Pt}$. In a more detailed analysis of O_2 sticking the individual fractional areas A_i with $N_{Pt,i}$ Pt layers were additionally taken into account. Using IRAS, these can be easily discriminated by adsorbing small amounts of CO; in the absence of dynamical dipole coupling, i.e., at low CO coverages Θ_{CO}, discrete bands of $\nu_{C\text{-}O}$ (C-O stretch mode) have been observed at 2085.5, 2094, and 2098 cm^{-1} for $N_{Pt} = 1$, 2, and 3 ML, respectively.[18] For $\nu_{O\text{-}O}$ of chemisorbed O_2 such a discrimination is impeded by the fact that the respective vibrational bands at 860–880 cm^{-1} are quite broad. This is why, prior to oxygen adsorption, each Pt layer deposited onto

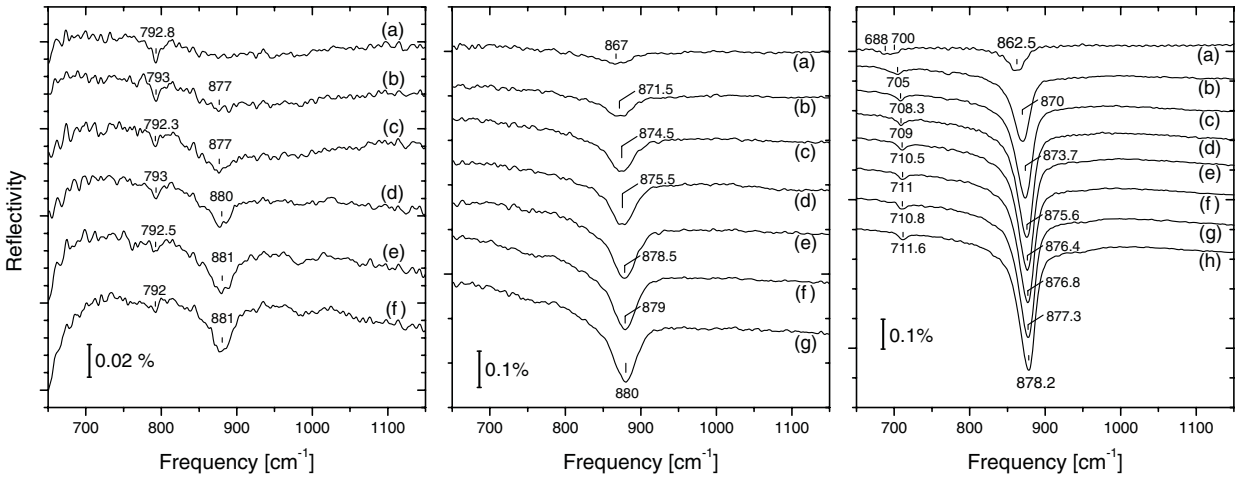

FIG. 3. Infrared absorption spectra of increasing amounts of molecularly adsorbed $^{16}O_2$ on epitaxially grown Pt/Ru(0001) films: (left) N_{Pt} = 1.3 ML, T_G = 600 K; (center) N_{Pt} = 2.0 ML, T_G = 600 K; (right) N_{Pt} = 10 ML, T_G = 700 K. Accumulated O_2 exposures at T_{ads} = 80 K as indicated in Fig. 4(a). Maximum O_2 exposures in the left, center, and right series of IR-spectra were 235 L, 520 L, and 18 L, respectively. All spectra were obtained at T_m = 80 K using a lq. N_2 cooled MCT detector and at a spectral resolution of 4 cm^{-1}.

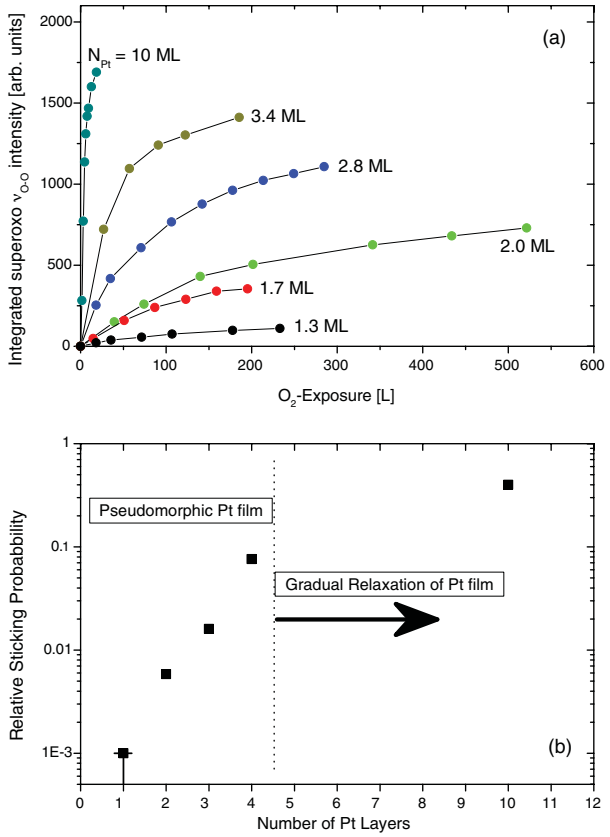

FIG. 4. (a) Integrated intensities of the ν_{O-O} bands of the superoxo O_2 species as the oxgen exposure is increased (T_{ads} = 80 K). The individual curves refer to Pt/Ru(0001) layers of different thicknesses, as indicated in the figure. The relative error in the given exposures is estimated to be ±10%. (b) Extracted sticking coefficients of impinging O_2 (thermal beam) for an increasing number of Pt layers. The quoted values refer to low O_2 coverages ($\Theta_{O_2} \leq 5\%$), and they are given with respect to O_2 adsorption on Pt(111). The value of 10^{-3} for N_{Pt} = 1 ML represents an upper limit.

Ru(0001) has been characterized by CO adsorption at low T ≃ 80 K (flashed away lateron); the low temperatures thereby suppress lateral motion and ensure negligible interlayer transport during CO adsorption. From these spectra the fractional areas A_i with $N_{Pt,i}$ Pt layers were determined. The average amount of deposited Pt (which scaled nicely with the integrated flux of deposited Pt) then equals $\bar{N}_{Pt} = \sum A_i \cdot N_{Pt,i}$.

The derived, averaged sticking coefficients (see Fig. 4(a)) are then used to extract the values for individual N_{Pt} (see Fig. 4(b)). The most striking finding of the adsorption experiments presented in this work is the very low sticking coefficient of oxygen molecules on the Pt/Ru(0001) monolayer, despite an efficient oxygen uptake for the pristine close-packed surfaces of platinum[12,23,32] and ruthenium[47] (sticking coefficients for thermal beams amount to 0.5 and beyond). Moreover, it is found that sticking greatly increases, as thicker layers are grown.

Comparison of the findings regarding O_2 adsorption on the 10 ML Pt film and on Pt(111) yields a somewhat lower sticking probability for the epitaxially grown film along with a minor ν_{O-O} frequency shift, which is attributed to the not yet fully relaxed evaporated Pt film. Similar observations have been reported for ν_{C-O} frequencies of isolated CO species on increasingly thicker Pt layers which approach the value observed on Pt(111) only little by little.[18] Note that Pt layers grow pseudomorphically for $N_{Pt} \leq 4$ ML and relaxation of the strained (compressed) Pt lattice proceeds very gradually for thicker layers, and is accompanied by the formation of a dislocation network.[8,18] Using monochromatic molecular beams, the sticking of O_2 on Pt(111) has been analyzed in detail by Luntz *et al.*;[23] based on their data an absolute sticking coefficient of about 0.6 is to be expected for a thermal beam such as ours, impinging perpendicularly onto Pt(111), and accordingly lower values for the Pt/Ru(0001) films.

The negligible sticking of O_2 on the Pt monolayer is confirmed by vibrational spectra of coadsorbed CO (Fig. 5). Here it is essential that the internal stretch frequency of CO on Pt is sensitively influenced by coadsorbates. For example, for N_{Pt} = 10 ML Pt on Ru(0001) ν_{C-O} experiences blue shifts of about 20 and 10 cm^{-1} when coadsorbed with either O_2 or atomic oxygen, respectively, in favorable agreement with findings of CO on Pt(111).[48] Similar observations were made for CO on Ru(0001) surrounded by various chemisorbed coadsorbate species.[49–52] In Fig. 5 the curves (a)–(f) correspond to the layers in the left panel of Fig. 3. Due to a heavy CO dose just before the oxygen adsorption series was conducted, the oxygen

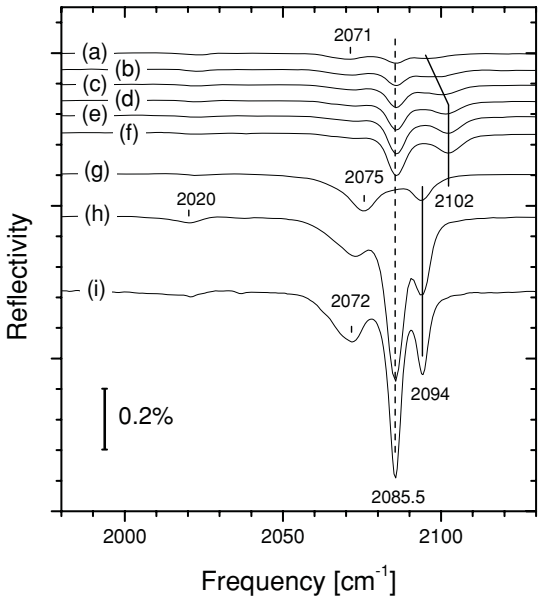

FIG. 5. Infrared absorption spectra of CO used as a tracer to monitor adsorption of molecular oxygen on an epitaxially grown Pt/Ru(0001) film (N_{Pt} = 1.3 ML). The curves (a)–(f) represent the spectra in Fig. 3 (left panel) in the spectral region of the C-O stretch mode. Due to minute amounts of CO in the O_2 gas, oxygen uptake at 80 K was accompanied by the growth of the ν_{C-O} modes at 2070–2100 cm^{-1} (curves (a)–(f)). (g): Layer in (f) after annealing to 175 K; (h): layer in (g) after annealing to 600 K (thereby desorbing CO entirely) and with 0.02 ML CO adsorbed at 80 K thereafter. For comparison the IR spectrum of 0.02 ML CO adsorbed at 80 K on the native Pt/Ru(0001) layer (i.e., before oxygen according to curves (a)–(f) has been admitted) is displayed as well (curve (i)). The spectra were obtained at T_m = 80 K using a lq. N_2 cooled MCT detector and at a spectral resolution of 4 cm^{-1} (curves (a)–(h)) or 2 cm^{-1} (curve (i)).

gas contained tiny amounts of CO which accumulated on the Pt/Ru(0001) surface as the O_2 exposure increased; in curve 5(f) the CO coverage amounts to 0.005 ML. Thanks to a notable chemical shift of $\nu_{C\text{-}O}$ in the vicinity of coadsorbed oxygen atoms or molecules, CO can be used as a probe molecule to detect adsorbed oxygen on Pt/Ru(0001). As $\nu_{C\text{-}O}$ displays characteristic line shifts for increasing N_{Pt} (see supplementary material[46] and Ref. 18) this analysis has the advantage of being layer sensitive.

Specifically, it is found that, independent of O_2 exposure, $\nu_{C\text{-}O}$ at 2085.5 cm^{-1} (ascribed to CO on the Pt/Ru(0001) monolayer) (Ref. 53) remains unchanged with respect to CO on a clean Pt/Ru(0001) monolayer. This observation of a nondistorted $\nu_{C\text{-}O}$ band for $N_{Pt} = 1$ ML stands even after quite high oxygen exposures of several hundred L have been admitted, in accordance with a zero (or close to) adsorption probability for O_2 on this layer. For thicker Pt layers, on the other hand, $\nu_{C\text{-}O}$ displays substantial line shifts if molecularly or atomically chemisorbed oxygen is coadsorbed. Specifically, for CO located in sub-areas with 2 ML Pt/Ru(0001), O_2 exposure leads to a narrow line at 2102 cm^{-1} (see Figs. 5(d)–5(f)), i.e., chemisorbed O_2 induces a +8 cm^{-1} blue shift with respect to 2094 cm^{-1} expected for CO on the clean Pt/Ru(0001) bilayer film. A closer inspection of this band (curves (a)–(e) in Fig. 5) reveals a gradual shift 2094 → 2102 cm^{-1}, which we attribute to the decreasing distances between CO and O_2 as the O_2 exposure/coverage increases.

Upon annealing to 175 K (Fig. 5(g)), this $\nu_{C\text{-}O}$ blue shift is nullified again. Evidently, negligible amounts of molecularly chemisorbed O_2 convert to atomic oxygen on these Pt mono and bilayer films, i.e., chemisorbed O_2 largely desorbs upon thermal annealing. On Pt(111) or thick Pt/Ru(0001) films a substantial fraction (roughly a quarter, or even more for O_2 submonolayer coverages) dissociates upon annealing. It is suspected that a lower binding energy of O_2 (favoring desorption at lower T), in conjunction with a slightly higher activation energy for the dissociation channel are responsible for this reduced efficiency in O_2 dissociation. Just for completion we note that CO molecules, initially located on the Pt/Ru monolayer (2085.5 cm^{-1} band) become mobile at $T > 100$ K and leave these areas; their preferred locations, populated upon annealing, are Pt step edges (2075 cm^{-1}) and, probably, areas with $N_{Pt} = 2$ ML (2094 cm^{-1}).

As mentioned above, exposure of the Pt/Ru(0001) monolayer to molecular oxygen at low T exhibits a novel spectral feature at about 790 cm^{-1}. This species forms already for low O_2 exposures, which is at striking variance to the peroxo and superoxo species which are formed only very gradually for thin Pt films on Ru(0001), or, they may not form at all on the Pt/Ru(0001) monolayer; moreover, the 790 cm^{-1} band disappears as soon as higher Pt layers were grown (see Figs. 6(a)–6(d)). Since the 790 cm^{-1} band saturates at quite low intensities (and exposures), it is concluded that it must be associated with some special minority site and that these sites may get populated readily due to an increased bond strength; Pt monolayer terraces, on the other hand, remain virtually oxygen-free.

A straightforward candidate to explain the 790 cm^{-1} band would be O_2 located at Pt steps, as such species

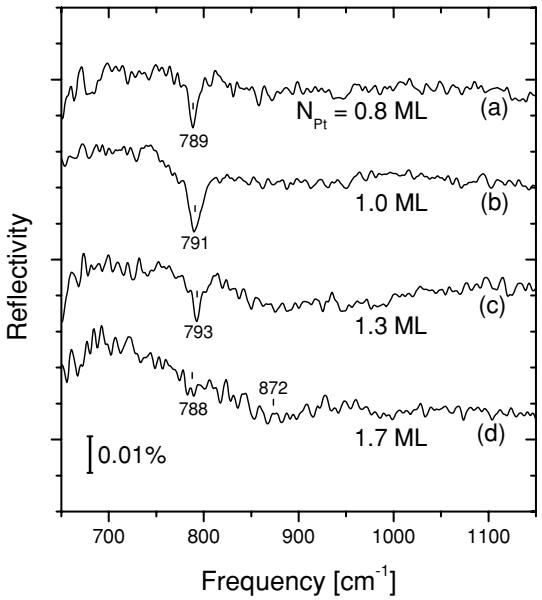

FIG. 6. Infrared absorption spectra of ultrathin Pt/Ru(0001) films (Pt layer thickness ranging from 0.8–1.7 ML, as indicated in the figure) which have been exposed to molecular oxygen at 80 K: (a) 5 L; (b) 25 L; (c) 18 L; (d) 15 L. All Pt/Ru(0001) layers have been grown at $T_G = 600$ K.

have been observed by STM (Refs. 26 and 36) and these oxygen molecules seem to be more strongly bound than O_2 on terraces;[2,12,13,40–42] such stronger bonding would be in accordance with the reported higher desorption temperature and a suggested larger fraction of O_2 dissociation as compared to O_2 on the plain terraces of Pt(111).[3,54]

Another evidence is provided by vibrational spectroscopy: Oxygen adsorption on a stepped Pt(111) surface (B-type of steps with ⟨111⟩ microfacets) indeed gave an extra vibrational band at 820 cm^{-1}, not observed previously (Fig. 7). For Pt(335) substrates (i.e., substrates with A-type of steps) a similar molecular oxygen species with substantially reduced O-O stretch frequency (about 800–820 cm^{-1}) has been observed (using HREELS) and attributed to O_2 located at the ridges separating the rather short terraces.[2,41] Kind of puzzling, the assignment of the 790 cm^{-1} mode to a step species does not really explain why this band is not observed for Pt films beyond monolayer thickness. Possibly, the nearby and much stronger regular terrace O_2 mode screens the respective mode of the minority step edge species (electronic screening or by means of "intensity borrowing").[55–57] As no oxygen adsorbs on the terraces of the Pt/Ru(0001) monolayer, the observation of the weak step species is facilitated.

An alternative interpretation is associated with the special sites located at the boundaries of original Ru step edges and Pt monolayer areas attached to them in the course of the (step-flow) Pt deposition process at elevated T. While one cannot give a definitive answer, the close agreement of the vibrational frequency of this novel state and the O-O stretch frequencies of O_2 at Pt step edges gives clear support to the step edge geometry. Further corroboration to this interpretation comes from the enhanced sticking coefficient for stepped Pt(111) samples,[12,23] which agrees perfectly with the rapid

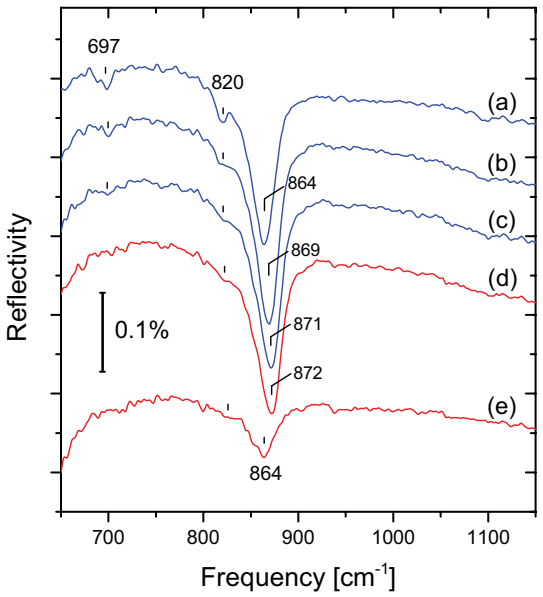

FIG. 7. Infrared absorption spectra of molecular oxygen adsorbed on a stepped Pt(111) surface (5° misorientation with B-type of steps, i.e., with (111) microfacets), and annealed to increasingly higher T thereafter: (a) exposure of 1.2 L O_2 at T_{ads} = 80 K; (b) layer in (a) +1.2 L O_2 at 80 K; (c) layer in (b) +3.6 L O_2 at 80 K; (d) layer in (c) annealed to T_{anneal} = 100 K; (e) layer in (d) annealed to T_{anneal} = 134 K. All spectra were taken after recooling to 80 K.

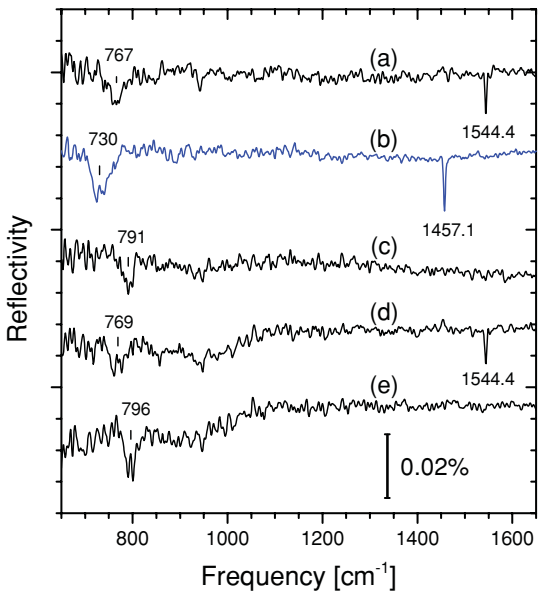

FIG. 8. IRAS spectra of physisorbed O_2 on bimetallic Pt/Ru(0001) layers: (a) N_{Pt} = 1.0 ML, grown at T_G = 600 K, exposed to 35 L $^{16}O_2$ at T_{ads} = 36 K; (b) N_{Pt} = 1.0 ML, grown at T_G = 600 K, exposed to 45 L $^{18}O_2$ at T_{ads} = 36 K; (c) N_{Pt} = 1.6 ML, grown at T_G = 800 K, exposed to 1.5 L $^{16}O_2$ at T_{ads} = 36 K; (d) layer in (c), additionally exposed to 25 L $^{16}O_2$ at T_{ads} = 36 K; (e) layer in (d), annealed to T_{ads} = 60 K. All spectra have been obtained at T_m = 36 K using an MCT detector and at a spectral resolution of 4 cm^{-1}.

uptake of this species despite zero sticking on the Pt/Ru(0001) monolayer for the regular terrace O_2 species.

D. Physisorbed O_2 and thermally induced conversion to chemisorbed O_2

In the following it is investigated whether the lack of O_2 adsorption on the Pt/Ru(0001) monolayer is associated with a kinetic barrier along the adsorption pathway, or, it is simply due to a much too shallow adsorption potential and unsufficient cooling of the sample at T = 80 K. Therefore, lq. He cooling is used in the following. According to the literature, O_2 exposures should predominantly lead to population of a physisorbed O_2 state at very low T.[23–27] A transition into the molecularly chemisorbed O_2 states then can be initiated by slight thermal annealing to 40–70 K; it appears likely that population of the weakly bound precursor state will be transient only, when applying the O_2 gas at elevated surface temperatures (60–120 K). Moreover, the activation barriers stabilizing the physisorbed state on Pt(111) vary slightly for the different adsorption sites underneath, so that the relative ratio of peroxo and superoxo species produced upon annealing depends critically on the adsorption temperature.[26,27]

Figure 8 shows IRAS data of oxygen gas applied to ultrathin Pt/Ru(0001) layers at T = 36 K. In the range of 1400–1600 cm^{-1} a single vibrational mode at 1544.4 cm^{-1} (1457.1 for the $^{18}O_2$ isotopic species; k_{iso} = 0.9435) due to physisorbed O_2 is observed (see curves 8(a) and 8(b)). The internal vibration of this weakly bound molecule apparently has a quite small dynamic dipole moment perpendicular to the surface and its O-O stretch frequency is red shifted by ~12 cm^{-1} as compared to the respective mode of the free O_2 molecule[28] (and blue shifted by 1 cm^{-1} with respect to O_2 on the Pt(111) surface[27]).

The only extra band detected for these layers is located at about 765–800 cm^{-1} for $^{16}O_2$. Interestingly, this band is subject to a red shift by about 25 cm^{-1} when physisorbed oxygen is present (see curves (c) and (d) of Fig. 8). This shift is reversible after physisorbed O_2 has desorbed (Fig. 8(e)). In Sec. III C this feature has been attributed to molecular oxygen at some kind of defect sites, most likely at the step edges of Pt-terraces. Clearly, there exists an isotopic shift 767 → 730 cm^{-1} (k_{iso} = 0.952), when $^{16}O_2$ is replaced by the $^{18}O_2$ isotopic species (see curves (a) and (b) of Fig. 8).

In accordance with the adsorption studies at T = 80 K (see Fig. 6), the 790 cm^{-1} species forms readily, even for rather low exposures (Fig. 8(c)). As the growth of the physisorbed oxygen starts only with some delay, it appears reasonable that there exists a non-activated exit channel of the physisorbed state. It is obvious that these special high reactivity sites of the Pt/Ru(0001) surface are associated with the molecular chemisorbed state with $\tilde{\nu}_{\text{O-O}}$ at about 790 cm^{-1}. It seems that only after these sites have been occupied, the physisorbed oxygen represents a stable (observable) state.

The well-known superoxo and peroxo species, on the other hand, experience shallow but nevertheless effective activation barriers along their adsorption pathways. Referring to molecularly chemisorbed O_2 (superoxo species) with $\tilde{\nu}_{\text{O-O}}$ expected in the range of 850-900 cm^{-1}, no infrared absorption bands are observed for $N_{\text{Pt}} \leq 2$ ML when O_2 dosage is performed at 36 K (apart from a slight baseline instability at

800–1000 cm^{-1} in Figs. 8(d) and 8(e)). With an increasing number of Pt layers, i.e., for $N_{Pt} = 3$ ML and beyond, the filling of the physisorbed O_2 state is accompanied by the growth of a weak band at 870 cm^{-1}. It is attributed to the superoxo state of chemisorbed O_2, in accordance with the adsorption series at 80 K (see Fig. 3). This band gains considerably in intensity upon annealing to 80 K which transforms physisorbed O_2 to the molecularly chemisorbed state on Pt(111).[23–27] Note that the $\nu_{O\text{-}O}$ mode of the superoxo species at about 870 cm^{-1} likewise is subject to a slight red shift (about 6 cm^{-1}) in the presence of physisorbed O_2 (not shown). Such frequency shifts of chemisorbed species in the presence of physisorbates are quite common.[49,50] Interestingly, this shift is substantially weaker for superoxo O_2 as compared to the defect (step) related species with $\tilde{\nu}_{O\text{-}O} = 790$ cm^{-1}. It is invoked that the more compact arrangement[26,36] of the superoxo species (870 cm^{-1}) attenuates the influence of nearby physisorbed O_2. In addition, the effect of second layer O_2 (physisorbed O_2 above islands of superoxo O_2) is expected to be a lot weaker as compared to first layer physisorbed O_2; such behavior has been noticed before for the system CO + Xe/Ar on Ru(0001) and it is in accordance with a negligible work function change of second layer vs. first layer physisorbed species.[50]

For Pt(111) physisorbed oxygen can be readily transformed into molecularly chemisorbed O_2 simply by heating to about 40 K.[24] For Pt/Ru(0001) layers such a transfer works efficiently only for $N_{Pt} \geq 3$ ML. For $N_{Pt} = 1$ ML such annealing fully desorbs physisorbed O_2 and for $N_{Pt} = 2$ ML the amount of produced chemisorbed O_2 is negligibly small. Only by applying extended oxygen exposures at 80 K notable signals of chemisorbed O_2 could be obtained. Further annealing to T $\geq$ 130 K desorbed O_2; as a consequence, atomic oxygen could not be produced on mono and bilayer Pt/Ru(0001). This conclusion is based on the lack of detecting $\nu_{Pt\text{-}O}$ of atomic oxygen and the absence of any oxygen induced $\nu_{C\text{-}O}$ line shifts when using CO as a probe molecule (see Fig. 5, above).

IV. DISCUSSION

In a detailed *ab initio* local-spin-density calculation, the adsorption of oxygen on Pt(111) has been analyzed[30,58] and it turned out that the *d*-band is contributing most significantly to the bonding. Based on the model developed by Hammer and Nørskov[59,60] it has been further shown, that the binding energies of various adsorbate species, such as CO molecules and, in particular, oxygen atoms are linearly lowered as the *d*-band center departs from the Fermi level.[21,61,62]

In previous work an elegant way to modify the surface electronic structure, e.g., the location of the *d*-band, by growing bimetallic layers has been presented.[8] Specifically, clear evidence that the first monolayers of Pt on Ru(0001) grow pseudomorphically and are laterally compressed by 2.5% has been found. According to theory,[21,22,59–61] such a compression yields a stronger overlap of neighboring Pt *d*-band orbitals and an accordingly energetically broadened *d*-band. For Pt on Ru(0001), both of them being transition metals with more than half-filled *d*-band, the energetic position of the *d*-band center is then shifted downward from the Fermi level to ensure charge neutrality of bulk and surface. In the calculations of Mavrikakis and co-workers this shift, as well as variations in adsorbate binding energies have been directly correlated with lattice strain.[21] On the experimental side, this trend of reduced bond strength of adsorbate (oxygen) species on compressed lattices is documented for the Ru(0001) surface, locally strained by means of nanoscale protrusions caused by subsurface Ar-filled cavities after Ar^+-ion bombardment and implantation.[7,20]

The adsorption geometry and energetics of atomic and molecularly chemisorbed oxygen on Pt/Ru(0001) layers have been investigated theoretically by M. Lischka *et al.*[22] Using density-functional theory (DFT) the binding sites of molecularly chemisorbed oxygen on Pt/Ru(0001) have been identified and their adsorption energies determined. For reference, similar calculations have been performed for Pt(111) substrates and their data agreed favorably with other published theoretical calculations on Pt(111),[30,58] as well as with experimental findings: O_2 adsorbs in two configurations, the superoxo ($\tilde{\nu}_{O\text{-}O} \simeq 870$ cm^{-1}) and the peroxo state ($\tilde{\nu}_{O\text{-}O} \simeq 690$ cm^{-1}), which are centered above bridge and threefold hollow sites, respectively. Their binding energies on Pt(111) (0.78 eV for superoxo – O_2 and 0.80 eV for peroxo – O_2) are found to decrease substantially upon lateral compression of Pt(111) down to the Ru(0001) lattice constant (eventually reaching 0.56 eV for superoxo – O_2 and 0.53 eV for peroxo – O_2). Interestingly, the calculated values for oxygen molecules adsorbed on laterally compressed Pt(111) and on pseudomorphic 3 ML Pt/Ru(0001) films are virtually identical.[22] This finding corroborates an earlier conclusion stating that the influence of the Pt/Ru interface is negligible for Pt layer thicknesses of $N_{Pt} = 3$ ML and beyond.[8] Only for $N_{Pt} = 2$ ML and especially for the Pt/Ru(0001) monolayer the substrate influence is substantial, leading to additional reductions of the oxygen-Pt interaction strength.

At variance to expectation based on calculated binding energies of O_2 on Pt/Ru(0001) monolayers,[22] the molecular chemisorbed superoxo – O_2 species could not be detected in our experiments. For Pt bilayers this species is formed, albeit at a slow rate due to the small sticking probability; upon annealing molecular oxygen desorbs entirely, i.e., no transition to the atomic state could be initiated on Pt bilayers. To visualize these differences, a schematic picture of the potential curve as seen by impinging O_2 is displayed in Fig. 9. Despite its simplicity it may nevertheless provide an intuitive picture of the findings of this study regarding the sticking of oxygen on the various Pt/Ru(0001) layers.

In our TD spectra (see supplementary material[46]) we observe an increase in O_2 desorption (peak) temperature $T_{max} = 115 \rightarrow 135$ K for $N_{Pt} = 2$-5 ML (heating rate 1 K/s); for thicker Pt films gradual strain relaxation within the Pt film adds another 5–10 K. This finding is in accordance with theoretical predictions[22] that adsorption energies E_i of the molecular chemisorbed state of oxygen increase with layer thickness (and also upon Pt lattice relaxation). The binding energy of the physisorbed O_2 species (E_{phys}), on the other hand, is expected to be largely independent of Pt layer thickness. By means of numerical integration of an Arrhenius rate equation (assuming first order desorption kinetics and a constant

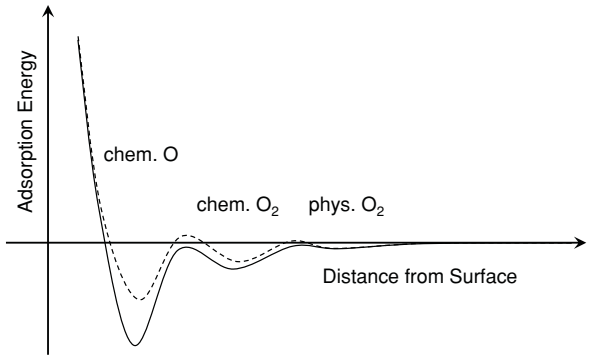

FIG. 9. Schematic view of the binding energies and the transition barriers between the various adsorption states of oxygen on Pt(111), such as physisorbed O_2, molecularly chemisorbed O_2, and atomically chemisorbed oxygen (full line). Approximate values of the activation barriers and potential depths were taken from Luntz *et al.*[23,24] For the bimetallic Pt on Ru(0001) system a lower binding energy for chemisorbed oxygen on the Pt/Ru(0001) mono and bilayers probably leads to an increase of the transition barriers which obstructs transition of physisorbed O_2 into the chemisorbed state, as well as suppresses dissociation of molecularly chemisorbed O_2 (dashed curve).

standard prefactor of $k_0 = 10^{13}$ 1/s), the respective adsorption energies E^{ads} have been derived from a comparison to the thermal desorption spectroscopy traces of desorbing O_2; for $N_{Pt} = 2$–10 ML values of 0.3–0.4eV were obtained. Since no chemisorbed O_2 can be produced for monolayer Pt/Ru(0001), the associated binding energy E_1 must remain open; it is likely that E_1 is significantly lower than E_2. On Pt(111), the adsorption energy of O_2 has been experimentally determined by Luntz *et al.*[23] to be 37 kJ/mol (0.38 eV). This energy is reasonably close to the value derived for $N_{Pt} = 10$ ML in this work, which is not a big surprise since the 10 ML Pt film already started to relax structurally and its lattice constant gradually approaches the Pt(111) value.

The experimentally derived value for superoxo O_2 on Pt(111) is about 50% lower than calculated using DFT.[22,30,58] For the Pt/Ru(0001) layers this factor amounts to 30–40% (Ref. 22) and even though the deviations in absolute values are notable, the derived trend for different Pt/Ru(0001) layer thicknesses is quite clear and correlates well with experimental data. Assuming a similar "correction" factor of 0.6-0.7 to apply for the Pt/Ru(0001) monolayer, the energies from DFT calculations[22] may be employed to extrapolate a fictitious value of $\tilde{E}_1^{ads} \simeq (0.34\ \text{eV}) \cdot 0.65 \simeq 0.22$ eV, leading to $T_1^{des} \approx 80$ K, if a standard prefactor (10^{13} 1/s) for the desorption process is assumed. As liquid N_2 cooling is insufficient to stabilize such a weakly bound surface species on the Pt/Ru(0001) monolayer, liquid He cooling is required to avoid rapid desorption out of this state once it is populated. However, neither extended exposures at low T $\simeq$ 36 K nor annealing of physisorbed O_2 could produce molecular chemisorbed oxygen on the Pt/Ru(0001) monolayer (except for a defect-related state with $\tilde{\nu}_{O\text{-}O} \approx 790$ cm^{-1}). Apparently, the transition from the physisorbed state to chemisorbed O_2 is hindered for Pt/Ru(0001) monolayer substrates, which is attributed to a higher activation barrier as compared to desorption of physisorbed O_2. It is invoked that the less deep adsorption potential of O_2 on the Pt/Ru(0001) monolayer is the primary cause for this increased barrier height. For 2 ML Pt/Ru(0001), the increased depth of the superoxo chemisorption potential reduces the barrier between the physisorbed and molecular chemisorbed O_2 states sufficiently to allow a transition by heating the sample to about 50 K. Such a correlation between activation barriers and the ground state energies of educt or product species is known as the Brønstedt-Evans-Polanyi principle.[63,64] In particular, when it comes to predict catalytic behavior and to describe trends, a renewed interest in these concept exist.[65,66]

In order to end up in the atomically chemisorbed state (as observed for chemisorbed O_2 on Pt(111) (Refs. 24 and 34)), the O_2 molecules eventually have to dissociate, e.g., by controlled annealing of the layers. For bimetallic Pt/Ru(0001) layers with $N_{Pt} = 2$ ML desorption sets in prior to dissociation. A transition into the atomic state is found only for ≥ 3 ML Pt layers; we suspect that a similar scenario as described above applies to the atomically chemisorbed state (E_{at}), i.e., an enhanced bonding of oxygen atoms to thick Pt layers reduces the barrier towards dissociation. It is suggested that both, the residual electronic effect of the Ru(0001) substrate as well as lattice strain within the pseudomorphic Pt layers, contribute to the modified chemical properties of Pt/Ru(0001) with respect to Pt(111). While the former has virtually vanished for $N_{Pt} \geq 3$ ML, the strain effect remains active for thicker layers and is only gradually released for $N_{Pt} \geq 5$ ML by the formation of dislocations.[8,18] According to the present findings the contribution due to strain seems to be of minor importance, as compared to the electronic influence of the Ru(0001) substrate (including the Pt/Ru interface), at least for the studied transition of physisorbed O_2 into chemisorbed O_2, as well as the dissociation into the atomic state.

V. SUMMARY

In conclusion, infrared absorption and thermal desorption spectroscopy have been employed to study the adsorption behavior of oxygen on epitaxially grown, pseudomorphic Pt layers on Ru(0001). Thereby, drastically modified chemical properties with respect to oxygen adsorption on Pt(111) are revealed. Specifically, sticking of O_2 and occupation of the molecularly chemisorbed peroxo and superoxo states is found to depend critically on Pt layer thickness, which is attributed to an increasingly higher kinetic barrier for thin Pt films. For the Pt monolayer occupation of these states is entirely suppressed; quite similarly, the transition between the molecular chemisorbed and the atomic oxygen states is kinetically hindered and O_2 dissociation proceeds only for $N_{Pt} \geq 3$ ML.

Irrespective of the Pt film thickness, the spectroscopic signature (line position, line width, intensity) of the prominent O_2 superoxo state at about 880 cm^{-1} agrees favorably with O_2 on Pt(111); such similarities have been noticed before for CO on these Pt/Ru(0001) films.[18] Even though the characteristics of the adsorption states once formed might not be that different, kinetic processes proceed at vastly different rates and may dramatically influence the accessible adsorption states and possible reaction intermediates.

In brisk contrast to the zero sticking of O_2 on Pt/Ru(0001) monolayer films, a novel molecular chemisorbed O_2 species,

located at some minority site, most likely at step edges of the Pt monolayer, has been identified; this species readily forms without any indication of a kinetic barrier.

ACKNOWLEDGMENTS

This work has been funded by the Deutsche Forschungsgemeinschaft (DFG) through Sonderforschungsbereich 338.

[1]T. Zambelli, J. Wintterlin, J. Trost, and G. Ertl, Science **273**, 1688 (1996).
[2]D. V. Heyd, R. J. Scharff, and J. T. Yates, Jr., J. Chem. Phys. **110**, 6939 (1999).
[3]P. Gambardella, Ž. Šljivančanin, B. Hammer, M. Blanc, K. Kuhnke, and K. Kern, Phys. Rev. Lett. **87**, 056103 (2001).
[4]J. A. Rodriguez, Surf. Sci. Rep. **24**, 225 (1996).
[5]M. Tsuda and H. Kasai, Phys. Rev. B **73**, 155405 (2006).
[6]T. Diemant, H. Rauscher, and R. J. Behm, J. Phys. Chem. **112**, 8381 (2008).
[7]M. Gsell, P. Jakob, and D. Menzel, Science **280**, 717 (1998).
[8]A. Schlapka, M. Lischka, A. Groß, U. Käsberger, and P. Jakob, Phys. Rev. Lett. **91**, 016101 (2003).
[9]B. Hammer and J. K. Nørskov, Adv. Catal. **45**, 71 (2000).
[10]J. J. Mortenson, B. Hammer, and J. K. Nørskov, Surf. Sci. **414**, 315 (1998).
[11]M. H. Koch, P. Jakob, and D. Menzel, Surf. Sci. **367**, 293 (1996).
[12]A. Winkler, X. Guo, H. R. Siddiqui, P. L. Hagans, and J. T. Yates, Jr., Surf. Sci. **201**, 429 (1988).
[13]A. Rar and T. Matsushima, Surf. Sci. **318**, 89 (1994).
[14]H. Rauscher, T. Hager, T. Diemant, H. Hoster, F. B. de Mongeot, and R. J. Behm, Surf. Sci. **601**, 4608 (2007).
[15]H. Hartmann, T. Diemant, A. Bergbreiter, J. Bansmann, H. E. Hoster, and R. J. Behm, Surf. Sci. **603**, 1439 (2009).
[16]J. Paul and F. M. Hoffmann, Surf. Sci. **172**, 151 (1986).
[17]F. Buatier de Mongeot, M. Scherer, B. Gleich, E. Kopatzki, and R. J. Behm, Surf. Sci. **411**, 249 (1998).
[18]P. Jakob and A. Schlapka, Surf. Sci. **601**, 3556 (2007).
[19]C. Günther, J. Vrijmoeth, R. Q. Hwang, and R. J. Behm, Phys. Rev. Lett. **74**, 754 (1995).
[20]P. Jakob, M. Gsell, and D. Menzel, J. Chem. Phys. **114**, 10075 (2001).
[21]M. Mavrikakis, B. Hammer, and J. K. Nørskov, Phys. Rev. Lett. **81**, 2819 (1998).
[22]M. Lischka, C. Mosch, and A. Groß, Electrochim. Acta **52**, 2219 (2007).
[23]A. C. Luntz, M. D. Williams, and D. S. Bethune, J. Chem. Phys. **89**, 4381 (1988).
[24]A. C. Luntz, J. Grimblot, and D. E. Fowler, Phys. Rev. B **39**, 12903 (1989).
[25]W. Wurth, J. Stöhr, P. Feulner, X. Pan, K. R. Bauchspiess, Y. Baba, E. Hudel, G. Rocker, and D. Menzel, Phys. Rev. Lett. **65**, 2426 (1990).
[26]B. C. Stipe, M. A. Rezaei, W. Ho, S. Gao, M. Persson, and B. I. Lundqvist, Phys. Rev. Lett. **78**, 4410 (1997).
[27]K. Gustafsson and S. Andersson, J. Chem. Phys. **120**, 7750 (2004).
[28]K. P. Huber and G. Herzberg, *Constants of diatomic molecules*, Molecular spectra and molecular structure Vol. 4 (Van Nostrand, New York, 1971).
[29]D. A. Outka, J. Stöhr, W. Jark, P. Stevens, J. Solomon, and R. J. Madix, Phys. Rev. B **35**, 4119 (1987).
[30]A. Eichler and J. Hafner, Phys. Rev. Lett. **79**, 4481 (1997).
[31]C. Puglia, A. Nilsson, B. Hernäs, O. Karis, P. Bennich, and N. Mårtensson, Surf. Sci. **342**, 119 (1995).
[32]J. L. Gland, B. A. Sexton, and G. B. Fisher, Surf. Sci. **95**, 587 (1980).
[33]S. Lehwald, H. Ibach, and H. Steininger, Surf. Sci. **117**, 342 (1982).
[34]H. Steininger, S. Lehwald, and H. Ibach, Surf. Sci. **123**, 1 (1982).
[35]N. Canning and M. Chesters, J. Electron Spectrosc. Relat. Phenom. **29**, 69 (1983).
[36]B. C. Stipe, M. A. Rezaei, and W. Ho, J. Chem. Phys. **107**, 6443 (1997).
[37]T. Matsushima, Surf. Sci. **127**, 403 (1983).
[38]K. H. Allers, H. Pfnür, P. Feulner, and D. Menzel, J. Chem. Phys. **100**, 3985 (1994).
[39]K. H. Allers, H. Pfnür, P. Feulner, and D. Menzel, Z. Phys. Chem. (Munich) **197**, 253 (1996).
[40]M. Sano, Y. Seimiya, Y. Ohno, T. Matsushima, S. Tanaka, and M. Kamada, Surf. Sci. **421**, 386 (1999).
[41]H. Wang, R. G. Tobin, D. K. Lambert, C. L. DiMaggio, and G. B. Fisher, Surf. Sci. **372**, 267 (1997).
[42]T. Yamanaka, T. Matsushima, S. Tanaka, and M. Kamada, Surf. Sci. **349**, 119 (1996).
[43]U. Engstrøm and R. Ryberg, Phys. Rev. Lett. **82**, 2741 (1999).
[44]P. Feulner and D. Menzel, J. Vac. Sci. Technol. **17**, 662 (1980).
[45]H. E. Hoster, A. Bergbreiter, P. M. Erne, T. Hager, H. Rauscher, and R. J. Behm, Phys. Chem. Chem. Phys. **10**, 3812 (2008).
[46]See supplementary material at http://dx.doi.org/10.1063/1.3598957 for figures S1–S3.
[47]T. E. Madey, H. A. Engelhardt, and D. Menzel, Surf. Sci. **48**, 304 (1975).
[48]J. Yoshinobu and M. Kawai, J. Chem. Phys. **103**, 3220 (1995).
[49]F. M. Hoffmann, N. D. Lang, and J. K. Nørskov, Surf. Sci. **226**, L48 (1990).
[50]R. L.C. Wang, H. J. Kreuzer, P. Jakob, and D. Menzel, J. Chem. Phys. **111**, 2115 (1999).
[51]A. Schiffer, P. Jakob, and D. Menzel, Surf. Sci. **389**, 116 (1997).
[52]P. Jakob and A. Schiffer, Surf. Sci. **603**, 1135 (2009).
[53]A. Schlapka, U. Käsberger, D. Menzel, and P. Jakob, Surf. Sci. **502**, 129 (2002).
[54]Ž. Šljivančanin and B. Hammer, Surf. Sci. **515**, 235 (2002).
[55]R. M. Hammaker, S. A. Francis, and R. P. Eischens, Spectrochim. Acta **21**, 1295 (1965).
[56]M. Moskovits and J. E. Hulse, Surf. Sci. **78**, 397 (1978).
[57]B. N. J. Persson and R. Ryberg, Phys. Rev. B **24**, 6954 (1981).
[58]A. Eichler, F. Mittendorfer, and J. Hafner, Phys. Rev. B **62**, 4744 (2000).
[59]B. Hammer and J. K. Nørskov, Nature (London) **376**, 238 (1995).
[60]B. Hammer and J. K. Nørskov, Surf. Sci. **343**, 211 (1995).
[61]A. Ruban, B. Hammer, P. Stoltze, H. L. Skriver, and J. K. Nørskov, J. Mol. Catal. A: Chem. **115**, 421 (1997).
[62]B. Hammer, Y. Morikawa, and J. K. Nørskov, Phys. Rev. Lett. **76**, 2141 (1996).
[63]J. N. Brønstedt, Chem. Rev. **5**, 231 (1928).
[64]M. G. Evans and M. Polanyi, Trans. Faraday Soc. **34**, 11 (1938).
[65]J. K. Nørskov, T. Bligaard, A. Logadottir, S. Bahn, L. B. Hansen, M. Bollinger, H. Bensgaard, B. Hammer, Ž. Šljivančanin, M. Mavrikakis, Y. Xu, S. Dahl, and C. J. H. Jacobson, J. Catal. **209**, 275 (2002).
[66]C. H. Christensen and J. K. Nørskov, J. Chem. Phys. **128**, 182503 (2008).

Oxygen adsorption on Pt/Ru(0001) layers

Peter Jakob*, Andreas Schlapka and Pawel Gazdzicki

Fachbereich Physik und Wissenschaftliches Zentrum für Materialwissenschaften,
Philipps-Universität Marburg, D-35032 Marburg, Germany

* To whom all correspondance should be addressed (email: peter.jakob@physik.uni-marburg.de)

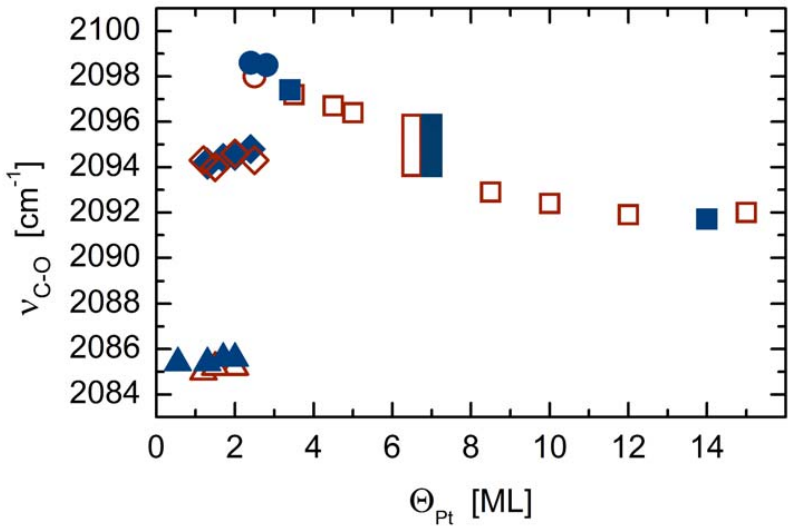

S1 Internal C-O stretch frequency (ν_{C-O}) of CO (coverage $\Theta_{CO} \approx 0.01$ ML, sample temperature 80 – 100 K) adsorbed on various Pt_N/Ru(0001) overlayers (number of Pt layers N_{Pt} = 0.3 – 15 ML). Pt has been deposited onto a Ru(0001) substrate held at 600 – 700 K at a rate of $R \approx 10^{-3}$ ML/s. Pt grows pseudomorphically on Ru(0001) up to at least 4 ML [1, 2]. Thereby ν_{C-O} is influenced by two effects [1, 2]:
(i) strain within the Pt film (lattice mismatch $\Delta a/a = 2.5\%$); this effect remains constant as long as the Pt layers retain their pseudomorphic structure, i.e. up to N_{Pt} = 4 – 5 ML.
(ii) an electronic influence due to the underlying Ru(0001) substrate and the presence of the Pt/Ru interface; this effect is dominant for few Pt layers and vanishes for $N_{Pt} \geq 3$ ML.

The elongated bars refer to broadened vibrational bands: for such layer thicknesses the strained pseudomorphic Pt_N/Ru(0001) layers start to relax structurally and begin to adopt/approach the Pt lattice constant.
Open symbols refer to data obtained very recently, bold symbols to data taken several years ago. Slight deviations in peak position are due to variations in CO coverage and associated line shifts due to lateral interactions. Note that the line positions refer to the low coverage limit and the quoted variations in line positions amount to few tenth of cm^{-1} only.

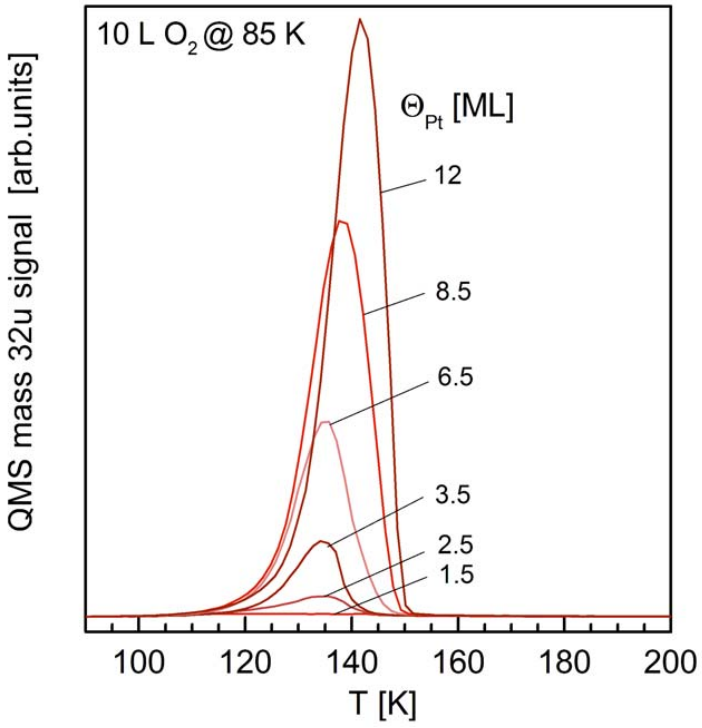

S2 Series of thermal desorption spectra (heating rate dT/dt = 1 K/s) obtained from O_2 adsorbed on various Pt_N/Ru(0001) overlayers (N_{Pt} = 1.5 – 12 ML). Pt has been deposited onto a Ru(0001) substrate held at 700K at a rate of R ≈ 10^{-3} ML/s. An identical O_2 exposure of 10 L has been applied to Pt_N/Ru(0001) and the variation in the amount of desorbing O_2 reflects the dramatic increase of the O_2 sticking coefficient with Pt layer thickness. The thermal desorption spectra were obtained using a glass enclosure to ensure desorption from the front face of our sample only and to enhance desorption signals in the quadrupole mass spectrometer. Note that the integrals of the displayed curves do not reflect the entire amount of adsorbed O_2 since a certain fraction dissociates during annealing. A quantitative evaluation of this fractional amount can be attained by means of CO post-adsorption and CO + O → CO_2 formation (and desorption).

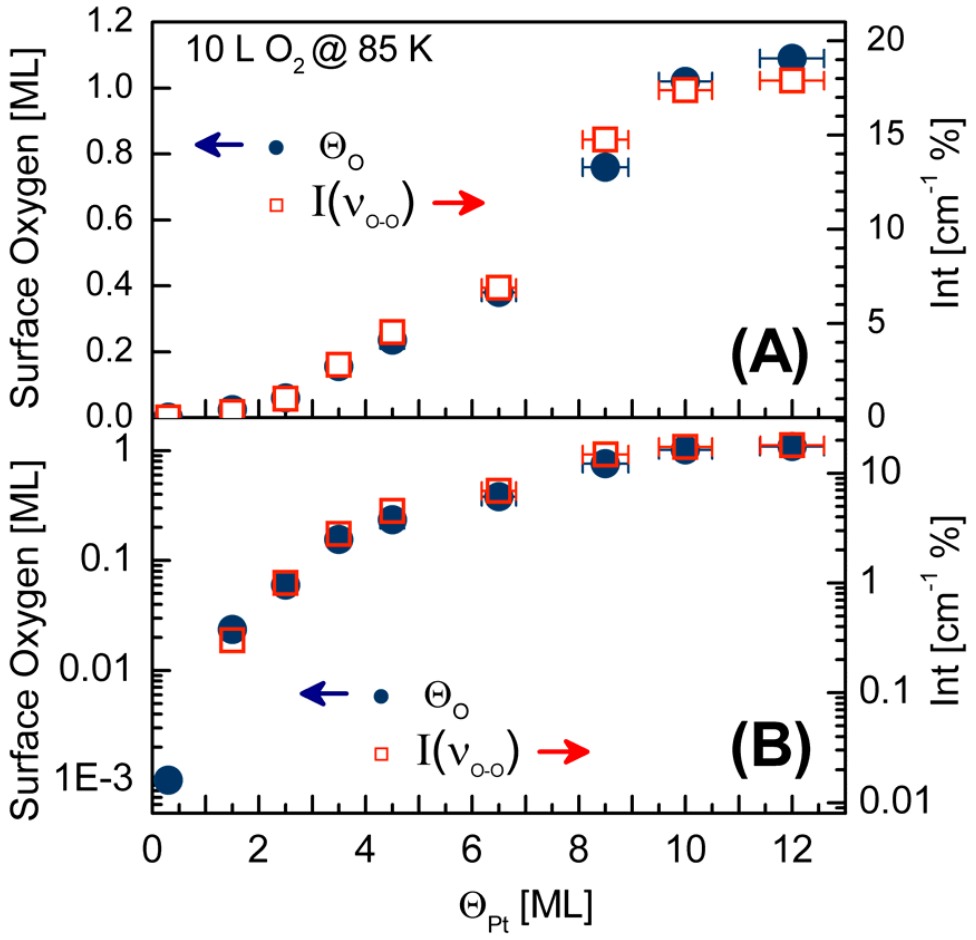

S3 Comparison of the superoxo O-O stretch mode intensity $I(\nu_{O\text{-}O})$ and of the surface oxygen coverage Θ_O on various Pt_N/Ru(0001) overlayers (N_{Pt} = 0.3 – 12 ML), as a result of a 10 L exposure to molecular oxygen at 85 K. $I(\nu_{O\text{-}O})$ has been derived from the integrated IR absorption signal of the O-O stretch mode located at about 880 cm^{-1}. Θ_O is obtained from thermal desorption spectra and is the sum of two contributions: (i) desorbing molecular O_2 at about 130 K; (ii) associative CO_2 desorption after CO post-adsorption, which consumes left-over atomic oxygen from dissociated O_2 after the run (i). Calibration of oxygen coverages and TDS desorption yields has been attained using XPS for the 12 ML Pt/Ru(0001) sample. In panels A and B identical data are displayed, either in a linear or a logarithmic scale, respectively. Note that the fractional ranges of the two log scales (on the left and right of panel B) are identical and differ only by a constant offset. The parallel evolution of IR intensities and oxygen coverages therefore confirms the linear dependence of $I(\nu_{O\text{-}O})$ and of Θ_O, i.e. $I(\nu_{O\text{-}O}) = c \cdot (\Theta_O)^n$ with n = 1.

[1] A. Schlapka, M. Lischka, A. Groß, U. Käsberger, and P. Jakob, Phys. Rev. Lett. **91**, 016101-1 (2003).

[2] P. Jakob and A. Schlapka, Surf. Sci. **601**, 3556 (2007).

6.5 Article V: Oxidation of Methanol on Oxygen Covered Pt_n/Ru(0001) Layers

[1]Final version available at *J. Phys. Chem. C 115, 23013 (2011).*

Oxidation of Methanol on Oxygen covered Pt_n/Ru(0001) Layers

Pawel Gazdzicki, Sebastian Thussing, and Peter Jakob
Fachbereich Physik und Zentrum für Materialwissenschaften,
Philipps-Universität Marburg, Renthof 5, 35032 Marburg, Germany

Thin pseudomorphic as well as thick "Pt(111)-like" Pt/Ru(0001) bimetallic substrates have been used to study the oxidation of methanol (CD_3OH) to CO_2. Specifically, molecular (cold deposited) and ordered atomic (annealed) oxygen precovered Pt_n/Ru(0001) layers with $n = 1 - 15$ ML have been studied. Thereby the thickness of the Pt films primarily influences the adsorption probability of O_2 and much less the energy barriers for methanol reactions. In particular, no indication of a strain effect could be detected and the reactions of methanol on Pt_n/Ru(0001) multilayer films closely follow the known reaction scheme on Pt(111) substrates: On O_2/Pt_n/Ru(0001) methanol is directly oxidized to formate (DCOO) and eventually desorbs as CO_2 (300 K). The formate producing reaction is thereby promoted by dissociating O_2 molecules (130 K) and, at higher temperatures (130-200 K), by disordered atomic oxygen. This is in contrast to methanol post-adsorbed onto ordered atomic oxygen covered Pt_n/Ru(0001) layers which exhibit formaldehyde formation and decomposition to CO and H. Interestingly, during methanol dissociation at 160-200 K a remarkable fraction of methanol molecules experiences an H $\leftrightarrow$ D exchange of the hydroxyl group hydrogen, leading to the dominant desorption of CD_3OD. Our observation that the relative fraction of desorbing CD_3OH is exceptionally low implies a bold primary isotope effect which we attribute to the dissimilar zero point energies associated with OH and OD vibrations of methanol.

PACS numbers:

I. INTRODUCTION

In this study methanol (CD_3OH) reactions on (molecular and atomic) oxygen precovered Pt_n/Ru(0001) layers with $n = 1 - 15$ ML (monolayers) have been investigated using infrared absorption spectroscopy (IRAS) and temperature programmed desorption (TPD). These systems exhibit reactivity towards complete methanol oxidation and thus formation of CO_2. In general, catalysts which convert methanol to CO_2, as opposed to CO accumulation at the electrodes, are of high interest with respect to the direct methanol fuel cell (DMFC).[1–8] Due to such CO poisoning, catalysts which dehydrogenate methanol without complete oxidation may be unsuitable for practical use.

On Pt(111) no methanol reactions are observed in the absence of preadsorbed oxygen.[9] Referring to IRAS and thermal desorption experiments by Liu et al.[10] and Endo et al.[11], methanol activation can be initiated by coadsorption with atomic or molecular oxygen. Thereby, abstracted hydrogen readily removes all surface oxygen and desorbs as water. For submonolayer methanol coverages on $O(2 \times 2)$/Pt(111) layers formaldehyde was additionally found as a stable surface intermediate which decomposes to CO and H at elevated T; further oxidation of H_2CO to formate merely represents a minority reaction pathway.[10] For saturation methanol coverages on $O(2\times2)$ layers no stable intermediates were observed except for CO which eventually desorbs at $\approx$ 500 K. Methanol coadsorbed with chemisorbed molecular oxygen on Pt(111) is reported to undergo oxidation to formate. Interestingly, this reaction occurs at temperatures as low as $T \simeq 70$ K, i.e. well below the dissociation temperature of molecular oxygen on Pt(111).[11,12]

Reactions of methanol on Ru(0001) have recently been analyzed by us.[13,14] On the oxygen-free surfaces methoxy as well as its decomposition product, CO, were identified as the only stable surface intermediates. Ordered $O(2\times2)$ or $O(2 \times 1)$ overlayers on Ru(0001), on the other hand, turned out to be entirely unreactive under the conditions of our experiment. This does not apply to residual oxygen (few percent) on clean Ru(0001) which induces a direct H-transfer from the methanol hydroxyl group to surface oxygen which is then removed from the surface as water.

The growth of Pt on Ru(0001) has been studied extensively with IRAS and STM in the submonolayer and multilayer regime.[15–19] It has been found that Pt grows pseudomorphically at least up to the 4^{th} atomic layer.[17,19] For higher layers the strain relaxes and the Pt lattice constant gradually approaches the Pt(111) value. The (short range) electronic influence of the Ru(0001) substrate dominates for few layer Pt films and vanishes starting with the third Pt layer. This peculiarity allows us to study the effect of laterally compressed "Pt(111)" on the surface reactivity. Experimental evidence for such an influence of strain on adsorption energies has been provided by Gsell, Jakob and Menzel.[20,21] DFT calculations explain this phenomenon by means of strain induced shifts of metal *d*-bands with respect to the Fermi level.[22] For the system O_2/Pt_n/Ru(0001) it has been shown that the sticking probability of oxygen is virtually zero for the first Pt layer and increases step by step, approaching the value of Pt(111) for thick layers.[23,24] It therefore appeared interesting to analyze more complex reactions, involving a variety of different bonds. In the case of methanol reactions activation barriers now separate two surface species, both of them subject to strain and/or the electronic influence of the Pt/Ru interface, as opposed to the O_2 stick-

ing reaction which involves surface species only on the product side. The fundamental question therefore was, whether adsorption energies of transition states and of reaction products and educts scale evenly, or they are more or less decoupled.

In our study we will first present results on methanol adsorption and reactions for O_2 precovered Pt_n/Ru(0001) layers with n denoting the number of deposited Pt layers. Subsequently, reactions on O covered Pt_n/Ru(0001) substrates will be discussed. To the best of our knowledge no UHV-studies on thermally induced methanol reactions on oxygen precovered or clean Pt_n/Ru(0001) multilayers have been published up to now.

II. EXPERIMENTAL

The experiments were performed in a UHV chamber at a base pressure of $p = 6 \times 10^{-11}$ mbar. The sample is a Ru(0001) crystal (5N purity) with 10 mm in diameter and a thickness of 2 mm. It can be cooled with liquid He or N_2 and heated up to 1570 K (limited by the type K thermocouple) with linear heating rates of 0.1-10 K/s. The quadrupole mass spectrometer (Balzers QMA112) is equipped with a Feulner cup[25] (glass enclosure) to ensure desorption from the front face of the sample only and to enhance the desorption signals. The Fourier transform infrared spectrometer (FTIRAS) is a Bruker IFS 66v with evacuable optics (p < 1 mbar). Polarized IR radiation is produced by a water cooled blackbody source (Globar) in conjunction with a wire grid polarizer. Within this work a LN_2 cooled MCT (HgCdTe) detector was used, allowing for measurements in the spectral range of 750-4000 cm^{-1}. All infrared absorption (IRAS) spectra were taken at a resolution of 2 cm^{-1} with 500-2000 scans coadded. For the IRAS measurements the sample was positioned in a dedicated IR-cell, which contained also a titanium sublimation pump. A uniform gas dosage at the IR measurement position is provided by a multi-capillary array with individual diameters of $\approx$ 10 μm. The sample was cleaned by Ar^+ sputtering (1.4 keV, 1 μA) and multiple O_2 dosing cycles combined with flashing the sample up to 1570 K.

For Pt deposition an e^--beam evaporator was used. The typical deposition rate was 0.03 ML min^{-1} at a growth temperature T_g = 700 K. During the evaporation time the pressure increases up to 2×10^{-10} mbar. A more detailed description of the experimental setup has been published recently.[13,14] The prepared Pt/Ru(0001) layers were characterized by monitoring the ν(CO) mode of adsorbed CO with IRAS.[17,18] The error of the Pt coverage is estimated to 5%. Referring to the notation Pt_n/Ru(0001), n denotes the number of deposited Pt monolayers (ML). In the following a monolayer (ML) refers to the ratio of the number of adsorbates to the number of substrate atoms in the topmost layer.

Methanol was cleaned by repeated freeze-and-thaw cycles. All methanol exposures in this paper are specific to our experimental setup only and are given as the product of the pressure in our gas dosing system and the exposure time; the units used are mTorr·s. 10 mTorr·s of methanol approximately leads to 10% saturation of the first layer and equals 0.04 ML referring to the above definition as determined by XPS (integral of the O_{1s} peak) and comparing the result to O(2 × 2)/Ru(0001)[26]. An oxygen exposure of 1 Langmuir (L) equals to 30 mtorr·s. For Pt_n/Ru(0001) with $n \geq 10$ ML an exposure of 10 L O_2 at 80 K leads to an O_2 coverage equivalent to a surface oxygen coverage of $\Theta_O = 1$ ML. The correlation of Θ_O and n for a constant O_2 exposure has been published recently.[24]

The isotopic purity of the used gases was 99.8% for CD_3OH, 99.8% for CD_3OD, 95% for $CH_3^{18}OH$, and 98.73% for $^{18}O_2$.

The data shown in this work primarily comprises the CD_3OH isotope, as its vibrational modes exhibit somewhat sharper line shapes as compared to regular methanol. In addition, CD_3O (methoxy) on Ru(0001) exhibits a 10 times stronger umbrella mode $\delta_s(CD_3)$ (symmetric CD_3 stretch) than CH_3O which allows a more accurate quantitative analysis.[13] A similar observation was reported in the literature for methanol on oxidized Ag(111).[27] On Cu(111) the umbrella mode was not at all observed for CH_3O but for CD_3O only.[28,29] The reason for such dissimilar oscillator strengths for two methoxy isotopes is that mode coupling with the nearby ν(CO) mode enhances the intensity of $\delta_s(CD_3)$.

III. RESULTS AND DISCUSSION

A. Methanol on O_2/Pt_n/Ru(0001)

In this section methanol reactions on Pt_{3-15ML}/Ru(0001) substrates precovered with chemisorbed O_2 will be analyzed. We like to state right at the beginning that the methanol reaction intermediates and product yields, as well as reaction and desorption temperatures are largely independent of the Pt-film thickness for $n = 3 - 15$ ML; as Pt films grow pseudomorphically for $n < 5$ ML and relax for thicker layers we conclude that strain within the Pt film has a marginal influence on the reaction pathway (discussed later). Due to negligible oxygen uptake and dissociation for Pt mono- and bilayers on Ru(0001),[24] the thermal evolution of methanol on these layers has been analyzed in the absence of coadsorbed oxygen; however, no evidence for methanol activation has been found under the conditions of our experiment.

Oxygen adsorption on Pt_n/Ru(0001) proceeds similar to Pt(111)[30,31], i.e. O_2 adsorbs molecularly at $T <$ 120 K.[24] Upon annealing a fraction of the oxygen desorbs molecularly at about 130 K while another fraction dissociates to atomic oxygen and desorbs recombinatively at around 800 K.

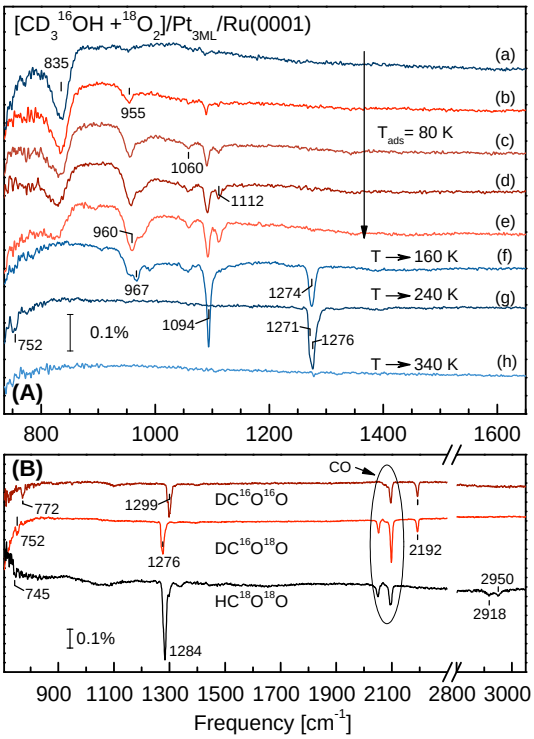

FIG. 1: **(A):** IRAS spectra of CD_3OH adsorbed onto $Pt_{3\ ML}/Ru(0001)$ precovered with $^{18}O_2$ (exposure: 60 L). Spectrum (a) shows the $O_2/Pt_n/Ru(0001)$ layer alone. Increasing exposures of CD_3OH (up to 40 mTorr·s) are displayed in spectra (b)-(e). Spectra (f)-(h) show the sample after annealing to increasingly higher temperatures as denoted in the figure. **(B):** IRAS spectra of $[CD_3OH + {}^{18}O_2]$, $[CD_3OH + {}^{16}O_2]$ and $[CH_3^{18}OH + {}^{18}O_2]$ coadsorbate layers on $Pt_{3ML}/Ru(0001)$; the layers have been annealed to 240-260 K in order to analyze isotopic shifts of the observed formate vibrational modes. All adsorbates were deposited at $T_{\rm ads} = 80$ K. The exposures of preadsorbed O_2 were $50 - 60$ L.

In Fig. 1A IRAS spectra of CD_3OH postadsorbed onto $^{18}O_2$ precovered $Pt_{3ML}/Ru(0001)$ are displayed for increasing methanol coverages (b)-(e) and increasing annealing temperatures (f)-(h) as indicated in the figure. 60 L $^{18}O_2$ were dosed at 80 K, leading to a prominent stretch $\nu_{\text{O-O}}$ mode at 835 cm^{-1}. Spectrum (a) depicts the $O_2/Pt_{3ML}/Ru(0001)$ layer prior to the methanol exposure. After methanol has been added all vibrational bands, while being fully compatible to equivalent data of CD_3OH on clean Ru(0001),[13] display rather broad lines, which lead us to conclude that the coadsorbates build a heterogeneous layer. The following spectral features are attributed to methanol: ν(CO) at 955 cm^{-1}, and several $\delta(CD_3)$ bendings at 1060-1112 cm^{-1}. In the region of C-D stretch modes spectral features at 2193, 2220, and 2246 cm^{-1} have been identified (not shown), similar to spectra on Ru(0001).

At 160 K molecular oxygen ($^{18}O_2$) has partly desorbed (see thermal desorption experiments in Fig. 3B, below) while another fraction dissociates, both of which contribute to the vanishing of the 835 cm^{-1} vibrational band. In parallel, the $\delta(CD_3)$ mode of CD_3OH at 1094 cm^{-1} has increased significantly. The observed change of the spectral signature is likely due to the replacement of molecular oxygen by atomic oxygen which implies an altered chemical environment of adsorbed methanol. Moreover, no desorption of methanol is observed in this temperature range as will be discussed below. Analogous vibrational features of intact methanol have been detected on atomic oxygen precovered $Pt_{12ML}/Ru(0001)$ after heating to 160 K (see below).

A particular interesting set of vibrational bands (located at 752, 1276 and 2192 cm^{-1}) appears after annealing to 240 K; they are assigned to the symmetric O-C-O bend, δ_s(OCO), symmetric O-C-O stretch, ν_s(OCO), and the C-D stretching mode, ν(CD), of a formate species (DCOO) with a local C_{2v} symmetry. To corroborate this assignment, additional experiments with various methanol and oxygen isotopes have been performed. In Fig. 1B the spectra of three different formate isotopes are displayed. Thereby, all vibrational modes of a C_{2v}-formate expected in the spectral range $700 - 3000$ cm^{-1} could be identified. Analogous to the methanol oxidation on $O/Cu_{1\ ML}/Ru(0001)$[32] the reactively produced formate species consists of one oxygen from methanol and another one due to preadsorbed oxygen; otherwise no shift in the line positions would be observed for the O-C-O modes if preadsorbed $^{16}O_2$ is replaced by $^{18}O_2$. The assignment of the observed formate modes (summarized in Tab. I) agrees with literature data regarding formate on Pt(111)[11,12,33], Ru(0001)[34], Cu(110)[35], Ag(111)[27] or Ni(110)[36]. Moreover, our detection of formate as a prominent intermediate in methanol oxidation is in agreement with electro-chemical experiments over Pt electrodes.[51]

Interestingly, formate containing regular hydrogen exhibits two peaks at 2800-3000 cm^{-1}; one of them is due to the C-H stretch and the other one is a combination mode, $\nu_{\rm comb} = \nu_{as}$(OCO)+$\delta$(CH), of the forbidden in-plane anti-symmetric O-C-O stretching and in-plane C-H bending modes. Group theory confirms that their combined excitation contains the totally symmetric representation and thus is dipole allowed. This combination band, observed on numerous surfaces (see Tab. I), was first reported by the group of Bradshaw[35,37] for the system HCOO/Cu(110).

On Pt(111) Sawada et al.[12] reported that (preadsorbed) O_2 and CH_3OH react to HCOO even below 80 K. In Fig. 1 no indication for formate ($DC^{16}O^{18}O$) is found at 80 K. However, in the case of the IRAS spectrum of the $DC^{16}O^{16}O$ isotope shown in Fig. 2 the ν(OCO) mode at 1294 cm^{-1} could be clearly observed at 80 K confirming the finding of Sawada et al.[12] The authors concluded that formate formation is caused by an attractive interaction between O_2 and methanol which leads to the dissociation of O_2 even below 80 K. Endo et al.[11], on the other hand, postulated that formate formation is initiated by "hot"

TABLE I: Vibrational modes (frequencies given in cm^{-1}) of formate (C_{2v} symmetry) on various metal surfaces. The values in parentheses refer to low formate coverages. ν(OCO) frequencies of the $HC^{16}O^{18}O$ and $HC^{16}O^{16}O$ isotopes on Pt_n/Ru(0001) are found at 1293 and 1316 cm^{-1} (low formate coverage values, see Fig. 7). All literature data refer to species containing the regular oxygen isotope.

Pt_n/Ru(0001), this work			Pt(111)[33]	Ru(0001)[34]	Cu(110)[35]	Ni(110)[36]	Ag(111)[27]		mode
$DC^{16}O^{16}O$	$DC^{16}O^{18}O$	$HC^{18}O^{18}O$	HCOO	HCOO	HCOO	HCOO	HCOO	DCOO	assignment
772	752	745	790	784	-	777	-	-	δ_s(OCO)
1299 (1294)	1276 (1271)	1284 (1278)	1340	1361	1350	1362	1320	1296	ν(OCO)
2192	2192	2918	-	2851	2900	2850	2808	2126	ν(CH)
-	-	2953	2950	2939	2950	2944	2882	-	ν_{comb}

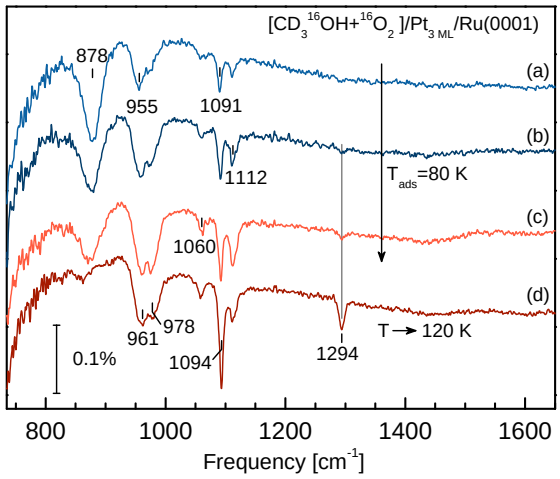

FIG. 2: IRAS spectra of increasing coverages of CD_3OH adsorbed at 80 K on $^{16}O_2$ (exposure: 50 L) precovered $Pt_{3\ ML}$/Ru(0001), (a-c), and after annealing to 120 K (d). In addition to bands due to intact methanol (≈960, 1060, ≈1094, 1112 and 2050-2250 cm^{-1}), the ν(OCO) and ν(CD) modes of DCOO at 1294 and 2192 cm^{-1} (not shown) are clearly discernible already at 80 K. Upon slight annealing to 120 K, they both gain in intensity.

oxygen atoms produced in the course of O_2 dissociation around 130 K.

According to our data, the amount of DCOO produced at low temperatures and even during O_2 dissociation is rather small. In fact, this reaction seems to proceed significantly more effective at $T \approx 140 - 200$ K (compare with Fig. 3A), i.e. at temperatures with atomic oxygen instead of O_2 present. This observation strongly suggests that the formation of formate is not primarily promoted by dissociating O_2 as proposed by Endo et al.[11] but it is also due to disordered atomic oxygen, especially at $T > 130$ K. The high reactivity of such disordered oxygen atoms towards methanol activation has been reported recently for the Cu/Ru(0001) monolayer.[32] In accordance with Sawada et al.[12] we believe that low temperature formate observed at 80 K in Fig. 2 implies an alternative process and may involve some special sites of O_2.

In spectrum (g) in Fig. 1A the formate vibrational band at 1274 cm^{-1} actually represents a double-peak feature with individual maxima at 1271 and 1276 cm^{-1} for the $DC^{16}O^{18}O$ isotope. At $T \leq 160$ K the low frequency mode is dominant and the second peak at 1276 cm^{-1} only appears as a separate feature upon heating the sample to 180-190 K. In Fig. 3A the combined integrated IRAS intensities of the two modes as well as of the various $\delta(CD_3)$ modes of CD_3OH (1050-1120 cm^{-1}) are plotted versus the annealing temperature. It is apparent that the somewhat delayed growth of the 1276 cm^{-1} peak is the reason for the extra increase of the DCOO intensity at 180-190 K. Furthermore, this process correlates with the vanishing of CD_3OH related vibrational bands; this latter observation, however, is, at least partially, caused by methanol desorption proceeding in parallel.

The prominent desorption of CO_2 at 300 K is clearly correlated with the decomposition of formate (bullets) at 250-300 K in Fig. 3A. The final reaction step is therefore DCOO→D+CO_2 with produced CO_2 desorbing instantaneously. At variance to quite substantial CO_2 evolution in the TPD spectra, no D_2 (4 u) desorption is observed in this temperature range. It is suggested that D reacts with residual surface oxygen (^{18}O in our experiment) and desorbs as water ($D_2^{18}O$, 22 u) rather than it desorbs molecularly as D_2. Indeed the 22 u signal exhibits a distinct peak at 300 K which explains the missing 4 u desorption signal. The detected mass 12, 18, 28, and 30 u signals at 300 K represent ionization fragments of $C^{16}O^{18}O$. To avoid confusion, we note that the mass 30 u signal observed at 130 K is due to $C^{18}O$ formed from desorbing $^{18}O_2$ and C at the filament of our QMS, as it closely follows the 36 u trace of desorbing $^{18}O_2$; in experiments with preadsorbed $^{16}O_2$ a corresponding peak appears for mass 28 u ($C^{16}O$).

The QMS traces of various masses in the 170-190 K range in the TPD in Fig. 3B deserve a closer inspection. Surprisingly, the masses 36 u and 34 u exhibit significant desorption signals which cannot be ascribed to the initially adsorbed CD_3OH methanol isotope (35 u) or fragments thereof. Furthermore, the outcome of such an experiment was independent of the isotopic nature of preadsorbed oxygen. Yet, these desorption signals provide clear evidence for significant CD_3OD desorption as verified by the comparison of mass 29-36 u QMS signal levels in Fig. 4: data from a TPD experiment equiva-

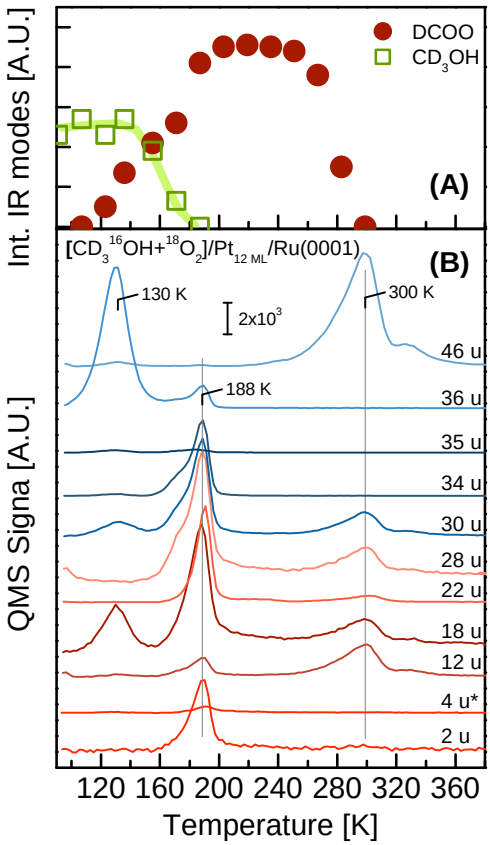

FIG. 3: **(A):** Thermal evolution of methanol (CD_3OH) and formate (DCOO) as monitored by the integrated IR intensities of various $\delta(CD_3)$ modes at 1050-1120 cm^{-1} and $\nu(OCO)$ modes at $\approx 1270 - 1280$ cm^{-1}, respectively. The sample was prepared by dosing 50 L $^{18}O_2$ and CD_3OH (dose: 40 mTorr·s) at 80 K onto $Pt_{12\ ML}/Ru(0001)$. The individual IRAS spectra contributing to these curves were measured while ramping the surface temperature at a rate of 0.2 K/s. **(B):** Multi-mass TPD of [CD_3OH + $^{18}O_2$] on $Pt_{12\ ML}/Ru(0001)$ prepared as described above. The sample was heated with 1 K/s from 80 to 500 K. (*) The 4 u signal was taken from a second TPD experiment with a slightly lower Pt/Ru(0001) film thickness of 9 ML Pt under otherwise identical conditions; for this run QMS desorption traces of masses 28-36 are virtually identical to those displayed here.

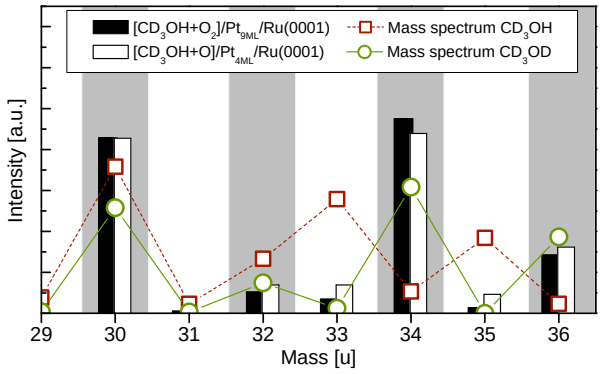

FIG. 4: QMS signal levels associated with different methanol isotopes. The squares and circles denote the respective QMS signals as CD_3OH or CD_3OD is admitted to our chamber. Slight contributions of CD_3OH in the dosed CD_3OD gas, most likely due to isotopic exchange of the OD hydroxyl group at the walls of the gas dosing system, have been subtracted. The black and white bars correspond to the desorption signals at 188 K for $[CD_3OH{+}O_2]/Pt_{9\ ML}/Ru(0001)$ and at 203 K for $[CD_3OH{+}O]/Pt_{4\ ML}/Ru(0001)$, respectively (see Supporting Information). For better comparison the two thermal desorption data sets have been aligned for mass 30 u. In both cases the observed QMS signals of desorbing methanol are independent of the isotopic nature of preadsorbed oxygen.

lent to Fig. 3B (black bars) are compared with the mass spectra of CD_3OH (squares) and CD_3OD (circles) which have been introduced into our UHV system. Evidently, the data from Fig. 3B and Fig. 4 suggest a substantial prevalence of the CD_3OD over the CD_3OH isotope, as the distribution of mass intensities closely resembles CD_3OD and deviates notably from CD_3OH. We suggest that this bold isotope effect (preference of CD_3OD) is caused by the lower zero point energy of CD_3OD as compared to CD_3OH, in conjunction with the low temperatures sufficient for this isotopic exchange reaction to occur.

The slight discrepancies in the relative intensities (bars and symbols) in Fig. 4 probably are due to different dosing conditions: The thermal desorption spectra have been taken with the sample directly in front of the glass enclosure of the QMS (distance $\approx$ 2 mm). The mass spectra, on the other hand, were measured by dosing methanol through an MCA doser in our chamber (facing the QMS at a distance of $\approx$ 10 cm). Also we should keep in mind that a notable fraction of introduced CD_3OD actually converts to CD_3OH at the chamber walls of the gas dosing system, i.e. the QMS raw data correspond to a mixture of both isotopic species. The QMS signal levels of CD_3OD have therefore been corrected for this CD_3OH contribution so that the QMS values displayed in Fig. 4 (open circles) refer to nominally 100% CD_3OD.

The mechanism which leads to CD_3OD formation and desorption at $T \approx 170 - 190$ K is proposed to be an exchange of the hydrogen from methanol's OH group by surface deuterium or hydrogen. Note that methanol dehydrogenation and oxidation to formate starts already at 120 K producing surface hydrogen and deuterium with a ratio of 1:2. As no evidence for surface CD_3OD is found, its formation presumably occurs close to the desorption temperature only. Regarding the details of this exchange process it is worth mentioning that a recombination of a methoxy (CD_3O) species with surface D to produce desorbing CD_3OD can be ruled out as there is no evidence for the presence of surface methoxy despite a high detection sensitivity of less than 0.01 ML for such a species (see also below). For a related system, methanol coadsorbed with deuterium on Ru(0001), the total lack of H

- D exchange reactions of the methanol hydroxyl group has been associated with the irreversible dehydrogenation of methanol to a strongly bound methoxy species.[14] This observation strongly suggests that the formation of a stable methoxy precludes the reversible H ↔ D exchange of the hydroxyl hydrogen with surface H/D.

At variance to the methanol hydroxyl group, the CD_3 group of intact methanol is not affected by such an H↔D exchange; otherwise the IRAS spectra of formate should exhibit not only C-D but also a C-H stretching mode, in addition to an isotopically shifted ν(OCO) mode of formate (expected at about 1320 cm^{-1}). However, under no circumstances did we observe such bands in the course of our experiments using CD_3OH. For unsaturated hydrocarbon species CH bonds may in fact undergo isotopic exchange with coadsorbed D. Specifically, for benzene coadsorbed with hydrogen on Ru(0001) various combinations of isotopically labeled C_6 H_n D_{6-n} species have been identified after slight annealing, and a prevalence of CD versus CH bonds have been found.[38,39] In that case, a hydrogenation - dehydrogenation sequence (with a short-living C_6H_6D intermediate) has been proposed, a process that is not accessible to a saturated hydrocarbon species, or a methyl group.

The overall reaction can be described as follows:

$$CD_3^{16}OH^{(s)} + CD_3^{16}OH^{(s)} + {}^{18}O^{(s)} \longrightarrow$$
$$CD_3^{16}OH^{(s)} + DC^{18}O^{16}O^{(s)} + 2D^{(s)} + H^{(s)} \longrightarrow$$
$$CD_3^{16}OD^{(g)} + DC^{18}O^{16}O^{(s)} + D^{(s)} + 2H^{(s)},$$

with $^{(s)}$ and $^{(g)}$ denoting stable surface intermediates and desorbing species, respectively.

An analogous exchange reaction, $CD_3OH + D \rightarrow CD_3OD + H$, has been observed for methanol coadsorbed with atomic oxygen on Pt_n/Ru(0001) (white bars in Fig. 4). Yet, in this case H and D atoms are provided by a dehydrogenation reaction of methanol to surface formaldehyde and not to formate (see below). In both cases remaining abstracted hydrogen atoms (H and D) react with surface ^{18}O to water which desorbs in parallel to CD_3OD at 190-200 K. The 22 u desorption peak can be taken as unambiguous evidence for reactively produced $D_2^{18}O$ because no methanol cracking product is expected at mass 22 u. The other masses which exhibit peaks at 180-200 K (2, 12, 28, 30 u, and partially 18 u), on the other hand, do represent methanol ionization fragments produced in the mass spectrometer.

An estimate of the CD_3OD : CD_3OH preference K must take into account the vibrational partition functions of both species at $T \approx 160 - 200$ K.[40] As the majority of modes do not shift upon OH ↔ OD exchange and therefore merely give a factor close to unity, the OH (OD) stretch and bending modes will enter the analysis through their different zero point energies. Due to their much lower vibrational frequencies, the bending modes contribute only little and may be approximately compensated by an inverse factor due to adsorbed surface D (H), so that consideration of the hydroxyl stretching

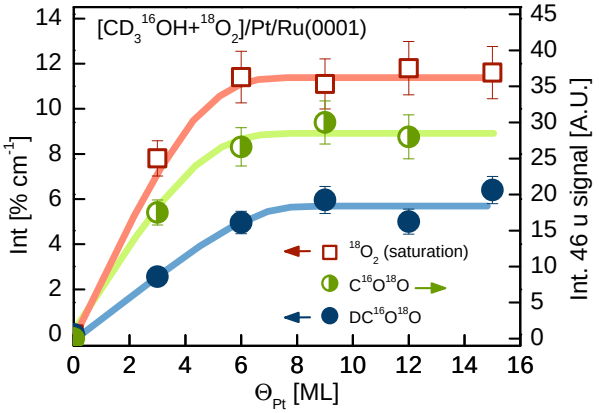

FIG. 5: Comparison of $^{18}O_2$ coverages (integrated IRAS intensities of the $\nu(^{18}O-^{18}O)$ mode at 835 cm^{-1} after $50-60$ L exposure at 80 K for $n \leq 9$ and $20-30$ L for $n > 9$ ML), the amount of reactively produced formate $DC^{16}O^{18}O$ (integrated IRAS intensities of the ν(OCO) mode at 1275 cm^{-1} after annealing to 200-220 K) and the amount of desorbing $C^{16}O^{18}O$ (integrated desorption peak of mass 46 u signal at $\approx$ 300 K) as a function of Pt_n/Ru(0001) film thickness. All layers were exposed to 40 mTorr·s CD_3OH at 80 K.

modes at 3500 (2500) cm^{-1}[14] suffices to obtain an approximate value. Specifically, we obtain K values of the order of 40 - 100 for $T \approx 160 - 200$ K, explaining the dominance of the CD_3OD over the CD_3OH isotope in the detected methanol desorption yield.

As the water formation reaction occurs in parallel to the described D ↔ H exchange of methanol and differences in OH (OD) stretch zero point energies are similar, one may invoke as to why the water formation does not exhibit a similar preference for the heavier hydrogen isotope. The reason is that the applicability of such a thermodynamic argument (different zero point energies) is closely related to the question, whether the H ↔ D exchange process is reversible or not. Apparently, methanol (CD_3OD and CD_3OH) is able to release its hydroxyl H(D) reversibly. For water and OH this is not true; as water does not dissociate on Pt(111) and adsorbed OH likewise represents a rather stable compound, produced OD or D_2O won't be able to take profit of their even more stable configurations as compared to OH or H_2O, i.e. adsorbed oxygen accepts whichever isotope, H or D, initiates the reaction, and keeps it permanently. Therefore, the water formation path is not selective in terms of H or D. Actually, the higher zero point energy of adsorbed surface H would imply a reduced O + H → OH reaction barrier as compared to O + D → OD, in accordance with our observations. Another process which may contribute to the prevalence of H_2O in the water formation yield, especially at the low T side of the corresponding desorption peak is a direct H-transfer of the hydroxyl H to nearby surface oxygen. Such a process has been unambiguously established for [methanol + D] on

Ru(0001)[13] and it may well contribute to the observed high fraction of CD_3OD in methanol desorption.

The yield of reactively produced formate and of desorbing CO_2 is depicted in Fig. 5 as a function of the number of Pt layers. Specifically, Fig. 5 comprises the integrated intensities of vibrational modes associated with $^{18}O_2$ ($\nu_{O\text{-}O}$ mode at 835 cm^{-1}) and of $DC^{18}O^{16}O$ ($\nu_{O\text{-}C\text{-}O}$ modes at 1270-1280 cm^{-1}), as well as the (integrated) desorption peaks of $C^{18}O^{16}O$ for nominally saturated $O_2/Pt_n/Ru(0001)$ layers (exposures: $50-60$ L for $n \leq 9$ ML and $20-30$ L for $n > 9$ ML) and an initial methanol coverage of 40 mTorr·s (0.16 ML). Apparently, the quantities of produced formate and CO_2 scale with the amount of initially adsorbed molecular oxygen. For thin Pt films of less than 6 ML Pt this value becomes smaller, as a result of the decreasing sticking probability of O_2.[24] For thicker layers ($n > 6$ ML) the efficiency towards methanol oxidation remains constant and probably equals the value of the Pt(111) surface.

In Fig. 6 integrated intensities of methanol and the dominant reaction intermediate (formate) are plotted versus the surface annealing temperature for various Pt coverages. Obviously, the formation and decomposition temperatures of the observed species do not vary with n, i.e. the activation energies of the individual reaction steps are largely independent of n. Consequently, the thermal evolution proceeds identically on laterally compressed (pseudomorphic[19]) $Pt_n/Ru(0001)$ and on relaxed Pt films (> 10 ML) with lattice constants close to Pt(111).

DFT calculations concerning Cu/Ru(0001) and Pd/Ru(0001)[41], as well as pseudomorphic $Pt_n/Ru(0001)$ layers[19] show that for thin ($n = 1-2$ ML) films the electronic influence of the substrate is dominant compared to the effect caused by strain. Thus, it would be interesting to study methanol reactions also on oxygen covered single monolayer Pt films. Yet, such experiments are virtually impossible as the sticking probability of O_2 for $n = 1-2$ ML is negligible.[24]

The integrated CO_2 desorption signal for the samples with $n > 6$ ML equals 0.08(±10%) ML, i.e., the fraction of CD_3OH molecules which becomes oxidized to formate adds up to about 50% for an initial methanol coverage of 0.16(±10%) ML. A calibration of the absolute values of desorbing CO_2 has been achieved by means of TPD, monitoring the signals of masses 28, 32 and 44 u of reactively produced CO_2 from coadsorbed CO and O ($\Theta_O \simeq 0.13$ ML, measured with XPS; $T_{ads} = 80$ K) on $Pt_{15\ ML}/Ru(0001)$.

B. Methanol on $O/Pt_n/Ru(0001)$

In this section methanol adsorption and reactions on ordered atomic oxygen ($T \rightarrow 300$ K) precovered $Pt_n/Ru(0001)$ layers are described. In each case O_2 has been adsorbed at 80 K and the layers annealed to 300 K to induce at least partial ordering of preadsorbed oxygen. In accordance with findings for preadsorbed O_2 the reaction pathways again seem to be independent of the Pt film thickness and the amount of adsorbed oxygen represents the primary factor affecting the reaction yields on $Pt_n/Ru(0001)$ films of different thicknesses. IRAS spectra of CD_3OH adsorbed at 80 K on $Pt_{12ML}/Ru(0001)$ precovered with 0.15 ML ^{16}O and annealed to increasingly higher temperatures are depicted in Fig. 7A. At 80 K intact isolated methanol molecules are visible with the following modes: out-of-phase $[\delta(OH)+\rho_{inplane}(CD_3)]oop$ mode at 872 cm^{-1}, $\nu(CO)$ stretching mode at 947 cm^{-1}, in-phase $[\delta(OH)+\rho_{inplane}(CD_3)]ip$ mode at 1280 cm^{-1}, and $\delta(CD_3)$ stretching modes at $1060-1100$ cm^{-1}. The *ip* and *oop* modes are characteristic for isolated methanol

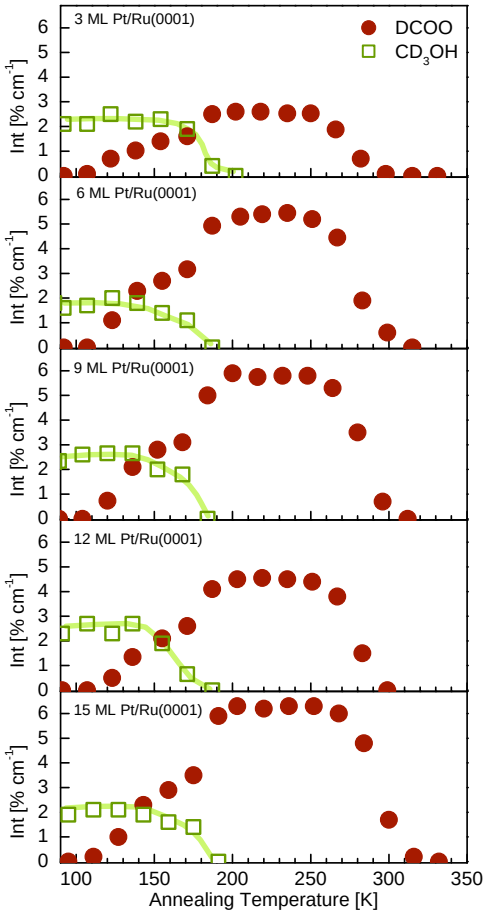

FIG. 6: Thermal evolution of CD_3OH (integrated IR intensities of the $\delta(CD_3)$ modes at 1050-1120 cm^{-1}) and of DCOO (integrated IR intensities of the $\nu(OCO)$ modes at $\approx 1270-1280$ cm^{-1}) on various $O_2/Pt_n/Ru(0001)$ layers, with $n = 3$, 6, 9, 12, and 15 ML. The oxygen exposures at 80 K were 50−60 L for $n \leq 9$ and 20−30 L for $n \geq 12$ ML. The individual IRAS spectra contributing to these curves have been measured while ramping the surface temperature at a rate of 0.2 K/s.

and therefore provide unambiguous evidence for intact methanol because both the CD_3 and the OH group participate in these vibrations.[14] The bands around 2100 cm^{-1} are due to a slight CO contamination accumulated during the O_2 exposure.

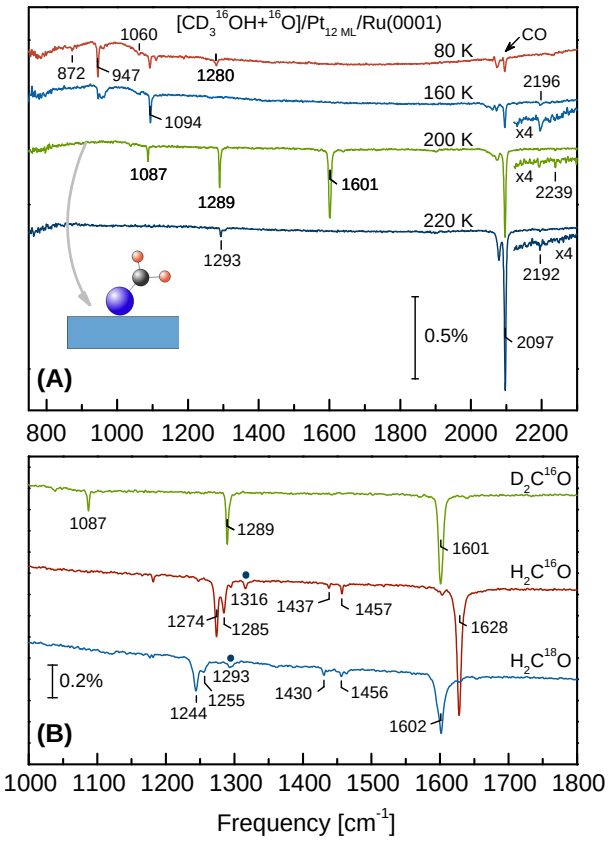

FIG. 7: **(A):** IRAS spectra of ≈ 0.15 ML CD_3OH adsorbed at 80 K onto $O/Pt_{12\ ML}/Ru(0001)$ with $\Theta_O \approx 0.15$ ML (1 L $^{16}O_2$ adsorbed at 80 K and annealed to 300 K). The spectra at 80 and 160 K show intact isolated methanol (872, 947 and 1280 cm^{-1} bands) and clustered methanol (∼960 and 1094 cm^{-1} bands), respectively. At 200 K formaldehyde (D_2CO) is observed (∼ 1087, 1289, and 1601 cm^{-1}). At 220 K minute amounts of formate (DCOO) are discernible (vibrational bands at 1293 and 2192 cm^{-1}), while the spectrum is dominated by the strong bands at 2075 and 2097 cm^{-1} due to CO (from formaldehyde decomposition) located at Pt(111) steps and terraces, respectively. The cartoon illustrates the binding geometry of formaldehyde. **(B):** IRAS spectra obtained after annealing the [methanol + oxygen] coadsorbate layers on $Pt_{12ML}/Ru(0001)$ to produce η^1-formaldehyde. Top: [CD_3OH + O], $T \rightarrow 200$ K; center: [CH_3OH + O], $T \rightarrow 190$ K; bottom: [$CH_3^{18}OH$ + O], $T \rightarrow 180$ K. All spectra have been recorded after recooling to 80 K. The full circles identify modes belonging to formate.

Upon heating the sample to 160 K, the modes at ≈ 960, 1060 and 1094 cm^{-1}, assigned to clustered methanol molecules, gain in intensity, while the characteristic *ip* and *oop* modes of isolated methanol are weakened substantially. The IRAS spectra of methanol on O/Pt(111) reported in the literature[10] agree with our spectra. However, Liu et al.[10] assigned the various vibrational modes at 160 K to a surface methoxy species. Yet, this assignment adheres to earlier HREELS measurements published by Sexton[42]. In our opinion, the spectral features look significantly different from methoxy on transition metal surfaces[13,27,29,43,44] which in all cases exhibits a prominent Fermi resonance signature in the methyl group stretching region. While we cannot exclude that small amounts of methoxy may be present after annealing to 160 K we attribute the dominant peaks at ≈960, 1060, 1094 cm^{-1} to intact methanol as already mentioned above.

After annealing to 200 K the spectrum changes dramatically. Specifically, the C-O stretching mode at $900 - 1000$ cm^{-1} has disappeared and new strong bands appear at 1087, 1289 and 1601 cm^{-1}, respectively. Again, the vibrational spectrum obtained by Liu et al.[10] on Pt(111) looks very similar; they assigned two of these bands, at 1087 and 1601 cm^{-1}, to the $\rho(CD_2)$ and $\nu(CO)$ modes of η^1-formaldehyde, respectively, with the C-O axis tilted as shown in the cartoon in Fig. 7A and as proposed by Anton et al.[45] for formaldehyde on Ru(0001). Note that the mirror plane of the molecule containing all atoms is still perpendicular to the surface. Regarding the assignment of the vibrational peak observed at about 1290 cm^{-1} Liu et al. concluded that this band does probably not belong to D_2CO but to a different species which could not be identified.[10] According to our data these three peaks belong to the same species produced after methanol dehydrogenation for the following reasons:

(i) all three features correlate closely in intensity for all annealing temperatures and they are observed in a narrow temperature range only $(180 - 200$ K) (see Supporting Information);

(ii) the line positions are not affected by the isotopic nature of preadsorbed oxygen (see Supporting Information). This latter point definitely excludes species such as formate which contain two oxygen atoms.

On the oxygen precovered Rh(111) surface, heating to 240 K converts methanol to a η^1-H_2CO species as well, as deduced from HREELS data.[46] According to our data formaldehyde formation is also found for the Rh/Ru(0001) monolayer (see Supporting Information).

The interpretation of the observed vibrational bands to a tilted η^1-D_2CO formaldehyde is in agreement with findings of Anton et al.;[45] an assignment of the vibrational bands observed at 200 K in Fig. 7A, along with a comparison to literature data, is given in Tab. II. In particular, the observed isotopic shift of the $\rho(CD_2)/\rho(CH_2)$ mode by +200 cm^{-1} upon D↔H exchange is in agreement with data of formaldehyde on Ru(0001)[45]. Note that the $\nu(CD_2)$ and $\nu(CH_2)$ stretching vibration of the sp^2-hybridized CD_2- (CH_2-) group of formaldehyde is located at $100 - 200$ cm^{-1} higher energies than the $\nu(CD_3)$ and $\nu(CH_3)$ stretching modes of the sp^3-hybridized methyl

group of methoxy,[13] providing further support for a η^1-formaldehyde with a C-O double bond as the observed surface species. According to Mavrikakis and Barteau[49] the reduced electron density in the vicinity of surface oxygen should, quite generally, lead to a preferred adsorption of formaldehyde in the η^1-configuration as opposed to η^2-formaldehyde, in accordance with our conclusions.

In order to further corroborate the identity of this species we performed additional experiments with various isotopically labeled methanol molecules as depicted in Fig. 7B. The assignment of the 1601 cm^{-1} peak to a C-O stretching vibration of formaldehyde is thereby assured by the isotope substitution of the methanolic oxygen $CH_3^{16}OH \leftrightarrow CH_3^{18}OH$ which causes a frequency shift 1628 $\leftrightarrow$ 1602 cm^{-1}.

At 1289 cm^{-1} the frequency of the suggested $\delta_s(CD_2)$ scissor mode is remarkably high. Comparing the data of matrix isolated formaldehyde[47] and formaldehyde adsorbed on Ru(0001)[45] (see Tab. II) the shift of this mode upon adsorption amounts to +86 cm^{-1} for D_2CO, starting at 1104 cm^{-1}. On Pt_n/Ru(0001) or Pt(111) the frequency of this band is even higher by another +100 cm^{-1}, reaching 1289 cm^{-1} for our layers.

The dependency of the $\delta(CD_2)$ and $\rho(CD_2)$ line positions on the frequency of the ν(CO) stretch mode is depicted in Fig. 8; the plot comprises data of D_2CO on O/Pt_n/Ru(0001) (this work), O/Rh_{1ML}/Ru(0001) (this work), O/Ru(0001)[45], and of matrix isolated D_2CO[47]. Obviously, the $\delta(CD_2)$ and $\rho(CD_2)$ line positions exhibit the higher values the lower the frequency of the C-O stretch. This effect seems to be related to the distortion of gas phase formaldehyde upon adsorption which appears particularly severe on Pt_n/Ru(0001) and on Pt(111) surfaces[10]. H_2CO on Rh(111), on the other hand, displays vibrational frequencies (measured with HREELS) which largely match those of matrix isolated H_2CO[48]. Interestingly, the Rh/Ru(0001) monolayer leads to substantially stronger shifts of formaldehyde modes as compared to Rh(111) (see Supporting Information).

The spectra for H_2CO and $H_2C^{18}O$ both exhibit two peaks in the regions of the $\delta(CH_2)$ and $\rho(CH_2)$ modes at about 1450 and 1250 - 1300 cm^{-1}, respectively. As the isotopic shifts of these modes are very similar (see Tab. II) they are both attributed to formaldehyde, however, located in two slightly different local environments.

Much weaker bands located at 1038 and 1182 cm^{-1} for D_2CO and H_2CO, respectively, may indicate the presence of some unknown species. An alternative interpretation would be a slight off-plane tilt rendering the $\omega(CH_2)$ of formaldehyde dipole active.

By further heating to temperatures above 200 K formaldehyde vanishes suddenly and the strong band at around 2100 cm^{-1} associated with reactively produced CO from formaldehyde decomposition grows to its maximum height. Additionally, a tiny peak appears at 1293 cm^{-1}. Analogous experiments with preadsorbed ^{18}O confirm the existence of this latter peak, however, significantly shifted to 1271 cm^{-1} (compare with Fig. 1B and Supporting Information). Hence, its assignment to the ν(OCO) mode of formate, produced in the course of formaldehyde oxidation, is straightforward. The corresponding ν(CD) stretch at 2192 cm^{-1} agrees perfectly with corresponding frequencies given in Tab. I and with experiments on Pt_n/Ru(0001) with preadsorbed O_2.

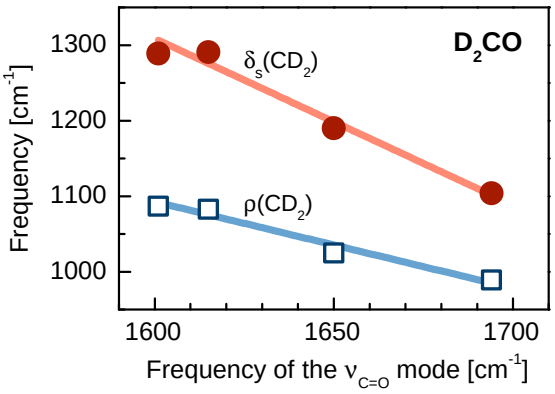

FIG. 8: Dependence of the $\delta_s(CD_2)$ and $\rho(CD_2)$ line positions on the frequency of the respective ν(CO) stretching mode of formaldehyde in different environments: adsorbed on O/Pt_n/Ru(0001) (1601 cm^{-1}, this work), O/Rh_{1ML}/Ru(0001) (1615 cm^{-1}, this work), O/Ru(0001)[45] (1650 cm^{-1}), and of matrix isolated D_2CO[47] (1694 cm^{-1}).

Fig. 9 shows a thermal desorption spectrum of CD_3OH on Pt_{12ML}/Ru(0001) precovered with 0.15 ML atomic oxygen. The strong peaks at about 200 K are due to desorbing methanol and water, as well as various cracking products thereof. Note that this temperature range corresponds to the temperature where formaldehyde bands develop in the IRAS spectra. Analogous to the O_2 precovered Pt_n/Ru(0001) layers, an isotopic exchange $CD_3OH+D \rightarrow CD_3OD+H$ during the methanol decomposition and desorption process occurs as well, leading to desorption of CD_3OD (compare with Fig. 4). Surface H and D are thereby provided by the dehydrogenation reaction of methanol to formaldehyde in the temperature range 180-200 K. Interestingly, the D_2CO reaction intermediate is observed in a narrow temperature range only and becomes dehydrogenated already at 200-210 K. In addition, we actually noticed a weak isotope effect, as formaldehyde formation and decomposition occurs at about 10 K lower temperatures for CH_3OH than for CD_3OH. This finding is in accordance with the higher activation energy for dehydrogenation of the CD_3- as compared to the CH_3-methyl group, due to a lower zero-point energy for the former. Regarding formaldehyde it is worth mentioning that our detected mass 32 u signal at 203 K is entirely due to an ionization fragment of desorbing methanol, i.e. there is no indication for D_2CO desorption.

By looking at the mass 18, 19 and 20 u signals of reactively produced and desorbing water (various isotopes)

TABLE II: Vibrational modes (frequencies given in cm^{-1}) of adsorbed tilted η^1-formaldehyde and of matrix isolated formaldehyde isotopes. If not specified otherwise, then O refers to the regular 16-oxygen isotope. Mode notation: stretching ν, scissor δ_s, rocking ρ.

this work			Ru(0001)[45]		Rh(111)[48]	matrix isolated[47]			mode
D_2CO	H_2CO	$H_2C^{18}O$	D_2CO	H_2CO	H_2CO	D_2CO	H_2CO	$H_2C^{18}O$	assignment
2239	3055	3054	2200	2970	2850	2187	2874	2859	$\nu(CH_2)$
1601	1628	1602	1650	1670	1740	1694	1740	1707	$\nu(CO)$
1289	1457/1437	1456/1430	1190	1456	1500	1104	1505	1495	$\delta_s(CH_2)$
1087	1285/1274	1255/1244	1025	1220	1240	989	1250	1244	$\rho(CH_2)$

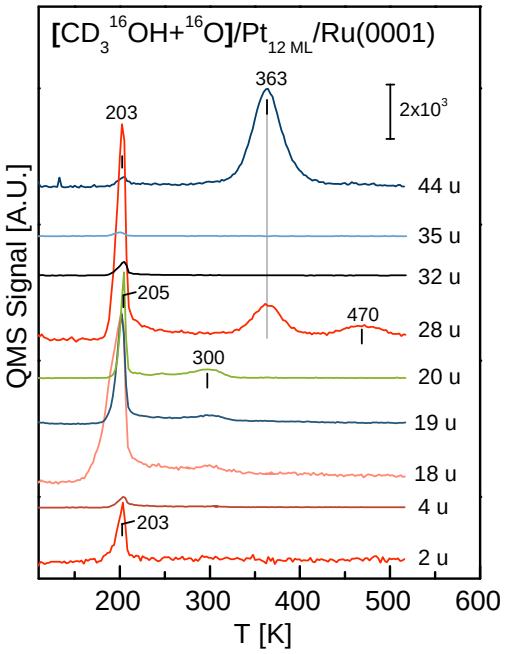

FIG. 9: Multi-mass TPD of $[CD_3OH+^{16}O]$ on $Pt_{12\ ML}/Ru(0001)$. 1 L O_2 was dosed at 80 K and annealed to 300 K to dissociate oxygen leading to $\Theta_O \approx 0.15$ ML in advance of the methanol exposure (30 mTorr·s at 80 K). The sample was heated with 1 K/s from 80 to 600 K.

in more detail, we notice that the H-containing species prevails at ≈ 180 K, i.e. during formaldehyde formation, while D_2O desorption is observed as a sharp feature during formaldehyde decomposition only. This observation is in accordance with expectation as both hydrogen isotopes are released during D_2CO formation while exclusively deuterium is liberated in the course of its decay.

Actually, the fractions of desorbing HDO and D_2O water isotopes at $T < 180$ K are considerably below expectation, if equal amounts of adsorbed H and D (from methanol to formaldehyde conversion) contribute to the overall water formation. Two explanations appear reasonable: (i) the hydroxyl group efficiently transfers its H atom directly to surface oxygen, similar to our observations on Ru(0001)[13] or (ii) abstracted D atoms are consumed in the exchange reaction $CD_3OH + D \rightarrow CD_3OD + H$ as discussed above, effectively replacing D by H as a surface species. While there is clear evidence for the latter process (see discussion related to Fig. 4, above), process (i) appears likely, but must remain speculative for now.

CO produced in the course of formaldehyde decomposition at about 200 K partially desorbs instantaneously, or it stays behind as a surface compound and leaves the surface at higher temperatures: at 360 K a strong mass 44 u peak indicates the reaction of accumulated CO and surface oxygen to CO_2; the 28 u signal evolving in parallel represents a CO_2 ionization fragment. In contrast, the small 28 u peak around 470 K is due to desorption of remaining CO after all surface oxygen has been consumed.

An analysis of the ionization fragments of desorbing methanol yields yet another surprise. Namely, the signal of mass 28 u at 200 K is way beyond expectation as a methanol ionization fragment. Purely thermal CO desorption at temperatures as low as 200 K appears unlikely as well. As the CO evolution correlates with formaldehyde decomposition, a non-equilibrated CO species produced during abstraction of both D-atoms may explain our observation. Note that bonding of formaldehyde is via the oxygen atom and a flipping of the CO core is required to produce adsorbed CO. While a 'one by one' abstraction of the two D leads to a chemical bonding of the C-atom to the substrate, eventually producing (upright) CO, a 'two at once' abstraction would leave the CO in an unfavorable, non-bonding upside-down configuration, leading to instantaneous desorption.

It is left to mention that there is no indication for the scission of methanol's C-O bond. DFT calculations of Greeley and Mavrikakis[8] show that on Pt(111) the energetic barrier for C-O bond breaking is 3 times higher than for C-H or O-H bands. In various experimental studies[10,12,13,44,50] dealing with methanol on transition metal surfaces a C-O bond breaking path has been ruled out as well. In contrast to methanol on $O/Cu_{1\ ML}/Ru(0001)$[32] and to the hydrogenation of oxygen on Pt(111)[53] no stable surface hydroxyl could be detected in the course of this study.

IV. CONCLUSIONS

In this work the adsorption and reactions of methanol on oxygen covered $Pt_n/Ru(0001)$ multilayers have been

investigated with IRAS and TPD. Specifically, the reactions of methanol on atomic and molecular oxygen covered Pt_n/Ru(0001) layers are found to proceed significantly different. In the latter case the formation of a formate species prevails with no stable intermediate detected in between. To some extent this reaction occurs even below the O_2 dissociation temperature at $T < 100$ K, probably at some special sites; much higher rates, however, have been achieved at slightly higher $T \approx 140 - 200$ K, after O_2 has dissociated and most likely involves disordered oxygen atoms. Once preadsorbed oxygen layers have been annealed, formate is produced as a minority species only and formaldehyde (η^1-D_2CO) is identified as the dominant stable reaction intermediate in the temperature range 180 - 210 K.

A central finding of this investigation is that the methanol reaction pathway on Pt_n/Ru(0001) multilayers looks very similar to Pt(111) and depends only weakly on the thickness of the Pt_n/Ru(0001) film. Strain within the Pt overlayers seems to influence the reactivity of methanol on these surfaces only marginally. The only relevant aspect to be considered when analyzing reactions on few layer Pt_n/Ru(0001) substrates is the sticking coefficient of oxygen which depends dramatically on n[24] and consequently affects the methanol reactions indirectly.

In addition to literature findings related to O_2 or O precovered Pt(111)[12]. isotopic labeling experiments allowed us to develop a more intricate description of the reaction schemes. Specifically, we found that H and D atoms abstracted during methanol decomposition lead to two different reactions both of them proceeding at relatively low $T \leq 200$ K: (i) hydrogenation of surface oxygen to gas phase water, and (ii) H $\leftrightarrow$ D exchange between methanol's OH group and surface H/D leading the preferential desorption of CD_3OD instead of the initially adsorbed CD_3OH. Our analysis of this latter process revealed a remarkable primary isotope effect which we attribute to the difference in zero point energies associated with OH and OD vibrations of methanol.

Referring to the DMFC where hydrogen acts as the energy provider, the easy reaction of hydrogen released during methanol decomposition with surface oxygen to produce gas phase water (180 - 200 K) on Pt multilayers constitutes a severe drawback. A possible way-out of this dilemma would be to enhance the adsorption energy of oxygen, e.g. by employing Pt_xRu_{1-x} surface alloys, thereby lowering the affinity of oxygen on Pt(111) towards hydrogenation; ideally, this may proceed without impairing its beneficial role in CO oxidation.

We note that application of our findings to realistic catalytic processes is not straightforward and some caution is advised. For example, the clean Pt(111) surface is non-reactive under UHV conditions (reactions occur on defects only[9]); under steady-state electrochemical conditions, however, this surface exhibits higher current densities upon methanol oxidation than the Pt(110) surface which is more reactive in UHV.[6] This surprising finding has been attributed to rapid CO poisoning of Pt(110) under continuous methanol flow conditions as a result of the relatively high reactivity of methanol on this surface.[52] Nevertheless, our investigation provides an in-depth view of the individual reaction steps and produced reaction intermediates. Interestingly, strain within the Pt films does only marginally influence the reaction pathways and yields of methanol on an oxygen precovered Pt surface. This is attributed to the fact that strain primarily affects adsorption energies; assuming that the energetic positions of transition states shift accordingly, the activation barrier separating two adsorbed species will stay the same (at least to a first approximation).

Supporting Information Available

- Ionization fragments of methanol desorbing from oxygen pre-covered Pt_n/Ru(0001) surfaces (figure)
- Formaldehyde formation on $Pt_{12\ ML}$/Ru(0001). (figure)
- Water desorption from [$CD_3^{16}OH$ + ^{16}O] and [D + ^{16}O] coadsorbate layers on Pt_n/Ru(0001) substrates. (figure)

This material is available free of charge via the Internet at http://pubs.acs.org.

[1] Ralph, T.R.; Hogarth, M.P., Platinum Metals Rev. **2002**, 46, 3.
[2] Ralph, T.R.; Hogarth, M.P., Platinum Metals Rev. **2002**, 46, 117.
[3] Iwasita, T.; Hoster, H.; John-Anacker, A.; Lin, W. F.; Vielstich, W., Langmuir **2000**, 16, 522.
[4] Hoster, H.; Iwasita, T.; Baumgärtner, H.; Vielstich, W., Phys. Chem. Chem. Phys. **2001**, 3, 337.
[5] Iwasita, T., J. Braz. Chem. Soc. **2002**, 13, 401.
[6] Waszczuk, P.; Lu, G.Q.; Wieckowski, A.; Lu, C.; Rice, C.; Masel, R. I., Electrochim. Acta **2002**, 47, 3637.
[7] Jusys, Z.; Kaiser, J.; Behm, R. J., Electrochim. Acta **2002**, 47, 3693.
[8] Greeley, J.; Mavrikakis, M., J. Am. Chem. Soc. **2004**, 126, 3910.
[9] Gibson, K.D.; Dubois, L.H., Surf. Sci. **1990**, 233, 59.
[10] Liu, Z.; Sawada, T.; Takagi, N.; Watanabe, K.; Matsumoto, Y., J. Chem. Phys. **2003**, 119, 4879.
[11] Endo, M.; Matsumoto, T.; Kubota, J.; Domen, K.; Hirose, C., J. Phys. Chem. B **2000**, 104, 4916.
[12] Sawada, T.; Liu, Z.; Takagi, N.; Watanabe, K.; Matsumoto, Y., Chem. Phys. Lett. **2004**, 392, 334.
[13] Gazdzicki, P.; Jakob, P., J. Phys. Chem. C **2010**, 114, 2655.

[14] Gazdzicki, P.; Uvdal, P.; Jakob, P., J. Chem. Phys. **2009**, 130, 224703.
[15] Buatier de Mongeot, F.; Scherer, M.; Gleich, B.; Kopatzki, E.; Behm, R.J., Surf. Sci. **1998**, 411, 249.
[16] Käsberger, U.; Jakob, P., Surf. Sci. **2003**, 540, 76.
[17] Jakob, P; Schlapka, A., Surf. Sci. **2007**, 601, 3556.
[18] Schlapka, A.; Käsberger, U.; Menzel, D.; Jakob, P., Surf. Sci. **2002**, 502, 129.
[19] Schlapka, A.; Lischka, M.; Groß, A.; Käsberger, U.; Jakob, P., Phys. Rev. Lett. **2003**, 91, 016101.
[20] Gsell, M.; Jakob, P.; Menzel, D., Science **1998**, 280, 717.
[21] Jakob, P.; Gsell, M.; Menzel, D., J. Chem. Phys. **2001**, 114, 10075.
[22] Mavrikakis, M.; Hammer, B.; Nørskov, J. K., Phys. Rev. Lett. **1998**, 81, 2819.
[23] Lischka, M.; Mosch, C.; Groß, A., Electrochim. Acta **2007**, 52, 2219.
[24] Jakob, P.; Schlapka, A.; Gazdzicki, P., J. Chem. Phys. **2011** 134, 224707.
[25] Feulner, P.; Menzel, D., J. Vac. Sci. Technol. **1980**, 17, 662.
[26] Koch, M. H.; Jakob, P.; Menzel, D., Surf. Sci. **1996**, 367, 293.
[27] Sim, S.W.; Gardner, P.; King, D.A., J. Phys. Chem. **1995**, 99, 16002.
[28] Mudalige, K.; Warren, S.; Trenary, M., J. Phys. Chem. B **2000**, 104, 2448.
[29] Chesters, M. A.; McCash, E. M., Spectrochim. Acta, Part A **1987**, 43, 1625.
[30] Gland, J.L., Surf. Sci. **1980**, 93, 487.
[31] Gland, J.L.; Sexton, B.A.; Fisher, G.B., Surf. Sci. **1980**, 95, 587.
[32] Gazdzicki, P.; Jakob, P., J. Phys. Chem. C **2011**, 115, 16555.
[33] Columbia, M.R.; Crabtree, A.M.; Thiel, P.A., J. Am. Chem. Soc. **1992**, 114, 1231.
[34] Weisel, M.D.; Chen, J.G.; Hoffmann, F.M., J. Electron Spectrosc. Relat. Phenom. **1990**, 54, 787.
[35] Hayden, B.E.; Prince, K.; Woodruff, D.P.; Bradshaw, A.M., Surf. Sci. **1983**, 133, 589.
[36] Haq, S.; Love, J. G.; Sanders, H. E.; King, D. A., Surf. Sci. **1995**, 325, 230.
[37] Hayden, B.E.; Prince, K.; Woodruff, D.P.; Bradshaw, A.M., Phys. Rev. Lett. **1983**, 51, 475.
[38] Jakob, P.; Menzel, D., Surf. Sci. **1988**, 201, 503.
[39] Jakob, P.; Menzel, D., Langmuir **1991**, 7, 134.
[40] Wolfsberg, M., Acc. Chem. Res. **1972**, 5, 225.
[41] Laurent, G.; Busnengo, H.F.; Riviere, P.; Martin, F., Phys. Rev. B **2008**, 77, 193408.
[42] Sexton, B. A., Surf. Sci. **1981**, 102, 271.
[43] Uvdal, P.; Weldon, M. K.; Friend, C. M., Phys. Rev. B **1994**, 50, 12258.
[44] Gazdzicki, P.; Jakob, P., J. Phys. Chem. C **2011**, 115, 1961.
[45] Anton, A.B.; Parmeter, J.E.; Weinberg, W.H., J. Am. Chem. Soc. **1986**, 108, 1823.
[46] Houtman, C.; Barteau, M.A., Langmuir **1990**, 6, 1558.
[47] Tso, T.L.; Lee, E.K.C., J. Phys. Chem. **1984**, 88, 5475.
[48] Houtman, C.; Barteau, M.A., Surf. Sci. **1991** 248, 57.
[49] Mavrikakis, M.; Barteau, M.A., J. Mol. Catal. A. **1998** 131, 135.
[50] Mudalige, K; Trenary, M., Surf. Sci. **2002**, 504, 208.
[51] Chen, Y. X.; Miki, A.; Ye, S.; Sakai, H.; Osawa, M., J. Am. Chem. Soc. **2003**, 125, 3680.
[52] Wang, J.; Masel, R.I., Surf. Sci. **1991**, 243, 199.
[53] Germer, T.A.; Ho, W., Chem. Phys. Lett. **1989**, 163, 449.

Supporting information for:

Oxidation of Methanol on Oxygen covered Pt_n/Ru(0001) Layers

Pawel Gazdzicki, Sebastian Thussing, and Peter Jakob*

Fachbereich Physik und Zentrum für Materialwissenschaften, Philipps-Universität Marburg, Renthof 5, 35032 Marburg, Germany

E-mail: peter.jakob@physik.uni-marburg.de

*To whom correspondence should be addressed

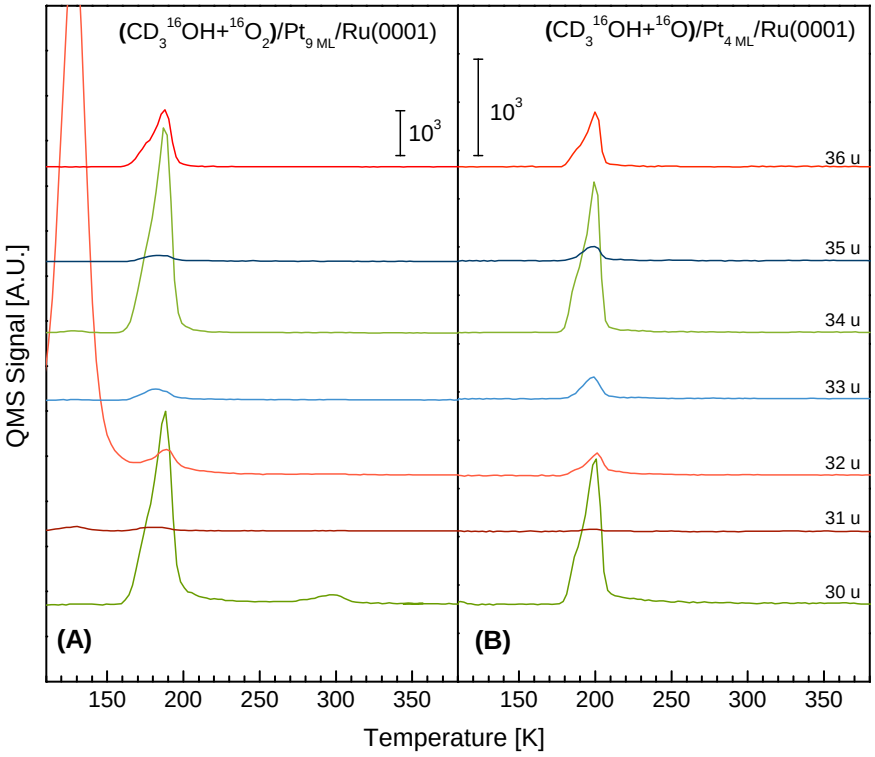

Figure 1: **Ionization fragments of methanol desorbing from oxygen pre-covered Pt_n/Ru(0001) surfaces** Multi-mass thermal desorption spectra (1 K/s) of $[CD_3^{16}OH + {}^{16}O_2]/Pt_{9\ ML}$/Ru(0001) (panel A) and $[CD_3^{16}OH + {}^{16}O]/Pt_{4\ ML}$/Ru(0001) (panel B). The oxygen exposures were 30 L and 40 L for the layers in (A) and (B), respectively; in the latter case the oxygen layer has been annealed to 300 K inducing dissociation and some ordering of preadsorbed oxygen. To both layers ≈ 0.15 ML methanol was added at 80 K. Our comparison of intensity ratios of the mass 30-36 u QMS signals in the temperature range 160 - 210 K demonstrate the occurrence of an isotope effect in the $CD_3OH+D \leftrightarrow CD_3OD+H$ exchange reaction, discussed in detail in the main article: even though the surface was exposed to the CD_3OH isotope only (dominant peaks expected at 35 u and 33 u) the data suggest a strong prevalence of CD_3OD (dominant peaks at 36 u and 34 u). Note that the figure focuses on signals associated with desorbing methanol (and various ionization fragments thereof) and other relevant masses have been blanked out.

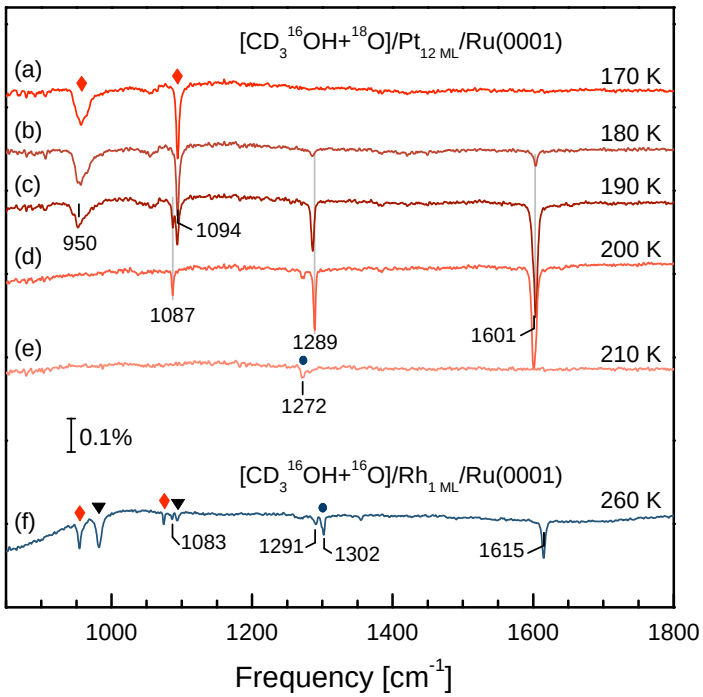

Figure 2: **Formaldehyde formation on $Pt_{12\,ML}$/Ru(0001).** IRAS spectra of the coadsorbate layer [$CD_3^{16}OH$ + ^{18}O] on $Pt_{12\,ML}$/Ru(0001) in the temperature range $170-210$ K (spectra (a)-(e)) demonstrating the increase and decay of the peaks associated with surface formaldehyde (gray lines). Identical peak positions with respect to an equivalent layer ([$CD_3^{16}OH$ + ^{16}O], see Fig. 7, main article) confirm that surface oxygen is only indirectly involved in the formaldehyde formation, e.g. by accepting abstracted H(D) atoms from methanol. Note that the distinctly different frequencies detected for formate (1272 cm^{-1} versus 1293 cm^{-1} in Fig. 7 in the main article) demonstrate the incorporation of surface oxygen to produce formate (DCOO). In addition, spectrum (f) shows formaldehyde (characteristic modes at 1087, 1291, and 1615 cm^{-1}) produced on 1 ML Rh/Ru(0001) after annealing a [$CD_3^{16}OH$ + ^{16}O] coadsorbate layer. Both surfaces have been exposed to 1 L of oxygen (annealed to 300 K) before methanol admission ($\Theta_{methanol} \approx 0.15$ ML) at 80 K. The samples were heated to the temperatures indicated in the figure and recooled to 80 K for data acquisition. Vibrational bands belonging to species other than formaldehyde have been individually labeled: methanol (rhombus), methoxy (triangles), and formate (bullets). Each set of peaks has been identified by its characteristic thermal evolution.

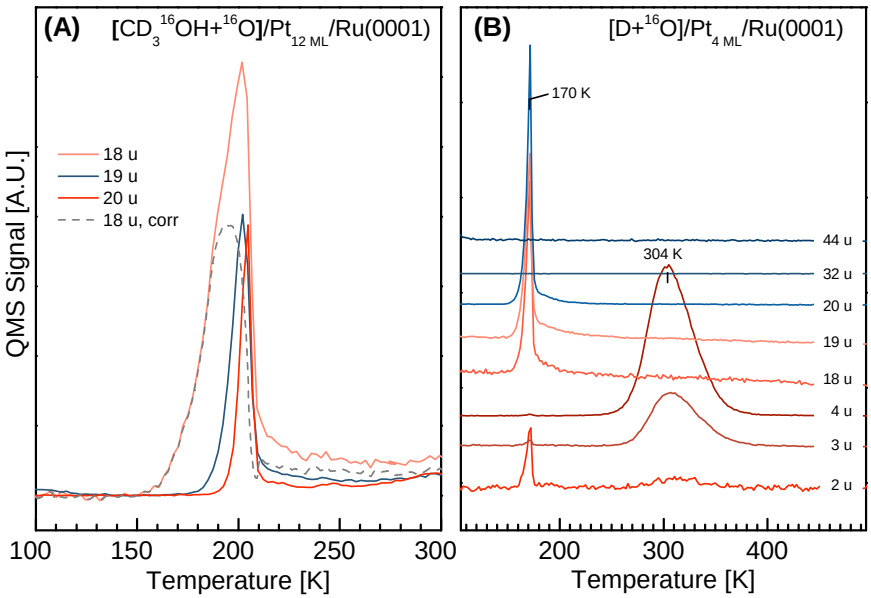

Figure 3: **Water desorption from [$CD_3^{16}OH$ + ^{16}O] and [D + ^{16}O] coadsorbate layers on Pt_n/Ru(0001) substrates. (A):** Enlarged view of mass 18, 19 and 20 u TPD traces (see Fig. 9, main article) of reactively produced water. The 18 u,corr curve represents the signal of desorbing H_2O and it corresponds to the 18 u signal with contributions due to ionization fragments of other species (methanol, HDO and D_2O) desorbing in parallel subtracted: 18 u,corr = 18 u - 4 $\times$ 32 u - 0.3 $\times$ 20 u - 0.15 $\times$ 19 u. The prevalence of desorbing H_2O at temperatures below 200 K points at an efficient transfer of hydroxyl H to coadsorbed oxygen atoms. HDO and D_2O evolution, on the other hand, only sets in after formaldehyde formation has started, which provides an extra D atom from the CD_3 methyl group. As outlined in the main paper, water formation is accompanied by the preferential incorporation of D into methanol, i.e. $CD_3^{16}OH + D \rightarrow CD_3^{16}OD + H$. **(B):** Thermal desorption spectra of the coadsorbate system [D+^{16}O] on $Pt_{4\ ML}$/Ru(0001) showing reactively produced desorbing water at 170 K. After all oxygen has been consumed, the remaining hydrogen desorbs at around 300 K. O_2 was dosed at 80 K and annealed to 300 K prior to D_2 exposure at 80 K. Note that the sample contains a slight H contamination leading to the desorption of H_2O, HDO (19 u), H_2 (2 u), and HD (3 u). The steep exponential increase and decrease of the water desorption rate leading to the narrow line shape (FWHM = 5 K) of the peak at 170 K confirms the autocatalytic water formation reaction reported in the literature [Sachs *et al.*, Science 293 (2001) p.1635, and references therein]. It is apparent that water formation occurs at higher temperatures for the methanol + oxygen coadsorbate layer which suggests that abstraction of hydrogen is the rate limiting step.

6.6 Article VI: Reactions of Methanol on Clean and Oxygen Covered Pt_xRu_{1-x}/Ru(0001) Surface Alloys

[1]Final version available at *J. Phys. Chem. C 115, 25379 (2011).*

Reactions of Methanol on Clean and Oxygen Covered Pt_xRu_{1-x}/Ru(0001) Surface Alloys

Pawel Gazdzicki, Sebastian Thussing, and Peter Jakob
Fachbereich Physik und Zentrum für Materialwissenschaften, Philipps-Universität Marburg, Renthof 5, 35032 Marburg, Germany

In this study the adsorption and reactions of methanol (CD_3OH) on clean and oxygen precovered Pt_xRu_{1-x}/Ru(0001) surface alloys with $x = 0 - 0.8$ have been investigated using Fourier transform infrared spectroscopy and thermal desorption. Particular interest has been devoted to the influence of coadsorbed (atomic) oxygen. For increasing amounts of Pt the clean surface becomes gradually passivated in agreement with the inert full Pt/Ru(0001) monolayer. On such oxygen-free layers the reaction pathway proceeds similar to clean Ru(0001). Yet, Pt increases the thermal stability of the methoxy (CD_3O) intermediate which represents the only stable reaction product species besides CO. On oxygen precovered Pt_xRu_{1-x}/Ru(0001) surface alloys the primary activation of methanol again leads to methoxy. Depending on the Pt concentration within the Pt/Ru(0001) surface alloy subsequent reactions, however, vary substantially. For $x < 0.4$ total dehydrogenation to CO prevails, while for $x > 0.4$ formate (DCOO) is produced, eventually leading to CO_2 desorption. Formaldehyde formation and desorption is observed for $x = 0.1 - 0.8$. Similar to methanol reactions on O/Ru(0001) and O/Pt_n/Ru(0001) no experimental evidence for surface hydroxyl has been found.

PACS numbers:

I. INTRODUCTION

In this study methanol (CD_3OH) reactions on clean and atomic oxygen covered Pt_xRu_{1-x}/Ru(0001) surface alloys have been investigated using infrared absorption spectroscopy (IRAS) and temperature programmed desorption (TPD). This bimetallic system exhibits reactivity toward complete oxidation of methanol and CO_2 desorption and is therefore of high relevance as a catalyst material for a direct methanol fuel cell (DMFC).[1–8]

The reactions of methanol on Ru(0001)[9,10] and Pt_n/Ru(0001)[11] layers have been presented recently. It has been found that the clean Ru(0001) surface is reactive toward methanol dehydrogenation to CO via a stable methoxy intermediate (CD_3O). In contrast, ordered oxygen overlayers, such as $O(2\times2)$ or $O(2\times1)$, passivate the surface completely. Low oxygen coverages of few percent of a monolayer, however, induce a direct H-transfer from the methanol hydroxyl group to surface oxygen leading to the desorption of water.[9]

On Pt_n/Ru(0001)[11] and Pt(111)[12–14] the situation is different: on the clean surfaces no reactions occur and surface oxygen is needed to activate methanol. Preadsorbed disordered (cold deposited) atomic or chemisorbed molecular oxygen oxidizes methanol directly to DCOO without any stable surface intermediates in between.[11,14,15] When ordering of the atomic oxygen layer is induced by annealing, adsorbed methanol decomposes to CO via a stable formaldehyde (D_2CO) surface species. The continued oxidation of formaldehyde to formate (DCOO) thereby represents a minor path only.

The properties of bimetallic surface alloys have been studied extensively establishing that the behavior of foreign atoms embedded in the surface layer of a host material (surface alloy) behave substantially different than bulk alloys or elemental surfaces.[16,17] A key parameter to describe the chemical properties of bimetallic alloys is represented by the number of specific surface sites needed to activate a certain species (geometric or ensemble effect)[17,18]; other relevant influences are the electronic interaction between different types of atoms involved in the reaction (electronic or ligand effect)[17,18], and strain introduced by the difference in atom sizes[19].

Hence, referring to methanol reactions, the pathways may be tailored based on which of the effects described above dominates. The properties of surfaces with high concentrations of Pt where the ensemble effect due to Pt is expected to dominate should behave different from alloys with low amounts of Pt dominated by ligand effects (Pt-Ru interaction) within the first layer.

Notably, epitaxially grown bimetallic Pt/Ru(0001) films, studied in previous work as a catalyst for methanol reactions, converts into such a surface alloy upon annealing of submonolayer Pt films to 1300 K.[20,21] Surface alloy means that Pt atoms intermix with Ru atoms within the topmost layer, while diffusion of Pt into Ru bulk remains negligible. According to Hoster et al.[21], a statistical distribution of Pt and Ru atoms prevails and conservation of the number of Pt atoms in the topmost layer is ensured for $\Theta_{Pt} \leq 0.8$ ML.

There exist a number of steady-state electrochemical studies regarding methanol oxidation on PtRu alloys[3–5,7], nano-particles[6], and Ru/Pt surfaces[3–5] performed with various methods, such as cyclic voltammetry, mass spectrometry and FT-IRAS. An important question in these studies concerns the influence of the surface structure[3–6] and composition[3–7] on the catalytic activity. All groups agree that PtRu catalysts exhibit reactivity toward methanol oxidation and a high resistance against CO poisoning. Furthermore, rough PtRu alloys seem more reactive than smooth ones.[4] For realistic anode potentials a Ru content of 20-50% for both the PtRu bulk alloys[5–7] as

well as for the Ru/Pt surfaces[3,5] yielded the highest current density. Using IRAS, Chen et al.[22] unambiguously identified formate as an intermediate in methanol electrooxidation over a Pt electrode. This specific result is in accordance with our previous findings on $O_2/Pt_n/Ru(0001)$ layers.[11]

To the best of our knowledge no UHV-studies on thermally induced methanol reactions on oxygen precovered or clean $Pt_xRu_{1-x}/Ru(0001)$ surface alloys have been published up to now.

II. EXPERIMENTAL

The experiments were performed in an UHV system at a base pressure of $p = 6 \times 10^{-11}$ mbar. The sample is a Ru(0001) crystal (5N purity) with 10 mm in diameter and a thickness of 2 mm. It can be cooled with liquid He or N_2 and heated up to 1570 K (limited by the type K thermocouple) with linear heating rates of 0.1-10 K/s. The quadrupole mass spectrometer (Balzers QMA112) is equipped with a Feulner cup[23] (glass enclosure) to ensure desorption from the front face of the sample only and to enhance the desorption signals. The Fourier transform infrared spectrometer (FTIR) is a Bruker IFS 66v with evacuable optics ($p < 1$ mbar). Polarized IR radiation is produced by a water cooled blackbody source (Globar) in conjunction with a wire grid polarizer. Within this work a LN_2 cooled MCT (HgCdTe) detector was used, allowing for measurements in the spectral range 700-4000 cm^{-1}. All infrared absorption spectra were taken at a resolution of 2 cm^{-1} with 500-2000 scans coadded. For the IRAS measurements the sample is positioned in a dedicated IR cell, which contained a titanium sublimation pump. A uniform gas dosage is provided by a multicapillary array with individual diameters of ≈ 10 μm. The sample was cleaned by Ar^+ sputtering (1.4 keV, 1 μA) and multiple O_2 dosing cycles combined with flashing the sample up to 1570 K.

For Pt deposition a thermal evaporator was used. The typical deposition rate was 0.03 ML min^{-1} at a growth temperature $T_g = 700$ K. During the evaporation time the pressure increases up to 2×10^{-10} mbar. A more detailed description of the experimental setup has been published recently.[9,10] The prepared Pt/Ru(0001) layers were probed by measuring the ν(CO) mode of adsorbed CO with IRAS.[24,25] The error of the Pt coverage is estimated to 5%.

In order to induce alloy formation, the sample was annealed to 1300 K for 3-5 min. The conservation of the amount of surface Pt, as reported by Hoster et al.[21], is confirmed by XPS measurements of the Pt $4f_{5/2}$ and $4f_{7/2}$ peaks before and after alloy formation. The integrated intensities of these peaks remain constant within $\pm 5\%$.

Methanol was cleaned by repeated freeze-and-thaw cycles. The isotopic purities of CD_3OH, $CH_3^{18}OH$, and $^{18}O_2$ are 99.8%, 95%, and 98.73%, respectively. All methanol exposures in this paper are specific to our experimental setup only and are given as the product of the pressure in our gas dosing system and the exposure time; the units used are mTorr·s. 10 mTorr·s of methanol approximately leads to 10% saturation of the first layer and equals 0.04 ML referring to the above definition as determined by XPS (integral of the O_{1s} peak) and comparing the results with perfect $O(2 \times 2)/Ru(0001)$ layers at an oxygen coverage $\Theta_O = 0.25$ ML, prepared according to Koch et al.[26].

The data presented in this work primarily comprises the CD_3OH isotope, as its vibrational modes exhibit somewhat sharper line shapes as compared to regular methanol. In addition, CD_3O (methoxy) on Ru(0001) exhibits a 10 times stronger umbrella mode $\delta_s(CD_3)$ (symmetric CD_3 stretch) than CH_3O which allows a more accurate quantitative analysis.[9] A similar observation was reported in the literature on Ag(111)[27] and on Cu(111)[28,29]. The reason for such dissimilar oscillator strengths for two methoxy isotopes is that coupling among modes of equal symmetry depends on their spectral separation;[29] in our case, the nearby ν(CO) mode considerably enhances the intensity of $\delta_s(CD_3)$ but not of $\delta_s(CH_3)$.

III. RESULTS AND DISCUSSION

In this section the reactions of methanol on clean and on atomic oxygen precovered $Pt_xRu_{1-x}/Ru(0001)$ surface alloys ($x = 0 - 0.8$) will be described. Thereby x denotes the relative amount of Pt atoms with respect to the total number of atoms in the topmost layer. Note that on Ru(0001) and $Pt_xRu_{1-x}/Ru(0001)$ O_2 adsorbs dissociatively with a high probability, while sticking of O_2 on a single Pt/Ru(0001) monolayer is zero.[30] Thus, a non-constant s_0 is also expected for $Pt_xRu_{1-x}/Ru(0001)$ surface alloys. Since we applied a constant O_2 exposure (4 langmuirs) to all $Pt_xRu_{1-x}/Ru(0001)$ surface alloys, the layers with a low concentration of Pt atoms should exhibit higher oxygen coverages than layers with high x. In general, the oxygen layers have not been annealed before exposure to methanol, as heating of the oxygen layers to 600 K prior to methanol exposures largely passivates the surface in terms of methanol reactions. This is most likely due to the formation of ordered oxygen layers, e.g. (2×2)-O or (2×1)-O overlayers, which are known to be unreactive.[9,31–35] This finding strictly holds for Ru(0001) only, while for $Pt_xRu_{1-x}/Ru(0001)$ surface alloys minute amounts of reactively produced DCOO are observed. Yet, these quantities correspond to only 10% of the amounts produced on cold-deposited O-layers.

In our study using IRAS and TPD experiments we first present the reactions of methanol on oxygen-free surface alloys. Subsequently, the effect of preadsorbed oxygen on alloys with $55 - 70\%$ Pt ($x = 0.55 - 0.70$) will be discussed. Finally, we will analyze the influence of the Pt/Ru ratio within the surface alloys.

A. Methanol on Clean Pt_xRu_{1-x}/Ru(0001)

On oxygen-free Pt_xRu_{1-x}/Ru(0001) surface alloys the methanol reactions proceed similar to the reactions on clean Ru(0001)[9,10]: methanol adsorbs intact at 80 K and undergoes an O-H bond cleavage upon heating to 180 K leading to an upright methoxy species. Methoxy is stable at intermediate temperatures only and decays by means of hydrogen abstraction, producing CO. This correlation is illustrated in Fig. 1A showing the decrease of IRAS peaks associated with methoxy and the increase of the CO stretch mode for both layers, the clean Ru(0001) surface (blue symbols) and an alloy with $x = 0.4$ (red symbols). In contrast to Ru(0001) this decay proceeds at significantly higher temperatures for the Pt_xRu_{1-x}/Ru(0001) surface alloy. With increasing x the corresponding transition temperature shifts from 250 to 305 K for $x = 0.4$ and 315 K for $x = 0.6$ (see Fig. 1A and B and Fig. 5C below). For increasing $x > 0.5$ all vibrational bands associated with methoxy gradually lose intensity (see Fig. 1C) which is in agreement with the zero reactivity of methanol on the full Pt/Ru(0001) monolayer[11] and on Pt(111)[12].

A second characteristic associated with Pt-Ru surface alloys is the influence of Pt on the vibrational modes of methoxy as demonstrated in 1C. Specifically, the C-O stretching mode at 980 cm^{-1}, attributed to methoxy on clean Ru(0001), looses in intensity very quickly with increasing x and is replaced by an equivalent mode at 997 cm^{-1}. Even for low $x = 0.14$ the 980 cm^{-1} peak has less intensity than the one at 997 cm^{-1}, associated with the presence of Pt in the surface layer; for $x \geq 0.4$ the 980 cm^{-1} peak has vanished almost completely. These observations suggest that only few, probably isolated, Pt atoms are needed to change the vibrational signature of methoxy significantly. Hence, a strong ligand effect is most likely the reason for this behavior.

Besides the C-O mode, the Fermi resonance appearance of the methoxy methyl group is influenced by the local binding geometry as well. Such a dependence of these vibrations on the local chemical environment has also been observed for methoxy on clean Ru(0001) post-exposed to increasing amounts of oxygen (see Supporting Information). Specifically, for increasing x (and similarly Θ_O), the prominent and strongest Fermi resonance band at 2066 cm^{-1} seems to split up into weaker bands at 2053 and 2070 cm^{-1}. One may invoke that incorporated Pt atoms as well as coadsorbates lead to significant line shifts of the methyl bending and stretching modes. However, this conclusion is erroneous, as no such peak doubling is observed when replacing CD_3OH by CH_3OH.

In Fig. 2 the well-known spectra of CD_3O and CH_3O on Ru(0001) are reproduced and compared to the respective methoxy species produced on $Pt_{0.3}Ru_{0.7}$/Ru(0001). It is apparent that the 30% fraction of Pt within the surface layer does shift the methoxy ν(CO) mode, but leaves the modes in the C-H stretch region virtually unchanged. This finding agrees with the expectation that

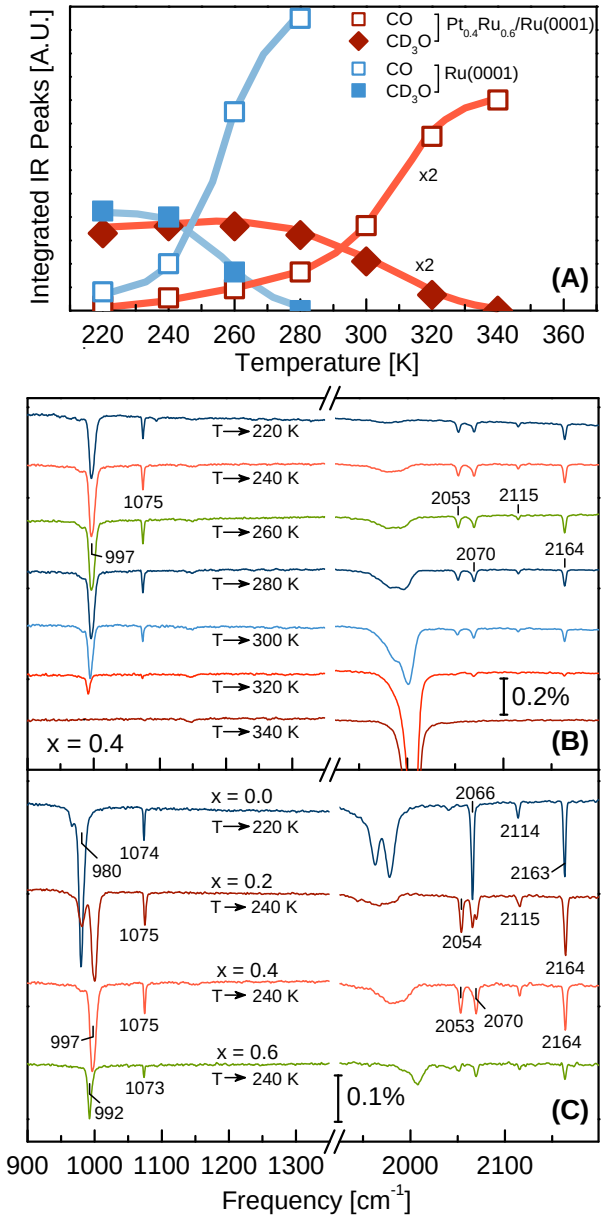

FIG. 1: **(A):** Decomposition of CD_3O (diamonds) to CO (squares) on clean Ru(0001) (blue symbols) and on Pt_xRu_{1-x}/Ru(0001) (brown symbols). The data points correspond to integrated IRAS intensities of methoxy (ν(CO) modes at 980 and 997 cm^{-1} for $x = 0$ and 0.4, respectively) and CO (ν(CO) mode at 2000-2100 cm^{-1}). **(B):** IRAS spectra of CD_3O on Pt_xRu_{1-x}/Ru(0001) with $x = 0.4$ obtained after annealing to increasingly higher temperatures from top to bottom as indicated in the figure. **(C):** IRAS spectra of CD_3O on Pt_xRu_{1-x}/Ru(0001) surface alloys with x increasing from top to bottom as indicated in the figure. In all panels methanol (covarege: 0.15 ML) was adsorbed at 80 K, annealed as indicated in the figure and recooled to 80 K for data acquisition.

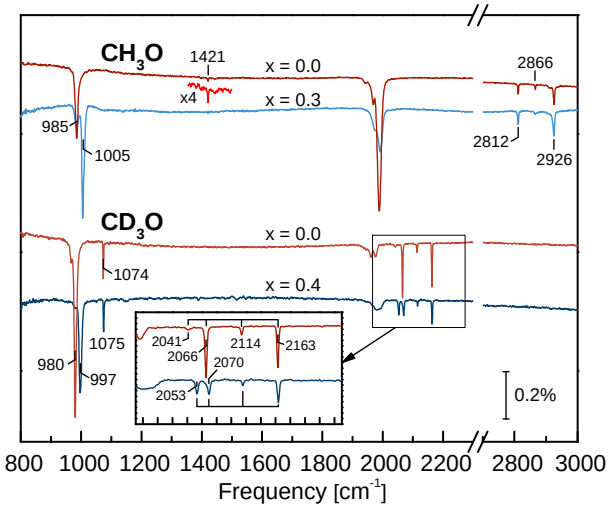

FIG. 2: IRAS spectra of methoxy on clean Ru(0001) and on Pt_xRu_{1-x}/Ru(0001) surface alloys. The top spectra correspond to CH_3O on surfaces with $x = 0.0$ and 0.3. The bottom spectra represent CD_3O on surfaces with $x = 0.0$ and 0.4. To all samples about 0.15 ML methanol was added at 80 K and annealed to 220 K to produce methoxy prior to data acquisition at 80 K.

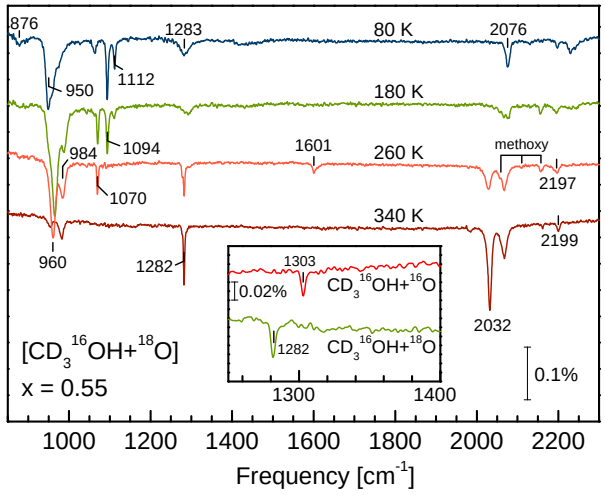

FIG. 3: IRAS spectra of $[CD_3OH + {}^{18}O]$ coadsorbate layer on a $Pt_{0.55}Ru_{0.45}$/Ru(0001) surface alloy. Methanol and oxygen exposures at 80 K were 40 mTorr·s (0.15 ML) and 4 langmuirs (0.3 ML), respectively. All spectra were taken at 80 K after heating (1 K/s) to the temperatures indicated in the figure. In the spectral range above 2300 cm^{-1} no vibrational peaks have been observed. The inset shows IRAS spectra of $[CD_3^{16}OH+{}^{16}O]$ and $[CD_3^{16}OH+{}^{18}O]$ on $Pt_{0.3}Ru_{0.7}$/Ru(0001) after heating to 320 K to produce formate.

the large distance of the methyl group from the surface plane renders the methyl group insensitive to modifications at the surface. In accordance with Sim et al.[27] the doublet at 2040-2080 cm^{-1} is attributed to the effect of another 'overtone' band, the $[\nu(CO) + \delta_s(CD_3)]$ combination band, interacting with the (fundamental) symmetric $\nu_s(CD_3)$ mode.

Actually, for the clean Ru(0001) surface ($x = 0$) the $[\nu(CO) + \delta_s(CD_3)]$ combination band is also visible at 2041 cm^{-1} (inset of Fig. 2), i.e. red shifted due to the lower $\nu(CO)$ frequency and the apparent repulsion from the fundamental $\nu_s(CD_3)$ mode via Fermi resonance coupling. What we observe is therefore not a splitting of the 2060 cm^{-1} band but a redistribution in oscillator strength between the $\nu_s(CD_3)$ fundamental mode and the $[\nu(CO) + \delta_s(CD_3)]$ combination band.

In agreement with a negligible coupling among the overtone and combination bands of the Fermi resonance (Darling-Dennison constants),[36–39] the remaining CD_3O modes at 2100-2200 cm^{-1} stay virtually the same, independent of Pt alloying or oxygen coadsorption.

A quantitative analysis of the Fermi resonance coupling yields a coupling $W_{ab} = 12 \pm 1$ cm^{-1} between $[\nu(CO) + \delta_s(CD_3)]$ and $\nu_s(CD_3)$ (for a full account of the various coupling constants etc., see Supporting Information). Our analysis additionally provides the anharmonic coupling between the $\nu(CO)$ and $\delta_s(CD_3)$ modes of CD_3O which amounts to $\delta\nu_{anh} = 9\pm1$ cm^{-1}.

In the following, the more heterogeneous reactions of coadsorbed methanol and oxygen on Pt_xRu_{1-x}/Ru(0001) surface alloys will be discussed.

A second characteristic associated with Pt-Ru surface alloys is the influence of Pt on the vibrational modes of methoxy as demonstrated in Fig. 1C. Specifically, the C-O stretching mode at 980 cm^{-1}, attributed to methoxy on clean Ru(0001), looses in intensity very quickly with increasing x and is replaced by an equivalent mode at 997 cm^{-1}. Even for low $x = 0.14$ the 980 cm^{-1} peak has less intensity than the one at 997 cm^{-1}, associated with the presence of Pt in the surface layer; for $x \geq 0.4$ the 980 cm^{-1} peak has vanished almost completely. These observations suggest that only few, probably isolated, Pt atoms are needed to change the vibrational signature of methoxy significantly. Hence, a strong ligand effect is most likely the reason for this behavior.

B. Methanol on O Covered Pt_xRu_{1-x}/Ru(0001): Infrared Spectroscopy

In Fig. 3 the thermal evolution of IRAS spectra of CD_3OH on a ^{18}O precovered $Pt_{0.55}Ru_{0.45}$/Ru(0001) surface alloy are depicted. This mixture of Pt:Ru surface atoms has been chosen because it provides a representative overview of the various surface processes and intermediates encountered in the course of methanol activation and beyond. Modifications hereof and the dependence on x will be discussed thereafter. Oxygen and methanol have been adsorbed at 80 K and then annealed to the temperatures indicated in the figure before data acquisition at 80 K. The topmost spectrum

shows intact CD_3OH molecules with the following vibrational modes: $[\delta(OH)+\rho_{ip}(CD_3)]$ in phase and out of phase modes at 1283 and 876 cm^{-1}, respectively, $\nu(CO)$ mode at 950 cm^{-1}, as well as $\delta(CD_3)$ modes at 1060-1112 cm^{-1}; various $\nu(CD_3)$ stretching modes in Fermi Resonance[29,37,39,40] with $\delta(CD_3)$ bending overtones are located at 2000-2200 cm^{-1}. Clear evidence for intact methanol adsorption is thereby provided by the detection of the two peaks at 876 and 1283 cm^{-1}; for methanol on Ru(0001) this set of modes has been unambiguously assigned to the $[\delta(OH)+\rho_{ip}(CD_3)]$ out of phase and $[\delta(OH)+\rho_{ip}(CD_3)]$ in phase modes of methanol.[10]

At 180 K methanol begins to transform into methoxy due to abstraction of the hydroxyl hydrogen and transfer to surface oxygen as evidenced by $H_2^{18}O$ desorption at 175 K (see Fig. 4A below). Thereby methoxy is identified on the basis of its prominent bands $\nu(CO)$ at 984 and $\delta(CD_3)$ at 1070 cm^{-1}; the characteristic Fermi resonance at 2000-2200 cm^{-1} is barely visible but still discernible. Note that after annealing to $T > 200$ K the spectral range at $2030-2080$ cm^{-1} becomes more and more dominated by reactively produced CO from methoxy decomposition. Even though a fraction of methanol molecules has decayed, the intensity of the bands associated with methanol remain about constant; yet, shifts in line positions are observed. These modifications are probably due to a reorganization of the methanol layer, most likely clustering caused by hydrogen bonding, similar to methanol on clean Ru(0001)[10].

Annealing to 260 K leads to the gradual disappearance of (intact) methanol's vibrational modes, partially due to molecular desorption (208 K), or due to the continued conversion to methoxy. Moreover, entirely new peaks show up at 1282 and 1601 cm^{-1}, with only the former surviving further annealing to 340 K. These new bands therefore belong to two different surface species. While the 1601 cm^{-1} band is characteristic for a η^1-formaldehyde species, the 1282 cm^{-1} peak, along with the tiny band at 2197 cm^{-1}, can be attributed to formate. This interpretation is supported by the observed isotopic shift 1282 $\leftrightarrow$ 1303 cm^{-1} for the $[CD_3^{16}OH + {}^{16}O]$ and $[CD_3^{16}OH + {}^{18}O]$ coadsorbate layers on $Pt_{0.3}Ru_{0.7}$/Ru(0001) after heating to 320 K (see the inset of Fig. 3). The vibrational frequencies fit well to formate on Pt_n/Ru(0001)[11] and Ru(0001)[41] as revealed by Tab. I. Specifically, the observed bands at 1282 and 1303 cm^{-1} can be ascribed to the formate isotopes $DC^{16}O^{18}O$ and $DC^{16}O^{16}O$, respectively.

The identity of the 1601 cm^{-1} peak as a vibrational mode of formaldehyde (D_2CO) is ensured by the fact that its frequency does not depend on the isotopic nature of preadsorbed oxygen; this species is therefore formed solely due to the dehydrogenation of methanol or possibly of methoxy. Referring to Liu et al.[13], Anton et al.[42] and our recent experiments on Pt_n/Ru(0001) layers[11] the 1601 cm^{-1} peak is assigned to the $\nu(CO)$ stretching mode of an inclined η^1-formaldehyde (D_2CO). Details regarding the adsorption geometry, however, must remain open,

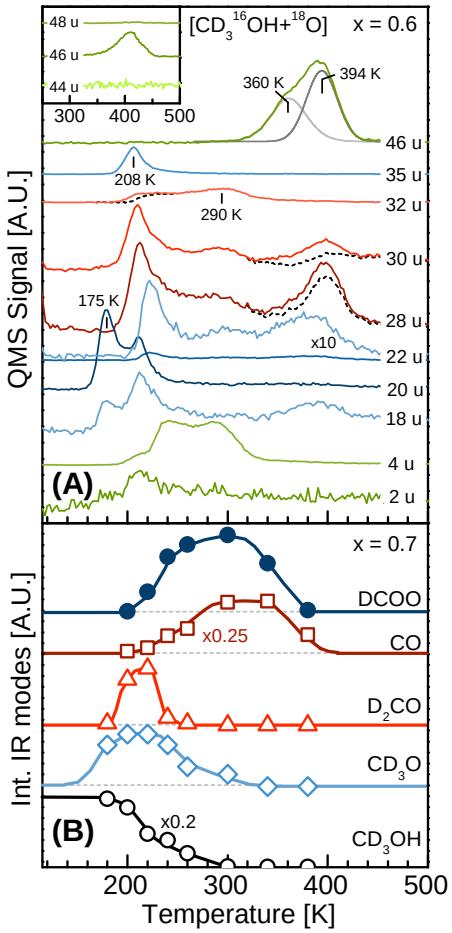

FIG. 4: **A:** Multi-mass TPD of $[CD_3OH + {}^{18}O]$ coadsorbate layer on $Pt_{0.6}Ru_{0.4}$/Ru(0001). Methanol and oxygen exposures at 80 K equal to 40 mTorr·s (0.15 ML) and 4 langmuirs (0.3 ML), respectively. The sample was heated with 1 K/s from 80 to 600 K. The dashed lines (mass 28 u and 30 u) correspond to 28 u,corr = 28 u - 0.16 × 46 u and 30 u,corr = 30 u - 0.17 × 46 u with contributions of desorbing $C^{16}O^{18}O$ (46 u) subtracted. The dashed line of 32 u correspond to the original 32 u signal (solid line) with contributions of desorbing methanol (35 u) subtracted. The relative ratios of the individual $C^{16}O^+$ and $C^{18}O^+$ fragments are known from reactively produced $C^{16}O+{}^{18}O \rightarrow C^{16}O^{18}O$ on Pt_n/Ru(0001). The gray lines at 46 u are fit curves to estimate the contributions of the two desorption features. The inset shows an analogous TPD for $Pt_{0.3}Ru_{0.7}$/Ru(0001) with masses 44, 46 and 48 u recorded. **B:** Temperature dependent integrated IRAS signals of CD_3OH ($\nu(CO)$ mode at 960 cm^{-1}), methoxy ($\nu(CO)$ mode at 980 cm^{-1}), D_2CO ($\nu(CO)$ mode at 1601 cm^{-1}), DCOO ($\nu(OCO)$ mode at 1300-1305 cm^{-1}), and CO ($\nu_{C\text{-}O}$ mode at 2020-2060 cm^{-1}). 4 L ${}^{16}O_2$ followed by 40 mTorr·s $CD_3^{16}OH$ were adsorbed at 80 K on $Pt_{0.7}Ru_{0.3}$/Ru(0001) before the sample was heated (1 K/s) to increasingly higher temperatures. The colored lines are guides to the eye. The individual curves are offset vertically for a better clarity of presentation.

TABLE I: Vibrational modes (frequencies given in cm^{-1}) of formate (C_{2v}-symmetry) on Pt_xRu_{1-x}/Ru(0001), Pt_n/Ru(0001), and Ru(0001). Note that the mode notation refers to DCOO.

Pt_xRu_{1-x}/Ru(0001)			Pt_n/Ru(0001)[11]		Ru(0001)[41]	mode
$DC^{16}O^{16}O$	$DC^{16}O^{18}O$	$HC^{16}O^{16}O$	$DC^{16}O^{16}O$	$DC^{16}O^{18}O$	$HC^{16}O^{16}O$	assignment
1303	1282	1336	1294	1276	1363	ν(OCO)
2193	2197	2926	2192	2192	2851	ν(CD)

as only the strongest mode of D_2CO is observed. Additional support for the assignment of the 1601 cm^{-1} peak to the C-O stretching vibration ($\nu_{C=O}$) of formaldehyde is provided by our isotope substitution of the methanolic oxygen $CH_3^{16}OH \leftrightarrow CH_3^{18}OH$ which causes a frequency shift 1626 $\leftrightarrow$ 1602 cm^{-1} (the closeness of the ν(CO) frequencies of $H_2C^{18}O$ and $D_2C^{16}O$ is accidental).

In the course of our investigation no experimental evidence for the formation of surface hydroxyl (OH) has been found in contrast to the reactions of methanol on oxygen precovered Cu/Ru(0001)[32] monolayers. Furthermore, we did not find any indication for the scission of methanol's C-O bond which would represent an alternative activation channel of methanol. DFT calculations of Greeley and Mavrikakis[8] show that on Pt(111) the energetic barrier for C-O bond breaking is 3 times higher than for C-H or O-H bands. In various experimental works[9,13,15,43,44] dealing with methanol on transition metal surfaces the C-O bond breaking path has been ruled out as well.

C. Thermal Desorption Spectroscopy

A multi-mass TPD spectrum of methanol postadsorbed onto an oxygen precovered $Pt_{0.6}Ru_{0.4}$/Ru(0001) surface alloy is displayed in Fig. 4A, along with the integrated intensities of vibrational modes associated with various surface intermediates produced upon thermal annealing (panel B). Even though the complexity of the surface structure and composition is substantial, the multitude of accessible spectral information allows us to develop a clear picture of the various surface processes encountered during the thermal evolution.

A closer look at the data depicted in Fig. 4 (and keeping the IRAS findings in mind) reveals that, once methoxy is formed, the further reactions proceed via different pathways (for clarity abstracted hydrogens have been omitted; '^{s}' and '^{g}' denote surface and gas phase species, respectively):

- *Pathway I*: total dehydrogenation path, leading to surface CO,
  $CD_3OH^s \rightarrow CD_3O^s \rightarrow CO^s \rightarrow CO^g$
- *Pathway II*: partial dehydrogenation path, producing surface formaldehyde,
  $CD_3OH^s \rightarrow CD_3O^s \rightarrow D_2CO^s \rightarrow D_2CO^g$
- *Pathway III*: oxidation path, leading to CO_2 via a formate (DCOO) intermediate,
  $CD_3OH^s + O^s \rightarrow CD_3O^s + O^s \rightarrow DCOO^s \rightarrow CO_2^g$

In the following these will be discussed in more detail.

1. *Initial Activation of Methanol and Water Formation*

The first desorption peak referring to the annealing temperature in panel (A) is the one of 20 u observed at 160-180 K which is due to reactively produced water ($H_2^{18}O$). In experiments with initially adsorbed [$CH_3^{18}OH + ^{16}O$] and with mass 18 u and 20 u monitored, only the 18 u signal exhibits a desorption signal around 170 K. It is therefore concluded that desorbing water exclusively contains preadsorbed oxygen atoms and not oxygen from methanol; this finding excludes any C-O bond breaking to act as the primary activation process of methanol. Furthermore, the contribution of deuterium from the CD_3 group is negligible as the desorption signal of 22 u ($D_2^{18}O$) at 175 K is zero. Consequently, the involved hydrogen stems from the methanol hydroxyl group only; this observation additionally renders C-D bond breaking of intact methanol unlikely.

The proposed reaction (primary activation of methanol) is therefore

$$2CD_3^{16}OH^{(s)} + {}^{18}O^{(s)} \longrightarrow 2CD_3^{16}O^{(s)} + H_2^{18}O^{(g)},$$

where $^{(s)}$ and $^{(g)}$ denotes surface and gas phase species, respectively. Deuterium from the methanol methyl group does, however, contribute to the water desorption at 200-230 K; in accordance with the easier abstraction of the hydroxyl H, desorption of $H_2^{18}O$ (mass 20 u signal) proceeds at 10-15 K lower temperatures (212 K) as compared to $D_2^{18}O$ (mass 22 u peak at 225 K).

As the water desorption at 175 K and 200-230 K represent two distinct features, they are ascribed to different water formation processes. Specifically, the desorption at 200-230 K is attributed to the recombination of surface D and ^{18}O, as it correlates with methoxy decomposition, releasing D atoms from its methyl group. In contrast, $H_2^{18}O$ evolution at 175 K is likely due to a direct H-transfer from the methanol's OH-group to a surface oxygen atom (^{18}O). Unambigeous evidence for such a reaction has been provided for methanol on Ru(0001)[9].

In parallel to methanol decomposition the mass 35 u peak at 208 K indicates desorbing CD_3OH, in accordance with the decrease of the CD_3OH IRAS signal (circles in panel B). Other desorption peaks (32, 30, 28, 20, 18, 4,

and 2 u) which evolve in parallel to the 35 u peak are due to methanol cracking fragments produced during ionization in the QMS. At variance to methanol on oxygen precovered Pt_n/Ru(0001) layers[11] no isotopic exchange $CD_3OH + D \rightarrow CD_3OD + H$, involving abstracted D from the concurrent $CD_3OH + O_2 \rightarrow DCOO + O + 2D + H$ reaction, is found here.

2. Formaldehyde Formation and Desorption

The next desorption feature in the energetic order is of mass 32 u and extends over a broad temperature range 230-320 K. Incidentally, these temperatures coincide with the vanishing of characteristic methoxy and formaldehyde vibrational features (squares and triangles in panel B). As the mass 32 u signal is not accompanied by a corresponding peak of mass 35 u, its identity as formaldehyde (D_2CO), as opposed to a cracking fragment of CD_3OH, is ensured. The D_2CO cracking products DCO^+ and CO^+ with masses 30 and 28 evolving in parallel support this conclusion.

Interestingly, deuterium desorption (mass 4 u signal) proceeds in the same temperature range which may point at a common origin. According to Fig. 4B methoxy decomposition represents such a mechanism which naturally could explain the evolution of both species. At T $<$ 250 K D_2CO desorption is still slow and this species is detected as a surface compound. At higher T D_2CO exists as a transient species only which desorbs soon after its formation from methanol or methoxy decomposition, similar to methanol on O/Cu_{1ML}/Ru(0001)[32] layers. In order to separate signals of genuine D_2CO desorption from those of the methanol ionization fragment (at 208 K), we subtracted the latter contribution which gave the 32 u,corr trace (dashed line).

For $x = 0.1$ desorption of D_2CO occurs at high temperatures ($T = 378$ K) only, in agreement with the high decomposition temperature of the parent methoxy species for such low Pt concentrations. As this process represents the rate limiting factor in formaldehyde desorption (rather than desorption itself) no surface formaldehyde is observed in IRAS. Only for $x = 0.3 - 0.8$ such species have been detected; the amount is found to be only weakly dependent on the Pt content and corresponds to about 0.2% ML. Note that this quantity refers to surface D_2CO only, while the total amount of produced formaldehyde including the desorbing (transient) species is much larger (about 0.02-0.03 ML). For thick Pt layers on Ru(0001) similar amounts of formaldehyde have been detected as a stable surface compound; however, at variance to the present findings, D_2CO easily dissociates to produce CO.[11] As this process occurs already at 220 K, no formaldehyde desorption takes place. As to the further dehydrogenation of D_2CO towards CO on the O/Pt_xRu_{1-x}/Ru(0001) surface alloys, we consider such a decomposition unlikely as intact desorption of D_2CO is observed in a broad temperature range up to 300 K, i.e. until all methoxy and methanol is consumed. This conclusion is corroborated by the intact desorption of formaldehyde around 275 K for H_2CO adsorbed on the oxygen precovered Ru(0001)-(2 $\times$ 2)-O surface[42].

Hence, as mentioned above, formaldehyde represents the final reaction product of the partial dehydrogenation *Pathway II*.

3. Formate Formation and CO_2 Desorption

The desorbing $C^{18}O^{16}O$ molecules (46 u) in panel (A) of Fig. 4 are the final products of *Pathway III*. They are produced due to the dissociation of surface formate (solid circles in Fig. 4B). The inset depicts desorption signals of the masses 44, 46 and 48 u for a sample with coadsorbed [$CD_3^{16}OH + {}^{18}O$]. As only the mass 46 u exhibits a significant desorption signal it is invoked that the CO_2 molecules consist of one oxygen from methanol and a second one due to the preadsorbed surface oxygen. The same applies to CO_2 produced on Cu/Ru(0001)[32], and Pt/Ru(0001)[11] again involving a formate precursor intermediate. The observation of formate as a key intermediate in methanol oxidation to CO_2 is in agreement with electro-chemical experiments over a Pt electrode.[22]

In parallel to the $C^{18}O^{16}O$ (46 u) desorption we observe peaks of 28 and 30 u which are ascribed to $C^{16}O^+$ and $C^{18}O^+$ ionization fragments of desorbing $C^{16}O^{18}O$. The ratios of 28u/46u and 30u/46u for desorbing $C^{18}O^{16}O$ are known from TPD experiments with coadsorbed [CO + ^{18}O] on Pt_{12ML}/Ru(0001) which produces desorbing $C^{18}O^{16}O$.[11] Subtraction of these contributions yield the true $C^{16}O$ and $C^{18}O$ desorption signals (dashed lines in Fig. 4A). While the 30 u signal entirely represents a $C^{18}O^{16}O$ fragment, there is indeed a proper $C^{16}O$ desorption which we associate with methoxy decomposition (*Pathway I*). The desorption of $C^{16}O$ as opposed to $C^{18}O$ is corroborated by our observation of surface $C^{16}O$ using IRAS in the temperature range 260-380 K (squares in Fig. 4B) while vibrational bands due to $C^{18}O$ are missing.

One possibility for the formation of DCOO is the oxidation of the stable CD_3O intermediate similar to methanol on O/Cu_{1ML}/Ru(0001)[32]; an alternative reaction path would be the direct oxidation of methanol, i.e. without other stable intermediates, similar to methanol on disordered O/Pt_n/Ru(0001) layers with $n = 3 - 15$ ML[11]. These conclusions are based on the correlated increase of the DCOO vibrational modes (solid circles) and the decrease of CD_3OH as well as CD_3O bands (open circles and diamonds). As methoxy is clearly observed as a surface compound in our experiments and it represents an obvious intermediate on the way to DCOO we suggest that methoxy represents the precursor species of DCOO (*Pathway III*). The formation of formate from formaldehyde is unlikely as there is clear evidence for molecular desorption of D_2CO even at temperatures when formate production is completed. Yet, as this reaction

has indeed been observed on ordered O/Pt(111)[13] and O/Pt_{12ML}/Ru(0001)[11] it cannot be ruled out completely.

Remarkably, no D_2 (4 u) desorption is observed in parallel to CO_2 desorption at around 390 K, even though formate decay (DCOO → CO_2 + D) should release some D. This puzzle is resolved by mass 22 u in Fig. 4A which exhibits a tiny peak at 350-400 K (see enlarged curve) indicative of a reaction of D and residual surface ^{18}O to gas phase $D_2^{18}O$ (22 u).

4. *Influence of Pt/Ru Ratio on the Abundance of Surface Species and Desorption Yields*

A general observation in the course of our study was that the initial activation always led to a methoxy intermediate, with the abstracted hydrogen being oxidized by surface oxygen to desorbing water. Depending on the concentration of Pt in the surface layer the decay of methoxy, however, proceeds in different ways as described above. As *Pathway II* (formaldehyde formation and desorption) is largely independent of x, it won't be discussed in the following.

The dependence of *Pathways I* and *III* on the content x of Pt atoms within the Pt_xRu_{1-x}/Ru(0001) surface alloy is illustrated in Fig. 5A. Specifically, the integrated intensities of surface DCOO (vibrational spectra obtained after annealing to 320 K) and of desorbing CO and CO_2 (thermal desorption peaks) are plotted versus x. It is apparent, that the amount of desorbing CO_2 closely follows the intensity of surface DCOO, confirming the DCOO→CO_2 decomposition reaction proposed above. The intensity of desorbing CO shows an inverse behavior, i.e. for x increasing from 0 to 0.8 the amount of desorbing CO_2 increases, while a decrease is observed for the CO desorption yield. In other words, methanol oxidation to CO_2 prevails for surface alloys with $x > 0.4$. In contrast, total dehydrogenation to CO dominates for $x < 0.4$. The quadratic dependence of the CO_2 and DCOO signals on the amount of Pt in the range $x = 0 - 0.4$ clearly suggest an ensemble effect involving at least two neighboring Pt atoms to be responsible for this oxidation reaction; in case of a dominant ligand effect a linear increase of these data should prevail.

For $x = 0.8$ the DCOO signal lies significantly below the corresponding CO_2 signal; the reason for this deviation is the onset of formate decomposition and CO_2 desorption which decreases with increasing x as depicted in Fig. 5B. Thus, the reduced amount of adsorbed DCOO for $x = 0.8$ as compared to $x = 0.6$ after annealing to 320 K is simply due to incipient DCOO decomposition and CO_2 desorption, both of which start slightly below 300 K for $x = 0.8$.

In general, the thermal stability of methoxy on the oxygen covered alloys seems significantly higher than on clean Ru(0001), see Fig. 5C (blue diamonds). Interestingly, this effect appears more pronounced on Ru(0001) as compared to Pt rich Pt_xRu_{1-x}/Ru(0001) surface alloys. For example, CD_3O on clean Ru(0001) which is

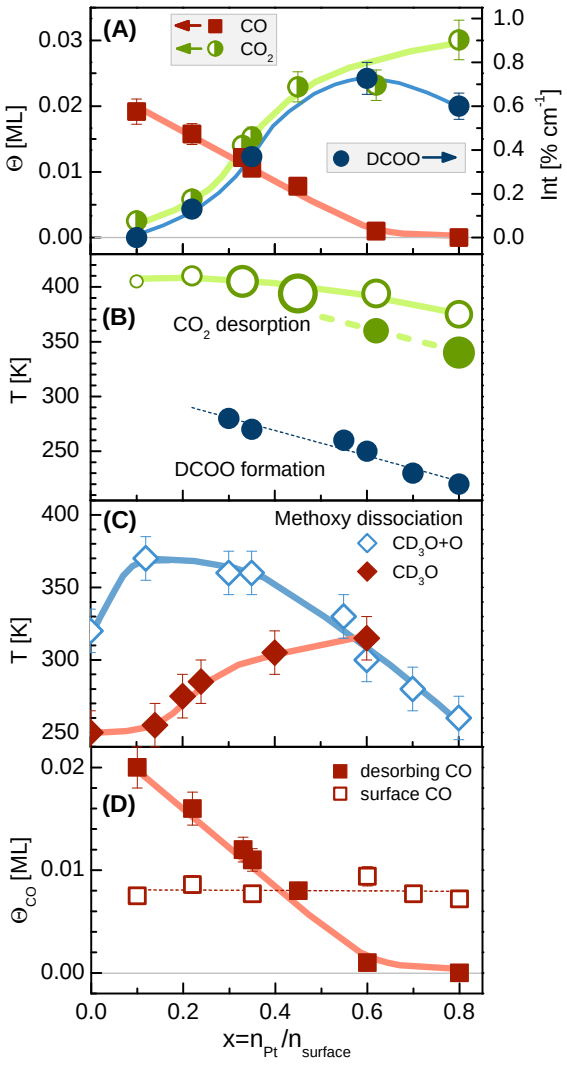

FIG. 5: **A:** Integrated IRAS intensities of formate (ν(OCO) mode at 1300−1305 cm^{-1}) after annealing to 320 K, as well as absolute amounts of CO_2 and of CO determined from the integrated thermal desorption peaks of 44 u and 28 u−0.35×44 u, respectively, as a function of x. **B:** Temperature range of DCOO formation and of CO_2 desorption for the samples in panel A versus x. The empty and full green symbols correspond to the two maxima in the CO_2 desorption trace in Fig. 4A; the areal size of the symbols thereby corresponds to the the respective integrals. **C:** Dissociation temperature of methoxy on oxygen precovered (open diamonds) and oxygen-free (solid diamonds) surface alloys. The point at 320 K for $x = 0$ refers to methoxy on clean Ru(0001) to which 1 L oxygen was added at 80 K after its formation at 220 K. **D:** Absolute amounts of surface CO (ν(CO) mode at 300-320 K) and of desorbing CO (28 u−0.35 × 44 u) as a function of x. All samples were exposed to 4 L oxygen and to 40 mTorr·s CD_3OH, both at 80 K. The data points associated with CO and CO_2 desorption have been obtained simultaneously.

observed in the temperature range 200 - 260 K only, becomes stabilized when 1 L oxygen is added, and 320 K are needed to dissociate half of the methoxy molecules to CO and D. We attribute this observation to the low reactivity of ordered oxygen layers on Ru(0001). For the alloys with high x things are more complex and it is necessary to assess the contributions of incorporated Pt atoms and of coadsorbed oxygen separately. For the oxygen-free surface alloy increasing amounts of Pt also lead to an increase of the thermal stability of methoxy up to 315 K for $x = 0.6$ (solid red diamonds). Remarkably, the combination of adsorbed O and increasing x initially improves the thermal stability of methoxy for $x < 0.2$, while an accelerated decay is observed for $x > 0.3$, reaching 260 K for $x = 0.8$ (blue diamonds). The reason for this latter effect is the onset of the $CD_3O + O \rightarrow DCOO + D_2$ oxidation reaction, which effectively consumes all methoxy molecules. According to panel B in Fig. 5 (blue solid circles) the DCOO formation temperature shifts down from 270 to 220 K for x increasing from 0.35 to 0.8. This accelerated methoxy to formate reaction for Pt rich alloys in conjunction with a stabilization of methoxy with respect to dehydrogenation to CO at low x naturally explains the observed selectivity change in the methanol reaction pathway on Pt_xRu_{1-x}/Ru(0001) surface alloys.

Fig. 5D depicts the amounts of surface CO N^S_{CO} (integrated IR intensities at 300-320 K) and of desorbing CO N^{des}_{CO} (TPD peak areas) as a function of x. Apparently, these two signals behave completely different; the amount of surface CO remains about constant while desorbing CO exhibits the trend known from panel A. In the following we need to treat the two cases of (i) $N^S_{CO} < N^{des}_{CO}$ and (ii) $N^S_{CO} > N^{des}_{CO}$ separately.

(i) The higher amount of desorbing CO as compared to surface CO for $x < 0.4$ is simply due to the increased thermal stability of methoxy for such low concentrations of Pt as evidenced in panel C: at annealing temperatures of 300-320 K, applied to our sample before surface CO is monitored (empty symbols), the decomposition of methoxy is not yet completed; actually, only a small fraction has decayed (see Supporting Information). Higher annealing temperatures decompose methoxy, but nonetheless won't increase N^S_{CO} due to the onset of CO desorption. Similarly, the high temperatures required for methoxy to decay prevents any surface formaldehyde to build up, even though this reaction channel is definitey operative, as evidenced by a pronounced mass 32 u desorption peak of D_2CO at 378 K (see Supporting Information).

(ii) For $x > 0.4$ methoxy decomposition occurs at lower T and does not interfere with CO desorption. At high x the amount of detected surface CO therefore reflects the true yield of *Pathway I* and the lack of detecting desorbing CO has a different reason. From thermal desorption experiments on alloys with $x \geq 0.5$ we know that the reaction $CO + O \rightarrow CO_2$ takes place at 300-400 K. Based on these findings we suggest that the lack of desorbing CO at high x is caused by an efficient reaction of surface CO with oxygen. Consequently, the CO_2 desorption yield in Fig. 5A contains contributions (up to 20%) due to CO oxidation, in addition to the formate decay channel. The low bias of CO towards oxidation at low x even though surface oxygen is available is confirmed by observations of a marginal $CO + O \rightarrow CO_2$ reaction yield for Ru(0001) as compared to Pt(111) under UHV conditions. In contrast to Pt(111), this recombinative desorption does not consume all oxygen atoms on the Pt-Ru surface alloy. We conclude that active and passive surface sites with respect to this reaction exist, which points at a marked ensemble effect: only locations with a high local concentration of Pt represent active regions.

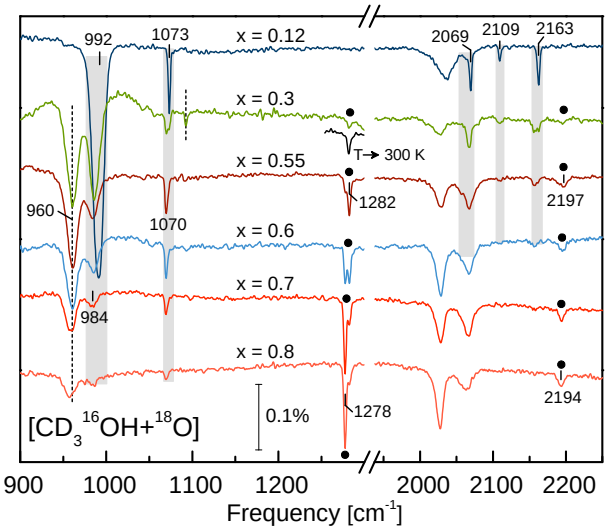

FIG. 6: IRAS spectra of the coadsorbate system $[CD_3OH+^{18}O]$ on Pt_xRu_{1-x}/Ru(0001) surface alloys with $x = 0.12-0.8$ emphasizing formate and methoxy as stable surface intermediates. The spectra of the layers with $x = 0.3-0.8$ were recorded after annealing to 260 K. The samples with $x = 0.12$ was heated to 300 K in order to desorb all residual methanol and present methoxy as the only intermediate (note that no formate is produced). For the layer with $x = 0.3$ the formate band at 1282 cm^{-1} is additionally shown after heating to 300 K, because slightly higher T are required to initiate formate formation at low x. Vibrational bands belonging to residual methanol (dashed lines), methoxy (gray bars), and formate (solid circles) are labeled in the figure. The broad bands at 2000-2080 cm^{-1}, which overlap with the 2070 cm^{-1} peak of methoxy, are due to reactively produced CO. The weak band at 1601 cm^{-1} due to formaldehyde is not shown.

In Fig. 6 a series of IR spectra obtained from $[CD_3{}^{16}OH + {}^{18}O]$ on various Pt_xRu_{1-x}/Ru(0001) surface alloys with $x = 0.12 - 0.8$ and after annealing to 260 K are displayed. For low x the reaction scheme resembles Ru(0001) and less formate but more methoxy is produced, exhibiting the classic Fermi resonance signature of methoxy on Ru(0001). Note that the observed bands at 992, 1073, 2069, 2109 and 2163 cm^{-1} are slightly offset with respect to methoxy on clean Ru(0001)[9] which are

located at 980, 1074, 2066, 2114 and 2163 cm^{-1}.

For $x \geq 0.3$ slight frequency shifts of the methoxy modes are observed, e.g. the 1073 cm^{-1} band shifts to 1070 cm^{-1}, which we attribute to the influence of Pt atoms participating in the bonding to methoxy. In parallel, the Fermi resonance bands (2070-2170 cm^{-1}) become significantly broadened for $x \geq 0.3$ as compared to $x = 0.12$; for $x \geq 0.55$ they are missing almost entirely. Considering the fact that the oxygen precovered Pt_xRu_{1-x}/Ru(0001) alloys provide a much larger variety of local binding geometries of methoxy than clean Pt_xRu_{1-x}/Ru(0001) alloys or (CD_3O+O)/Ru(0001) layers, it is likely that this heterogeneity led to the observed broadening and eventually the vanishing of the Fermi resonance modes at high Pt concentrations.

According to our series of IR spectra in Fig. 6, DCOO formation gradually sets in for $x \geq 0.2$ as evidenced by the 1282 cm^{-1} band ($DC^{16}O^{18}O$ isotope). At low x about 300 K are needed to produce formate and this annealing temperature slightly shifts to lower values for increasing Pt concentration, as depicted in Fig. 5B. For $x \geq 0.55$ an additional $\nu_{\text{O-C-O}}$ mode emerges at 1278 cm^{-1}, as demonstrated in Fig. 6 ($x = 0.55 - 0.8$); for $x = 0.8$ the 1278 cm^{-1} peak accounts for more than 80% of the total formate yield. In this respect we note that the formate signals in Fig. 4B and Fig. 5A represent the sum of both formate peaks. The corresponding features of the regular $DC^{16}O^{16}O$ isotope are located at 1304 and 1300 cm^{-1}, respectively. Thereby the high-frequency peak survives about 20-40 K higher annealing temperatures; moreover the presence of the two $\nu_{\text{O-C-O}}$ modes correlates with the observation of the double peak structure of the CO_2 desorption peak with individual maxima at $\approx$ 360 and 390-400 K in Fig. 4A. Specifically, TPD spectra of samples with $x < 0.6$ exhibit only a single CO_2 desorption peak at around 400 K. We conclude that two formate species with slightly different local environments and binding energies are formed. The presence of two formate species with different vibrational frequencies of the O-C-O stretch have also been reported on Cu/Ru(0001)[32] and Pt/Ru(0001)[11].

From the quantities of the desorbing reaction products D_2CO, CO_2 and CO, the relative amount of methanol which undergo a reaction is estimated to be approximately 35% for an initial methanol coverage of 0.16 ML and for $x = 0.6$. Note that the calibration procedures of the absolute amounts of desorbing CO, CO_2 and D_2CO have been reported previously.[9,32]

IV. CONCLUSIONS

In this work the adsorption and reactions of methanol on clean and oxygen covered Pt_xRu_{1-x}/Ru(0001) surface alloys have been investigated using IRAS and TPD. On oxygen-free Pt_xRu_{1-x}/Ru(0001) surface alloys the reactions proceed similar to Ru(0001), with Pt primarily enhancing the thermal stability of the methoxy intermediate and lowering the CO desorption temperature. In agreement with expectations regarding the inert full Pt/Ru(0001) monolayer, the amount of produced methoxy gradually decreases for $x \to 0.6$.

With cold deposited oxygen preadsorbed, methoxy again represents the primary reaction intermediate. Depending on the Pt concentration the further thermal evolution, however, varies: At low $x < 0.4$, methoxy preferentially dissociates to CO which eventually desorbs at about 400 K. In contrast for $x > 0.4$, methoxy undergoes oxidation to surface formate (DCOO) at 200-300 K. This species is rather stable and its decay can be monitored by detection of desorbing CO_2. The maximum amount of DCOO, as deduced from the CO_2 desorption yield, is obtained for Pt_xRu_{1-x}/Ru(0001) alloys with $x = 0.6-0.8$ and equals 15% of the initially adsorbed methanol molecules. In addition and largely independent of x, the partial dehydrogenation of methoxy to surface formaldehyde is observed; this reaction intermediate is found to desorb moleculary.

Referring to the DMFC where hydrogen acts as the energy provider, the easy reaction of hydrogen (released during methanol decomposition) with surface oxygen to produce gas phase water constitutes a severe disadvantage of Pt(111)[13,14]. For Pt_xRu_{1-x}/Ru(0001) surface alloys this reaction channel is suppressed (most probably due to a much stronger bonding of oxygen to Ru atoms) and hydrogen from methoxy decomposition (250-300 K) eventually desorbs molecularly rather than reacts with surface oxygen. Still, water formation associated with the initial activation of methanol (abstraction of the hydroxyl hydrogen), as well as formaldehyde production and desorption represent loss channels with respect to the total H production yield.

Another important aspect to be considered when analyzing the various substrate materials in terms of applications in DMFC is CO poisoning. On Ru(0001) CO represents a persistent surface compound due to the strong Ru-CO bonding and its negligible CO + O $\rightarrow$ CO_2 reaction activity (at least under UHV conditions). For Pt_xRu_{1-x}/Ru(0001) surface alloys this reaction is possible at $T > 300$ K for $x > 0.5$. In addition, the incorporation of Pt atoms within the Ru(0001) surface lowers the CO desorption temperature considerably by about 60 K for $x = 0.7 - 0.8$.[45,46] Our suggestion for a reasonably well performing anode catalyst is therefore a Pt:Ru ratio of $x = 0.6 - 0.8$ in the surface layer.

Supporting Information Available

- IRAS spectra of methoxy (CD_3O) on O/Ru(0001) and on $Pt_{0.4}Ru_{0.6}$/Ru(0001). (figure)
- Optimized parameters of the methoxy Fermi resonance. (table)
- Thermal evolution of [CD_3OH + ^{16}O] on Pt_xRu_{1-x}/Ru(0001) for $x \approx 0.1$. (figure)

This material is available free of charge via the Internet at http://pubs.acs.org.

[1] Ralph, T.R.; Hogarth, M.P., Platinum Metals Rev. **2002**, 46, 3.
[2] Ralph, T.R.; Hogarth, M.P., Platinum Metals Rev. **2002**, 46, 117.
[3] Iwasita, T.; Hoster, H.; John-Anacker, A.; Lin, W. F.; Vielstich, W., Langmuir **2000**, 16, 522.
[4] Hoster, H.; Iwasita, T.; Baumgärtner, H.; Vielstich, W., Phys. Chem. Chem. Phys **2001**, 3, 337.
[5] Iwasita, T., J. Braz. Chem. Soc. **2002**, 13, 401.
[6] Waszczuk, P.; Lu, G.Q.; Wieckowski, A.; Lu, C.; Rice, C.; Masel, R. I., Electrochim. Acta **2002**, 47, 3637.
[7] Jusys, Z.; Kaiser, J.; Behm, R. J., Electrochim. Acta **2002**, 47, 3693.
[8] Greeley, J.; Mavrikakis, M., J. Am. Chem. Soc. **2004**, 126, 3910.
[9] Gazdzicki, P.; Jakob, P., J. Phys. Chem. C **2010**, 114, 2655.
[10] Gazdzicki, P.; Uvdal, P.; Jakob, P., J. Chem. Phys. **2009**, 130, 224703.
[11] Gazdzicki, P.; Thussing, S.; Jakob, P., submitted to J. Phys. Chem. C.
[12] Gibson, K.D.; Dubois, L.H., Surf. Sci. **1990**, 233, 59.
[13] Liu, Z.; Sawada, T.; Takagi, N.; Watanabe, K.; Matsumoto, Y., J. Chem. Phys. **2003**, 119, 4879.
[14] Endo, M.; Matsumoto, T.; Kubota, J.; Domen, K.; Hirose, C., J. Phys. Chem. B **2000**, 104, 4916.
[15] Sawada, T.; Liu, Z.; Takagi, N.; Watanabe, K.; Matsumoto, Y., Chem. Phys. Lett. **2004**, 392, 334.
[16] Rodriguez, J.A.; Goodman, D.W., Science **1992**, 257, 897.
[17] Rodriguez, J.A., Surf. Sci. Rep. **1996**, 24, 223.
[18] Liu, P.; Nørskov, J. K., Phys. Chem. Chem. Phys. **2001**, 3, 3814.
[19] Mavrikakis, M.; Hammer, B.; Nørskov, J. K., Phys. Rev. Lett. **1998**, 81, 2819.
[20] Buatier de Mongeot, F.; Scherer, M.; Gleich, B.; Kopatzki, E.; Behm, R. J., Surf. Sci., **1998**, 411, 249.
[21] Hoster, H.E.; Bergbreiter, A.; Erne, P.M.; Hager, T.; Rauscher, H.; and Behm, R.J., Phys. Chem. Chem. Phys., **2008**, 10, 3812.
[22] Chen, Y. X.; Miki, A.; Ye, S.; Sakai, H.; Osawa, M., J. Am. Chem. Soc. **2003**, 125, 3680.
[23] Feulner, P.; Menzel, D., J. Vac. Sci. Technol. **1980**, 17, 662.
[24] Jakob, P; Schlapka, A., Surf. Sci. **2007**, 601, 3556.
[25] Schlapka, A.; Käsberger, U.; Menzel, D.; Jakob, P., Surf. Sci. **2002**, 502, 129.
[26] Koch, M. H.; Jakob, P.; Menzel, D., Surf. Sci. **1996**, 367, 293.
[27] Sim, S.W.; Gardner, P.; King, D.A., J. Phys. Chem. **1995**, 99, 16002.
[28] Mudalige, K.; Warren, S.; Trenary, M., J. Phys. Chem. B **2000**, 104, 2448.
[29] Chesters, M. A.; McCash, E. M., Spectrochim. Acta, Part A **1987**, 43, 1625.
[30] Jakob, P.; Schlapka, A.; Gazdzicki, P., J. Phys. Chem. **2011** 134, 224707.
[31] Ryberg, R., J. Chem. Phys. **1985**, 82, 567.
[32] Gazdzicki, P.; Jakob, P., J. Phys. Chem. C **2011**, 115, 16555.
[33] Russell, J. N. Jr.; Gates, S. M.; Yates, T. J. Jr., Surf. Sci. **1985**, 163, 516.
[34] Francis, S.M.; Leibsle, F.M.; Haq, S.; Xiang, N.; Bowker, M., Surf. Sci. **1994**, 315, 284.
[35] Davies, P.R.; Bowker, M., Catal. Today **2010**, 154, 31.
[36] Darling, B.T.; Dennison, D.M., Phys. Rev. **1940**, 57, 128.
[37] Herzberg, G., Infrared and Raman Spectra of Polyatomic Molecules (D. Van Nostrand Company, 1960).
[38] Duncan, J.L.; McKean, D.C.; Speire, G.K., Mol. Phys. **1972**, 24, 553.
[39] Asmundsson, R.; Uvdal, P., J. Chem. Phys. **2000**, 112, 366.
[40] Uvdal, P.; Weldon, M. K.; Friend, C. M., Phys. Rev. B **1994**, 50, 12258.
[41] Weisel, M.D.; Chen, J.G.; Hoffmann, F.M., J. Electron Spectrosc. Relat. Phenom. **1990**, 54, 787.
[42] Anton, A.B.; Parmeter, J.E.; Weinberg, W.H., J. Am. Chem. Soc. **1986**, 108, 1823.
[43] Gazdzicki, P.; Jakob, P., J. Phys. Chem. C **2011**, 115, 1961.
[44] Mudalige, K; Trenary, M., Surf. Sci. **2002**, 504, 208.
[45] Rauscher, H.; Hager, T.; Diemant, T.; Hoster, H.; Buatier de Mongeot, F.; Behm, R.J., Surf. Sci. **2007**, 601, 4608.
[46] Diemant, T.; Bansmann, J.; Rauscher, H., ChemPhysChem **2010**, 11, 1482.

Supporting information for:

Reactions of Methanol on Clean and Oxygen Covered Pt_xRu_{1-x}/Ru(0001) Surface Alloys

Pawel Gazdzicki, Sebastian Thussing, and Peter Jakob*

Fachbereich Physik und Zentrum für Materialwissenschaften, Philipps-Universität Marburg, Renthof 5, 35032 Marburg, Germany

E-mail: peter.jakob@physik.uni-marburg.de

*To whom correspondence should be addressed

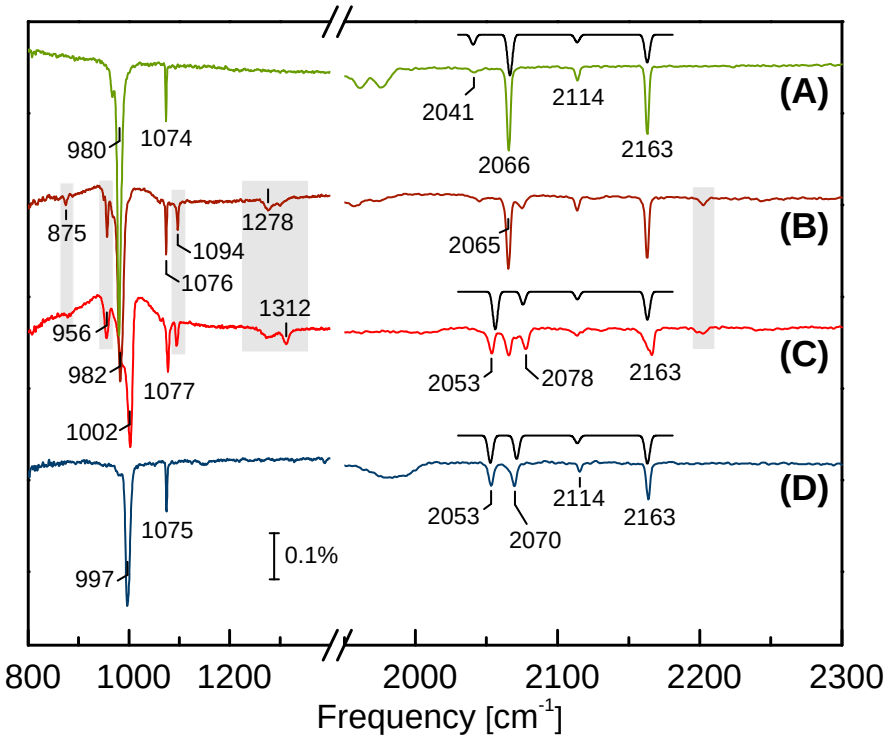

Figure 1: **IRAS spectra of methoxy (CD_3O) on O/Ru(0001) and on $Pt_{0.4}Ru_{0.6}$/Ru(0001).** Spectrum (A) shows methoxy on clean Ru(0001) after heating adsorbed methanol ($\Theta_{\mathrm{Meth}} = 0.1 - 0.15$ ML) to 220 K to produce methoxy. Spectrum (B) has been obtained in a similar way as spectrum A, but with 0.1 ML oxygen preadsorbed. In spectrum (C) the layer in (B) has been exposed to an extra oxygen dose of 0.6 L at 80 K and again annealed to 220 K. The peaks labeled by the gray boxes are due to residual intact methanol. Specifically, the peaks at 1278 and 1312 cm^{-1} can be associated with isolated methanol molecules embedded in a (2×2)-O and a (2×1)-O matrix, respectively;[1,2] note that 250 K are required to fully desorb methanol from O/Ru(0001) layers. Spectrum (D) refers to CD_3O on a $Pt_{0.4}Ru_{0.6}$/Ru(0001) surface alloy with 40% Pt atoms in the surface layer. 0.15 ML methanol was adsorbed at 80 K and annealed to 220 K to produce methoxy prior to data acquisition at 80 K. The modes located at 2030 - 2180 cm^{-1} are attributed to Fermi resonance multiplets of methoxy comprising the symmetric $\nu_s(CD_3)$ fundamental mode interacting with several overtone and combination bands of this species; among them are the symmetric and the twofold degenerate asymmetric methyl C-D bending modes, $\delta_s(CD_3)$ and $\delta_{as}(CD_3)$, as well as the $[\nu(CO)+\delta_s(CD_3)]$ combination band. Their mixing has been calculated as described below by adjusting their unperturbed line positions and the respective Fermi resonance coupling constants. Simulated spectra (black curves) with parameters summarized in Table 1 and using Gaussian functions with a FWHM$= 4$ cm^{-1} have been added in the spectral range $2030 - 2180$ cm^{-1} for comparison.

The parameters of the methoxy Fermi resonance observed in Figure 1 have been derived from an analysis of the mutual coupling of the contributing modes similar to the analysis performed by Asmundsson and Uvdal,[3] except for the fact that an additional mode, the [ν(CO)+δ_s(CD_3)] combination band is included. These modes (with unperturbed frequencies ν_i) have identical symmetry and the interaction between them (Fermi resonance coupling constants, W_{ij}) can be described by the symmetric effective Hamiltonian matrix H:[4,5]

$$H = \begin{pmatrix} \nu_1 & & & \\ W_{21} & \nu_2 & & \\ 0 & W_{32} & \nu_3 & \\ 0 & W_{42} & 0 & \nu_4 \end{pmatrix}. \tag{1}$$

Thereby the couplings between the overtone and combination modes (Darling-Dennison constants)[6,7] are neglected as they are significantly weaker than the Fermi resonance coupling constants.[8] The matrices of eigenvalues E and of eigenvectors Ψ of the equation

$$H = \Psi E \Psi^{-1} \tag{2}$$

then provide the perturbed peak positions and peak intensities, respectively.

An optimized set of parameters which (almost) perfectly reproduces the three independent experimental data sets (spectra A, C, and D of Figure 1) is presented in Table 1. Here the unperturbed frequencies of all modes associated with the methyl group have been kept constant for all three data sets, i.e. only the value of the [δ_s(CD_3)+ν(CO)] combination band has been changed to simulate the individual spectra. Note that the respective line shifts of this band were directly taken from the experimentally observed line shifts of the methoxy ν(CO) band. Of course the individual Fermi resonance coupling constants were kept constant for all three data sets.

Our analysis additionally provides the anharmonic coupling between the ν(CO) and δ_s(CD_3) modes of CD_3O which amounts to $\delta\nu_{anh}$ = 9±1 cm^{-1}; here we assume that ν(CO) and δ_s(CD_3) are not affected by dynamic dipole shifts, which would reduce $\delta\nu$ accordingly.

Table 1: Optimized parameters of the methoxy Fermi resonance. The vibrational modes (frequencies given in cm^{-1}) of CD_3O (C_{3v} symmetry) refer to the spectra A, C, and D in Figure 1. The values have been obtained by a systematic variation of the parameters in Eq. (1) and optimizing congruency with the experimental spectra. Note that the high values of the coupling constant W_{42} and the intensity of the $2\delta_{as}$ mode are because of the twofold degeneracy of this mode.

mode	coupling	unperturbed peak positions			perturbed peak positions		
		A	**C**	**D**	**A**	**C**	**D**
$\nu_1 = \delta_s(CD_3)+\nu(CO)-\delta\nu_{anh}$	$W_{21} = 12$	2045	2070	2062	2041	2056	2053
$\nu_2 = \nu_s(CD3)$		2099	2099	2099	2067	2076	2071
$\nu_3 = 2\delta_s(CD3)$	$W_{32} = 27$	2104	2104	2104	2114	2114	2114
$\nu_4 = 2\delta_{as}(CD3)$	$W_{42} = 37$	2136	2136	2136	2163	2163	2163

References

(1) Gazdzicki, P.; Uvdal, P.; Jakob, P., J. Chem. Phys. **2009**, 130, 224703.

(2) Gazdzicki, P.; Jakob, P., J. Phys. Chem. C **2011**, 115, 16555.

(3) Asmundsson, R.; Uvdal, P., J. Chem. Phys. **2000**, 112, 366.

(4) Califano, S., Vibrational States (Wiley, New York, 1976).

(5) Wilson, E.B.; Decius, J.C.; Cross, P.C., Molecular Vibrations (Dover, New York, 1980).

(6) Darling, B.T.; Dennison, D.M., Phys. Rev. **1940**, 57, 128.

(7) Herzberg, G., Infrared and Raman Spectra of Polyatomic Molecules (D. Van Nostrand Company, 1960).

(8) Duncan, J.L.; McKean, D.C.; Speire, G.K., Mol. Phys. **1972**, 24, 553.

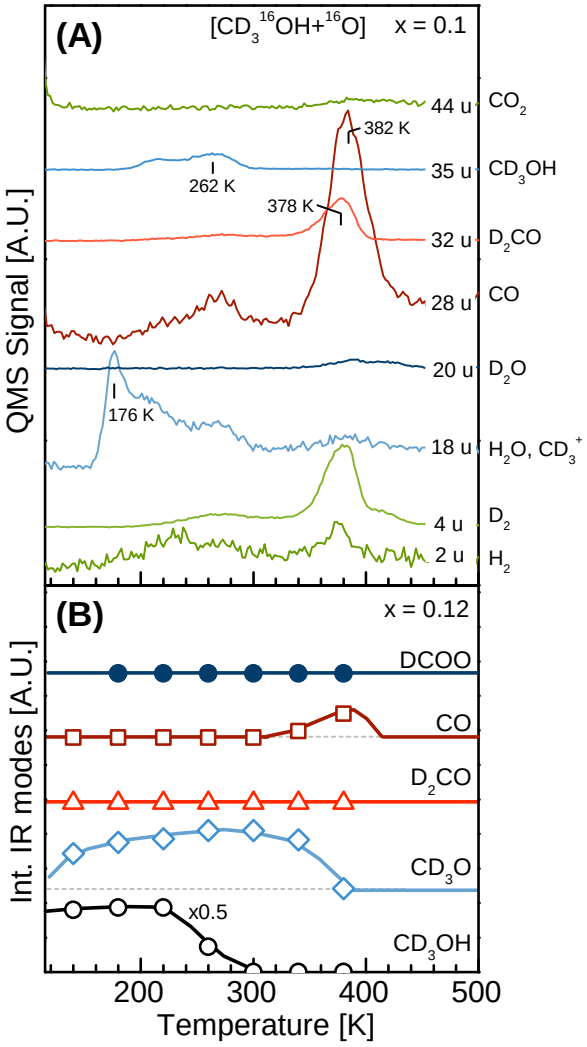

Figure 2: **Thermal evolution of [CD_3OH + ^{16}O] on Pt_xRu_{1-x}/Ru(0001) for $x \approx$ 0.1.**
A: Multi-mass TPD (heating rate 1 K/s) comprising masses of various desorbing species labeled at the right. The methanol exposure at 80 K corresponds to 40 mTorr·s (leading to a coverage of about 0.15 ML) and has been applied to an oxygen covered PtRu alloy surface ($\Theta_O \approx 0.4$ ML).
B: Integrated IR intensities of characteristic modes associated with the various surface species after annealing to increasingly higher temperature: methanol ν(CO) mode at 957 cm^{-1}, methoxy ν(CO) mode at 992 cm^{-1}, carbon monoxide ν(CO) mode at 1950-2000 cm^{-1}. No other stable surface intermediates (formate, formaldehyde, ...) have been observed. Methanol and oxygen exposures as in **(A)**; annealing of the sample to the indicated temperatures used a linear ramp of 1 K/s. The colored lines are guides to the eye. The individual curves are vertically offset for better clarity of presentation.

References

[1] J. W. Erisman, M. A. Sutton, J. Galloway, Z. Klimont, and W. Winiwarter, Nature Geosci. **1**, 636 (2008).

[2] G. Ertl, Angew. Chem. Int. Ed. Engl. **29**, 1219 (1990).

[3] J. A. Rodriguez and D. W. Goodman, Science **257**, 897 (1992).

[4] M. P. Hogarth and T. R. Ralph, Platinum Metals Rev. **46**, 146 (2002).

[5] K. A. Mauritz and R. B. Moore, Chem. Rev. **104**, 4535 (2004).

[6] K. Schmidt-Rohr and Q. Chen, Nat. Mater. **7**, 75 (2008).

[7] M. P. Hogarth and G. A. Hards, Platinum Metals Rev. **40**, 150 (1996).

[8] A. Hamnett, Catal. Today **38**, 445 (1997).

[9] T. R. Ralph and M. P. Hogarth, Platinum Metals Rev. **46**, 117 (2002).

[10] L. Liu et al., Electrochim. Acta **43**, 3657 (1998).

[11] H. Liu et al., J. Power Sources **155**, 95 (2006).

[12] P. Waszczuk et al., Electrochim. Acta **47**, 3637 (2002).

[13] Z. Jusys, J. Kaiser, and R. J. Behm, Electrochim. Acta **47**, 3693 (2002).

[14] H. B. Harry Hoster, Teresa Iwasita and W. Vielstich, Phys. Chem. Chem. Phys **3**, 337 (2001).

[15] T. Iwasita, H. Hoster, A. John-Anacker, W. F. Lin, and W. Vielstich, Langmuir **16**, 522 (2000).

[16] T. Iwasita, J. Braz. Chem. Soc. **13**, 401 (2002).

[17] T. R. Ralph and M. P. Hogarth, Platinum Metals Rev. **46**, 3 (2002).

[18] R. T. Vang, E. Laegsgaard, and F. Besenbacher, Phys. Chem. Chem. Phys. **9**, 3460 (2007).

[19] P. Stoltze and J. K. Nørskov, Phys. Rev. Lett. **55**, 2502 (1985).

[20] J. Hrbek, R. A. de Paola, and F. M. Hoffmann, J. Chem. Phys. **81**, 2818 (1984).

[21] J. Hrbek, R. de Paola, and F. M. Hoffmann, Surf. Sci. **166**, 361 (1986).

[22] A. A. Deckert, J. L. Brand, C. H. Mak, B. G. Koehler, and S. M. George, J. Chem. Phys. **87**, 1936 (1987).

[23] T. Sasaki, Y. Itai, and Y. Iwasawa, Surf. Sci. **443**, 44 (1999).

[24] R. Barros, A. Garcia, and L. Ilharco, J. Phys. Chem. B **105**, 11186 (2001).

[25] R. Barros, A. Garcia, and L. Ilharco, J. Phys. Chem. B **108**, 4831 (2004).

[26] P. Gazdzicki, P. Uvdal, and P. Jakob, J. Chem. Phys. **130**, 224703 (2009).

[27] J. Russell Jr., S. Gates, and J. Yates Jr., Surf. Sci. **163**, 516 (1985).

[28] B. A. Sexton, Surf. Sci. **88**, 299 (1979).

[29] J. Greeley and M. Mavrikakis, J. Catal. **208**, 291 (2002).

[30] I. E. Wachs and R. J. Madix, J. Catal. **53**, 208 (1978).

[31] M. A. Chesters and E. M. McCash, Spectrochim. Acta, Part A **43**, 1625 (1987).

[32] R. Ryberg, J. Chem. Phys. **82**, 567 (1985).

[33] R. Ryberg, Phys. Rev. Lett. **49**, 1579 (1982).

[34] J. P. Camplin and E. M. McCash, Surf. Sci. **360**, 229 (1996).

[35] K. Mudalige and M. Trenary, Surf. Sci. **504**, 208 (2002).

[36] A. Groß and S. Sakong, J. Phys. Chem. **111**, 8817 (2007).

[37] P. Singnurkar et al., J. Phys. Chem. C **112**, 14034 (2008).

[38] D. H. Ehlers, A. Spitzer, and H. Lth, Surf. Sci. **160**, 57 (1985).

[39] K. Gibson and L. Dubois, Surf. Sci. **233**, 59 (1990).

[40] B. A. Sexton, Surf. Sci. **102**, 271 (1981).

[41] S. Akhter and J. White, Surf. Sci. **167**, 101 (1986).

[42] J. Wang, M. A. DeAngelis, D. Zaikos, M. Setiadi, and R. I. Masel, Surf. Sci. **318**, 307 (1994).

[43] W. T. Lee, F. Thomas, and R. I. Masel, Surf. Sci. **418**, 479 (1998).

[44] M. Endo, T. Matsumoto, J. Kubota, K. Domen, and C. Hirose, J. Phys. Chem. B **104**, 4916 (2000).

[45] M. Endo, T. Matsumoto, J. Kubota, K. Domen, and C. Hirose, Surf. Sci. **441**, L931 (1999).

[46] T. Sawada, Z. Liu, N. Takagi, K. Watanabe, and Y. Matsumoto, Chem. Phys. Lett. **392**, 334 (2004).

[47] Z. Liu, T. Sawada, N. Takagi, K. Watanabe, and Y. Matsumoto, J. Chem. Phys. **119**, 4879 (2003).

[48] S. Desai, M. Neurock, and K. Kourtakis, J. Phys. Chem. B **106**, 2559 (2002).

[49] J. Greeley and M. Mavrikakis, J. Am. Chem. Soc. **126**, 3910 (2004).

[50] J. Greeley and M. Mavrikakis, J. Am. Chem. Soc. **124**, 7193 (2002).

[51] C. Houtman and M. A. Barteau, Langmuir **6**, 1558 (1990).

[52] F. Solymosi, A. Berk, and T. Tarnczi, Surf. Sci. **141**, 533 (1984).

[53] N. Kruse, G.-K. Chuah, G. Abend, D. Cocke, and J. Block, Surf. Sci. **189-190**, 832 (1987).

[54] J. Davis and M. Barteau, Surf. Sci. **197**, 123 (1988).

[55] J. Davis and M. Barteau, Surf. Sci. **187**, 387 (1987).

[56] X. Guo, L. Hanley, and J. T. Yates, J. Am. Chem. Soc. **111**, 3155 (1989).

[57] W. S. Sim, P. Gardner, and D. A. King, J. Phys. Chem. **99**, 16002 (1995).

[58] A. L. Schwaner and J. M. White, J. Phys. Chem. B **101**, 10414 (1997).

[59] P. Uvdal, M. K. Weldon, and C. M. Friend, Phys. Rev. B **50**, 12258 (1994).

[60] P. Uvdal and A. D. MacKerell, Surf. Sci. **393**, 141 (1997).

[61] J. L. Gland, B. A. Sexton, and G. B. Fisher, Surf. Sci. **95**, 587 (1980).

[62] J. L. Gland, Surf. Sci. **93**, 487 (1980).

[63] S. Francis, F. Leibsle, S. Haq, N. Xiang, and M. Bowker, Surface Science **315**, 284 (1994).

[64] P. R. Davies and M. Bowker, Catal. Today **154**, 31 (2010).

[65] R. Ryberg, Chem. Phys. Lett. **83**, 423 (1981).

[66] K. Mudalige, S. Warren, and M. Trenary, J. Phys. Chem. B **104**, 2448 (2000).

[67] M. N. D. Cordeiro, A. S. Pinto, and J. A. Gomes, Surf. Sci. **601**, 2473 (2007).

[68] M. Gsell, P. Jakob, and D. Menzel, Science **280**, 717 (1998).

[69] P. Jakob, M. Gsell, and D. Menzel, J. Chem. Phys. **114**, 10075 (2001).

[70] M. Mavrikakis, B. Hammer, and J. K. Nørskov, Phys. Rev. Lett. **81**, 2819 (1998).

[71] A. Ruban, B. Hammer, P. Stoltze, H. Skriver, and J. Nørskov, J. Mol. Catal. A: Chem. **115**, 421 (1997).

[72] B. Hammer and J. K. Nørskov, Nature **376**, 238 (1995).

[73] B. Hammer, O. Nielsen, and J. Nørskov, Catal. Lett. **46**, 31 (1997).

[74] A. Schlapka, M. Lischka, A. Groß, U. Käsberger, and P. Jakob, Phys. Rev. Lett. **91**, 016101 (2003).

[75] J. E. Houston, C. H. F. Peden, D. S. Blair, and D. W. Goodman, Surf. Sci. **167**, 427 (1986).

[76] K. Christmann, G. Ertl, and H. Shimizu, Thin Solid Films **57**, 247 (1979).

[77] C. Günther, J. Vrijmoeth, R. Q. Hwang, and R. J. Behm, Phys. Rev. Lett. **74**, 754 (1995).

[78] F. Buatier de Mongeot, M. Scherer, B. Gleich, E. Kopatzki, and R. J. Behm, Surf. Sci. **411**, 249 (1998).

[79] U. Käsberger and P. Jakob, Surf. Sci. **540**, 76 (2003).

[80] A. Schlapka, U. Käsberger, D. Menzel, and P. Jakob, Surf. Sci. **502-503**, 129 (2002).

[81] Y. He, A. P. Seitsonen, and H. Over, Phys. Rev. B **72**, 075432 (2005).

[82] B. Eisenhut, J. Stober, G. Rangelov, and T. Fauster, Phys. Rev. B **47**, 12980 (1993).

[83] D. G. O'Neill and J. E. Houston, Phys. Rev. B **42**, 2792 (1990).

[84] J. R. Kitchin, J. K. Nørskov, M. A. Barteau, and J. G. Chen, Phys. Rev. Lett. **93**, 156801 (2004).

[85] S. Kneitz, J. Gemeinhardt, and H. P. Steinrück, Surf. Sci. **440**, 307 (1999).

[86] G. Laurent, H. F. Busnengo, P. Riviere, and F. Martin, Phys. Rev. B **77**, 193408 (2008).

[87] G. Anger, A. Winkler, and K. Rendulic, Surf. Sci. **220**, 1 (1989).

[88] G.-J. Kroes, Prog. Surf. Sci. **60**, 1 (1999).

[89] H. Shimizu, K. Christmann, and G. Ertl, J. Catal. **61**, 412 (1980).

[90] T. E. Madey, H. Albert Engelhardt, and D. Menzel, Surf. Sci. **48**, 304 (1975).

[91] R. Otero et al., Surf. Sci. **550**, 65 (2004).

[92] F. Habraken, E. Kieffer, and G. Bootsma, Surf. Sci. **83**, 45 (1979).

[93] J. Rodriguez, Surf. Sci. Rep. **24**, 223 (1996).

[94] P. Liu and J. K. Nørskov, Phys. Chem. Chem. Phys. **3**, 3814 (2001).

[95] H. E. Hoster et al., Phys. Chem. Chem. Phys. **10**, 3812 (2008).

[96] T. Diemant, J. Bansmann, and H. Rauscher, ChemPhysChem **11**, 1482 (2010).

[97] H. Rauscher et al., Surf. Sci. **601**, 4608 (2007).

[98] A. Bergbreiter, H. E. Hoster, and R. J. Behm, ChemPhysChem **12**, 1148 (2011).

[99] H. Hartmann et al., Surf. Sci. **603**, 1439 (2009).

[100] A. Bergbreiter, O. B. Alves, and H. E. Hoster, ChemPhysChem **11**, 1505 (2010).

[101] A. Schiffer, PhD thesis, Technische Universität München, 1998.

[102] H. Engelhardt, P. Feulner, H. Pfnür, and D. Menzel, J. Phys. E **10**, 1133 (1977).

[103] A. Bradshaw and E. Schweizer, *Advances in Spectroscopy: Spectroscopy of Surfaces*, chapter 8, pages 413–483, John Wiley & Sons Ltd, 1988.

[104] Y. J. Chabal, Surf. Sci. Rep. **8**, 211 (1988).

[105] B. Hayden, *Methods of Surface Characterization*, chapter 7, pages 267–343, Plenum, 1987.

[106] P. Dirac, Proc. Roy. Soc. (London) **114**, 243 (1927).

[107] G. Herzberg, *Infrared and Raman Spectra of Polyatomic Molecules*, D. Van Nostrand Company, 1960.

[108] E. Bright Wilson, J. Decius, and P. C. Cross, *Molecular Vibrational*, Dover Publications, inc. New York, 1980.

[109] B. Hayden, K. Prince, D. Woodruff, and A. Bradshaw, Surf. Sci. **133**, 589 (1983).

[110] B. E. Hayden, K. Prince, D. P. Woodruff, and A. M. Bradshaw, Phys. Rev. Lett. **51**, 475 (1983).

[111] J. D. Head, Int. J. Quantum Chem. **77**, 350 (2000).

[112] R. Asmundsson and P. Uvdal, J. Chem. Phys. **112**, 366 (2000).

[113] M. Andersson, P. Uvdal, and A. MacKerell, J. Phys. Chem. B **106**, 5200 (2002).

[114] J. Fan and M. Trenary, Langmuir **10**, 3649 (1994).

[115] D. C. Harris and M. D. Bertolucci, *Sammetry and Spectroscopy*, Dover, 1989.

[116] B. N. J. Persson, F. M. Hoffmann, and R. Ryberg, Phys. Rev. B **34**, 2266 (1986).

[117] F. M. Hoffmann and B. N. J. Persson, Phys. Rev. B **34**, 4354 (1986).

[118] E. Schweizer, B. Persson, M. Tüshaus, D. Hoge, and A. Bradshaw, Surf. Sci. **213**, 49 (1989).

[119] P. Jakob and B. N. J. Persson, Phys. Rev. B **56**, 10644 (1997).

[120] P. Jakob, J. Chem. Phys. **108**, 5035 (1998).

[121] H. Pfnür, D. Menzel, F. M. Hoffmann, A. Ortega, and A. M. Bradshaw, Surf. Sci. **93**, 431 (1980).

[122] P. Jakob and A. Schiffer, Surf. Sci. **603**, 1135 (2009).

[123] B. N. J. Persson and R. Ryberg, Phys. Rev. B **24**, 6954 (1981).

[124] W. Herres and J. Gronholz, Comp. Appl. Lab. **2**, 216 (1984).

[125] J. Gronholz and W. Herres, Instruments & Computers **3**, 10 (1985).

[126] D. A. King, Surf. Sci. **47**, 384 (1975).

[127] D. Menzel, *Interactions on Metal Surfaces*, volume 4, chapter Desorption phenomena, pages 101–142–142, Springer Berlin / Heidelberg, 1975.

[128] P. Redhead, Vacuum **12**, 203 (1962).

[129] H. Pfnür, P. Feulner, and D. Menzel, J. Chem. Phys. **79**, 4613 (1983).

[130] P. Feulner and D. Menzel, J. Vac. Sci. Technol. **17**, 662 (1980).

[131] H. Schlichting, PhD thesis, Technische Universität München, 1990.

[132] H. Schlichting and D. Menzel, Surf. Sci. **285**, 209 (1993).

[133] D. R. Lind, editor, *Handbook of CHEMISTRY and PHYSICS*, CRC Press, 73 edition, 1992-1993.

[134] J.-P. Lange, Catal. Today **64**, 3 (2001).

[135] G. Chinchen, K. Waugh, and D. Whan, App. Catal. **25**, 101 (1986).

[136] K. Waugh, Catal. Today **15**, 51 (1992).

[137] M. Bowker, R. A. Hadden, H. Houghton, J. N. K. Hyland, and K. C. Waugh, J. Catal. **109**, 263 (1988).

[138] K. Klier, *Methanol Synthesis*, volume Volume 31, pages 243–313, Academic Press, 1982.

[139] M. Qian, M. A. Liauw, and G. Emig, Appl. Catal. A **238**, 211 (2003).

[140] M. Mavrikakis and M. A. Barteau, J. Mol. Catal. A: Chem. **131**, 135 (1998).

[141] A. Schiffer, P. Jakob, and D. Menzel, Surf. Sci. **465**, 198 (2000).

[142] N. Brønsted, Chem. Rev. **5**, 231 (1928).

[143] M. G. Evans and M. Polanyi, Trans. Faraday Soc. **34**, 11 (1938).

[144] P. Gazdzicki, Diploma Thesis, Philipps-Universität Marburg, 2008.

[145] T. H. Ellis and H. Wang, Langmuir **10**, 4083 (1994).

[146] Y. X. Chen, A. Miki, S. Ye, H. Sakai, and M. Osawa, J. Am. Chem. Soc. **125**, 3680 (2003).

[147] D. Kreikemeyer-Lorenzo et al., Phys. Rev. Lett. **107**, 046102 (2011).

[148] J. R. B. Gomes and J. A. N. F. Gomes, J. Mol. Struct. **463**, 163 (1999).

[149] S. Sakong and A. Gro, J. Catal. **231**, 420 (2005).

[150] I. Bak and G. Plinks, Surf. Sci. **600**, 3809 (2006).

[151] F. Delbecq and P. Sautet, Langmuir **9**, 197 (1993).

Personal Data

Pawel Gaździcki

pawel@gazdzicki.de

∗ 09.03.1982, Warsaw

Education

since 08/2008	PhD Student, Faculty of Physics, Philipps-Universität Marburg Supervisor: Prof. Dr. P. Jakob Thesis: Adsorption and Thermally Induced Reactions of Methanol on Bimetallic X/Ru(0001) Layers (X = Cu, Pt)
10/2002 – 07/2008	Study of Physics, Philipps-Universität Marburg Focus: surface science Thesis: Adsorption and Thermal Evolution of Methanol on Functionalized Ru(0001) Graduation 07/2008: Dipl.-Phys.
06/2002	Albert Einstein-Gymnasium, Maintal University entrance qualification (Abitur)

Publications

11/2011	P. Gazdzicki, S. Thussing and P. Jakob, *Reactions of Methanol on Clean and Oxygen Covered Pt_xRu_{1-x}/Ru(0001) Surface Alloys*, J. Phys. Chem. C. 115, 25379 (2011).
10/2011	P. Gazdzicki, S. Thussing and P. Jakob, *Oxidation of Methanol on Oxygen Covered Pt_n/Ru(0001) Layers*, J. Phys. Chem. C. 115, 23013 (2011).
07/2011	P. Gazdzicki and P. Jakob, *Methanol Oxidation on Monolayer Cu/Ru(0001)*, J. Phys. Chem. C 115, 16555 (2011).
06/2011	P. Jakob, A. Schlapka and P. Gazdzicki, *Oxygen Adsorption on Pt/Ru(0001) Layers*, J. Chem. Phys. 134, 224707 (2011).
12/2010	P. Gazdzicki and P. Jakob, *Methoxy on Cu/Ru(0001) Layers*, J. Phys. Chem. C 115, 1961 (2011).
01/2010	P. Gazdzicki and P. Jakob, *Reactions of Methanol on Ru(0001)*, J. Phys. Chem. C 114, 2655 (2010).
05/2009	P. Gazdzicki, P. Uvdal, and P. Jakob, *Adsorption of Intact Methanol on Ru(0001)*, J. Chem. Phys. 130, 224703 (2009).